

AD-A052 420

SYSTEMS CONTROL INC PALO ALTO CALIF AERONAUTICAL AND--ETC F/G 21/5
F100 MULTIVARIABLE CONTROL SYNTHESIS PROGRAM. VOLUME 1. DEVELOP--ETC(U)

UNCLASSIFIED

JUN 77 R L DE HOFF, W E HALL, R J ADAMS

F33615-75-C-2053

AFAPL-TR-77-35-VOL-1

NL

1 of 4

AD-A052420



AD A 052420

18
19
AFAPL-TR-77-35-VOL-1
Volume I

2
B.S.

6
**F100 MULTIVARIABLE CONTROL SYNTHESIS PROGRAM,
Volume I. Development of F100 Control System.**

AERONAUTICAL & MARINE SYSTEMS SECTOR
SYSTEMS CONTROL, INC. (Vt)
1801 PAGE MILL ROAD
PALO ALTO, CALIFORNIA 94304

10
Ronald L. De Hoff, W. Earl Hall, Jr.,
Richard J. /Adams Narendra K. /Gupta

AD No.

DDC FILE COPY

11
JUN 77

12 324p.

DDC
APR 10 1978
F

9
TECHNICAL REPORT AFAPL-TR-77-35, Volume I
Final Report, 1 Aug 75 - 31 Dec 76

15 F33615-75-C-2053

16 3066

17 03
Approved for public release; distribution unlimited.

A0523 76 A052 346
AIR FORCE AERO-PROPULSION LABORATORY
AIR FORCE WRIGHT AERONAUTICAL LABORATORIES
AIR FORCE SYSTEMS COMMAND
WRIGHT-PATTERSON AIR FORCE BASE, OHIO 45433

410 132

mt

NOTICE

When Government drawings, specifications, or other data are used for any purpose other than in connection with a definitely related Government procurement operation, the United States Government thereby incurs no responsibility nor any obligation whatsoever; and the fact that the government may have formulated, furnished, or in any way supplied the said drawings, specifications, or other data, is not to be regarded by implication or otherwise as in any manner licensing the holder or any other person or corporation, or conveying any rights or permission to manufacture, use, or sell any patented invention that may in any way be related thereto.

This report has been reviewed by the Information Office (OI) and is releasable to the National Technical Information Service (NTIS). At NTIS, it will be available to the general public, including foreign nations.

This technical report has been reviewed and is approved for publication.

Charles A. Skira
CHARLES A. SKIRA
Project Engineer

FOR THE COMMANDER

Charles E. Bentz
CHARLES E. BENTZ
Tech Area Manager, Controls

"If your address has changed, if you wish to be removed from our mailing list, or if the addressee is no longer employed by your organization please notify AFAPL/TBC, W-PAFB, OH 45433 to help us maintain a current mailing list".

Copies of this report should not be returned unless return is required by security considerations, contractual obligations, or notice on a specific document.

SECURITY CLASSIFICATION OF THIS PAGE (When Data Entered)

DDC
RECEIVED
APR 10 1978
RECEIVED
F

UNCLASSIFIED

SECURITY CLASSIFICATION OF THIS PAGE(When Data Entered)

20. structure integral trim system produced specified steady-state performance and limit accommodation in the presence of simulated degradation effects and instrument errors.

The resulting control logic was extensively tested on a hybrid simulation of the F100 turbofan and will be used to control an engine in an altitude test cell. The details of the design procedure, linear model analysis and a summary of digital and hybrid simulation tests results are presented in this report.

ACCESSION for	
NTIS	Write Section <input checked="" type="checkbox"/>
DDC	B. H. Section <input type="checkbox"/>
UNANNOUNCED	<input type="checkbox"/>
JUSTIFICATION	
BY	
DISTRIBUTION/AVAILABILITY NOTES	
A	

UNCLASSIFIED

SECURITY CLASSIFICATION OF THIS PAGE(When Data Entered)

FOREWORD

This final report was submitted by Systems Control, Inc. (Vt), Palo Alto CA under Air Force Contract F33615-75-C-2053. The effort was sponsored by the National Aeronautics and Space Administration, Lewis Research Center, Cleveland OH, and the Air Force Aero-Propulsion Laboratory, Air Force Systems Command, Wright-Patterson Air Force Base OH under Project 3066, Task 306603 and Work Unit 30660370 with Charles A. Skira, AFAPL/TBC, as Project Engineer. This program was initiated with FY 75 Aero-Propulsion Laboratory Director's Funds. Dr. W. Earl Hall, Jr. of Systems Control, Inc. (Vt) was Project Manager for this effort. Project Engineer was Dr. Ronald L. De Hoff. Ms. Deborah Buenz responsible for the technical publication of this report.

The Air Force would like to gratefully acknowledge the following personnel for their invaluable contributions to this effort: Dr. Narendra K. Gupta and Ms. Karen Nakano of Systems Control, Inc. (Vt); Mr. Richard J. Adams of Champlain Technology Industries Division of Systems Control, Inc. (Vt), West Palm Beach FL; Messrs. Ronald D. Hackney and Ronald J. Miller of Pratt and Whitney Aircraft, Government Products Division, West Palm Beach, FL; Mr. Edward C. Beattie of Pratt and Whitney Aircraft, Commercial Products Division, East Hartford CT; Messrs. John R. Zeller, John R. Szuch, James F. Soeder, David S. Cwynar, Dr. Kurt Seldner and Dr. Bruce Lehtenin of the National Aeronautics and Space Administration, Lewis Research Center, Cleveland OH; and Mr. Lester L. Small of the Air Force Aero-Propulsion Laboratory, Wright-Patterson Air Force Base OH.

The Air Force would especially like to acknowledge Lt Col Walter J. Rabe formerly of the Air Force Office of Scientific Research who contributed greatly to the formulation of this research effort.

This report consists of two volumes:

Volume I - Development of F100 Control System

Volume II - Appendices A through K

Reference [1] and [2] describe associated efforts specifically related to the research effort discussed in this report. For a more complete description of this program, the reader should obtain these reports.

CONTENTS

CHAPTER		PAGE
I	INTRODUCTION AND SUMMARY	1
	1.1 INTRODUCTION	1
	1.2 SUMMARY	3
II	FUNDAMENTAL CONSIDERATIONS GOVERNING ENGINE CONTROL SYNTHESIS	7
	2.1 BACKGROUND	8
	2.2 A SUMMARY OF CONTROL REQUIREMENTS FOR ADVANCED AIRCRAFT ENGINES	10
	2.2.1 General Control Requirements	10
	2.2.2 Steady-State and Transient Operating Requirements Leading to Control Requirements	11
	2.2.3 Transient and Destabilizing Conditions Related to Operation Over Flight Condition Transition	20
	2.3 CURRENT CONTROL DESIGN METHODS	23
	2.3.1 Approaches to Existing Operational Engine Control Systems	24
	2.3.2 Multivariable Design Methods	28
	2.4 MULTIVARIABLE CONTROL DESIGN METHODOLOGY	29
	2.4.1 Modern and Classical Control	30
	2.4.2 Classical Control Synthesis	30
	2.4.3 Modern Control Synthesis Methods	31
	2.5 LQR APPROACH FOR LINEAR SYSTEM CONTROL SYNTHESIS	34
	2.5.1 Basis of the LQR Method	35
	2.6 APPLICATION OF LQR METHOD TO TURBOFAN ENGINES	37
	2.6.1 LQR Theory for Linear Systems	39
	2.6.2 Linearization of Nonlinear Simulation for Application of the LQR Method	41
	2.6.3 Gain Scheduling for Turbofan Engine Control	42
	2.6.4 Choice of States and the Design Points	43
	2.6.5 Rapid Accelerations and Set Point Change	45
	2.6.6 Parameter Insensitivity of the LQR Gains	46
	2.7 ENGINE DIGITAL CONTROL IMPLEMENTATION	46
	2.7.1 Digitization	47
	2.7.2 Word Size	48
	2.8 SUMMARY	49
III	LINEAR QUADRATIC REGULATOR SYNTHESIS TECHNIQUES	51
	3.1 OVERVIEW	51
	3.2 BASIS OF LINEAR QUADRATIC REGULATOR DESIGN METHOD	53

CONTENTS (Continued)

CHAPTER		PAGE
	3.2.1 Linear System Description	53
	3.2.2 Quadratic Cost Functional	54
	3.2.3 Solution to the Optimization	56
	3.2.4 Steady-State Solution	59
	3.2.5 Generalized Results	60
3.3	SELECTION OF PERFORMANCE INDEX	63
	3.3.1 Scale Factor Weightings (Bryson's Rule)	63
	3.3.2 Root Square Locus	64
	3.3.3 Modal Sensitivities	69
3.4	TECHNIQUES FOR AUGMENTING THE PERFORMANCE INDEX	70
	3.4.1 Weights on Control Rates and Accelerations	70
	3.4.2 Control Actuator Models	71
	3.4.3 Output Augmentation	74
3.5	TECHNIQUES FOR INTEGRAL CONTROL SYNTHESIS	75
	3.5.1 Optimal Control with State Augmentation	77
	3.5.2 Disturbance Estimation	79
	3.5.3 Spectral Decoupling Techniques	84
3.6	SYSTEM PARAMETER INSENSITIVITY	92
	3.6.1 Important Considerations	92
	3.6.2 Modal Sensitivities	93
	3.6.3 Techniques for Insensitive Controls ..	94
3.7	SIMPLIFICATION OF CONTROL LAWS	97
	3.7.1 Sensitivity Calculations	99
	3.7.2 Fixed Structure Optimization	101
3.8	DISCRETE OPTIMAL CONTROL PROBLEM	101
	3.8.1 Discrete Time Problem	102
3.9	SUMMARY	108
IV	DESIGN METHODOLOGY FOR A MULTIVARIABLE CONTROLLER ..	109
4.1	OVERVIEW	109
4.2	DETERMINISTIC NONLINEAR CONTROL	110
4.3	ENGINE MODELING FOR CONTROL	114
4.4	GAIN SCHEDULING AND ADAPTIVITY	130
	4.4.1 Analytical Approaches	131
	4.4.2 Direct Gain Schedule Development	134
4.5	TRANSITION CONTROL	141
	4.5.1 Requirements	141
	4.5.2 Generation of Transition Models	141
	4.5.3 Rate Design	147
4.6	INTEGRAL CONTROL DESIGN PROCEDURES	149
	4.6.1 Integral Control with Variable Structure	149

CONTENTS (Continued)

CHAPTER		PAGE
4.7	SENSOR COMPENSATION TECHNIQUES	154
4.7.1	Optimal Control in the Presence of Noise	154
4.7.2	Classical Techniques	158
4.7.3	Multivariable Filter Compensation	160
4.7.4	Sensor Error Models	163
4.7.5	Final Value Filter for Nonlinear System	165
4.8	SUMMARY	170
V	DESIGN OF A MULTIVARIABLE CONTROLLER FOR THE F100 ENGINE	171
5.1	INTRODUCTION AND OVERVIEW	171
5.2	F100 ENGINE SYSTEM	172
5.2.1	F100 Turbofan Engine	172
5.2.2	Sensor and Actuator Characteristics ..	172
5.2.3	Engine Envelope and Control Criteria .	177
5.3	OVERVIEW OF THE CONTROL STRUCTURE	183
5.4	REFERENCE POINT SCHEDULES	184
5.4.1	Purpose	184
5.4.2	Implementation Procedure	185
5.4.3	Approximation Techniques	186
5.4.4	Description of Implementation	186
5.5	ENGINE LINEAR MODEL DESCRIPTION	192
5.5.1	Linear Model Analysis	197
5.5.2	Principal Conclusions of Linear Model Analysis	200
5.6	LINEAR QUADRATIC REGULATOR DESIGNS	201
5.6.1	Introduction	201
5.6.2	Transient Control Criteria	201
5.6.3	Selection of Design and Evaluation Models	203
5.6.4	Design Model Structure and Performance Indices	206
5.7	DEVELOPMENT OF REGULATOR GAIN SCHEDULES	210
5.7.1	Introduction	210
5.7.2	Simplification of Feedback Matrices ..	211
5.7.3	Scheduling Parameter Development	211
5.7.4	Verification of Scheduled Response ...	214
5.8	INTEGRAL CONTROL DESIGN	215
5.8.1	Introduction	215
5.8.2	Set Point Vector Specification	219
5.8.3	Integral Control Design Results	229
5.8.4	Summary	233

CONTENTS (Continued)

CHAPTER		PAGE
	5.9 TRANSITION CONTROL DESIGN	234
	5.9.1 Introduction	234
	5.9.2 Transition Control Design Principles .	235
	5.9.3 Description of the Designs	236
	5.9.4 Implementation of Logic	240
	5.9.5 Summary	244
	5.10 FAN TURBINE INLET TEMPERATURE SENSOR COMPEN- SATION	244
	5.11 SUMMARY	248
VI	EVALUATION OF THE F100 MULTIVARIABLE CONTROLLER	251
	6.1 INTRODUCTION	251
	6.2 STEADY-STATE EVALUATION	252
	6.2.1 Introduction	252
	6.2.2 Reference Schedules	252
	6.2.3 Installation and Deterioration Effects	254
	6.2.4 Fan Exit Pressure Measurement	261
	6.2.5 Summary	263
	6.3 TRANSIENT EVALUATION	264
	6.3.1 Introduction	264
	6.3.2 Digital Evaluation	265
	6.3.3 Hybrid Evaluation	273
VII	SUMMARY, CONCLUSIONS AND RECOMMENDATIONS	285
	7.1 SUMMARY	285
	7.2 CONCLUSIONS	289
	7.3 RECOMMENDATIONS	290
	REFERENCES	293

ILLUSTRATIONS

FIGURE		PAGE
1.1	Management and Technical Integration - F100 Multivariable Control System Program	4
2.1	F100 Turbofan Engine	12
2.2	Typical Engine Operating Limitations	13
2.3	Typical Fan Map	17
2.4	Altitude Effects on Stability	18
2.5	Power Lever Transient Effects on Fan Stability ...	19
2.6	Power Lever Transient Effects on High Compressor Stability	20
2.7	Typical Steady-State Inlet Airflow Total Pressure Distortion	21
2.8	Typical Inlet Airflow Dynamic Pressure Variation .	22
2.9	Conventional Control Structures Using Hydromechan- ical Implementation	25
2.10	Procedure for Choosing Weights in the Performance Index	34
2.11	Perturbational Control Structure	36
2.12	Choice of States in Application of LQR Methods to a Nonlinear System	44
3.1	Illustration of Root Square Locus Technique for Approximating Closed-Loop Root Locations	67
3.2	Command Filter for Rate and Acceleration Limited Actuators	72
3.3	Controller Structure with Measured Actuator Inputs	73
3.4	Illustration of Multiplant Technique in Determin- ing Linearization Region Appropriate for a Single Design	98
4.1	F100 Turbofan Multivariable Control Structure	112
4.2	Schematic Flow Diagram of F100 Nonlinear Digital Simulation	115
4.3	States, Outputs, and Controls Modeled in F100 Linear Equations Generated from Nonlinear Digital Simulation Program	117

ILLUSTRATIONS (Continued)

FIGURE		PAGE
4.4	Normalized Eigenvector Components for Two Roots Lying in the Bandwidth of Control at Sea Level Static, Intermediate Power Condition for the F100 Turbofan Engine	123
4.5	Schematic Representation of Lightly Coupled Roots Within the Structure of a High Order Linear System	125
4.6	Example of Normalized Eigenvector Corresponding to a Lightly Coupled System in the 16th-Order Linear Models of the F100 Engine at Sea Level Static	127
4.7	Comparison of Small Perturbation Response of the F100 Turbofan Engine at Sea Level Static, Take-off Power Simulated by the Full Nonlinear Digital Deck, the 16th-Order Linearized Model and the Reduced Order Design Linear Model	129
4.8	Problems Caused by Extrapolation of Polynomial Gain Schedule for a Small Number of Design Points Include Sign Reversal and Overly Large Magnitude .	137
4.9	Linear Spline Interpolation of a Gain Scheduled Throughout a Bivariate Envelope Linking Design Points Within Each Region and Providing Well Behaved Extrapolation Properties	137
4.10	Univariate Schedule of Data Using Four Break Points	138
4.11	Average Error in Filtering Data for Increasing Number of Break Points	140
4.12	Asymptotic Solution to Linear System	144
4.13	Continuous State Asymptotic Solution to Linear System	145
4.14	Continuous Control Asymptotic Solution to Linear System	147
4.15	Operating Envelope Constraint Limits for the F100 Turbofan Engine	150
4.16	Complementary Filter Structure	160
4.17	Reduced Order Filter Implementation	163
4.18	Illustration of Step Response of a Nonlinear System During an Output Limited Transient	166
5.1	F100 Turbofan Engine	173
5.2	Linearized Actuator Dynamical Models	174

ILLUSTRATIONS (Continued)

FIGURE		PAGE
5.3	Fan Turbine Inlet Temperature (FTIT) Sensor Model	177
5.4	F100 Turbofan Multivariable Control Structure	183
5.5	Reference Schedule Algorithm	184
5.6	Reference Point Scheduling Algorithm - Overview ..	187
5.7	Fan Stream Reference Schedules	188
5.8	Relationship of Fan Component Parameters to $\Delta p/p$	189
5.9	Core Stream Reference Point Algorithm	190
5.10	Core Stream Uptrim Logic	191
5.11	Fan and Compressor Stability at Various Power Conditions, Altitudes, and Mach Numbers	194
5.12	Engine Protection Limits for Various Altitudes and Mach Numbers	196
5.13	Relative Operating Point Location and Significance Linear Model Generation Schedule	197
5.14	Linear Model Generation Points	199
5.15	Multivariable Feedback Control Law	201
5.16	Open- and Closed-Loop Root Locations for Six Design Point Models from LQR Synthesis	207
5.17	Normalized Linear Quadratic Regulator Weights, Intermediate Power	208
5.18	Gain Schedule	210
5.19	Gain Schedule Function for Power Level	213
5.20	Selected Elements of Regulator Gain Schedule - Intermediate Power	214
5.21	Dominant Open- and Closed-Loop Regulator Poles at Three Supersonic Evaluation Points Using Gains Scheduled from Subsonic Design Models and Calcu- lated on 16 th -Order Linear Systems at the Three Conditions	216
5.22	Rotor Speed Error Signal Response to Small Pertur- bation ($\Delta PLA = +3^\circ$) Step Input at Three Flight Conditions from Nonlinear Digital Evaluation	217
5.23	Integral Trim Logic	218
5.24	Implementation of Integral Trim - Overview	220

ILLUSTRATIONS (Continued)

FIGURE		PAGE
5.25	Priority Select Logic and Dead Zone in Integral Control Algorithm	221
5.26	Cyclic PLA Response Shows Nozzle Moving In and Out of Saturation	222
5.27	An Example of Integral Trim Accommodation of Control Saturation During a Step Power Lever Response	226
5.28	Example of Fuel Flow Integrator Switching During Cyclic PLA Input at Sea Level Static	227
5.29	Multivariable Controller Feedback Gain Matrix Structure Containing Regulator and Variable Set Point Integral Trim Terms	228
5.30	Transition Model	236
5.31	Illustration of the Differences Between Perturbation Error Signal and Reference Error in a Large Transient from Point A to Point B Shown as State Space Trajectory, Perturbation Trajectory, and Step Input Error Signal	237
5.32	Transition Trajectory Generation Algorithm is Formed from a Rate Limited Servomechanism Structure with Variable Rate Saturation Forming the Gross Trajectory and the Proportional Response Providing Continuity with the Steady-State Reference	241
5.33	Generation of Control Step Inputs as a Function of Power Lever Angle Change and Current Trajectory State	241
5.34	Illustration of Transient Trajectory Generation Algorithm for Cyclic PLA Input at Sea Level Static Conditions from Nonlinear Digital Simulation	242
5.35	Step Response of FTIT Sensor Models Indicating That Error in Using First Order Approximation is Small Compared to Overall Sensor Output Response .	246
5.36	Asymptotes of Frequency Response of FTIT Sensor Compensation Showing Pole-Zero Locations as Function of Estimator Gains and Feedforward Parameter	247
5.37	Implementation of Fan Turbine Inlet Temperature Estimator in Multivariable Control System	249
5.38	Example of Temperature Compensation Showing Compensator Output Leading Both the Actual Temperature Response and Sensor Output During a 75% Thrust Step at 10,000 ft, Mach Number 0.9 from Hybrid Simulation	250

ILLUSTRATIONS (Continued)

FIGURE		PAGE
6.1	Comparison of Hybrid Simulation of the Multivariable Controller Steady-State Operating Points with the Digital Simulation of the Production Controller at Three Flight Conditions - Net Thrust	255
6.2	Comparison of the Hybrid Simulation of the Multivariable Controller Steady-State Operating Points with the Digital Simulation of the Production Controller at Three Flight Conditions - Fan Speed	256
6.3	Effect of Deterioration and Installation on Net Thrust - Sea Level Static Conditions	258
6.4	Effect of Deterioration and Installation on Thrust Specific Fuel Consumption - Sea Level Static Conditions	259
6.5	Effect of Deterioration and Installation on Net Thrust (% of Point) at Altitude Points, Intermediate Power Level Shown as the Magnitude of the Variation	259
6.6	Effect of Deterioration and Installation on Thrust Specific Fuel Consumption (% of Point) at Altitude Points, Intermediate Power Level Shown as the Magnitude of the Variation	260
6.7	Schematic of Instrumentation for Fan Exit Pressure Measurement	262
6.8	Worst Case Performance Sensitivity to $(\Delta p/p)_{2.5}$ Sensing Accuracy	263
6.9	Hybrid Simulation of F100 and Multivariable Controller at NASA Lewis Research Center	264
6.10	Cyclic PLA Transient I at Sea Level Static Condition from Digital Multivariable Control Evaluation	267
6.11	Cyclic PLA Transient II at Sea Level Static Conditions from Multivariable Control Evaluation	268
6.12	Small Perturbation Step Response to Intermediate Power at Sea Level Static Conditions from the Multivariable Control Evaluation	270
6.13	Small Perturbation Response to a Step Input - Middle Power, Sea Level Static Conditions from the Multivariable Control Evaluation	271
6.14	Deceleration from Intermediate to Idle at 30,000 ft, $M_n = 0.9$, Holding the Minimum Burner Pressure Limit	272

ILLUSTRATIONS (Continued)

FIGURE		PAGE
6.15	Acceleration to Intermediate Power at Sea Level, $M_n = 1.2$ Showing Accommodation of Temperature and Pressure Limits	273
6.16	Accommodation of Pressure Disturbances at Sea Level Static Conditions	274
6.17	Acceleration from Idle Power at Sea Level Static Conditions with Full Specified Deterioration and Installation Effects	275
6.18	Acceleration from Idle to Intermediate Power with Fuel Flow Limit Lowered at Sea Level Static Conditions	275
6.19	Three Degree Power Lever Angle Step Response at an Off-Design Condition, 52/10K/1.2, from the Hybrid Simulation	277
6.20	Augmentor Control Logic Implementation Schematic	279
6.21	Simulated Augmentor Ignition Disturbance Accommodation Without Nozzle Area Feedforward (from Hybrid Simulation)	280
6.22	Frequency Response of Multivariable Controller and F100 Engine at 45K/0.9 from the Hybrid Evaluation Showing Thrust Response to PLA Inputs	282
6.23	Engine Response Comparison at Sea Level, Static Conditions for an Idle to Intermediate to Idle Input with the Fast Response Control Parameters (from the Hybrid Simulation)	284
7.1	F100 Turbofan Multivariable Control Structure ...	287

TABLES

TABLE		PAGE
2.1	F100 Performance Evaluation Points and Associated Operational Considerations	15
2.2	Performance Output Measures	16
2.3	Comparison of Modern Vs. Classical Design Methods	28
2.4	Application of Multivariable Control Design Using Linear Perturbational Techniques to Aircraft Turbine Engines	37
2.5	Application of LQR Theory to Control Design for Turbine Engines - State-of-the-Art	40
3.1	Organization of Chapter III	52
4.1	Elimination of Lightly Coupled Complex Pair by Performing Static Reduction on TT4LO	128
5.1	Characteristic Actuator Time Constants	175
5.2	Engine Sensor List	177
5.3	Summary of Control Criteria	178
5.4	Operating Points Chosen for Dynamic/Static Analysis	198
5.5	Typical Multivariable Design Cycle	209
5.6	Regulator Feedback Gain Matrix Structure After Reduction	212
5.7	Operating Points for Evaluation	218
5.8	Integral Set Point Vector Specification	219
5.9	Scheduled Rate Values and Derived Output Values Calculated as a Function of Ambient Conditions at Four Design Points	239
6.1	Operating Points for Evaluation	252
6.2	Digital Evaluation of Reference Point Schedules Comparing the Steady Operating Point of the Production and Multivariable Controller at Ten Study Flight Conditions	253
6.3	Typical Component Deterioration and Installation Effects for the F15	257
6.4	Conclusion Summary - Installation Sensitivity	260
6.5	Digital Computer Control Evaluation	265
6.6	Transient Simulation Data Index - Multivariable Controller Evaluation	266

SYMBOLS

A	measurement distribution matrix
A	state weighting matrix
A	switching matrix
a	linear interpolator slope
a	scalar state weight
A/B	afterburner
AJCL	jet area control signal
A _J	nozzle area
ANMIX	nozzle area
B	control weighting matrix
B	schedule bias
b	control scalar weight
b	integrator variable
b	linear interpolator intercept or slope
BLCCL	customer bleed flow control law output
BLD	customer bleed flow
C	regulator gain matrix
c	constant
c	linear interpolator intercept
c	row or element of modal control distribution matrix
CIVV	compressor inlet variable vanes
CIVVCL	compressor inlet variable vanes control law output
col	column vector
CWFMB	corrected main burner fuel flow
D	control feedforward matrix
d	element or row of control feedforward matrix
DEG	degrees
det	determinant
diag	diagonal matrix
DP25	$\Delta p/p$ averaged at fan exit station

SYMBOLS (Continued)

DP25SCH	$\Delta p/p$ scheduled at fan exit station
dt	time differential
E	auxiliary matrix
E(\cdot)	expected value
E	integrator error
e	error
e	exponential function
exp	exponential function
F	dynamics matrix
F	Fahrenheit
f	nonlinear dynamics function
F/A	fuel-to-air ratio
F_n	net thrust
FT	feet
FTIT	fan turbine inlet temperature
G	control distribution matrix
g	nonlinear function
g	scalar element or row of control distribution matrix
H	Hamiltonian
H	output distribution matrix
h	altitude
h	element or row of output distribution matrix
h	nonlinear algebraic output function
HP	horsepower
HPX	horsepower extraction
hr	hour
I	identity matrix
i	index
I_p	pxp identity matrix
IPCS	integrated propulsion control system

SYMBOLS (Continued)

J	cost functional
j	index
j	$\sqrt{-I}$
K	estimator gain matrix
K	thousand
L	integral weighting function
\mathcal{L}	linear functional
L	reduced order estimator gain matrix
LBF	pounds force
LBM	pounds mass
LF	logic flag
LQG	Linear Quadratic Gaussian
LQR	Linear Quadratic Regulator
M	follower output distribution matrix
M	state rate compatibility matrix
M	steady-state gain matrix
m	number of controls
MF	logical flag
MFLAG	integrator flag vector
M_i	<u>i</u> th model
Mn	Mach number
N	control state cross weighting matrix
n	index
n	number of states
N_1	fan speed
N_2	compressor speed
N_2C_2	compressor speed corrected to station 2
P	positive definite matrix
P	output jump matrix
P	parameter

SYMBOLS (Continued)

P_B	burner pressure
PLA	power lever angle
pps	pounds mass per second
PSIA	pounds per square inch (absolute)
P_{T2}	engine face total pressure
$P_{T2.5}$	fan exit total pressure
P_{T3}	compressor discharge total pressure
P_{T4}	high pressure turbine entrance total pressure
$P_{T4.5}$	low pressure turbine entrance total pressure
P_{T6C}	duct exit total pressure
P_{T6M}	augmentor volume entrance total pressure
P_{T7M}	augmentor volume exit total pressure
PUL	unlimited scheduled pressure
Q	output rate matrix
Q	process noise density
Q	quadratic weight
q	auxiliary variable
q	dynamic pressure
q	rank index
q	state index
R	measurement noise density
R	Rankine
R	scaling matrix
RCVV	rear compressor variable vanes
RCVVCL	rear compressor variable vanes control law output
Re	Reynolds number
R_k	residue at kth eigenvalue
RPM	revolutions per minute
r_u	control rate vector
r_x	state rate vector

SYMBOLS (Continued)

S	quadratic terminal miss weighting matrix
S	Riccati matrix
S	scaling matrix
S	state jump matrix
s	index
s	Laplace transformer variable
s	scalar factor
SEC	seconds
S_k	control residue at <u>k</u> th eigenvalue
SMAF	average fan stability margin
SMHC	compressor stability margin
SNCSCH	scheduled compressor speed
SNCSCR	scheduled corrected compressor speed
SNFSCR	scheduled corrected fan speed
S_{θ}^i	sensitivity of <u>i</u> th eigenvalue to parameter θ
T	output transfer factor matrix
T	sampling time
T	similarity transformation
t	term
t	time
TIT	turbine inlet temperature
tr	trace of a matrix
TSFC	thrust specific fuel consumption
T_{T2}	engine face total temperature
$T_{T2.5C}$	fan discharge total temperature - outer stream
$T_{T2.5H}$	fan discharge total temperature - inner stream
T_{T3}	compressor discharge total temperature
T_{T4}	high pressure turbine total temperature
T_{T4LO}	high pressure turbine entrance slow response temperature
T_{T4HI}	high pressure turbine entrance fast response temperature

SYMBOLS (Continued)

$T_{T4.5}$	low pressure turbine total temperature
$T_{T4.5LO}$	low pressure turbine entrance slow response temperature
T_{T5}	low pressure turbine exit temperature
T_{T6C}	duct discharge total temperature
T_{T6M}	augmentor entrance total temperature
T_{T7M}	augmentor exit total temperature
u	column eigenvector
u	control vector
\tilde{v}	auxiliary integrated state vector
v	measurement noise
v	row eigenvector
w	airflow
w	auxiliary control vector
w	disturbance
w	variable bias
WCF	fan corrected airflow
WFAB	augmentor fuel flow
WFMB	main burner fuel flow
WFMBCL	main burner fuel flow control law output
WFMBFB	main burner fuel flow feedback
X_i	<u>i</u> th break point
x	state vector
x	x data coordinate
x	covariance of x
Y_i	<u>i</u> th break point
y	output vector
y	y data coordinate
Z_i	<u>i</u> th break point
z	model coordinate
z	z data coordinate

SYMBOLS (Continued)

α	auxiliary variable
α	factor
α	independent rate
β	auxiliary variable
Γ	discrete control distribution matrix
Γ	disturbance distribution matrix
δ	perturbation
δ	pressure ratio, referenced to standard condition
ε	coupling term
ε	error
ε	small number
ζ	damping ratio
Θ	set of parameters
θ	ambient parameter vector
θ	parameter element
θ	reduced order filter state
θ	temperature ratio referenced to standard conditions
Λ	Block diagonal or diagonal matrix
λ	eigenvalue
$\lambda(\cdot)$	eigenvalue of matrix
λ	Lagrange multiplier
μ	auxiliary control variable
ν	exponent index
$\nu(t)$	innovation process
Σ	auxiliary factor matrix
φ	terminal weighting function
φ	transition matrix
ξ	modal coordinate
Ξ	modal control distribution matrix
χ	modified process noise element
ω	frequency

SYMBOLS (Continued)

ω_{CL}	closed-loop bandwidth
ω_n	natural frequency
ω_s	sampling frequency
Δp	pressure difference
$\Delta p/p$	pressure difference ratio $(P_T - P_S)/P_T$
Δ	determinant
Δ	change
ρ_2	engine face density
∂	partial differential
τ_c	time constant
τ	time variable
τ_L	lag time constant
χ	augmented state variable

Subscripts

ACT	actual
AS	area servo
a	actual
C	column
C	closed-loop
CS	vane servo
c	command
D	discrete
d	desired
d	discrete
f	final
HP	high power
i, j, k, l, m, n	indices
LP	low power
MV	metering value
m	model output

SYMBOLS (Continued)

m	measured
max	maximum
min	minimum
norm	normal
nom	nominal
OL	open-loop
o	initial value
o	nominal
PC	pump controller
R	row
RS	stator servo
r	reduced
r	index
S	static
SCH	scheduled
SM	stepper motor
SS	steady-state
SP	set point
STD	standard
s	index
s_i	i th output gain column
T	total
T	trim
+	right half plane
-	left half plane

Superscripts

T	transpose
-1	matrix inverse
•	time derivative
••	second time derivative

\wedge	estimate
+	right half plane
-	left half plane
-	modified matrix
-	logical not
*	scaled
*	modified
*	minimum
'	modified
°	degrees

Symbols

$ \cdot $	matrix norm
\approx	approximately equal to
\ll	much less than
ϵ	subset of
\cup	logical "and"
\cap	logical "or"
Σ	summation
$<$	less than
$>$	greater than
$!$	factorial
$\%$	per cent

Engine Station Numbers

0	ambient
2	engine face
2.5H	fan discharge - inner side
2.5C	fan discharge - outer side
3	compressor discharge
4	high pressure turbine entrance
4.5	low pressure turbine entrance
5	low pressure turbine exit
6C	duct discharge
6M	augmentor volume entrance
7M	augmentor discharge

CHAPTER I

INTRODUCTION AND SUMMARY

1.1 INTRODUCTION

Aircraft missions of the next decade and beyond are dictating the requirement for multimode integration of airframe and propulsion systems over wide operational envelopes. Aircraft engines have accordingly become more sophisticated in the evolutionary design process which must eventually meet these future requirements.

The provision for multimode propulsion response, without sacrificing efficiency or performance, is achievable by engines with variable geometry. Such engines are controlled by commanded internal geometrical changes. This capability is achieved at the expense of a significant increase in engine complexity, addition of actuators, and sensors. The subsequent control system requirement to maintain strict transient and steady-state performance specifications forces attention to more accurate and reliable controller implementations. Control synthesis techniques for such digital systems must therefore be developed and demonstrated to fill the need for accurate response, high reliability, and compatibility with state-of-the-art digital processing capability.

One potential control design technique for achieving these objectives is based on quadratic synthesis methods. These are usually identified as modern control, optimal control, linear-quadratic-Gaussian (LQG), or linear-quadratic-regulator (LQR) methods. They have undergone extensive theoretical development. The results have indicated that they can serve as the basis for a systematic, comprehensive procedure

to design practical multivariable digital controllers to satisfy complex engine performance requirements.

To evaluate the potential benefits of these multivariable design methods, the Air Force Aero-Propulsion Laboratory and the NASA Lewis Research Center have cooperatively sponsored a comprehensive research and development program of an advanced multivariable controller for the F100 turbofan engine.

The F100 Multivariable Control (MVC) program is designed to investigate the use of modern control theory as a design tool for advanced aircraft gas turbine engines. Specifically, linear quadratic regulator (LQR) theory is being investigated. The LQR techniques have been successfully used in the past and are well understood. From a performance standpoint, LQR methods result in a feedback controller and exploit the use of the loop interactions and cross-coupling effects of the engine in a constructive manner. The LQR control modes also can be designed to be insensitive to engine and sensor inaccuracies.

Although the test vehicle under this program is the Pratt & Whitney F100 engine, it should be noted that this program was designed to investigate the applicability of LQR theory and not to specifically design a controller for the F100 engine. This engine was chosen because: (1) detailed digital and analog/digital hybrid simulations of the F100 engine were available for detailed analysis, and (2) an actual F100 engine was available for testing at NASA LeRC. The F100 engine represents the current state-of-the-art in aircraft gas turbine technology. Although not as complex as some of the advanced cycles being proposed, it was felt that the F100 would be a worthy challenge for the LQR technique.

The program is distinctly different from previous efforts to evaluate LQR theory as a turbine engine design tool. The major issues involved were: (1) the capability to accomplish large power excursions without exceeding engine or actuator limits, (2) extending the controller authority to the entire

engine flight envelope, (3) including realistic nonlinear representations of the engine sensing and actuating components, and (4) including engine operating limits and constraints.

These issues are not new to the engine controls designer. Conventional loop-by-loop design methods must also contend with these problems. It should be noted that LQR techniques are set-point design methods and one cannot incorporate large transient criteria or control and plant constraints directly into the algorithm. LQR techniques form the basis of the controller but there is still a need for sound engineering judgment to make it work. The results of this program represent one of many possible solutions to the problem and are intended to stimulate the growth of ideas and discussion.

To accomplish these objectives, the AFAPL and NASA-LeRC contracted for the controller design to Systems Control, Inc. (Vt) and, for the F100 engine technology expertise, to Pratt & Whitney Aircraft Group, Government Products Division. The overall agency integration is illustrated in Figure 1.1.

1.2 SUMMARY

This report details the F100 multivariable controller design and the methodology used to develop that design. Although the report is as self-contained as possible, it primarily treats the controller design aspect of the program, with sufficient detail to provide both engine manufacturers and control agencies a comprehensive reference to the design process. Details of the engine modeling and control design criteria are given in Ref. 1. A comprehensive hybrid simulation evaluation of the controller performance is described in Ref. 2.

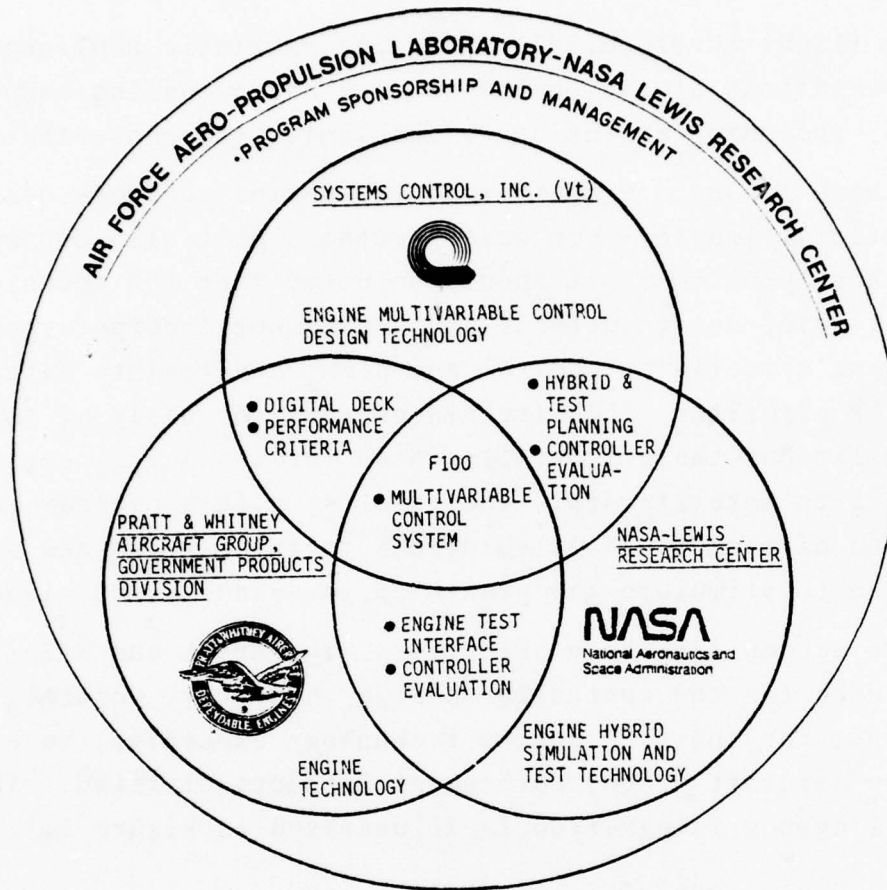


Figure 1.1 Management and Technical Integration -
F100 Multivariable Control System Program

This report is organized as follows:

- Chapter II, Fundamental Considerations Governing Engine Control Synthesis

This chapter is an overview of the background of previous engine control efforts and of the underlying dynamic, aerodynamic, and thermodynamic considerations upon which criteria for advanced engine controllers are based. A discussion is then presented which outlines essential elements of LQR design theory, stressing particular aspects which were used for the detailed F100 multivariable control (MVC) design.

- Chapter III, Linear Quadratic Regulator Synthesis Techniques

This chapter is a more detailed tutorial discussion of the theory and application of linear quadratic regulator control design methods. The method is shown to be highly automatable, if a rationale for engine mathematical modeling and performance index specifications is prescribed. The trade-offs in selecting integral controller structures are presented and the important issue of sensitivity of controller performance to modeling uncertainties is described.

- Chapter IV, Design Methodology for a Multivariable Controller

Various considerations must be evoked in producing a practical controller based on LQR techniques. In particular, the F100 engine is a highly complex nonlinear system. LQR methods address the control of small perturbations about specified operating points and on variable trajectories between the operating points. A practical engine controller must accommodate a diverse set of operating requirements, a broad flight envelope, a consequently wide variation in dynamic behavior, and a large set of measurements and controls. The application of LQR methods to such a system therefore requires a systematic procedure for engine modeling, scheduling gains, utilizing appropriate integral control options, and compensating for realistic sensor and actuator characteristics. This chapter discusses these considerations.

- Chapter V, A Multivariable Controller for the F100 Engine

The application of the design methodology described in Chapter IV to the F100 engine is detailed in this chapter. The controller is a highly modularized design, functionally containing the following elements: reference schedules, transition logic, integral control logic, gain scheduling logic, LQR gains, and sensor compensation. Development of each of these elements is presented in detail.

- Chapter VI, Evaluation of the F100 Multivariable Controller

The digital implementation performance of the controller is discussed in this chapter. In particular, discretization, desensitization to modeling errors, engine protection, and failure accommodation aspects

are examined. The hybrid evaluation is described and a summary of the digital and hybrid tests on the controller is presented.

- Chapter VII, Summary, Conclusions and Recommendations

This chapter reviews the controller design and design methodology. Significant issues identified in the evaluation phases are identified, and recommendations for future research and development are presented.

Each chapter of this report is intended to minimally depend on the material in the preceding or subsequent chapters. Chapter II is recommended for those interested in general turbine engine control considerations. For those interested in the theoretical foundations of the linear and nonlinear techniques used, Chapters III and IV should be addressed, respectively. Chapters V and VI are for those interested in the actual digital implementation and the results of the performance evaluations.

CHAPTER II

FUNDAMENTAL CONSIDERATIONS GOVERNING ENGINE CONTROL SYNTHESIS

The design of a multivariable controller for advanced engines requires simultaneous consideration of full flight envelope engine characteristics and state-of-the-art controller synthesis techniques. This chapter is an overview of how such a controller design methodology is approached, the significant engine modeling and controller requirements established, and the controller itself subsequently developed. As such, this chapter represents a summary of the background, objectives, methods, and performance evaluation criteria which are basic to the content of the subsequent chapters.

Section 2.1 summarizes the background of Government research and development objectives which led to this multivariable control synthesis program. Section 2.2 reviews the control requirements for advanced aircraft engines, which is followed, in Section 2.3, with a discussion of present controller design methods. Section 2.4 presents a short discussion of modern and classical control techniques. Section 2.5 presents an overview of multivariable LQR control design methodology in order to introduce Section 2.6, which summarizes applications of LQR techniques to aircraft gas turbine engines. Section 2.6 also extends the discussion of Sections 2.4 and 2.5 to the application of LQR methods to nonlinear systems. Section 2.7 presents the engine digital control implementation and test considerations.

2.1 BACKGROUND

The performance requirements of modern, high technology aircraft has placed severe demands on engine control capability. To provide this capability, advanced multivariable control synthesis methods, implemented digitally, are now the subject of intensive Government research and development [3]. Combining the basic analytical and test capabilities of NASA-LeRC and the applied operational engine flight and ground test capability of AFAPL, such joint efforts provide the technology to develop the advanced controls necessary to function in the rapidly expanding flight envelopes of present and future high performance aircraft.

A major example of this on-going development was the Integrated Propulsion Control System (IPCS) [4-7]. The objective of this program was the design and flight test of integrated operation of propulsion and inlet controls to eliminate adverse effects due to engine/inlet couplings. The final report on the F111E implementation and test phase of the IPCS program is given in Ref. 7.

Such an applications effort is based on extensive analysis and test programs being actively pursued at AFAPL and NASA-LeRC. Bentz [3], for example, discusses the specific role of computers in advanced propulsion systems, an active control system research program at AFAPL. Related AFAPL programs are directed toward sensor/interface/effector technology and system hardware technology. Advanced analytical hardware and test programs are also being accomplished at NASA-LeRC. In particular, notable effort in a digital computer propulsion control facility [8-12] has been achieved, and some of the most advanced inlet control analyses [13-16] (including optimal control theory [17]) and digital implementation of fuel control functions [18,19], have been performed at NASA-LeRC.

From the above programs, a number of significant conclusions concerning the development of advanced engine system controllers have been reached. Some of the most important of these, which are also relevant to this design program, are identified by Bentz and Zeller for the IPCS [4] and include the following:

- (1) Dynamic nonlinear engine simulations are necessary for the effective design and test of engine control systems.
- (2) The engine manufacturer should have the major responsibility for the simulation, which can also be used by the control manufacturer.
- (3) A significant step in the integration of the engine and airframe as well as for improving engine state performance and transient stability, is the development of an advanced engine controller. In particular, varying engine response to the environmental and operational requirements should be achieved by control regulation of each engine activation mechanism simultaneously.
- (4) One method of achieving such controller design is through optimal control techniques, as well as advanced "classical" control techniques.

In summary, the requirement for more precise engine control arises not only from the need for improved full flight envelope engine response, but also from the requirement to better integrate the engine with inlet and airframe controls [20-23]. These objectives must be based, however, on a high performance engine control regulator which will allow such integration. Such a control, because of the complexity of the engine processes, must couple many loops, and this can be most efficiently accomplished by use of multivariable design techniques, as opposed to design on a loop-by-loop basis. This fact has been demonstrated (analytically and operationally) in both aerodynamical and marine technologies [24-26].

2.2 A SUMMARY OF CONTROL REQUIREMENTS FOR ADVANCED AIRCRAFT ENGINES

In this section, the control requirements for advanced aircraft engines are reviewed. Basically, these requirements [27] state that the engines must exhibit desired transient and steady-state responses while remaining within safe margins of engine thermal, aerodynamic, and mechanical limits. In the following subsections, these and other requirements are reviewed.

2.2.1 General Control Requirements

Control requirements applied to gas turbine engines consist of ensuring safe, stable engine operation. Specific engine performance rating points are generally defined as basic steady-state design goals for the control. In addition to providing the regulation of engine operation required to meet the steady-state performance specified, the control must constrain the operation within the various aerodynamic, thermodynamic and mechanical design limits of the engine. Typical aerodynamic limits include fan and compressor stability, maximum allowable engine inlet airflow distortion, and turbulence. Thermodynamic limits include minimum main burner or augmentor fuel/air ratios for stable combustion, minimum fuel flow for ignition and maximum fuel/air ratios. Mechanical and structural limitations include maximum allowable rotor speeds, maximum allowable nozzle flap temperatures, maximum burner case pressure, rotor creep limits, and maximum average and peak values of turbine blade metal temperature.

The advent of additional performance requirements for today's supersonic fighter aircraft has amplified these basic limitations. Specifying aircraft performance capabilities

such as thrust to weight ratios of 1.0, high maneuverability, supersonic dash capabilities, efficient subsonic cruise and fast/stable power excursion, tend to broaden the steady-state engine rating requirements, and consequently, the control regulatory responsibility. Implicitly, these requirements also introduce a multitude of interactive and complicated control and engine operating problems.

Steady-state performance rating points at sea level static and altitude are specified in "General Specification for Turbojet and Turbofan Engines" (MIL-E-5007D) [27]. These specifications include engine power level rating points from idle to intermediate non-augmented, as well as minimum and maximum augmented, rating points.

Transient engine response characteristics are also specified in Ref. 27. No overspeed or overtemperature beyond stated transient limits and no main burner, augmentor, fan or compressor instability is acceptable for any power lever movement. Thrust response to these power lever movements is expressed as the time required to achieve 90 per cent of the thrust change. These requirements are discussed in detail in Ref. 1.

All of these specific steady-state and transient requirements must be satisfactorily demonstrated on any new control/engine design.

2.2.2 Steady-State and Transient Operating Requirements Leading to Control Requirements

A typical mixed stream, augmented turbofan engine as shown in Figure 2.1 may incorporate, in addition to main burner fuel flow and augmentor fuel flow, variable fan and compressor geometry, compressor bleeds, and variable exhaust nozzle geometry.

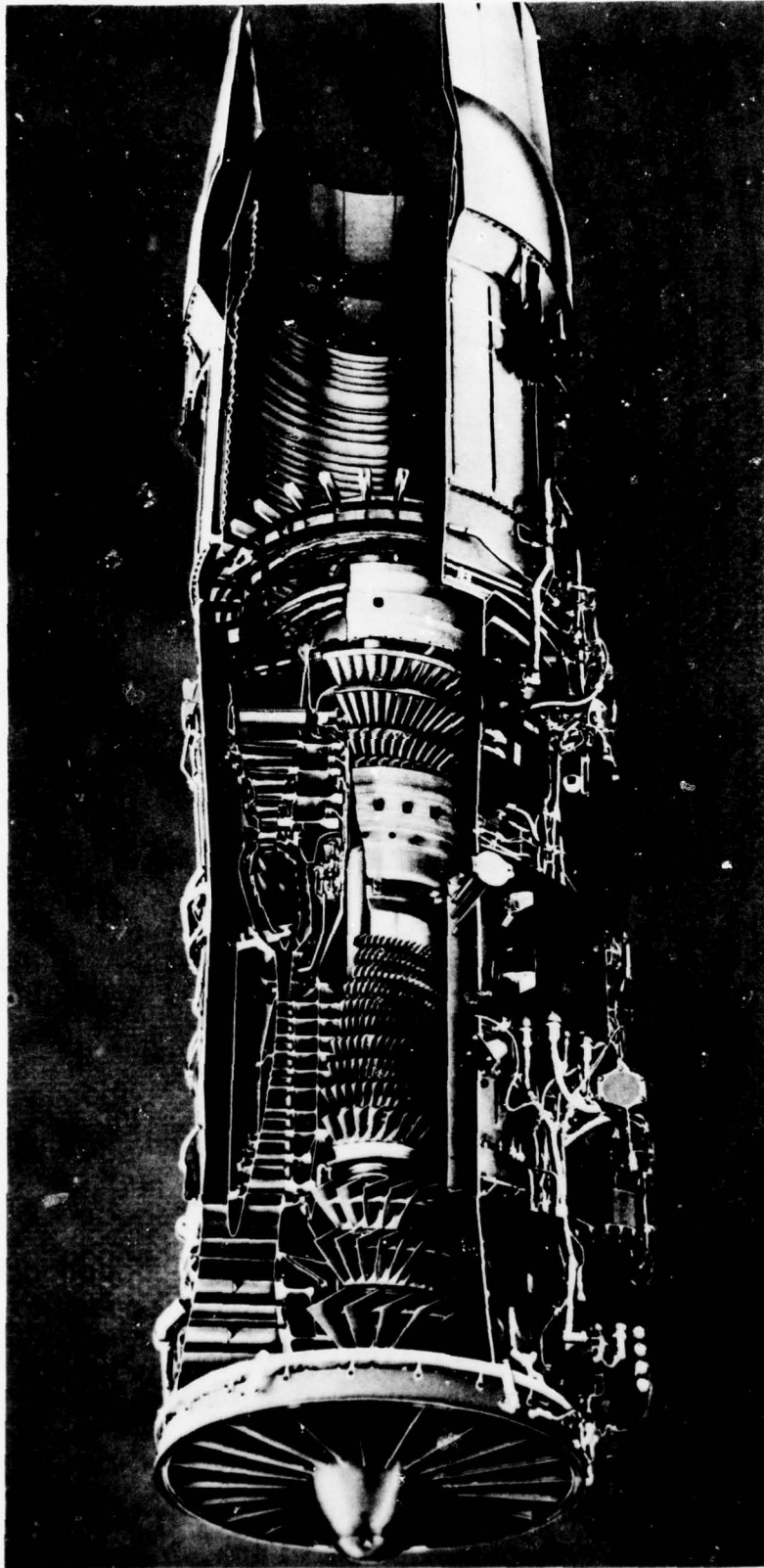


Figure 2.1 Typical Mixed Flow/Augmented Turbofan Engine

Significance of Envelope Flight Conditions

Specific flight conditions representative of engine operating requirements are the starting point for design. These conditions can be plotted as a function of Mach number and altitude as shown in Figure 2.2 to form the engine operating envelope. This illustration can then be used to deduce the general operational constraints indicated by the flight conditions. As shown on the figure, the basic flight envelope constraints are: maximum engine inlet pressure (P_{T2}) limit derived from burner case (P_B) structural limits and dynamic pressure blade loading considerations in the fan and compressor;

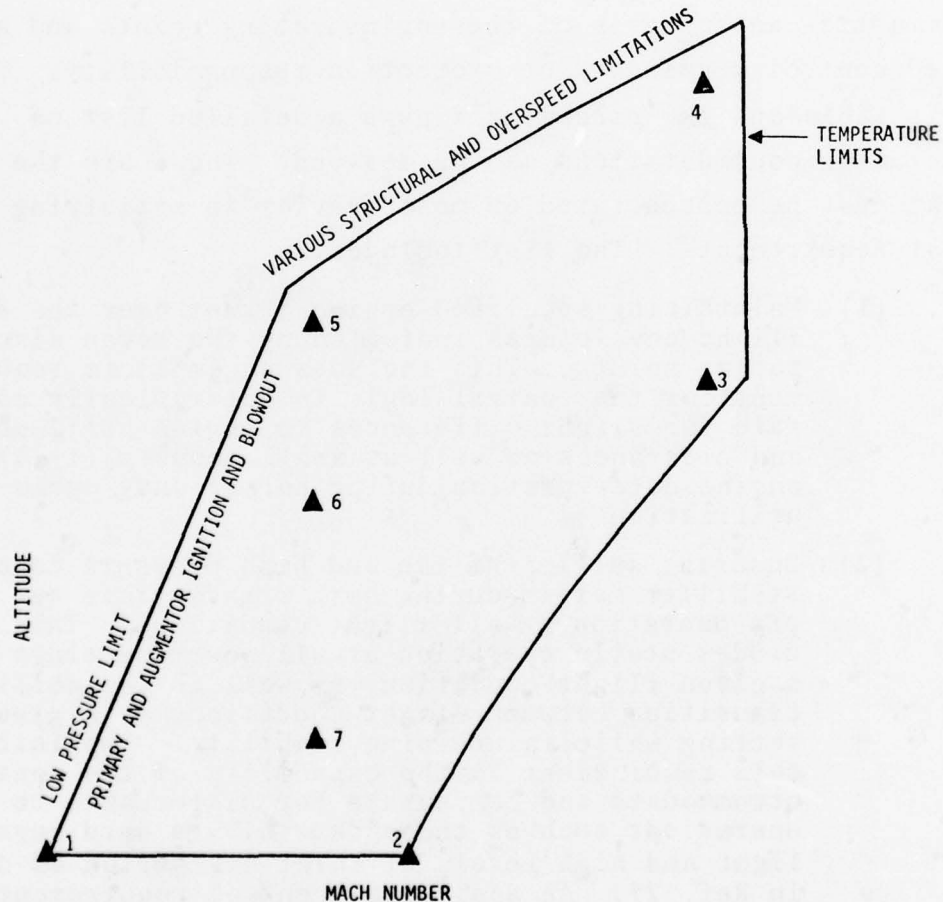


Figure 2.2 Typical Engine Operating Limitations

maximum engine inlet total temperature (T_{T2}) limit derived from the basic metal fatigue considerations throughout the engine but primarily at the high turbine inlet (T_{T4}) and on the nozzle flaps (T_{T7}) for augmented operations; and minimum P_{T2} derived from the minimum pressure requirements necessary to achieve stable combustion in the main burner and the augmentor or afterburner.

In addition to these basic engine operational limitations, each of the engine operating conditions, shown as points 1-7 on Figure 2.2, can be analyzed for specific steady-state and transient performance implications as well as for other implicit structural or mechanical constraints. Table 2.1 summarizes an analysis of the engine rating points and associated control regulatory or protection responsibility. From this table and the preceding figure a detailed list of operating considerations can be derived. These are the areas that must be concentrated on most heavily in satisfying control requirements. The list includes:

- (1) Maintaining specified engine thrust over the entire flight envelope as indicated by the seven discrete rating points. This includes an implicit requirement for the control logic to automatically compensate for slight differences in engine build-up areas and clearances as well as small amounts (1-2%) of engine deterioration during normal duty cycle utilization.
- (2) Ensuring sufficient fan and high pressure compressor stability margin during both steady-state and transient operation at all flight conditions. This includes stable operation at all power settings for a given flight condition, as well as the ability to transition between flight conditions at a given power setting while maintaining stability. Implicit in this requirement is the capability of the control to accommodate and compensate for disturbance to engine operations such as those caused by a hard augmentor light and high levels of inlet distortion as defined in Ref. 27. An additional control requirement is to compensate for degradation in stability (surge margin)

Table 2.1
Typical Engine Evaluation Points and Associated
Operational Considerations

POINT NO.	FLIGHT CONDITION	SIGNIFICANCE
1	Sea Level Take Off (SLTO)	Maximum non-augmented (intermediate) thrust and maximum augmented thrust rating points (T_{T4} , stability, thrust primary importance).
2	Sea Level Ram	Burner case pressure limit as well as extremely high fan and compressor blade and vane loading along this boundary. Structural and vibratory stress problems. Fan and compressor speed limits may be reached here.
3	Supersonic Dash	High steady state inlet distortion and subsequent reduced stability margin. Also, hard augmentor light off and/or blow out affects stability. Possible inlet disturbance due to popping or swallowing the inlet shock waves during maneuvers.
4	Extreme Flight Envelope Definition	Control gains must satisfy performance, stability, and safety limits. Also distortion and augmentor light problems as in 3. In addition, may reach or exceed fan and compressor speed limits.
5	Low Pressure Limited Flight Condition	Ignition limits for both main burner and augmentor occur along this boundary. Flame out and ignition problems typical. Augmentor flame holder ΔP too small to maintain combustion stability.
6	Subsonic Cruise and Combat Maneuvering Condition	Thrust Specific Fuel Consumption and therefore fuel flow and F/A ratio important. Transient engine response characteristics during combat mission. Also severe transient inlet distortion due to aircraft attitude changes.
7	NASA Test Capability (Also same as 6, i.e., air superiority rating and subsonic cruise)	Thrust Specific Fuel Consumption and therefore fuel flow and F/A ratio important. Transient engine response characteristics during combat mission. Also severe transient inlet distortion due to aircraft attitude changes.

due to Reynolds number effects at some flight conditions.

- (3) Maintaining acceptable operation within the physical constraints of maximum turbine blade temperature limits. This includes steady-state scheduling as well as ensuring the limits on turbine inlet temperature or temperature rates are not exceeded during start-up transients, acceleration or deceleration power level excursions.

Analysis of the engine performance evaluation points can be very useful in the development of steady-state and transient control requirements. Performance output measures associated with each of the evaluation points can be used to define

Table 2.2
Performance Output Measures

POINT NO.	FLIGHT CONDITION	PRIMARY CONTROL CONSTRAINTS
1	Sea Level Take Off	Thrust, overtemperature, stability (fan and compressor)
2	Sea Level Ram	Thrust, transient response (acceleration), overtemperature, stability, burner case pressure
3	Supersonic Dash	Thrust, overtemperature, transient response distortion tolerance, stability, hard augmentor lights, augmentation
4	Extreme Flight Envelope Definition	Thrust, overtemperature, transient response distortion tolerance, stability, hard augmentor lights, control gain scaling point
5	Low Pressure Limited Flight Condition	Thrust, temperature rate limits, blow out starting
6	Subsonic Cruise and Combat Maneuvering Condition	Thrust, fuel consumption, overtemperature, stability transient response
7	NASA Test Capability (Also same as 6, i.e., air superiority rating and subsonic cruise)	Thrust, fuel consumption, overtemperature, stability transient response

the operational limits imposed on the control design. Table 2.2 shows that thrust is the primary steady-state performance measure at all the flight envelope points. In addition, the table shows that turbine temperature limits, stability, and transient response are also common considerations at all of these engine rating points. The remaining engine operating points associated with the specified flight conditions are primarily associated with augmentor control and starting. In addition, Table 2.2 lists specific items which affect stability such as augmentor blow out or inlet distortion, all of which can be covered under the present general discussion of steady-state and transient operating requirements.

Use of Performance Maps for Determining Stability Requirements at Various Operating Points

Figure 2.3 is an illustration of a typical fan performance plot showing a steady-state operating line, the general location of some engine flight conditions of interest and the effects of jet area variations on a steady-state operating point. A qualitative definition of stability margin is how close the fan or compressor is operating to the surge line.

Keeping the definition of stability margin in mind and examining the performance points plotted on Figure 2.3, the

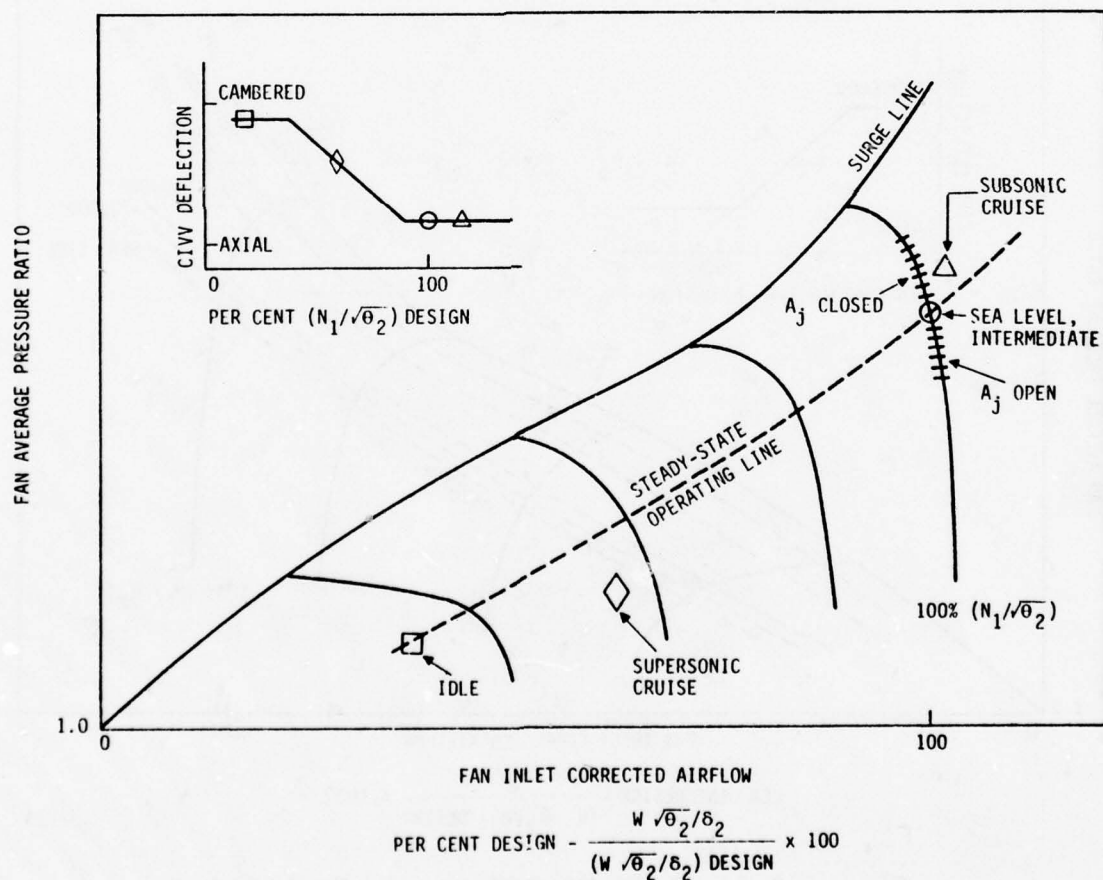


Figure 2.3 Typical Fan Map

next logical consideration is: What type of disturbances generally cause degradation of stability? At steady-state conditions, a loss of stability margin occurs during operation at altitude. Under normal conditions, the sea level steady-state fan and compressor operating lines move up and the surge line moves down with increasing altitude as a result of Reynolds number effects. Figure 2.4 illustrates the degradation in fan stability margin at 30,000 and 60,000 ft due to these effects. A high compressor map would show similar effects in operating and surge lines due to Reynolds number.

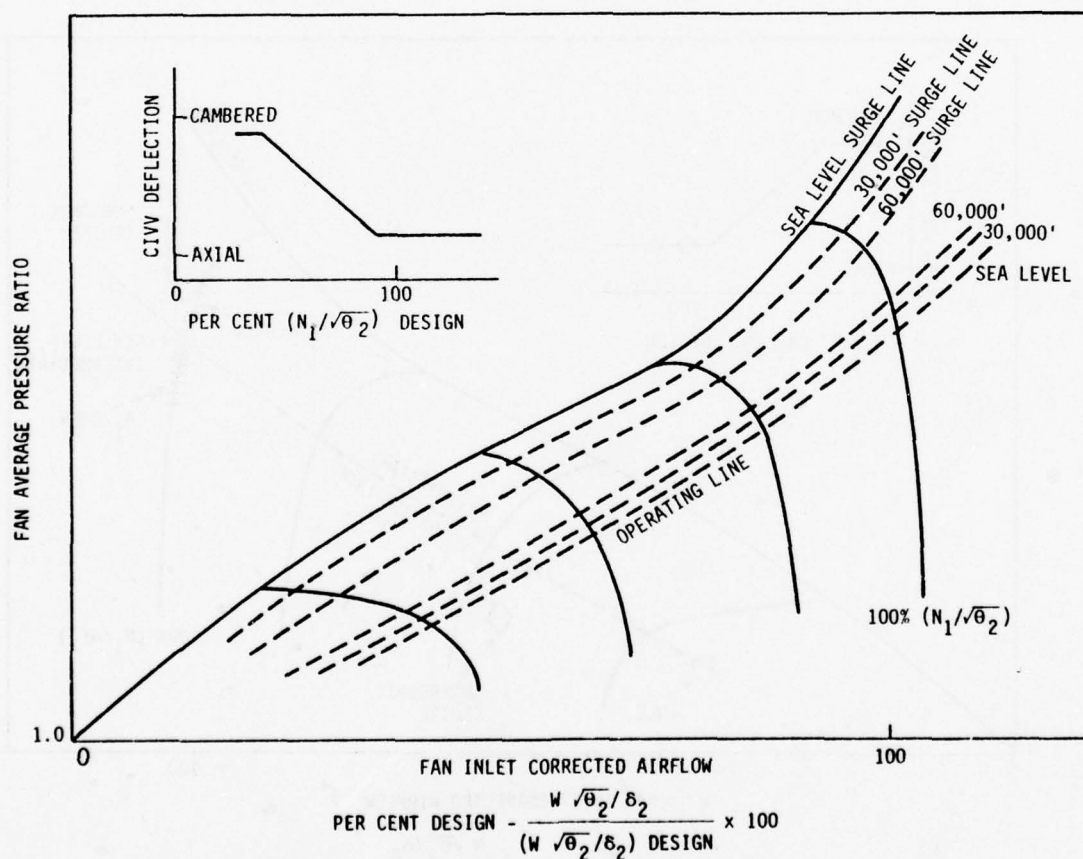


Figure 2.4 Altitude Effects on Stability

Similar destabilizing effects result from transient engine operations (power level excursions) from idle or part power to intermediate or maximum thrust. Figures 2.5 and 2.6 show the fan and compressor steady-state operating lines with typical acceleration and deceleration lines which these components follow as the engine power level is changed. It should be noted that deceleration leads to loss of stability margin on the fan while acceleration leads to loss of compressor stability margin. These general trends assume normal scheduling of the fan and compressor variable geometry as well as the exhaust nozzle exit area.

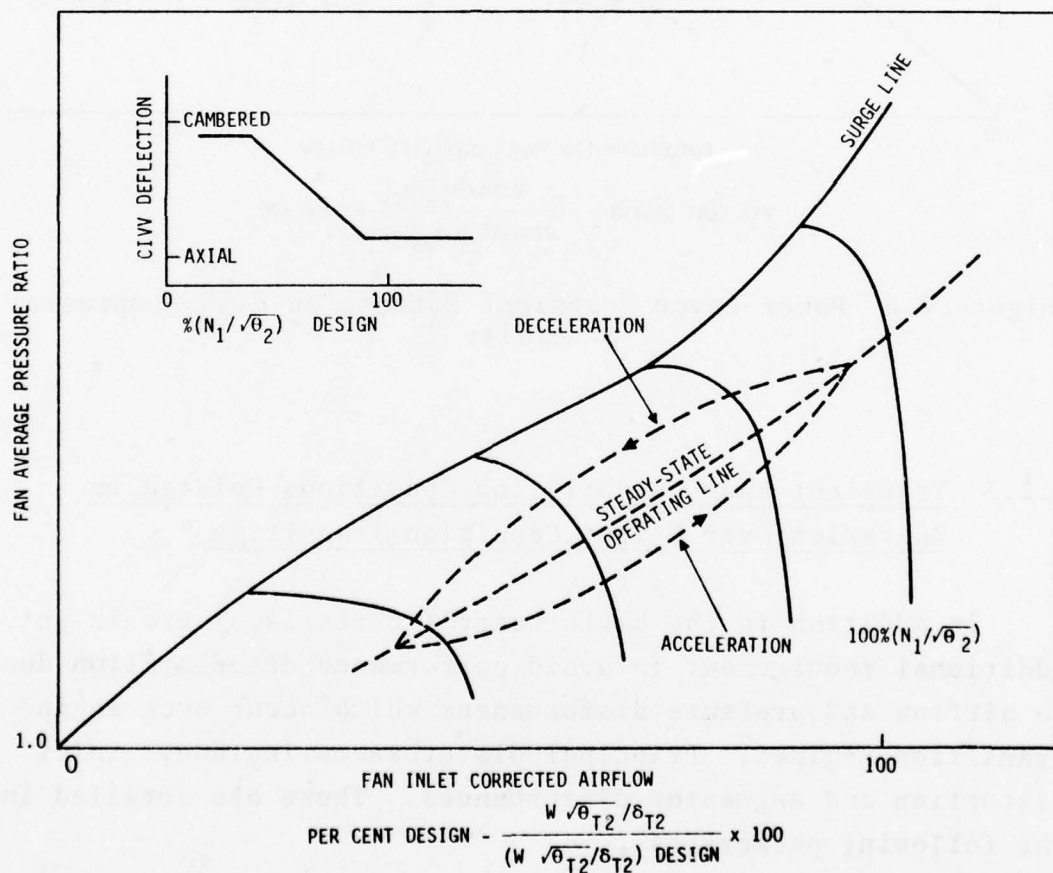


Figure 2.5 Power Lever Transient Effects on Fan Stability

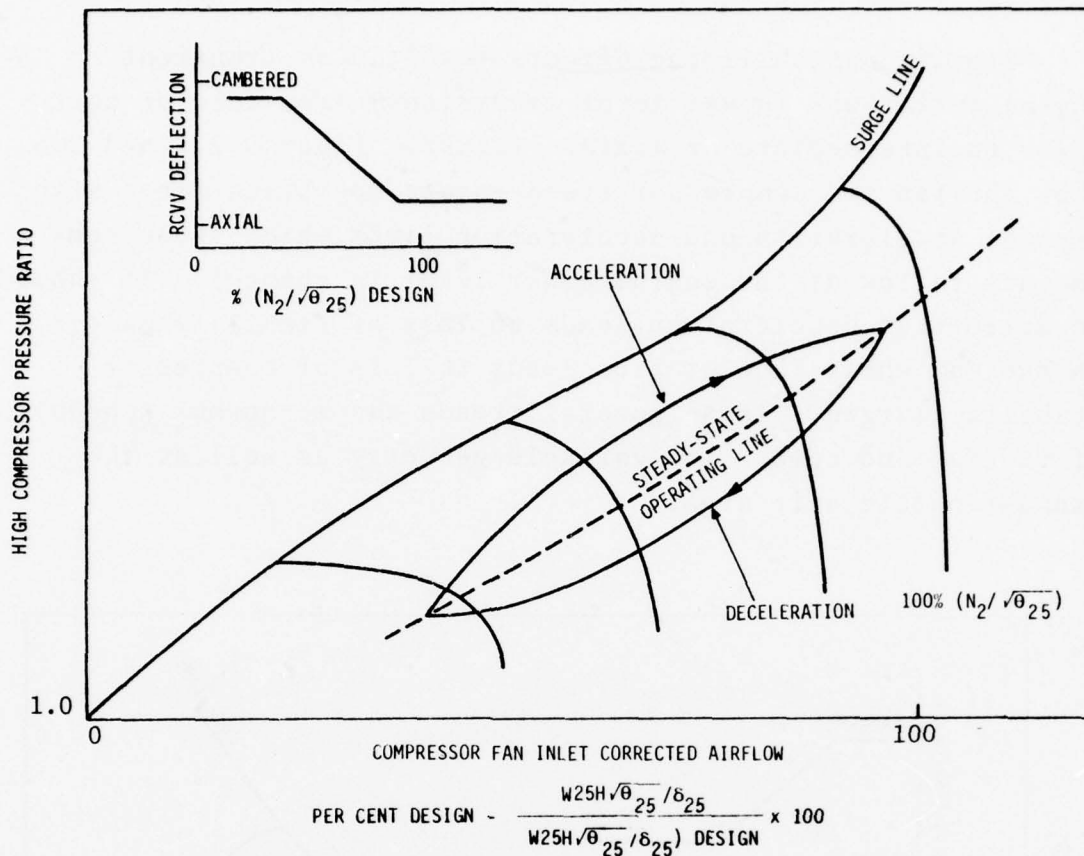


Figure 2.6 Power Lever Transient Effects on High Compressor Stability

2.2.3 Transient and Destabilizing Conditions Related to Operation Over Flight Condition Transition

In addition to the basic control criteria, there is an additional requirement to avoid performance deterioration due to airflow and pressure disturbances which occur over engine transition regimes. Principal disturbances include: inlet distortion and augmentor disturbances. These are detailed in the following paragraphs.

Distortion Effects on Stability

What really establishes the acceptability of a fighter inlet is its ability to supply uniform, undistorted airflow to the engine. Pressure recovery, circumferential inlet distortion, and inlet turbulence (time variant inlet distortion) define the quality of the inlet air. Pressure recovery is an average of all total pressures across the flow area. Distortion is the pressure recovery pattern and describes local peaks and valleys in terms of location and magnitude as shown in Figure 2.7. Turbulence is a dynamic characteristic which

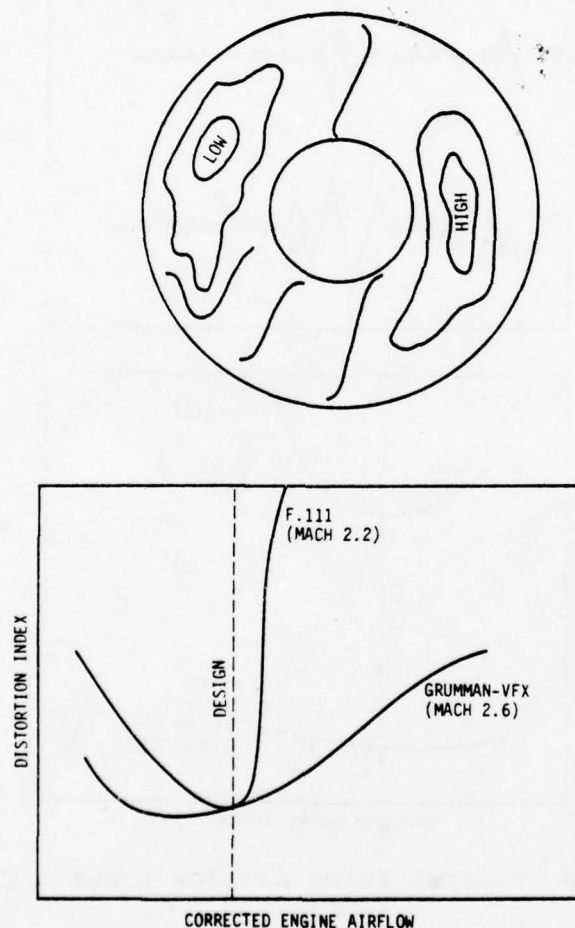


Figure 2.7 Typical Steady-State Inlet Airflow Total Pressure Distortion

indicates how certain areas of the distortion pattern are changing with time (Figure 2.8). Both distortion and turbulence will influence engine airflow, thrust and fuel consumption when certain high levels are reached, but their most pronounced effect is on engine operation in the form of decreased stability (or surge) which could occur in engine transition. For example, aircraft maneuvers such as high speed pull ups can severely distort the engine inlet airflow pattern

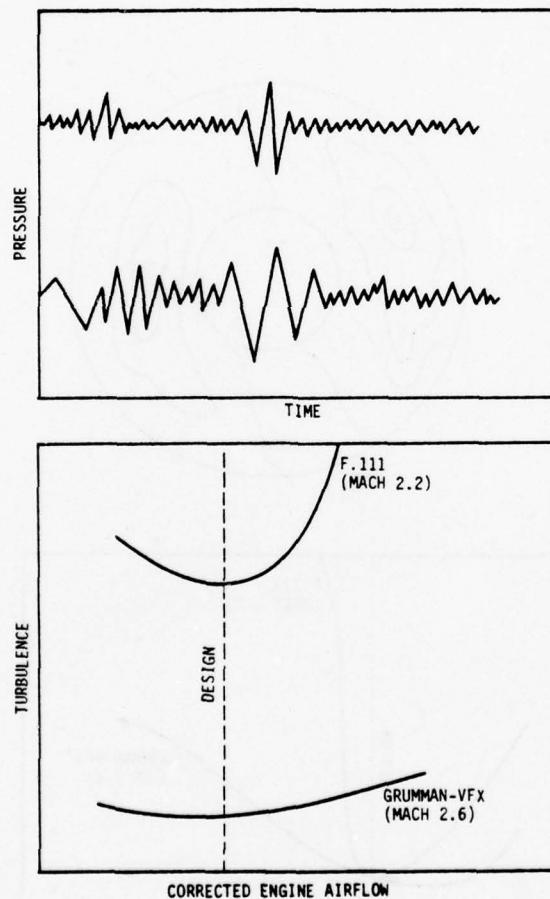


Figure 2.8 Typical Inlet Airflow Dynamic Pressure Variation

and create large areas or cells of low pressure, which can drive the engine into surge.

Augmentor Effects on Stability

The other primary engine component which directly affects stability is the augmentor. The turbofan has a flow path directly from the afterburner section to the fan discharge via the fan duct. Combustion disturbances, such as hard light-offs or blow-outs, cause rapid changes in fan back pressure which decreases stability margin (see Figure 2.3). Many things could then happen through a chain of events. If the fan stalls from back pressure, compressor flow may be distorted and lead to stall in the rear high pressure stages. This chokes up the compressor and produces a full engine stall.

It is obvious that these interactions must be anticipated and compensated in any suitable engine control scheme which is to accommodate augmented operation. Multivariable control theory is ideally suited to provide the necessary closed-loop compensation logic given the proper sensors are available with the necessary response and accuracy characteristics. For example, previous research on a non-mixed augmented turbofan [28,29] has shown the acceptability of fan exit and high compressor exit Mach number correlations as a stability indicator. This type of control input requires total and static or total and ΔP measurements.

2.3 ENGINE CONTROL DESIGN METHODS

The complexity of the requirements discussed in Section 2.2 introduces a formidable challenge to the control engineer. In this section, the present control methods as well as some advanced multivariable control synthesis (non-LQR) results are reviewed.

2.3.1 Approaches to Existing Operational Engine Control Systems

Classical linear control theory applied to gas turbine engines consists of developing the control logic required for safe, stable engine performance [30]. Current control design techniques concentrate on providing the required engine performance within the constraints imposed by these limitations. Early fuel controls regulated rotor speed scheduled as a function of ambient variables and throttle input [31]. The regulator provided full envelope performance with scheduled output limits for transient engine regulation. However, as engine performance requirements become more and more demanding, extremely complex hydromechanical implementations are required. The structure of those controls utilize the basic governor scheme with an electronic or hydromechanical trim computer to provide fine adjustment to the engine operating point to obtain rated performance (Figure 2.9).

Control schedules are generated to satisfy the performance ratings. Control loop interactions are resolved through trial-and-error modifications of the derived steady-state schedule control loop gains. Similarly, the operational limits are satisfied by an iterative modification of the schedules to avoid the undesirable aerodynamic, thermodynamic, or mechanical limits encountered. The desired engine response characteristics are achieved by modifying actuator limiting schedules where necessary to improve acceleration or deceleration characteristics. Finally, ground trim capability is provided on the current controls to compensate for engine-to-engine build tolerances and to provide uptrimming capabilities as performance deteriorates on a particular engine due to normal engine life-cycle wear. In summary, the current approach to control development concentrates on regulating the engine steady-state

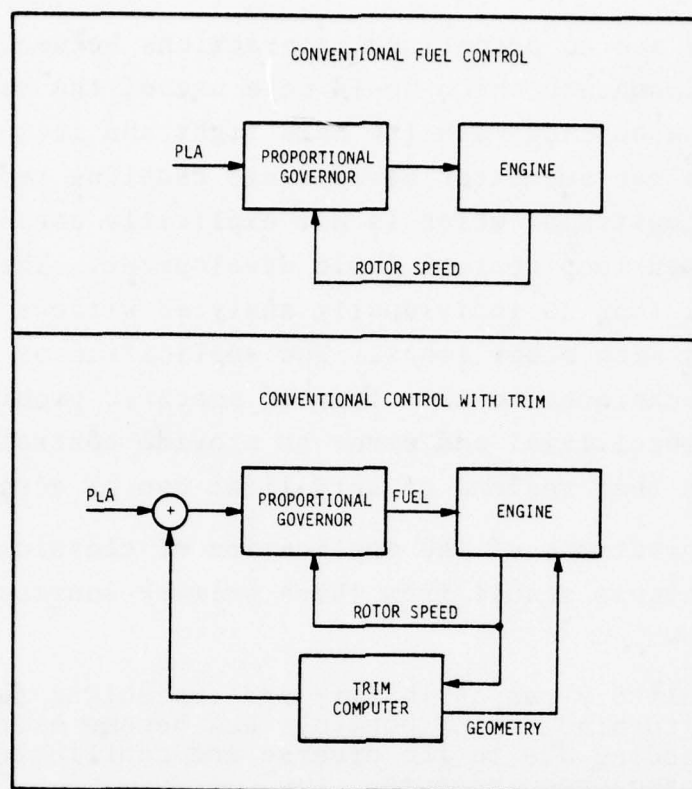


Figure 2.9 Conventional Control Structures Using Hydromechanical Implementation

performance as required while protecting the engine from encountering the operational limitations.

Although this classical approach to control design, control logic specification and control development has been in use for many years, certain inherent limitations exist in the technique. Engineering experience and intuition are required to solve control/engine interaction problems. The additional high performance requirements of supersonic aircraft vastly increase the magnitude, duration and scope of the "classical" solutions to control logic development.

Although current control design techniques could incorporate a sensed augmentor pressure to indicate the hard augmentor

light, there are no predefined interactions between fan and augmentor components which could make use of the sensed pressure pulse associated with the hard light and incipient fan surge. Such fan-augmentor aerodynamic coupling represents a real world constraint which is not explicitly considered in classical open-loop control logic development. This is because each control loop is individually analyzed without regard to interactions with other loops. The application of these classical techniques to this type of specific problem introduces additional trial and error to provide control schedule biasing such that regions of hard light can be accommodated.

The limitations of the application of classical control design techniques result from three primary sources. These are as follows:

- Regulatory responsibility and scheduling function of gas turbine engine controls has become extremely demanding due to the diverse and conflicting performance requirements.
- Protection of engine operating limits throughout the entire flight envelope for the range of missions typical of current generation air superiority aircraft becomes a greatly expanded trial-and-error process due to the cross-coupling effects and the associated compensatory logic. This process presents difficult problems due to conflicting performance and durability (temperature or pressure limits) or performance and stability (fan or compressor) trade-offs. Since it is a physical impossibility to test the control logic at all steady-state points within the flight envelope, it becomes a matter of engineering experience and intuition as to when the operational limitations have been sufficiently investigated.
- The resolution of specific control/engine, engine/augmentor or interactive engine component problem areas using the classical logic and simply adjusting steady-state schedules is not general enough an approach. Each particular problem is not foreseeable and the current techniques do not allow for sensor, component, actuator cross-coupling applicable to general, aerodynamic, thermodynamic, or mechanical interactions.

The previous discussion defined, in general terms, how current gas turbine control logic is developed and implemented. It presented a detailed discussion of known problems resulting from the limitations of classical control theory. What are the advantages of the current techniques? There are three primary advantages which are a direct result of the empirical approach to control logic design:

- (1) Although the iterative approach, using classical control analysis techniques and requiring a significant level of engineering judgment, is tedious and inefficient, the resulting control mode has proven to be realistic and capable of operating the gas turbine engine to the desired steady-state performance specifications.
- (2) The resulting control modes and schedules for low order systems have been physically simple enough to construct using hydromechanical and electromechanical techniques.
- (3) The practicality, reliability and acceptability of controls using the classical techniques have been demonstrated on a generation of gas turbine engines of various cycles for diverse applications from military reconnaissance/turbojet and air superiority/turbofan applications to the three spool cycle of the commercial transports.

The success of a given engine component design has never been used as a reason for halting advanced aerodynamic, thermodynamic or mechanical research. Similarly, the relative acceptability of classical control logic optimization techniques has not halted the basic study of control theory. Rather, the types of limitations discussed for the current gas turbine controls have led to the investigation of multi-variable (multi-input/multi-output) control techniques as a possible solution.

2.3.2 Multivariable Design Methods

Multivariable control theory can be used to resolve specific transient and steady-state operational limit problems by providing cross-coupling and decoupling logic which provides satisfactory transient response while maintaining all operational limits and providing specified steady-state performance (see Table 2.3). In addition to the interdependent control logic approach which inherently provides this cross-coupling capability, multivariable control theory employs sensed information in the compensation loops and provides variable gains where necessary to null out errors between scheduled and sensed variables at the desired steady-state engine operating points. In this manner, multivariable control theory can allow non-steady-state engine operation to be totally different

Table 2.3
Comparison of Modern Vs. Classical Design Methods

	ADVANTAGES	DISADVANTAGES
CLASSICAL CONTROL	<ul style="list-style-type: none">(1) Provides basis for engineering design decisions and evaluation (for low-order systems).(2) Inherent use of stability margin (e.g., gain and phase margins) to reduce controlled sensitivity to uncertainties in system parameters.(3) Best for single-input/single-output system.	<ul style="list-style-type: none">(1) Much trial-and-error in design, particularly for large systems such as engines.(2) Frequently leads to controls fighting each other.(3) Difficult to apply to multi-input/multi-output systems.
MODERN CONTROL	<ul style="list-style-type: none">(1) Leads to automatic synthesis of controls once performance index and model have been determined.(2) Designs are inherently minimally sensitive if proper P.I. is chosen.(3) Automatically includes optimum control and state cross-coupling.	<ul style="list-style-type: none">(1) Places more emphasis on correctness of model used for design (e.g., if model is in error, controlled system could be unstable) and relevance of performance index.(2) Many applications place too much confidence on automatic LQR methods to replace knowledge of system and model accuracy

from steady-state scheduled operations while maintaining accurate reference values for controlled engine variables. This technique allows for essentially independent, but compatible, steady-state and transient engine control such that closed-loop power and match point settings can be attained throughout the flight envelope without constraining the dynamic engine characteristics between power settings or between flight envelope points to the same set of empirically derived control schedules.

Two possible structures are shown for a full authority multivariable controller. Choice of the structure will be discussed below.

2.4 MULTIVARIABLE CONTROL DESIGN METHODOLOGY

The previous two sections have traced the development of controllers for advanced engines from highly complex control requirements through various "trial-and-error" control designs, including a recent design which includes many multivariable characteristics (e.g., LQR methods) [32,33]. It is concluded that a multivariable design method is necessary which has the following basic objectives:

- (1) The controller makes maximum use of the variable geometry capabilities of the engine.
- (2) The controller should not limit the performance capability of the engine by cross-coupling controls in such a way that controls are "fighting each other."
- (3) The design procedure should be systematic and place engineering judgment at certain critical points, not over the entire continuous spectrum of design development.

The basic controls research of the last three decades has produced a firm foundation for the synthesis of multivariable control systems. Application of this theory, principally in the aeronautical and marine technologies, has provided simple and effective multivariable designs.

2.4.1 Modern and Classical Control

The objective of control design is to determine a set of feedback, and possibly feedforward, gains which provide a system with desired response characteristics. Such desired characteristics include stability, frequency, damping, decoupling, and minimum error in following a specific command. This short section discusses the two main types of control synthesis which have been applied to various engine systems. These are denoted as classical control and modern control.

2.4.2 Classical Control Synthesis

Over forty years of successful control system designs have been achieved by what is now called classical synthesis. This approach is based on analysis of the transfer function representation of the system (e.g., the frequency domain relationship between input and output).

Examples of design techniques which have been used are the root locus method, the Nyquist method, and the Bode method (a derivative of the Nyquist method). The basic design approach is to analyze the transfer function with respect to desired system characteristics (e.g., gain and phase margin, transient response) and introduce compensating lead or lag filters to modify the response to that desired.

The compensators can provide lead or lag and may introduce a pure integral effect to eliminate steady-state errors from step inputs. Sufficient stability margin is provided such that small errors in the design parameter values do not affect the stability of the system. All modes can be made adequately fast and well damped within design requirements. These methods were originally devised for single-input, single-output systems and are difficult to use with multi-input, multi-output systems.

To resolve the difficulties of application of multi-input/multi-output classical methods, considerable research has been performed. One such notable attempt was performed in England for application to the Concorde jet engine. This work, by MacFarland, et al., was an extensive development and application of the inverse Nyquist method [34,35].

2.4.3 Modern Control Synthesis Methods

Modern control design methods have their basis in the state space representation of dynamic systems. The state space approach leads naturally to the description of both linear and nonlinear systems in time domain. The control inputs may be chosen to minimize a certain criterion function. This criterion function is a quantitative measure of the penalty for undesirable state response and the control input effort required (quadratic synthesis methods). For a general nonlinear system and criterion function, the control law may be very complicated. Alternately, the control may be selected by specifying the desired transient response characteristics of a system, and using algebraic synthesis techniques to solve for the required gains (e.g., pole placement methods, modal control methods, etc.).

In modern control synthesis development, linear systems have received special attention because they often lead to control laws which are both simple to design and easy to implement. The state, x , of a lumped parameter linear model follows the equation

$$\begin{aligned}\dot{x} &= Fx + Gu \\ 0 &\leq t \leq t_f \\ x(0) &= x_0\end{aligned}\tag{2.1}$$

where u is the control vector. Two basic methods have been used to determine control laws for such systems. The first approach, called the pole placement method, selects control gains to give adequate damping and speeds to the modes of the closed-loop system. In the second, control laws are determined to minimize certain criterion functions (e.g., LQR designs). These methods are now summarized.

Pole Placement Technique

If the control input is a fixed linear function of the state vector, i.e.,

$$u(t) = C x(t) \quad (2.2)$$

then the dynamics of the closed-loop system are

$$\dot{x} = (F + GC)x \quad (2.3)$$

It is clearly seen that the nature of the response is dependent on $(F + GC)$. The eigenvalues of $(F + GC)$ give the frequencies and dampings of various modes of the system, while the corresponding eigenvectors give the mode shapes. In the pole placement technique, the gain matrix C is selected so that all modes of the system have desired frequency and damping (this is always possible if the system is completely controllable). The solution is not unique for the multi-input case.

The solution is often unacceptable because the control law may not make economical use of various inputs (two inputs may be fighting each other). This disadvantage is particularly significant for the engine problem where many controls are available.

Linear Quadratic Design Techniques

A major control theory development occurred during the late 1950's and 1960's which was fostered by high-speed computers and an advanced technology space program. Now known under various names (quadratic synthesis, linear-quadratic Gaussian synthesis, modern optimal control theory, linear quadratic regulator theory), this development has been the subject of intensive theoretical research. Theoretically, it is known that optimal control has great potential since it is inherently a multi-input/multi-output linear system control design method also applicable to nonlinear systems. Much of the demonstration of the versatility of the method, however, has been limited to simulation studies, and the applications through actual implementation are not nearly as extensive.

The details of linear quadratic regulator (LQR) control theory design procedures are shown in Figure 2.10. At this point, it is only necessary to note the following:

- (1) Quadratic synthesis techniques design on a different objective than classical techniques. Instead of attempting to obtain a specific transient response (as do classical methods), LQR methods minimize the control energy required to keep the mean square response of the system as small as possible. The design parameters are weightings or penalties on deviations of states and controls (as well as the choice of augmented states and controls). Desirable transient response is obtained indirectly.
- (2) Quadratic synthesis techniques are highly automatic once the performance index and the design model have been selected.
- (3) Quadratic controls can produce simple control systems if the design process is conducted with an integrated understanding of the system physics. This is because many of the simplifications to an "optimal controller" can be based on certain types of analysis of the feedback structure and relating this structure to its actual effect on the system.

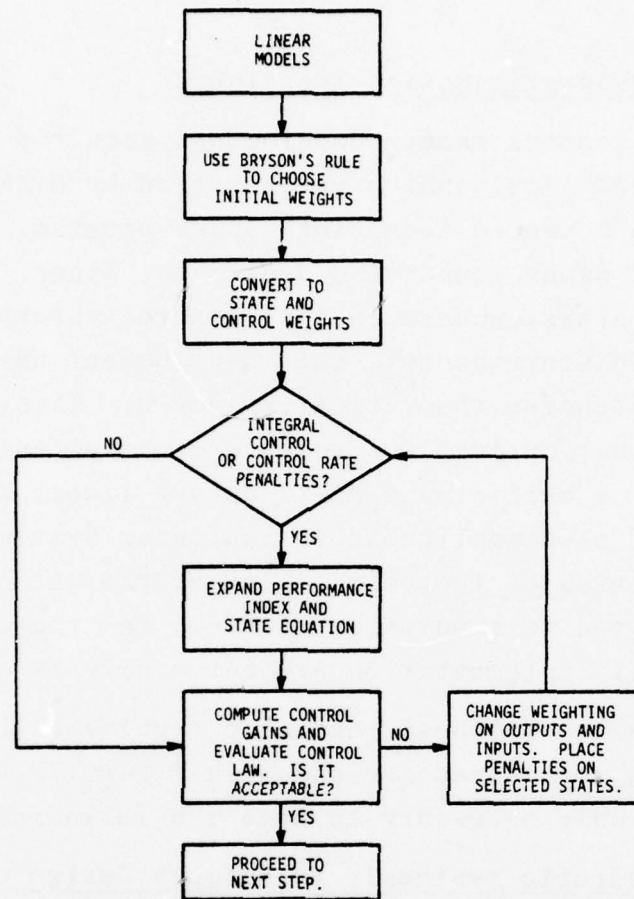


Figure 2.10 Procedure for Choosing Weights in the Performance Index

2.5 LQR APPROACH FOR LINEAR SYSTEM CONTROL SYNTHESIS

The last section discussed various approaches for the synthesis of control systems. It was mentioned there that modern control techniques have their basis in the state space representation of systems. For linear systems, with state vector, x , and input vector, u , the dynamic equations of motion can be written as

$$\dot{x} = Fx + Gu \quad (2.4)$$

This particular design methodology is directed to only deterministic design, so it is assumed for the purpose of this discussion that there is no random input. Control laws designed using modern design techniques are obtained by certain criterion functions, which are based on engineering experience and judgment of design goals required of the system to be controlled. Certain criteria have received special attention because of many desirable properties of the resulting controllers. The LQR approach is based on a particular form of the criterion function.

2.5.1 Basis of the LQR Method

The linear quadratic regulator method uses a linear system model [e.g., Eq. (2.4)] to design a regulator control law minimizing a matrix quadratic penalty function weighting state and control deviations about a nominal operation point. The optimization problem can be written as follows:

$$J^* = \min_{u(t)} \left\{ \frac{1}{2} x_f^T S_f x_f + \frac{1}{2} \int_0^{t_f} (x^T \mid u^T) \begin{pmatrix} A & \mid & N \\ \hline & & \\ N^T & \mid & B \end{pmatrix} \begin{pmatrix} x \\ \vdots \\ u \end{pmatrix} dt \right\} \quad (2.5)$$

where x_f and u_f are the state and control values at $t = t_f$; A , B and N are quadratic matrix weightings on the state and control deviations during a time interval $0 \leq t < t_f$; and S_f is a state penalty weighting at $t = t_f$. This problem has a particularly simple solution. The control u can be written as

$$u(t) = C(t) x(t) \quad (2.6)$$

where the control is implemented with the control structure shown in Figure 2.11. In other words, the control at any time is a linear function of the state at that time. If F , G , A , N and B are constants, and $t_f \rightarrow \infty$ constant, then a control gain C can be calculated. Constant gains are often used because of ease of implementation. This is called the linear quadratic regulator (LQR).

This approach has several characteristics including the following:

- (1) When the linear quadratic regulator is used, the control law gives a stable feedback system. Therefore, additional constraints to ensure that $F + GC$ has eigenvalues with negative real parts are not required. Note, however, that this desirable stability is guaranteed only if the system model Eq. (2.4), upon which the control is based, accurately represents the system. If significantly large modeling errors (e.g., errors in F) are present, the LQR law will not necessarily be stable. This warning is particularly applicable to the engine, whose analytical modeling can be quite difficult. This places considerable importance on engine modeling for LQR designs.
- (2) The optimal control input is a fixed linear combination of the state which can be precomputed. Cross-coupling of control on states is automatically included. This simplifies the implementation considerably.

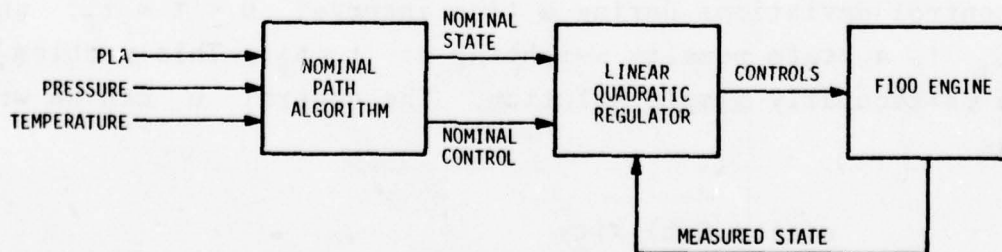


Figure 2.11 Perturbational Control Structure

Analytical issues relevant to the control design are summarized in Table 2.4 and are discussed in detail in Chapter III.

2.6 APPLICATION OF LQR METHOD TO TURBOFAN ENGINES

As discussed in Section 2.3, modern turbofan engines and anticipated propulsion systems of the future are extremely complex and involve interaction between several components.

Table 2.4
Application of Multivariable Control Design Using Linear Perturbational Techniques to Aircraft Turbine Engines

ISSUE	ELEMENT	APPROACH
TRANSITION CONTROL	Used during large transients	<ul style="list-style-type: none"> • Ramped set point/model • Follower approach
	First order approximation to trajectory produces acceptable temperature/surge excursions	<ul style="list-style-type: none"> • Constant acceleration models derived from linear systems
	Structure compatible with nonlinear trajectory generation	<ul style="list-style-type: none"> • Standard perturbation control
IMPLEMENTATION	Loop time (sampling cycle)	<ul style="list-style-type: none"> • Simplified schedule • Univariate gain functions • Multi-rate capability
	Program/parameter storage	<ul style="list-style-type: none"> • Nondimensional schedules • Gain matrix simplification
	Accuracy (fixed precision arithmetic)	<ul style="list-style-type: none"> • Gain matrix scaling
MODELING	State selection, dynamic elements	<ul style="list-style-type: none"> • Choose important performance rating quantities
	Generation of models	<ul style="list-style-type: none"> • Offset derivative from nonlinear simulation
	Reduction	<ul style="list-style-type: none"> • Eigenvector analysis and modal reduction
	Evaluation/verification	<ul style="list-style-type: none"> • Linear simulation and nonlinear deck
INTEGRAL CONTROL	Relevant trim point	<ul style="list-style-type: none"> • Choose fan match point for performance considerations
	Measurement accuracy	<ul style="list-style-type: none"> • Evaluate thrust losses due to expected scheduling and measurement errors
	Control saturation, dead zone, hysteresis	<ul style="list-style-type: none"> • Eliminate error term from feedback when saturated • Dead zone on errors

The dynamics of such engines follow nonlinear equations whose coefficients change with the speed and altitude of operation. There are acceleration and disturbance rejection requirements on engine performance and constraints on certain outputs.

The nonlinear turbofan equations of motion can be written as:

$$\dot{x} = f(x, u, \theta) \quad (2.7)$$

where x is the state vector, u is the vector of controls, and θ defines the ambient conditions (e.g., altitude and Mach number). The constraints on the outputs, such as thermal and mechanical limits, are usually independent of altitude and Mach number, i.e.,

$$y_{\min} \leq g(x, \tilde{u}) \leq y_{\max} \quad (2.8)$$

where y_{\min} , for example, could represent minimum acceptable thrust or fan stability margin and y_{\max} may indicate the maximum allowable value of high turbine inlet temperature. These outputs are related to the state variables through the functional form g .

There are additional constraints on control inputs and rates at which the control inputs can be changed

$$\begin{aligned} \dot{u}_{\min} &\leq \dot{u} \leq \dot{u}_{\max} \\ u_{\min} &\leq u \leq u_{\max} \end{aligned} \quad (2.9)$$

where \dot{u}_{\min} represents the maximum rate at which the control inputs can be decreased, \dot{u}_{\max} is the maximum rate at which they can be increased, and u_{\min} and u_{\max} are the extreme control positions. Usually,

$$\dot{u}_{\min} = -\dot{u}_{\max} \quad (2.10)$$

For maximum efficiency in steady-state operation, the controls must follow prespecified schedules as a function of the states:

$$u = g(x, \theta) \quad (2.11)$$

For example, in the F100 turbofan engine the position of the inlet guide vanes is a function of the corrected fan speed.

It is clear from the complexity of this problem, that the success of the application of the LQR approach to control synthesis depends on how the method is applied. It is also apparent from the discussion of the previous section that the regulator gains are obtained directly once the linear model and the performance index are specified.

Table 2.5 shows the state-of-the-art steps involved in successful application of the LQR theory to turbofan engines. Table 2.5 is discussed below.

2.6.1 LQR Theory for Linear Systems

From the discussion in Section 2.5, it is clear that the basic theory of the LQR approach is completely understood and has been widely applied. To apply the LQR approach, the non-linear system of Eqs. (2.7) to (2.11) must first be converted into the form of Eqs. (2.1) to (2.3). To accomplish this, an operating point is selected to determine state variables x_{ss} and u_{ss} . Next, small deviations around the state x_{ss} and u_{ss} are considered

Table 2.5
Application of LQR Theory to Control Design for Turbine
Engines - State-of-the-Art

STEPS IN CONTROL SYNTHESIS	STATE-OF-THE-ART	APPLICATION TO JET ENGINES AND OTHER NONLINEAR SYSTEMS	REMARKS
LQR Theory for Linearized Engine Models	Completely understood.	Wide class of applications. Several efficient programs exist to solve the Riccati equation; see, for example, Ref. 44.	Can be applied with confidence when the linearized model is correct.
Linearization of Nonlinear Systems for Application of LQR Theory	Two methods: (1) finite differences, and (2) use of advanced parameter estimation methods.	Applied on an ad hoc basis to engines and other systems.	Care should be exercised for complex systems, particularly when the nonlinear simulation has more states than the linearized model.
Gain Scheduling	Gain switching, or linear or quadratic interpolations.	Both linear and quadratic interpolation used on jet engines for sea level static condition.	Interpolation becomes complex when parameterized on more than one variable (in engine there are at least three). Possibility of simple gain switching needs further study.
Choice of States and Operating Points, Where the System is Linearized	Advanced identification method for choosing relevant states [45].	Applied in Ref. 46 for the high angle-of-attack problem (not in the context of control design). Computer programs available.	Important for designing a simple, yet effective, controller.
Quick Acceleration and Set Point Change	Acceleration controller applications [39]	Constant acceleration method used with helicopter.	Delay from integral control could cause poor accelerations.
Parameter Insensitive Control	Theory under development	Computer programs exist. Have been applied for satellite control.	Necessary for variations in engine and inlet conditions.

$$\delta x \triangleq x - x_{SS} \quad (2.12)$$

$$\delta u \triangleq u - u_{SS}$$

The nominal output and its deviation around the steady-state can be defined

$$y_{SS} \triangleq g(x_{SS}, u_{SS}) \quad (2.13)$$

$$\begin{aligned} \delta y &\triangleq y - y_{SS} \\ &= g(x, u) - g(x_{SS}, u_{SS}) \end{aligned} \quad (2.14)$$

For a linear system, Eq. (2.14) for the observed responses may be written in the form

$$y = H x + D u \quad (2.15)$$

where H is the observation matrix, and D is the feedforward control matrix.

2.6.2 Linearization of Nonlinear Simulation for Application of the LQR Method

Several methods have been used to derive linearized systems from nonlinear dynamic simulations [36]. The method must give correct poles as well as zeroes of the input/output transfer function. In other words, all elements of the linearized matrix must be correct. One of the most common methods is to compute F and G using the equations

$$F = \frac{f(x + \Delta x, u, \theta) - f(x - \Delta x, u, \theta)}{2\Delta x} \quad (2.16)$$

$$G = \frac{f(x, u + \Delta u, \theta) - f(x, u - \Delta u, \theta)}{2\Delta u} \quad (2.17)$$

where Δx and Δu must be chosen appropriately. The disadvantage of this method is that the nonlinear simulation may have many more state variables than one would like to include in the linear model. Approximation methods must then be used to eliminate the undesired states from the f function. An alternate approach is to use advanced parameter identification methods to estimate the linear model from the engine response around some point.

Matrices H and D in Eq. (2.15) can be determined by using finite difference formula of the type of Eqs. (2.16)-(2.17). Another method is to use linear regression between the output and the states and inputs.

2.6.3 Gain Scheduling for Turbofan Engine Control

The linearized equations of motion depend on the point around which the linearization is carried out and are parameterized on ambient variables. Different points in the envelope of the engine have different regulator gains, both because the linearized model changes and because the constraints on states and control change. Thus, as the engine enters into a different operating region, the control gains must be altered in a systematic manner.

There are two methods which have been used. In the first, the envelope is divided into several regions. Each region has its own control gains. As the system moves from one region to another, the control gains are switched. This reduces the on-line computer requirements, but more points must be chosen to compute gains. The controls will have step changes as the system moves from one region to another. The problem of step changes can be alleviated by placing weights on the control rates in the performance index as discussed in Chapter III.

The second method computes the gain by linear interpolation between adjacent points. In the engine, there are possibly three independent quantities on which the regulator gains can be parameterized. One set of scheduling parameters might be engine power level, altitude and Mach number. In this case, the gain matrix must be linearly interpolated between eight values. This can cause excessive real time computation requirements. A simplification of the above techniques is described in Chapter V.

2.6.4 Choice of States and the Design Points

When the LQR approach is applied to complex nonlinear systems like turbofan engines, the choice of states and design points is an important consideration both from the design and the implementation viewpoint. There are numerous states in the turbofan engine. The number of states must be reduced to get a reasonable control law. In addition, many of the states are not measurable or observable making it difficult to use them without extensive computation.

A natural solution to this problem results if advanced parameter identification methods are used for determining linear models from the nonlinear simulation. A certain state vector is chosen and the outputs are used to identify the state model. If the particular choice does not include all pertinent states, then the fit to the outputs will be poor because an insufficient set of state variables cannot describe the outputs completely. Thus, a poor fit to the outputs would indicate that further states should be included in the engine model. The inclusion of undesired states in the model would, on the other hand, make the problem overdetermined, which causes identifiability problems. Some of the state variables should be dropped. Figure 2.12 shows how this approach is used in an iterative manner. To select the states objectively, statistical tests can be used to evaluate the fit to the outputs. Reference 37 describes this approach in detail. A good design would attempt to determine pertinent state variables at representative operating points. It is clear from the above discussion that the set of adequate state variables depends on the outputs.

The next problem is the choice of the linearization points around which the regulator is designed. If the engine were always near a steady-state, at every flight condition, there is only one independent parameter which specifies the

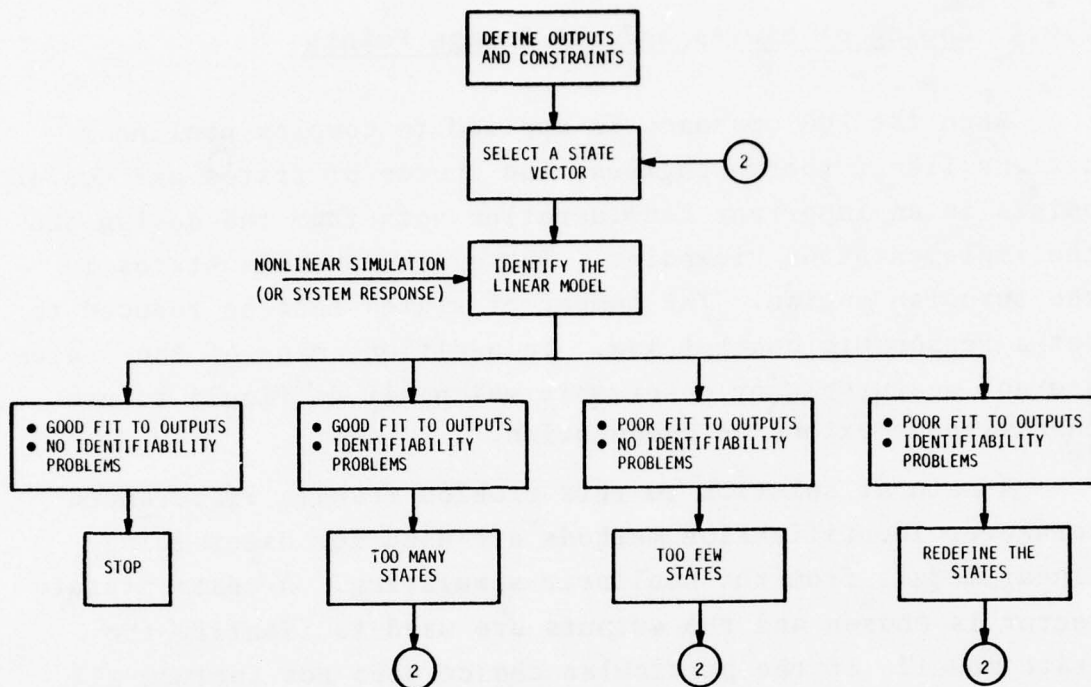


Figure 2.12 Choice of States in Application of LQR Methods to a Nonlinear System

linearized model. This parameter could be spool speed or engine pressure ratio. The model could be linearized along the steady-state line for the entire range of spool speed. In fast transients, particularly quick acceleration from low to high power, deviations from steady-state operating line may occur. It is very important, in the next step, to select design points in this envelope carefully so that a good nonlinear controller is obtained when the gain scheduling described in the last section is used. The basic idea is to choose fewer points in those regions where there are small changes in the linear models and to increase the density of design points in those regions where the linearized models are changing rapidly.

2.6.5 Rapid Accelerations and Set Point Change

One of the requirements in engine feedback control law design using the LQR method is the capability to rapidly accelerate the engine from low power to high power levels. This problem has received little attention in both the turbine engine problems and other nonlinear systems. Stone, et al. [38] reported that this is not a problem in the General Electric J85 engine. An integral approach is used by Michael, et al. [39,41]. Michael realizes some improvements in acceleration times over conventional controllers. The method requires an integral error to build up before the controls start moving.

One method for linear control systems was developed by Gupta and Bryson [42] for the rapid acceleration of helicopters carrying heavy slung loads. The technique suggested here can also be used for nonlinear systems. The method stems from an extension of the notion of steady-state. With reference to the linear model of Eq. (2.1), we define a steady-state

$$\dot{x} = \text{constant} = R \quad (2.18)$$

This is called the constant rate steady-state. The control required to maintain this steady-state is determined by differentiating Eq. (2.4) with respect to time:

$$\ddot{x} = F\dot{x} + G\dot{u} = 0 \quad (2.19)$$

This, with Eq. (2.18), gives both the control input and the input rate as a function R and the state variables. A maximum R is chosen such that no control, state, or output rate constraint is violated. The control derived from the above equations is used in a feedforward mode, while additional feedback control is applied to ensure that the engine follows

the desired trajectory. The details of this method are given in Ref. 42.

In the nonlinear engine control, this method must be modified to incorporate variations in the linear model with power output. The major variations would be the choice of the acceleration R and the functional variation of the feed-forward input component with engine power level and ambient conditions. The control law is general and provides the maximum acceleration from all starting points. This would be achieved with a modest increase in complexity.

2.6.6 Parameter Insensitivity of the LQR Gains

When the gain scheduling techniques of Section 2.6.3 are used together with the design point selection method of Section 2.6.4, the engine often operates away from the design points and the gains are not optimal for that operating point of the engine. In addition, as explained in Section 2.5, there are errors in the linearized engine models used for design purposes. Therefore, the requirement of having control gains which are relatively insensitive to the parameter values is even more important when the LQR method is used for nonlinear systems with scheduled gains. The methods applicable for linear systems can be applied at each design point.

2.7 ENGINE DIGITAL CONTROL IMPLEMENTATION

This section discusses the possible sources of controller errors which can be induced by digital implementation. It is recognized that the NASA-LeRC SEL 810B computer is very flexible. Recognizing the possible bandwidth problem, the following paragraphs detail how solutions may be integrated into the LQR design procedure if required.

2.7.1 Digitization

Several methods exist for implementing a control algorithm in a digital computer. The first and most commonly used method starts with a control law designed as a continuous system and uses one of several discrete approximation techniques (reviewed recently by Slater [43]). These techniques generally give good performance if the sample rate, ω_s , is significantly ($>$ factor of 10) faster than any of the closed-loop roots of the system. The closed-loop roots include the important actuator loop closures as well as the loops within the controller itself. The effect of the controller loops for a turbine application has been discussed recently by Cwynar, et al. [19]. For moderate sample rates ($\omega_s = 2 \rightarrow 5 \times$ closed-loop roots), discrete approximation techniques can lead to changes in performance including instabilities in extreme cases.

The change in performance arises from two sources. First, some high frequency information is lost by sampling instead of using the continuous signal. Second, there may be a dead time introduced by the computer computational delay. Cwynar showed that the dead time was the more significant of the two effects in a turbine control application.

An alternative to continuous design is to use a direct digital technique. Methods in this category include w-plane [44], z-plane Nyquist, and state space techniques [45]. All these methods eliminate the change in performance between analysis and implementation due to sampling and computation delay in the feedback loops. They do not eliminate the delay due to sampling the input command, however. These methods derive their accuracy in analysis by completely modeling the plant including any computation delays that may exist in the

physical implementation, a feature that fits easily into the discrete representation of a system, but is cumbersome in a continuous representation.

In early design iterations of an LQR controller, the increased complexity of computations and the loss of physical insight for direct digital design dictate that these methods should not be used. Once a design is established using continuous analysis, it is beneficial to evaluate the relationship between closed-loop roots and proposed sample rates to determine whether a discrete refinement of the design is warranted. Previous work [19] in a digital control implementation to a gas turbine concluded a sample rate 2 to 5 times faster than the fastest dynamic time constant was required for adequate control. Since the fastest closed-loop root is at approximately 10-15 rad/sec in the controller and a sampling rate of 20 msec could be achieved, then discrete refinement of the LQR designs was not required for implementation on the Lewis facility.

2.7.2 Word Size

For digital implementations, the effect of a finite computer word size can be important. The primary concern is the sensitivity of dynamic elements in the controller to imperfect coefficient storage due to a finite number of bits. This sensitivity decreases as the sample rate decreases; hence, the desirability to determine the slowest practical sample rate. This effect was found to be particularly important in the Apollo digital autopilot [46] and was found to lead to instabilities if not specifically accounted for in the design. Hybrid testing of the controller implementation is required to evaluate these effects.

2.8 SUMMARY

This chapter presents the performance requirements for typical turbofan engines, imposed by desired engine responses and aerodynamic, thermal, and mechanical constraints, on its components. The engine control operating within these constraints must provide safe and stable performance over the engine flight envelope.

Previous classical and modern techniques used for turbine engine control synthesis are discussed in detail to bring out the achievements and pitfalls of each approach. Next, the basic methods of the SCI (Vt) approach for the design of control systems for nonlinear systems, based on the linear quadratic regulator approach of modern control theory, is presented. These techniques have been applied successfully to other nonlinear systems, and are specialized to the engine control problem. The highlight of these methods for application to engine control is the complete integration of: (1) engine control requirements, (2) the role of nonlinear engine simulation, (3) the LQR approach, and (4) the control implementation environment including the NASA-LeRC altitude test facility and the related computer hardware.

The remaining chapters show specifically how these techniques were integrated to yield a procedure which designs a practical, effective controller for the Pratt & Whitney Aircraft F100 turbofan engine.

CHAPTER III

LINEAR QUADRATIC REGULATOR SYNTHESIS TECHNIQUES

3.1 OVERVIEW

The design of controls for nonlinear physical systems can be based on assumptions of nearly linear plant behavior about a nominal operating point. Using these assumptions, a wide spectrum of techniques for linear time and frequency domain analysis are available. Resulting controllers must then be verified on nonlinear simulations of the system or on the system itself.

Procedures for the design of linear multivariable control systems using optimal regulator theory are well known and many techniques for utilization of the theory to attack problems addressed in single-loop classical control have an abundant literature [47]. In this chapter, the foundations of the state variable formulation of the linear optimal regulator problem will be reviewed. Various structures and specific choice of optimal performance terms are presented from a physically intuitive point of view. Iterative procedures are discussed. A group of techniques for altering the formulation of the problem to accommodate physical limits and steady-state response are shown.

Systems designed with modern control methods have been criticized for being sensitive to parameter variations and too complex for practical implementation. Techniques are discussed for designing systems with minimal sensitivity to parameter variations using both explicit and implicit formulations. Simplification of the control law is discussed from an

eigenvalue sensitivity viewpoint and fixed structure optimization procedures are presented for comparison. Finally, discrete time forms are summarized and the conditions of equivalence to the continuous time solutions are reviewed. Table 3.1 summarizes the organization of the chapter and the important topics discussed.

Table 3.1
Organization of Chapter III

SECTION	IMPORTANT TOPICS
3.1	Overview
3.2	Theoretical Foundations <ul style="list-style-type: none"> • Regulator Solution • Alternate Forms
3.3	Performance Index Selection <ul style="list-style-type: none"> • Scaling • Root Square Locus • Modal Sensitivities
3.4	Augmenting the Performance Index <ul style="list-style-type: none"> • Control Rate/Acceleration Weighting • Actuator Models • Output Augmentation
3.5	Integral Control Synthesis <ul style="list-style-type: none"> • Direct Augmentation • Disturbance Estimation • Spectral Decoupling
3.6	System Parameter Insensitivity <ul style="list-style-type: none"> • Modal Sensitivities • Techniques for Sensitivity Reduction
3.7	Simplification of Control Laws <ul style="list-style-type: none"> • Sensitivity Calculations • Fixed Structure Optimization
3.8	Discrete Optimal Control Problem <ul style="list-style-type: none"> • Theoretical Development • Comparison to Continuous Time Solution
3.9	Summary

3.2 BASIS OF LINEAR QUADRATIC REGULATOR DESIGN METHOD

The linear optimal regulator solution is derived within the context of global optimization and perturbational forms for systems of differential equations written in state variable format.

3.2.1 Linear System Description

The linear quadratic regulator synthesis procedure operates on a set of first order, ordinary differential equations which, over some regime, describe system dynamic behavior. In the case of most physical systems, the dynamic variables, or states, describe perturbational motion from a nominal or equilibrium condition. The nonlinear development of the control will be considered in Chapter IV. In the following, the linear theory will be emphasized as to its applicability to often encountered problems in nonlinear systems.

The state variable description of a linear dynamic system can be represented in matrix notation as follows:

$$\dot{x}(t) = F(t)x(t) + G(t)u(t) \quad (3.1)$$

where the $(nx1)$ column vector of states, x , contains elements whose behavior in response to initial conditions and control inputs completely describes the important dynamic interactions. The $(mx1)$ control vector, u , contains elements corresponding to variables available to the controller which affect the response of the system. The (nxn) matrix, F , describes the dynamics of the states, and the (nmx) control distribution matrix, G , models the effect of control modulation on state response.

It should be noted that the state variable description in Eq. (3.1) implies that a knowledge of the control time history and the state vector at one instant of time is sufficient to determine the entire state time history. Often, quantities of interest to the control engineer outnumber the order of the dynamics in Eq. (3.1). In this case, the system model can be specified as in Eq. (3.1) along with a static relationship describing other important quantities or outputs of the system. This relation is described by the linear equations relating the (pxl) output vector, y , to the state and control variables by the (pxn) state output distribution matrix, H , and the (pxm) control output distribution matrix, D , as follows:

$$y(t) = H(t)x(t) + D(t)u(t) \quad (3.2)$$

The system of equations (3.1) and (3.2), called the design model, are the general dynamic description of the plant behavior used in quadratic synthesis.

3.2.2 Quadratic Cost Functional

Along with the design model, linear quadratic regulator synthesis requires a subjective judgment by the control designer on the character of the closed-loop dynamic behavior which is acceptable or desirable in a particular situation. Typically, control designs must accurately regulate the system in the presence of disturbances near a static equilibrium condition and provide a smooth transition from one operating point to another [47]. Quantification of this judgment requires specification of a cost functional for control given as follows:

$$J(x,u) = \varphi[x(t_f), t_f] + \int_{t_0}^{t_f} L[x(t), u(t), t] dt \quad (3.3)$$

where φ and L are functions of the state and control which penalize the terminal trajectory error and the sum of the trajectory errors over a specified interval, respectively.

Specialization of Eq. (3.3) to matrix quadratic forms simplifies the resulting control law. Objective functionals used in the linear quadratic optimal control problem may be of the following types [48]:

State/Control Weighting:

$$J(x,u) = x^T(t_f)S(t_f)x(t_f) + \frac{1}{2} \int_{t_0}^{t_f} [x^T(t)A(t)x(t) + u^T(t)B(t)u(t)] dt \quad (3.4)$$

Output Weighting:

$$J(x,u) = y^T(t_f)S(t_f)y(t_f) + \frac{1}{2} \int_{t_0}^{t_f} [y^T(t)Q(t)y(t)] dt \quad (3.5)$$

Follower:

$$J(x,u) = \frac{1}{2} \int_{t_0}^{t_f} \{ [y(t) - y_0(t)]^T Q(t) [y(t) - y_0(t)] + u^T(t)B(t)u(t) \} dt \quad (3.6)$$

The matrix S represents the quadratic penalty on terminal error and the matrices A , B , and Q represent quadratic penalties on the trajectory error. The function $y_0(t)$ represents a desired output trajectory. For the regulator problem, it is possible to assume that $S \rightarrow 0$ and $t_f \rightarrow \infty$ to eliminate the effect of the terminal miss [48]. However, S will be retained in the following to maintain generality. Each of the cost functionals shown above produces control laws involving state variable feedback. The particular form used by the designer is dependent on the control criteria of the desired system response.

3.2.3 Solution to the Optimization

The optimal control problem requires the calculation of the control time history $u(t)$ which minimizes the cost functional, $J(x,u)$, for a specified initial condition. The optimal control problem can be formally posed as follows:

$$\min_{u(t)} J(x,u) = \min_{u(t)} \int_{t_0}^{t_f} [x(t)^T A x(t) + u^T(t) B u(t)] \quad (3.7)$$

subject to the constraint,

$$\dot{x}(t) = F(t)x(t) + G(t)u(t) \quad (3.8)$$

and

$$x(t_0) = x_0 \quad (3.9)$$

The solution will be reviewed briefly and specialization to cost functions given in Eqs. (3.5) and (3.6) discussed.

Adjoining the constraint Eq. (3.8) to the cost function with Lagrange multipliers, $\lambda(t)$, yields the Hamiltonian function for the problem [47]:

$$\mathcal{H}(x, u, \lambda) = \frac{1}{2} x^T A x + \frac{1}{2} u^T B u + \lambda^T [f x + G u] \quad (3.10)$$

The necessary conditions for optimality are then as follows:

$$\dot{\lambda}^T = - \frac{\partial \mathcal{H}}{\partial x} \quad \lambda(t_f) = S(t_f) x(t_f) \quad (3.11)$$

$$0 = \frac{\partial \mathcal{H}}{\partial u} \quad (3.12)$$

The linear, two-point boundary value problem to be solved for the optimal control is specified by the Euler-Lagrange system of linear, homogeneous differential equations:

$$\begin{bmatrix} \dot{x} \\ \dot{\lambda} \end{bmatrix} = \begin{bmatrix} F & -GB^{-1}G^T \\ -A & -F^T \end{bmatrix} \begin{bmatrix} x \\ \lambda \end{bmatrix} \quad \begin{aligned} x(t_0) &= x_0 \\ \lambda(t_f) &= S(t_f)x(t_f) \end{aligned} \quad (3.13)$$

$$= H \begin{bmatrix} x \\ \lambda \end{bmatrix} \quad (3.14)$$

For the special case of constant system and weighting matrices, the dynamics matrix, H , of Eq. (3.14) has singularities that are symmetric about the real and imaginary axes in the complex plane. The solution to Eq. (3.13) with constant coefficients can be formulated for a point interior to the interval (t_0, t_f) using the modal decomposition of H [48].

The modal decomposition can be written as follows:

$$H = \mathcal{T} \Lambda \mathcal{T}^{-1} \quad (3.15)$$

where right eigenvectors of H form the transformation matrix as follows

$$\mathcal{T} = [u_1^+, u_2^+, \dots, u_n^+ \quad u_1^-, u_2^-, \dots, u_n^-] \quad (3.16)$$

and the right (+) and left (-) half plane eigenvalues are partitioned as follows:

$$\Lambda = \begin{bmatrix} \Lambda_+ & 0 \\ 0 & \Lambda_- \end{bmatrix} \quad (3.17)$$

The modal coordinate representation of the system in Eq. (3.13) is as follows:

$$\dot{z} = \Lambda z \quad (3.18)$$

The solution to Eq. (3.13) can be formally written for a point $t_0 < t < t_f$ as follows:

$$\begin{bmatrix} x(t) \\ \lambda(t) \end{bmatrix} = \begin{bmatrix} T_{11}^+ \\ \text{----} \\ T_{12}^+ \end{bmatrix} \varphi_+(t-t_f) z(t_f) + \begin{bmatrix} T_{11}^- \\ \text{----} \\ T_{12}^- \end{bmatrix} \varphi_-(t-t_0) z(t_0) \quad (3.19)$$

where T_{11}^+ and T_{12}^+ are partitions of the eigenvectors for positive eigenvalues and T_{11}^- and T_{12}^- are partitions of the eigenvectors for the negative eigenvalues. The following definitions have been made:

$$\varphi_+(\tau) = \exp(\Lambda_+ \tau) \quad (3.20)$$

$$\varphi_-(\tau) = \exp(\Lambda_- \tau) \quad (3.21)$$

Adjoining the constraint Eq. (3.8) to the cost function with Lagrange multipliers, $\lambda(t)$, yields the Hamiltonian function for the problem [47]:

$$\mathcal{H}(x, u, \lambda) = \frac{1}{2} x^T A x + \frac{1}{2} u^T B u + \lambda^T [f x + G u] \quad (3.10)$$

The necessary conditions for optimality are then as follows:

$$\dot{\lambda}^T = - \frac{\partial \mathcal{H}}{\partial x} \quad \lambda(t_f) = S(t_f)x(t_f) \quad (3.11)$$

$$0 = \frac{\partial \mathcal{H}}{\partial u} \quad (3.12)$$

The linear, two-point boundary value problem to be solved for the optimal control is specified by the Euler-Lagrange system of linear, homogeneous differential equations:

$$\begin{bmatrix} \dot{x} \\ \dot{\lambda} \end{bmatrix} = \begin{bmatrix} F & -GB^{-1}G^T \\ -A & -F^T \end{bmatrix} \begin{bmatrix} x \\ \lambda \end{bmatrix} \quad \begin{array}{l} x(t_0) = x_0 \\ \lambda(t_f) = S(t_f)x(t_f) \end{array} \quad (3.13)$$

$$= H \begin{bmatrix} x \\ \lambda \end{bmatrix} \quad (3.14)$$

For the special case of constant system and weighting matrices, the dynamics matrix, H , of Eq. (3.14) has singularities that are symmetric about the real and imaginary axes in the complex plane. The solution to Eq. (3.13) with constant coefficients can be formulated for a point interior to the interval (t_0, t_f) using the modal decomposition of H [48].

The modal decomposition can be written as follows:

$$H = \mathcal{T} \Lambda \mathcal{T}^{-1} \quad (3.15)$$

Using Eq. (3.12), the form of the control law is as follows:

$$u(t) = -B^{-1}G^T \lambda(t) \quad . \quad (3.22)$$

Since Eqs. (3.13) are homogeneous, the time-varying solutions are proportional to the initial state and the control law must have the form:

$$u(t) = -B^{-1}G^T C(t)x(t_0) \quad . \quad (3.23)$$

3.2.4 Steady-State Solution

If all elements in the system dynamics and the cost functional are constant and under some conditions of controllability and stability [48], the feedback law, Eq. (3.23), simplifies to a constant gain state feedback matrix determined, from the solution Eq. (3.19) of the Euler-Lagrange equations, at a time point far from the terminal conditions. Equation (3.19) reduces to the following:

$$x(t) = T_{11}^{-1} \varphi_-(t-t_0) z(t_0) \quad (3.24)$$

$$\lambda(t) = T_{12}^{-1} \varphi_-(t-t_0) z(t_0) \quad (3.25)$$

and

$$\lambda(t) = T_{12}^{-1}(T_{11}^{-1})^{-1} x(t) \quad .$$

The control law can be written from Eq. (3.24) as follows:

$$u(t) = -B^{-1}G^T T_{12}^{-1}(T_{11}^{-1})^{-1} x(t) \quad (3.26)$$

or

$$u(t) = Cx(t) \quad (3.27)$$

where C is the $(m \times n)$ constant state feedback gain matrix for the optimization problem; C will be referred to as the regulator solution.

Several properties of the closed-loop system should be noted. The closed-loop poles are the left half plane poles of the Euler-Lagrange system of Eq. (3.13). The resulting plant is always strictly stable if the characteristics of the F, G, A, and B matrices are satisfactory [48]. The technique described produces suboptimal solutions to the finite time problem. However, it often results in satisfactory controllers for multivariable linear systems. The simplicity of the state feedback control law makes this procedure attractive to the designer interested in utilizing the full range of couplings available in a large system.

3.2.5 Generalized Results

The control laws resulting from the cost functional shown in Eqs. (3.5) and (3.7) can be derived in an analogous procedure [49,50]. The important results are shown below.

Output Weighting

For $y = Hx + Du$, the following equations relate Eq. (3.5) to Eq. (3.4) [47]:

$$y^T Q y = x^T H^T Q H x + u^T D^T Q D u + x^T H^T Q D u + u^T D^T Q H x \quad (3.28)$$

and

$$J = \frac{1}{2} \int_{t_0}^{t_f} [x^T \quad u^T] \begin{bmatrix} H^T Q H & H^T Q D \\ \hline D^T Q H & D^T Q D \end{bmatrix} \begin{bmatrix} x \\ u \end{bmatrix} dt \quad (3.29)$$

This form is equivalent to the problem described in Sections 3.2.3 and 3.2.4 with the system of equations:

$$\dot{x} = [F - G(D^T Q D)^{-1} D^T Q H]x + Gu \quad (3.30)$$

$$J = \frac{1}{2} \int_{t_0}^{t_f} (x^T \bar{A} x + u^T \bar{B} u) dt \quad (3.31)$$

where

$$\bar{A} = Q - H^T Q D (D^T Q D)^{-1} D^T Q H \quad (3.32)$$

$$\bar{B} = D^T Q D \quad (3.33)$$

Follower Solutions [42,50]

Two forms of the follower solution are important in linear controls design. The general follower solution for the cost functional in Eq. (3.7) is easily derivable for the steady state optimal gains. The desired set of output trajectories is given as follows:

$$y_d = f(t) \quad (3.34)$$

and the actual output, $y(t)$, is described as a linear function of the states and controls,

$$y = Hx + Du \quad (3.35)$$

For the special case where $D \equiv 0$, Eq. (3.7) is written as follows:

$$J(x,u) = \frac{1}{2} \int_{t_0}^{t_f} [(Hx - y_d)^T Q (Hx - y_d) + u^T B u] dt \quad (3.36)$$

and the solution is given as follows:

$$u = Cx + w(t) \quad (3.37)$$

where C is calculated from the regulator solution given in Sections 3.3 and 3.4 with the state weighting matrix given by $H^T Q H$. The feedforward bias, $w(t)$, is found from the solution of the linear equation

$$\dot{q} = F_{CL}^T q + H^T Q y_d(t) \quad (3.38)$$

$$q(t_f) = 0 \quad (3.39)$$

$$w(t) = -B^{-1} G^T q(t) \quad (3.40)$$

where $F_{CL} = F + GC$.

A more useful result is obtained when the state and control time histories are completely specified. In this case,

$$x_d = f_x(t) \quad (3.41)$$

$$u_d = f_u(t) \quad (3.42)$$

with $f_x(t)$ assumed differentiable. The cost functional is written as follows:

$$J(x, u) = \frac{1}{2} \int_{t_0}^{t_f} [(x - x_d)^T A (x - x_d) + (u - u_d)^T B (u - u_d)] dt \quad (3.43)$$

The solution to the optimization problem is as follows [50]:

$$u = C[x(t) - x_d(t)] + w(t) \quad (3.44)$$

$$w(t) = -B^{-1} G^T q(t) + u_d(t) \quad (3.45)$$

$$\dot{q} = F_{CL}^T q + S[\dot{x}_d - Fx_d - Gu_d] \quad (3.46)$$

$$q(t_f) = 0$$

where S is a constant matrix ($G^T S = BC$).

The results in Eqs. (3.44) - (3.46) have strong implication in multivariable control design. The optimal feedback gain matrix is calculated independently of the follower problem. The control is implemented as perturbations away from the programmed trajectory with a control feedforward. If the trajectory is a solution to the open-loop dynamics of the plant, then the control law in Eq. (3.44) is equivalent to a perturbational controller regulating the system about a nominal trajectory specified by $w(t) = u_d(t)$. The results of this separation property of the regulator and follower are utilized directly in the formulation of the multivariable control structure discussed in Chapter IV.

3.3 SELECTION OF PERFORMANCE INDEX

The results of linear quadratic regulator theory are predicated on the selection of weightings in the performance index. Several methods are available to choose values in the A and B matrices which produce acceptable transient behavior.

3.3.1 Scale Factor Weightings (Bryson's Rule) [47]

Typically, the matrices weighting stages and controls in the regulator performance index, Eq. (3.4), are chosen to be diagonal. There are $m+n$ design parameters which determine the amount of control action used to null state deviations away from nominal. If scale factors are chosen for each state and control which determine a subjective equivalent (e.g., the amount of control to be used to null a given amount of state

deviation), then the design model Eq. (3.1) can be scaled, as follows:

$$\dot{x}^* = F^*x^* + G^*u^* \quad (3.47)$$

where

$$x^* = x/x_{nom} \quad (3.48)$$

$$u^* = u/u_{nom} \quad (3.49)$$

$$F_{ij}^* = F_{ij} x_{jnom}/x_{inome} \quad (3.50)$$

$$G_{ij}^* = G_{ij} u_{jnom}/u_{inome} \quad (3.51)$$

$$J = \frac{1}{2} \int_0^t (\dot{x}^{*T} A^* \dot{x}^* + u^{*T} B u^*) dt \quad (3.52)$$

The relationship between the regulator problem using Eqs. (3.8) and (3.9) and the problem using Eqs. (3.47) and (3.52) is as follows:

$$A_i = (1/x_{inome})^2 A_i^* \quad (3.53)$$

$$B_i = (1/u_{inome})^2 B_i^* \quad (3.54)$$

On the initial design iteration, A^* and B^* can be chosen as identity matrices and variations in the values of the matrix elements in subsequent iterations are directly identifiable as fractionally related to changes in the initial design.

3.3.2 Root Square Locus [51]

After initial evaluation of the closed-loop response of the regulated system, it is often desirable to modify the

weightings to improve the behavior either from a time domain or frequency domain point of view. Approximation of the pole movement with adjustments in performance index weighting permits the designer to satisfy bandwidth and damping requirements with direct adjustment to weighting elements. Also, if the frequency and damping are acceptable but the mode shape of the response is not acceptable, or if one or more controls are saturated by typical transient maneuvers, the state and control weightings can be varied in such a way that the closed-loop frequency and damping remain the same, but the modal response characteristics are improved with an improved distribution of control activity.

The root square locus procedure is applicable to single-input, multi-output (SIMO) or multi-input, single-output (MISO) systems. It has the advantage of using readily available transfer function information (see Appendix D, Section D.3) to determine the effect of state and control weightings on the closed-loop root locations. From Eq. (3.13), the characteristic equation of the Laplace transform of the equation can be written as follows:

$$\det \begin{bmatrix} sI - F & GB^{-1}G^T \\ A & sI + F^T \end{bmatrix} = 0 \quad (3.55a)$$

This expression can be expanded as follows:

$$\det(sI + F^T) \det[sI - F - GB^{-1}G^T(sI + F^T)^{-1}A] = 0 \quad (3.55b)$$

Using elementary determinant operations, the characteristic equation can be expressed as follows:

$$\det[B + G^T(-sI - F^T)^{-1}A(sI - F)^{-1}G] = 0 \quad (3.55c)$$

Defining $X(s)$ as the $(n \times m)$ system transfer function matrix,

$$X(s) = (sI - F)^{-1}G, \quad (3.55d)$$

the root square locus equation is given as follows:

$$\det[B + X^T(-s)A X(s)] = 0 \quad (3.55e)$$

These may be simplified to either the single-input or single-output case.

Thus, the closed-loop root locations for an optimal controller are found as the left half plane roots of the following expressions:

$$\text{SIMO: } b + x_C^T(-s) A x_C(s) = 0 \quad (3.55f)$$

$$\text{MISO: } \frac{1}{2} + x_R(s) B^{-1} x_R^T(-s) = 0 \quad (3.55g)$$

where

$$x_C(s) = \begin{bmatrix} \frac{x_1}{u}(s) \\ \vdots \\ \frac{x_n}{u}(s) \end{bmatrix} \quad (3.56a)$$

$$x_R(s) = \begin{bmatrix} \frac{x}{u_1}(s) & \vdots & \dots & \vdots & \frac{x}{u_m}(s) \end{bmatrix} \quad (3.56b)$$

Equation (3.55) can be solved using a standard multi-closure root locus procedure as illustrated in Figure 3.1. The transfer function poles and zeroes are plotted on the complex plane. The singularities are reflected over the imaginary axis. A root locus is then drawn. The locus parameter is the weighting ratio in the cost functional. The effects of weighting can be clearly exhibited before detailed design iteration.

SYSTEM: $\dot{x} = -\alpha x + \beta_1 u_1 + \beta_2 u_2$

COST: $J = \frac{1}{2} \int_0^\infty [\alpha x^2 + b_1 u_1^2 + b_2 u_2^2] dt$

ROOT SQUARE LOCUS EQUATION: $\frac{1}{a} + \frac{1}{b_1} \frac{\beta_1^2}{s^2 - \alpha^2} + \frac{1}{b_2} \frac{\beta_2^2}{s^2 - \alpha^2} = 0$

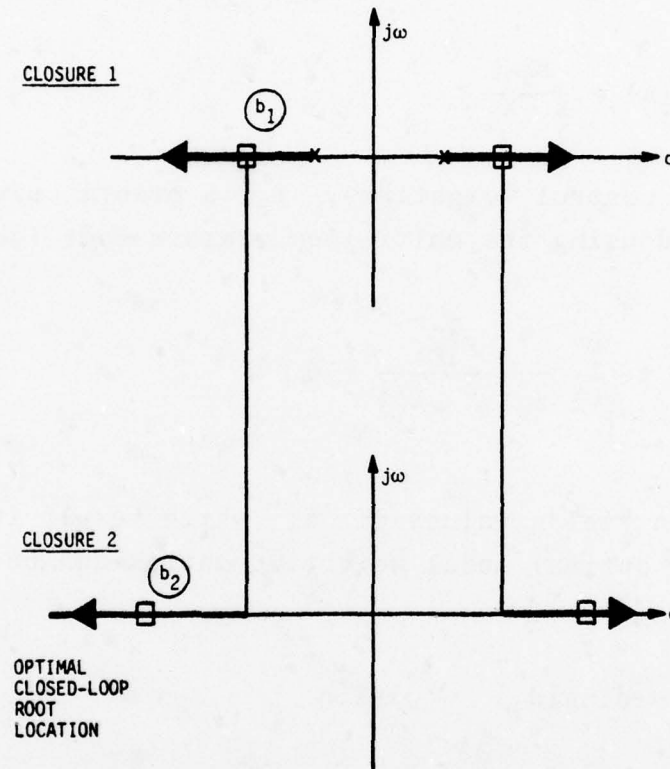


Figure 3.1 Illustration of Root Square Locus Technique for Approximating Closed-Loop Root Locations

The procedure can be extended to multi-input, multi-output systems using modal coordinates. The technique results in a multivariable pole placement algorithm. The development follows from Eqs. (3.55). The modal system is

$$\dot{x} = Tz \quad (3.57a)$$

Assuming real eigenvalues for simplicity of notation (the generalization to complex roots is straightforward)

$$\dot{\mathbf{z}} = \Lambda \mathbf{z} + \Xi \mathbf{u} \quad (3.57b)$$

or

$$\dot{z}_i = \lambda_i z_i + g_i^T \mathbf{u} \quad i=1,n \quad (3.57c)$$

and

$$\frac{z_i}{u_j}(s) = \frac{g_{ij}}{s - \lambda_i} \quad (3.57d)$$

Choosing the control weightings, B , a priori, each eigenvalue can be placed using the multi-loop closure root locus equation:

$$\frac{1}{\tilde{a}_i} + \sum_{i=1}^m \frac{g_i^T g_i}{b_k (s^2 - \lambda_i^2)} = 0 \quad (3.58a)$$

This equation yields values of \tilde{a}_i which result in roots at $s = \pm \lambda_i$. The optimal modal weighting matrix can be written as follows:

$$\tilde{A} = \text{diag}\{\tilde{a}_i\} \quad i=1,n \quad (3.58b)$$

and a corresponding optimal state feedback control problem can be solved for the feedback gains in terms of the original state variables:

$$J(\mathbf{x}, \mathbf{u}) = \min_{\mathbf{u}(t)} \frac{1}{2} \int_0^{\infty} [\mathbf{x}^T (\mathbf{T}^{-T} \tilde{A} \mathbf{T}^{-1}) \mathbf{x} + \mathbf{u}^T \mathbf{B} \mathbf{u}] dt \quad (3.58c)$$

where the state weighting matrix, $(\mathbf{T}^{-T} \tilde{A} \mathbf{T}^{-1})$, is not necessarily diagonal.

3.3.3 Modal Sensitivities [52]

An alternative to root square locus analysis exists for the development of an acceptable set of cost function weightings. This procedure is also attractive because it utilizes the model decomposition of the Euler-Lagrange system in the control gain calculation described in Section 3.2. This decomposition is repeated as follows:

$$H\mathcal{T} = \mathcal{T}\Lambda \quad (3.59)$$

where the similarity transformation \mathcal{T} consists of columns of eigenvectors of H , and Λ is a $2n \times 2n$ diagonal matrix of eigenvalues of H . Both \mathcal{T} and Λ contain complex elements. The LHP elements of Λ are the eigenvalues of the controlled system. Differentiation of Eq. (3.59) with respect to any element, θ , of H (i.e., elements of F , G , A , B , H , D , etc.) yields the following expression for the closed-loop eigenvalue sensitivity:

$$\frac{\partial H}{\partial \theta} \mathcal{T} = \mathcal{T} \frac{\partial \Lambda}{\partial \theta} \quad (3.60)$$

$$\frac{\partial H}{\partial \theta} = \mathcal{T} \text{diag}(\partial \lambda_i / \partial \theta) \mathcal{T}^{-1} \quad (3.61)$$

The sensitivity matrix, $\partial H / \partial \theta$, contains mostly zeroes and ones, depending on the element chosen as the independent variable. Calculation in Eq. (3.61) is then easily carried out in unison with the computation of the optimal control laws for elements of the state and control weighting matrices, A and B . The sensitivity of the eigenvalues is normally expressed as follows:

$$s_{\theta}^i = \frac{\partial \lambda_i}{\partial \theta_i / \theta_i} \quad (3.62)$$

where S_{θ}^i is a complex vector describing the magnitude and direction of closed-loop eigenvalue movement for a change in weighting element θ_i . Selecting weights to satisfy eigenvalue location requirements (e.g., frequency and damping) is systematic and efficient using the procedure. A discussion of an algorithm using only real arithmetic is included in Appendix A.

3.4 TECHNIQUES FOR AUGMENTING THE PERFORMANCE INDEX

The techniques described in Section 3.3 allow the designer to obtain a set of weightings in the performance index which satisfy the controls criteria. Sometimes, a given form of the performance index will not produce control inputs which are satisfactory for any set of weightings. In this case, the specific nature of the problem can be analyzed and an appropriate modification to the structure of the performance index made to accommodate the expanded criteria. A group of the procedures are described below.

3.4.1 Weights on Control Rates and Acceleration

Occasionally, an actuator will have a small rate saturation characteristic or a low bandwidth relative to the control system response so that the regulator will produce commands which cannot be accurately followed. This situation causes unsatisfactory and even unstable behavior. Similarly, force limited actuators have acceleration saturation which prevents acceptable response.

A cost functional can be written which explicitly weights actuator rates and acceleration as shown below [42]:

$$J = \frac{1}{2} \int_{t_0}^{t_f} (x^T A x + u^T B_0 u + \dot{u}^T B_1 \dot{u} + \ddot{u}^T B_2 \ddot{u}) dt \quad (3.63)$$

AD-A052 420

SYSTEMS CONTROL INC PALO ALTO CALIF AERONAUTICAL AND--ETC F/G 21/5
F100 MULTIVARIABLE CONTROL SYNTHESIS PROGRAM. VOLUME 1. DEVELOP--ETC(U)
JUN 77 R L DE HOFF, W E HALL, R J ADAMS F33615-75-C-2053

UNCLASSIFIED

AFAPL-TR-77-35-VOL-1

NL

2 OF 4

AD
A052420

[illegible]

This procedure is equivalent to formulating a new, augmented design model with the control deflections, deflection rates as additional states, and the control acceleration as the control variable.

To find the control that minimizes the new cost functional, a "new" control, $\mu = \ddot{u}$, is defined. The system state equation augmented by $u(t)$ and $\dot{u}(t)$ is as follows:

$$\dot{\chi}_a(t) = F_a(t) \chi_a(t) + G_a \mu(t) \quad (3.64)$$

where

$$\chi_a = \text{col}[x, u, \dot{u}]$$

and

$$F_a = \begin{bmatrix} F & G & 0 \\ 0 & 0 & I \\ 0 & 0 & 0 \end{bmatrix}; \quad G_a = \begin{bmatrix} 0 \\ 0 \\ I \end{bmatrix} \quad (3.65)$$

The optimal regulator law derived for Eqs. (3.65) and (3.63) is as follows:

$$\mu = C_x x + C_u u + C_{\dot{u}} \dot{u} \quad (3.66)$$

or

$$\ddot{u} - C_{\dot{u}} \dot{u} - C_u u = C_x x \quad (3.67)$$

Equation (3.67) describes a multivariable filter for the control command which limits rate and acceleration inputs to the actuator. Schematically, the implementation of the vector control law is shown in Figure 3.2.

3.4.2 Control Actuator Models

Often, actuators demonstrate bandlimited behavior within the frequency range of interest. Techniques demonstrated in Section 3.4.1 can be utilized to accommodate such situations.

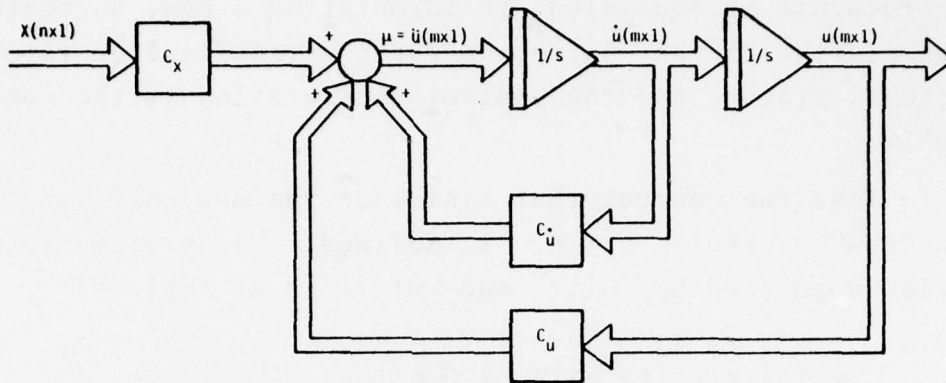


Figure 3.2 Command Filter for Rate and Acceleration Limited Actuators

Occasionally, direct measurements of the control deflection are available. For example, in the case of a servo-mechanism, feedback of actuator position in the servo loop might be in a form (e.g., an electronic signal) directly compatible with the controller. This situation eliminates the need for dynamic control elements and simplifies the physical implementation. A more detailed model of the actuator can be included in the design model without the necessity of additional implementation complexity (e.g., the command filter).

Typically, actuators can be modeled as follows:

$$\dot{u} = F_A u + G_A w \quad (3.68)$$

where F_A and G_A describe the linearized internal dynamics of the control actuator and u and w are internal actuator states and inputs, respectively.

The augmented design model becomes the following:

$$\frac{d}{dt} \begin{bmatrix} x \\ u \end{bmatrix} = \begin{bmatrix} F & G \\ 0 & F_A \end{bmatrix} \begin{bmatrix} x \\ u \end{bmatrix} + \begin{bmatrix} 0 \\ G_A \end{bmatrix} w \quad (3.69)$$

and the performance index is written as follows:

$$J = \int_{t_0}^{t_f} \left\{ [x^T \ u^T] \begin{bmatrix} A_1 & 0 \\ 0 & A_2 \end{bmatrix} \begin{bmatrix} x \\ u \end{bmatrix} + w^T B w \right\} dt \quad (3.70)$$

The optimal control law is written (and implemented) as follows:

$$w = C_x x + C_u u \quad (3.71)$$

where the control deflection, u , is directly measured. Figure 3.3 shows this system schematically.

The use of measured control deflections in the multivariable control law is beneficial only when actuator dynamics are significant in the bandwidth of control action. In this case, the direct feedback provides useful damping or lead in the control law.

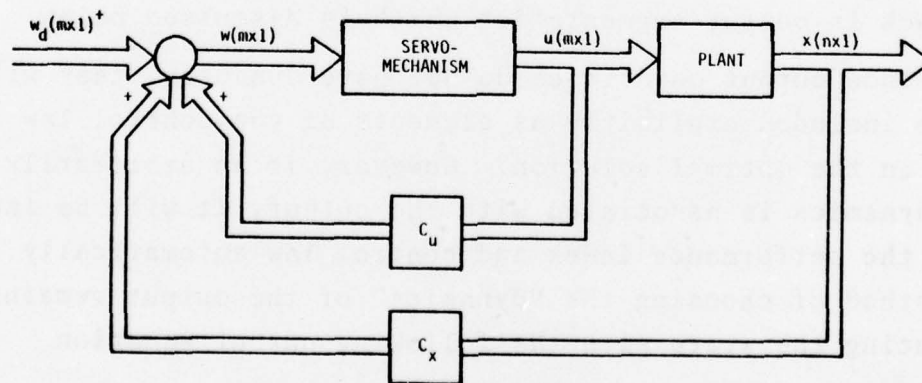


Figure 3.3 Controller Structure with Measured Actuator Inputs

3.4.3 Output Augmentation

Occasionally, an output parameter of the system is available as a convenient measurement (i.e., a high bandwidth, low noise signal), and various transient control criteria are expressed in terms of this output variable. For this reason, it could be desirable to include the variable as an explicit element of the cost functional and the control law. The reasoning behind the latter is twofold. First, by explicitly including the output, model parameter uncertainties do not affect the accuracy of the control law; i.e., there is an explicit loop "around" this variable. Since this variable is statically related to the other states, random errors associated with set point specification (described in Chapter IV) which cause the state vector to hang-off from its desired value can be reduced on the average by the inclusion of this added element.

The output feedback optimization problem can be solved using a direct numerical optimization algorithm. The resulting control law feedbacks lack only the system outputs in the regulator logic. There are no closed form solutions as in the state feedback formulation. It is known that output feedback cost functionals can be multi-modal and pose difficult numerical problems in their solution. An alternative to full output feedback is output augmentation which is discussed below.

Since output quantities do not have dynamics, they will not be included explicitly as elements of the control law given in the optimal solution. However, if an arbitrarily fast dynamics is associated with the output, it will be included in the performance index and control law automatically. The method of choosing the "dynamics" of the output remains. Augmenting the state with the following output equation

$$\dot{y} = -\lambda(y - h^T x - d^T u) \quad (3.72)$$

will cause the optimization to assign a gain to y in the control law and the following properties will hold if λ is large enough (relative to the time constants of F):

- (1) The dominant closed-loop dynamics of the system are independent of the value of λ .
- (2) The only weight in the performance index which affects the closed-loop root associated with the open-loop root $s = -\lambda$ is the weighting on y .

Thus, the precise choice of λ will not affect the gains associated with the other elements of the state vector and the particular output variable can be weighted directly.

3.5 TECHNIQUES FOR INTEGRAL CONTROL SYNTHESIS

Often a system must be designed to be insensitive to uncertainties in the knowledge of the dynamic behavior of the system and the disturbance acting upon it. The classical solution to the "high d.c. gain" requirement involves either lag compensation or integral control. Multivariable control techniques to accomplish this purpose are discussed below.

In general, a model for the response of a linear or linearized system is as follows:

$$\dot{x} = Fx + Gu + \Gamma w \quad (3.73)$$

$$y = Hx + Du$$

where Γ and w represent the effects of disturbances and equilibrium point mismatches.

Very often, physical specifications for steady-state can be written as follows:

$$y_{SP} = Hx_{SS} + Du_{SP} \quad t \rightarrow \infty \quad (3.74)$$

where the set point vector, y_{sp} , describes the point in state space, x_{ss} , which must be reached exactly for a given input, u_{sp} , and without knowledge of disturbances.

For the system (3.73) with the control law given by the following:

$$u = C_x x, \quad (3.75)$$

the steady state of the system can be written

$$x_{ss} = -(F + GC_x)^{-1} \Gamma w_{ss} \quad (3.76)$$

$$u_{ss} = C_x x_{ss} \quad (3.77)$$

$$y_{ss} = (H + DC_x) x_{ss} \quad (3.78)$$

Thus, using the state feedback law in Eq. (3.75) is unacceptable with regard to the requirements, Eq. (3.74), for an arbitrary constant disturbance because, in general, $y_{ss} \neq y_{sp}$ for all w_{ss} .

For example, in a scalar system, i.e., $n = m = p = 1$, a compensation network of the form

$$\frac{x(s)}{u(s)} = \frac{\tau_L s + 1}{\alpha \tau_L s + 1} \quad 0 < \alpha < 1 \quad (3.79)$$

produces a steady-state output to a constant disturbance as follows:

$$y_{ss} \propto \alpha \Gamma w_{ss}. \quad (3.80)$$

Thus, $y_{ss} \rightarrow 0$ as $\alpha \rightarrow 0$ and the system becomes insensitive to disturbances. Usually, τ_L can be made large enough, compared to the dominant dynamics, so that they are unaffected

by the phase lag associated with the compensation in Eq. (3.79). This procedure satisfies the steady-state requirements in single-loop systems with simple networks which are designed from a spectrally decoupled model, i.e.,

$$\frac{1}{\tau_L} \ll \omega_{CL} \quad (3.81)$$

The solution to steady-state hang-off problems in multi-variable systems can be formulated from a similar construction [49,53]. Define p set point quantities from Eq. (3.74) to be integrated outputs as follows:

$$\dot{b} = Hx + Du - y_{SP} \quad (3.82)$$

The control law designed for state equations (3.73) and (3.82) would have the following form [48]:

$$u = C_x x + C_b (b - y_{SP}) \quad (3.83)$$

In steady-state, $\dot{b} = 0$ and from Eq. (3.82), the design criteria, Eq. (3.74), would be satisfied. This conclusion is valid for any F , G , H , D , C_x , and C_b as long as the resulting system is stable.

3.5.1 Optimal Control with State Augmentation

From the discussion above, the linear optimal control solution for the augmented state equations may be written directly as follows

$$\begin{bmatrix} \dot{x} \\ \dot{b} \end{bmatrix} = \begin{bmatrix} F & 0 & x \\ H & 0 & b \end{bmatrix} + \begin{bmatrix} G \\ D \end{bmatrix} u - \begin{bmatrix} 0 \\ y_{SP} \end{bmatrix} \quad (3.84)$$

$$x(t_0) = x_0 \quad (3.85)$$

$$b(t_0) = b_0 \quad (3.86)$$

$$J = \frac{1}{2} \int_{t_0}^{t_f} (x^T A_1 x + b^T A_2 b + u^T B u) dt \quad (3.87)$$

The problem can be solved using the eigenvector decomposition technique discussed in Section 3.2 and the resulting control law, yielding a strictly stable closed-loop system, is

$$u = C_x x + C_b (b - y_{SP}) \quad (3.88)$$

The control law may be written in terms of a measured output quantity, y , as follows:

$$u = C_x x + \int_{t_0}^t C_b (y - y_{SP}) dt \quad (3.89)$$

The optimization problem is completely solved except for the choice of the initial conditions on the p integrators in Eq. (3.89). These are determined from the system initial conditions to produce the minimum cost on Eq. (3.87) [49].

The choice of weightings on the integrated state affects the closed-loop system roots. An initial choice of weights on b can be selected using Bryson's procedure:

$$a_{2ii} = \frac{1}{(\tau_C y_i)^2} \quad (3.90)$$

where τ_C is the time allowed to bring a nominal steady-state offset, y_i , to zero. Iterative techniques are almost always required to obtain satisfactory response since the state

augmentation procedure produces highly coupled, higher-order systems. The higher-order dynamic interactions can cause more sensitive regulator designs.

For modest uncertainties in the F , G , H and D parameters, the optimal controller, Eq. (3.89), will be stable and the steady-state requirements will be met exactly.

Several methods exist which more closely parallel classical loop gain modification. These procedures do not burden the designer with high-order regulator synthesis problems on large systems, and allow a degree of insight into the physical character of the problem. The optimality of the resulting system with regard to a particular performance index is relaxed in favor of more intuitive and subjective criteria of the closed-loop behavior.

3.5.2 Disturbance Estimation [49]

A method of accommodating disturbances directly into the synthesis procedure is presented below. Given a linear system model with a Γ matrix of known form and a set of p output quantities which must be held at predetermined values in the presence of the unknown, constant disturbance, w , the system equilibrium can be written as follows:

$$Fx_{SS} + Gu_{SS} + \Gamma w = 0 \quad (3.91)$$

$$Hx_{SS} + Du_{SS} - y_{SP} = 0 \quad (3.92)$$

where x_{SS} and u_{SS} are $(n+p)$ unknown quantities. Assuming w is known, the solution to Eqs. (3.91) and (3.92) is as follows:

$$\begin{bmatrix} x_{SS} \\ u_{SS} \end{bmatrix} = \begin{bmatrix} M_{xw} & M_{xy} \\ M_{uw} & M_{uy} \end{bmatrix} \begin{bmatrix} -\Gamma w \\ y_{SP} \end{bmatrix} \quad (3.93)$$

where M_{xw} , M_{xy} , M_{uw} , and M_{uy} are determined in one of the following ways depending on the conditions and dimensions of the problem:

- (1) For $p = m$, it may be possible to directly invert the system of equations, or:

$$\begin{bmatrix} M_{xw} & M_{wy} \\ M_{uw} & M_{uy} \end{bmatrix} = \begin{bmatrix} F & G \\ T & D \end{bmatrix}^{-1} \quad (3.94)$$

- (2) For $p < m$ or if direct solution in (1) is not possible, solve

$$J = \min_{x_{SS}, u_{SS}} (x_{SS}^T A x_{SS} + u_{SS}^T B u_{SS})$$

subject to Eqs. (3.91) and (3.92) where A and B are chosen to weight state hang-offs and control usage in steady-state.

- (3) For $p > m$, in general, there is no solution but rank deficient static equations can yield the type of problem in (1) or (2).

Assuming that the steady-state control or state vector, x_{SS} and u_{SS} , is determined from the above equation, the control law can be written as follows:

$$u = u_{SS} + C_x(x - x_{SS}) \quad (3.95)$$

or

$$u = + C_x x + C_y y_{SP} + C_w w \quad (3.96)$$

where

$$C_y = M_{uy} - C_x M_{xy} \quad (3.97)$$

$$C_w = -(M_{uw} - C_x M_{xw}) \Gamma \quad (3.98)$$

Since the disturbances, w , appear in the control law, implementation of Eq. (3.96) will use an estimate of w constructed as follows:

$$\dot{\hat{w}} = K[(Fx + Gu + \Gamma w) - \dot{x}] \quad (3.99)$$

where a stable filter results when K is chosen such that roots of

$$\det[sI - k] = 0 \quad (3.100)$$

are all LHP. The form of Eq. (3.99) is identical to the reduced order observer form discussed in Section 4.7. This modification allows implementation of Eq. (3.99) in a form without differentiation. In steady-state,

$$\hat{w} \rightarrow w \quad t \rightarrow \infty \quad (3.101)$$

and

$$y \rightarrow y_{SP} \quad t \rightarrow \infty \quad (3.102)$$

from Eq. (3.93). The implementation produces the modification to Eq. (3.96) as follows:

$$u = C_x x + C_y y_{SP} + C_w \hat{w} \quad (3.103)$$

Alternate formulation of this result ties together standard integral control and disturbance estimation. Insight into deviations in the output caused by equilibrium point matching errors can be gained.

Consider the control law Eq. (3.95) written as follows:

$$u = C_x x + C_b b(t) \quad (3.104)$$

where C_x is designed using linear optimal control synthesis without regard for the integral control structures. The (px1)

vector, b , and the (mxp) feedback matrix, C_b , will be derived below.

In steady-state, substituting Eq. (3.104) into Eqs. (3.76)-(3.78), the following is obtained:

$$y_{SS} = -(H + DC_x)(F + GC_x)^{-1}[GC_b b_o + \Gamma x] + DC_b b_o \quad (3.105)$$

$$= [\bar{H}G + D]C_b b_o + \bar{H} \Gamma w \quad (3.106)$$

where

$$\bar{H} = -(H - DC_x)(F + GC_x)^{-1} \quad (3.107)$$

$$b_o = b(\infty) \quad (3.108)$$

If b_o and C_b are chosen as follows,

$$b_o = y_{SP} - \bar{H} \Gamma w \quad (3.109)$$

and

$$(\bar{H}G + D)C_b = I \quad (3.110)$$

then

$$y_{SS} = y_{SP} \quad (3.111)$$

Since w is not known, b_o is not known. An estimate of b_o can be derived as follows:

$$b_o = y_{SP} - y_w \quad (3.112)$$

$$\dot{y}_w = 0 \quad (3.113)$$

$$\dot{\hat{y}}_w = K(y_w - \hat{y}_w) \quad (3.114)$$

or,

$$\dot{\hat{y}}_w = K[\bar{H}(\dot{x} - Fx - Gu) - \hat{y}_w] \quad (3.115)$$

where \hat{y}_w has the interpretation of the hang-off due to the constant disturbance which would occur if there was no integral control. Since the estimator is essentially predicting a constant value from transient information, Eq. (3.113) is justified.

Equation (3.115) is a reduced order estimator and implementation without differentiation is discussed in Chapter IV. The requirements for stability are that the matrix K be chosen as positive definite, in which case,

$$\dot{\hat{y}}_w \rightarrow y_w \quad (3.116)$$

$$\dot{\hat{y}}_w = 0 \quad (3.117)$$

$$b_o \rightarrow y_{SP} - \bar{H} \Gamma w \quad (3.118)$$

An equivalent form of Eq. (3.115) can be calculated by

$$\dot{v} = (Hx + Du - y_{SP}) \quad (3.119)$$

$$u = \bar{C}_x x + C_b (y_d - Kv) \quad (3.120)$$

$$\bar{C}_x = C_x + C_b K\bar{H} \quad (3.121)$$

An examination of the closed-loop dynamics of the following system shows that the $(n+p)$ roots are the roots of the $(sI - F - GC_x)$ system and the roots of the estimator $(sI - K)$. Thus, the design procedure for integral compensation is truly decoupled. Initially, a transient regulator is designed, i.e., C_x is calculated. The estimator is derived using Eq. (3.120) and a set of integral gains, C_b and K are calculated. The closed-loop control law governing the system is implemented according to Eq. (3.121). Notice that the state feedback term, C_x , has been modified by an additional proportional component of the control law. The modification to the state feedback counteracts for the dynamic interaction of the integral and plant states and maintains the regulator eigensystem of the original form.

The advantage of the control law shown in Eq. (3.121) is that it allows mode switching from one group of set point quantities to another without modification of the regulator dynamics. In this case, the processor implementation must store a $m(n+2p)$ quantities for each possible set point vector. In some applications, e.g., autopilot modes, this does not represent a problem.

An additional consideration in the design utilizing this method is that the character of the disturbance must be known. It was shown that even in the presence of uncertainty in the parameters, Γ , G , and F , that the system will reach the desired set point. In some nonlinear physical systems, the largest "disturbance" to the equilibrium is the non-equilibrium "force" due to set point mis-specification within the control itself. Such disturbances are dependent on the system control law. An alternative formulation is presented below.

3.5.3 Spectral Decoupling Techniques

The procedure of fully augmented linear quadratic regulator design does not allow direct control over the eigensystem of the $(n+p)$ th order closed-loop system. In the disturbance estimation method, the eigenvalues of the n th order and p th order system can be determined independently and the resulting eigensystem is determined exactly. The classical single-loop compensation procedure discussed above utilizes a frequency decoupling approach using only the closed-loop d.c. gain and cross-over frequency to determine the lag or integral compensation gain. A procedure using this philosophy along with multivariable techniques is described below.

Consider the control law form given in Eq. (3.103) and again below with C_x designed from transient criteria using linear optimal regulator synthesis:

$$u = C_x x + C_b b \quad (3.122)$$

If,

$$\dot{b} = [y_{SP} - (y_{SP})_m] \quad (3.123)$$

and the system is stable, then the steady-state is,

$$y_{SP} = (y_{SP})_m \quad (3.124)$$

and the control criteria is satisfied. Along with Eq. (3.124), the transient criteria used to design C_x above should not be violated by the augmented system. However, the precise location of the eigensystem given by the unaugmented design does not necessarily have to remain unchanged. It is desired that the integral trim dynamics be spectrally decoupled from the transient dynamics. The last specification is critical to realizing the simplicity of the procedure and is philosophically identical to the assumptions used to design lag compensation in classical synthesis.

If it is assumed that the states are in equilibrium in the time frame of integral action, the following relation is nearly true,

$$\dot{x} \approx 0 \quad (3.125)$$

and it follows that

$$y_{SS} = [-(H - DC_x)(F + GC_x)^{-1}G + D]C_b b_o \quad (3.126)$$

$$= H^*C_b b_o \quad (3.127)$$

where the disturbances have not been included since their magnitude and structure is assumed unknown.

The deviation of the set point can be written as follows:

$$\delta y = y_{SS} - y_{SP} \quad (3.128)$$

$$= H^*C_b(b - b_{SP}) \quad (3.129)$$

where

$$H^*C_b b_{SP} = y_{SP} \quad (3.130)$$

The dynamics of the integral system, from Eq. (3.123), is as follows:

$$\dot{b} = \delta y \quad (3.131)$$

$$= H^*C_b b \quad (3.132)$$

and in steady-state,

$$\dot{b} = 0 \quad (3.133)$$

and

$$y_{SP} = y_{SS} \quad (3.134)$$

The procedure described above is identical to the disturbance estimation at this point and a reduced order observer could be designed for δy as described in Section 3.5.2. The corresponding integral gain matrix C_b and an augmented proportional gain matrix, \bar{C}_x , could be calculated in order to maintain unchanged transient root locations. This procedure results in a complex implementation if many set point vectors, δy , are possible for a given system.

Considering the dynamics in Eqs. (3.73) and (3.131) (with $D = 0$), the closed characteristic equation is as follows:

$$\Delta(s) = \det \begin{bmatrix} sI - F_{CL} & -GC_b \\ -H & sI \end{bmatrix} = 0 \quad (3.135)$$

where $F_{CL} = F + GC_x$ is the system matrix with only the transient gains. Expanding Eq. (3.135), the characteristic equation can be factored as follows:

$$\det(sI_n - EF_{CL}) \det(sI_p - H(FE)^{-1}GC_b) = 0 \quad (3.136)$$

where

$$E = I + \Sigma \quad (3.137)$$

and

$$\Sigma = F^{-2}G C_b H \quad (3.138)$$

Considering a consistent matrix norm for Σ ,

$$||\Sigma|| < |1/\lambda_{CL_{\min}}| ||HF^{-1}GC_b|| \quad (3.139)$$

$$||\Sigma|| < |1/\lambda_{CL_{\min}}| |\lambda_{INT_{\max}}| \quad (3.140)$$

where $\lambda_{CL_{\min}}$ is the smallest transient eigenvalue of F_{CL} and $\lambda_{INT_{\max}}$ is the largest eigenvalue of the system

$$\dot{b} = (HF^{-1}GC_b)b \quad (3.141)$$

If

$$||\Sigma|| \ll 1 \quad (3.142)$$

then

$$E \approx I \quad (3.143)$$

and the roots of the transient and integral system are spectrally decoupled. In this case, Eq. (3.136) has the convenient form

$$\det(sI_n - F_{CL}) \det(sI_p - HF^{-1}GC_b) = 0 \quad (3.144)$$

The design process under assumption (3.142) can be separated into two portions: transient design using the unaugmented system, (3.73), and the integral design using Eq. (3.131). It must be recalled that the exact root locations of the full system given in Eq. (3.135) will be altered from the locations in the separate designs. However, if eigenvalues in the integral system are chosen slower than the transient system, dynamic decoupling will be approximately maintained.

The integral control design uses a system of the following form:

$$\dot{b} = H^*u \quad (3.145)$$

where H^* is given in Eq. (3.130). It is possible to use regulator synthesis directly on Eq. (3.145) with the cost functional,

$$J = \frac{1}{2} \int_{t_0}^{t_f} (b^T A b + u^T B u) dt \quad (3.146)$$

The characteristic equation of the Euler-Lagrange system is as follows:

$$\det \begin{bmatrix} sI & H^*B^{-1}H^{*T} \\ A & sI \end{bmatrix} = 0 \quad (3.147)$$

or

$$\det(s^2 I - H^* B^{-1} H^{*T} A) = 0 \quad (3.148)$$

which can be factored as follows:

$$\det(sI - P) \det(sI + P) = 0$$

where P is a positive definite matrix of rank q and

$$q = \max[\text{rank}(A), \text{rank}(H^* B^{-1} H^{*T})]$$

Normally, A will be chosen as positive definite, and $m = p$.
In this case, if

$$\text{rank}(H^* B^{-1} H^{*T}) = m,$$

then the eigenvalues of the closed-loop system are the negative square roots of the eigenvalues of the positive definite (mxm) matrix, $H^* B^{-1} H^{*T} A$. Typically, A and B can be chosen to produce acceptable integral transient response with a cut-and-try procedure analogous to Bryson's rule. The resulting closed-loop trim roots should maintain the separation specified in Eq. (3.140).

Alternately, a more systematic approach for optimal pole placement can be found using a modal decomposition of Eq. (3.145) assuming a full rank system:

$$z = Tb \quad (3.149)$$

$$\bar{u} = Tu$$

and

$$\dot{z} = \Lambda u \quad (3.150)$$

where

$$H^*T = TA \quad (3.151)$$

The system in Eq. (3.150) can be independently designed on a mode-for-mode basis, as will be shown below. The resulting optimal control law is then

$$\bar{u} = C_z z \quad (3.152)$$

where

$$C_z = \text{diag}(C_{z_1}, \dots, C_{z_n}) \quad (3.153)$$

or

$$u = C_b b \quad (3.154)$$

where

$$C_b = T^{-1} C_z T \quad (3.155)$$

A control weighting matrix B can be chosen to reflect the mix of control action desired for the trim function. Defining,

$$H^*B^{-1}H^*T = \bar{B} \quad (3.156)$$

the closed-loop squared dynamics matrix of Eq. (3.148) can be written in diagonal form:

$$\bar{B}T = TA \quad (3.157)$$

where

$$A = \text{diag}(a_i) \quad , \quad i=1, \dots, p.$$

Using Eq. (3.156), the values of A can be chosen to place the squared eigenvalues of the system at a desired location (e.g., from a transient response criteria) keeping the assumption in Eq. (3.140) true. Then, given A and B , the procedures of

optimal regulator synthesis can be used to calculate the trim gain matrix C_b .

A useful result can be derived for the case of a multi-input, single output or output modal coordinate system. Let

$$\dot{b} = gu \quad (3.158)$$

where b is a scalar and g is $1 \times m$. If the control weights, B_i , are chosen to determine the mix of control authority used to trim the error term, b , and the trim root is chosen to lie at

$$s = -\lambda_T \quad (3.159)$$

then

$$C_b = S \begin{bmatrix} g_1/b_1 \\ \vdots \\ g_m/b_m \end{bmatrix} \quad (3.160)$$

and

$$S = \lambda_T [g_1^2/b_1 + \dots + g_m^2/b_m]^{-1} \quad (3.161)$$

Techniques have been described to design controllers for spectrally decoupled systems defined as integrations of outputs shown in Eq. (3.145). The procedure stresses the decoupled assumptions important to satisfactory closed-loop behavior and use linear quadratic regulator theory as the foundation of the multivariable designs.

Phenomena such as set point switching, control saturation and unsaturation lead to slight modifications of the above procedures. Also, simplification of the gains for practical application must be considered. These topics will be discussed in detail in Chapter IV.

3.6 SYSTEM PARAMETER INSENSITIVITY

3.6.1 Important Considerations

A controller is implemented on a physical system for two reasons. First, steady-state requirements, namely operator inputs and environmental disturbances, must be interpreted as actuator commands to bring the operating point of the system to a satisfactory location so that the expected system outputs result. Secondly, the transitions caused by inputs and disturbances must be dynamically accommodated in a well-behaved manner. Modification of the system dynamics by the control law is required only for the second task. The first can be accomplished with open-loop trajectories and slow integral trim action. The sensitivity of the system to dynamic parameter variations is intimately tied to the amount of dynamic interaction necessary to produce the desired response.

For example, if a closed-loop controller is designed for a simple first order system and the required closed-loop time constant is τ_c , then the control is given as follows:

$$\text{plant:} \quad \dot{x} = -ax + gu \quad (3.162)$$

$$\text{control:} \quad u = Cx \quad (3.163)$$

$$\text{closed-loop:} \quad \dot{x} = -(1/\tau_c)x \quad (3.164)$$

$$\text{gain:} \quad c = 1/g (1/\tau_c - a) \quad (3.165)$$

Clearly, if $a = +1$ and $\tau_c = 100$, then only a small variation in g results in significant variation of the closed-loop dynamics; however, if $\tau_c = 1$, then there is no effect of variation of the parameter, g . Philosophically, systems are less sensitive to parameter uncertainties when the closed-loop and open-loop root locations are fairly close.

This is not always possible or desirable. In these cases, it is advantageous to include parameter sensitivities directly in the synthesis procedure to account for these effects.

3.6.2 Modal Sensitivities

Many procedures exist for evaluating parameter sensitivity of regulator designs. Several will be discussed below ranging from simple verification procedures to complex computer algorithmic exercises. The amount of modification of the dynamics required by an individual system is a measure of the sophistication of the technique required.

The sensitivity of the closed-loop root locations to model parameters is directly calculated from the modal decomposition of the closed-loop system (see Appendix A):

$$F_{CL} = F + GC \quad (3.166)$$

$$F_{CL}^T = T \Lambda_{CL} \quad (3.167)$$

$$\frac{\partial \Lambda_{CL}}{\partial \theta} = T^{-1} \frac{\partial F_{CL}}{\partial \theta} T \quad (3.168)$$

where θ is a parameter in the F or G matrix,

$$\frac{\partial \Lambda_{CL}}{\partial \theta} = \text{diag} \left[\frac{\partial \lambda_i}{\partial \theta} \right] \quad i=1,n \quad (3.169)$$

and λ_i are the closed-loop root locations. It is quite straightforward to evaluate the effect (to first order) of system parameter variations on the closed-loop roots.

The sensitivity to plant parameter variations is defined as follows:

$$S_{\theta}^i = \frac{\partial \lambda_i}{\partial \theta / \theta} \quad (3.170)$$

In general, typical values of uncertainty can be attached to the knowledge of the system parameters and the eigenvalue shifts can be evaluated. If large scale shifts are found to cause system response which fails to meet the transient criteria, the controller should be redesigned using more control weight or a modified state weighting matrix. Other techniques are available to produce insensitive controllers directly from the regulator design with cumbersome iterations. The computation overhead required by these procedures is justified only if significant plant parameter variation is expected.

3.6.3 Techniques for Insensitive Controls

There are several formal procedures for incorporating the uncertainty or variability of plant parameters into the control synthesis procedure and structure. A short discussion of these techniques is presented below.

Explicit Parameterization [54]

If parameters are variable or uncertain, they may be included as additional states with dynamics corresponding to the approximate correlation function of the parameter uncertainty. The nonlinear plant dynamics are as follows:

$$\dot{x} = f(x, u, \theta) \quad (3.171)$$

For linearizations of states, controls, and parameters, the perturbation form is as follows:

$$\delta \dot{x} = F \delta x + G \delta u + F_{\theta} \delta \theta \quad (3.172)$$

where

$$F_{\theta} = \partial f / \partial \theta \quad (3.173)$$

The dynamics of the parameter equations are

$$\delta \dot{\theta} = A \delta \theta + \Gamma w \quad (3.174)$$

where w is an assumed zero mean white noise and A is the dynamics of the time correlation of the $\delta \theta$ viewed as an equivalent stochastic process.

The dynamic equations in (3.172) and (3.174) form a state variable system in which the parameter uncertainty can be explicitly included. The regulator synthesis procedure can be carried out with the resulting control law:

$$\delta u = C_x \delta x + C_\theta \delta \theta \quad (3.175)$$

Since the parameter variations are not measured, they must be reconstructed from a suitable estimator.

Minimax and Multiplant Techniques [55]

It is assumed that for various regions of the system operating envelope, a single linear model adequately approximates the dynamic response. The variation of the response at operating points throughout this region can be viewed as parameter variations in the particular design model. There are two approaches to the design of a constant state feedback control for the entire linearization region. The minimax procedure minimizes the worst performance, and multiplant maximizes the average performance.

In the minimax formulation, the constant gain regulator is chosen to solve the following associated optimization problem:

$$J(t, \theta) = \frac{1}{2} \int_{t_0}^{t_f} [x^T(t, \theta) A x(t, \theta) + u^T(t, \theta) B u(t, \theta)] dt \quad (3.176)$$

$$J^* = \max_{\theta \in \Theta} \min_{C_x} J(t, \theta) \quad (3.177)$$

given that the control law is written as follows:

$$\delta u = C_x \delta x \quad (3.178)$$

where the system matrices are considered functions of external parameters, or

$$\dot{\delta x} = F(\theta) \delta x(t) + G(\theta) \delta u(t) \quad (3.179)$$

and

$$\theta \in \{\text{maximum range of parameter variation}\} \quad (3.180)$$

The computation requirements to perform the optimization can be significant for a relatively small number of states and parameters.

In the multiplant technique [55], a group of possible linear models for a particular design region are used simultaneously. These would correspond to various linearization points within a linearization region. The optimal control synthesis problem is to minimize the average cost associated with controlling each of the systems with a constant feedback gain. This can be written as follows:

$$M_i: \dot{\delta x} = F(\theta_i) \delta x + G(\theta_i) \delta u \quad i=1, N \quad (3.181)$$

$$J = \frac{1}{N} \sum_{i=1}^N J_i \quad (3.182)$$

$$J_i = \frac{1}{2} \int_{t_0}^{t_f} (\delta x^T A \delta x + \delta u^T B \delta u) dt \quad (3.183)$$

$$J^* = \min_{C_x} J \quad (3.184)$$

$$\delta u = C_x \delta x \quad (3.185)$$

The optimization is carried out numerically but for reasonably similar plant dynamics using a "close" starting point (e.g., an optimal regulator solution for one model), the convergence is rapid.

This method can be used to evaluate the linearization region. Suppose a linearization region is expanded to include another operating point. The optimal cost function for the multiplant system can be calculated for an arbitrary initial condition. If the minimum cost increases significantly with the inclusion of the extra operating point, it is due to the differing dynamic character of the linear model at the new operating condition compared to the average behavior at the other operating points. This criterion can be used to quantitatively determine appropriate regions of linearization where a single, average, linear model is suitable for design. This situation is shown in Figure 3.4.

There are several other techniques available to handle the parameter sensitivity problem (see Appendix A). In general, these techniques approximate the uncertainty in the system with an augmentation or modification of the optimization problem which produces a slightly different control law structure. The success of each method is markedly problem-dependent.

3.7 SIMPLIFICATION OF CONTROL LAWS

The state feedback matrices resulting from linear quadratic regulator designs contain $n \times m$ elements. The value of the performance index for a control law with fewer elements will always be larger than the minimum for full state feedback. Often, the increased cost associated with a smaller number of

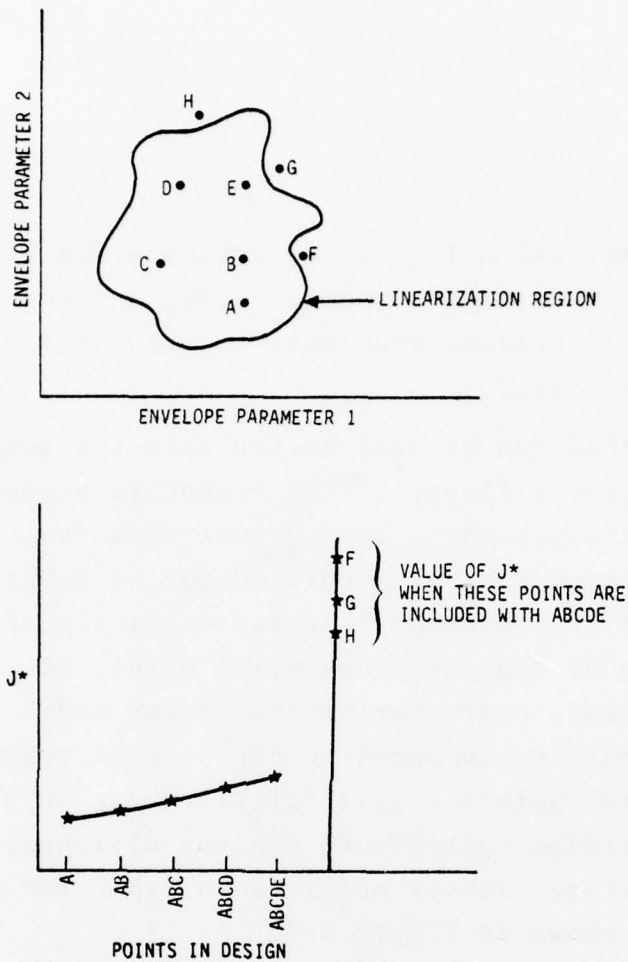


Figure 3.4 Illustration of Multiplant Technique in Determining Linearization Region Appropriate for a Single Design

gain elements produces a great savings in processor requirements. The savings in processor overhead obtained from gain matrix simplification can allow the freedom to utilize more sophisticated models which could not be ordinarily implemented in an unsimplified version. Various techniques for matrix reduction are discussed below which yield a slightly suboptimal, but minimally complex, implementation.

3.7.1 Sensitivity Calculations

The simplest procedure for gain matrix simplification is to use the sensitivity of the closed-loop eigensystem to changes in feedback gains. The closed-loop eigenvalues of the system are given by:

$$\det[sI - F - GC_x] = 0 \quad (3.186)$$

and reducing the closed-loop dynamics matrix to modal coordinates, sensitivity functions are calculated as follows:

$$F_{CL}^T = T\Lambda \quad (3.187)$$

and

$$\frac{\partial \Lambda}{\partial C_{ij}} = T^{-1} \frac{\partial F_{CL}}{\partial C_{ij}} T \quad (3.188)$$

where the derivative, $\partial F_{CL}/\partial C_{ij}$, is easily calculated. The derivative of the diagonal eigenvalue matrix can be written as follows:

$$\frac{\partial \Lambda}{\partial C_{ij}} = \text{diag}\{\partial \lambda_k / \partial C_{ij}\} \quad k = 1, \dots, n \quad (3.189)$$

The approximate change in the closed-loop roots due to the elimination of a gain element, is found as follows:

$$\Delta \lambda_k = (\partial \lambda_k / \partial C_{ij}) C_{ij} \quad (3.190)$$

The shift of the eigenvalue for the element of the gain matrix, C_{ij} , relative to the total shift caused by the feedback is given as follows:

$$s_{C_{ij}}^k = |\Delta \lambda_k| / |\lambda_k - \lambda_k(OL)| \quad (3.191)$$

where λ_k is the closed-loop eigenvalue, and $\lambda_k(OL)$ is the corresponding open-loop root location.

For a given gain matrix, it is possible to quickly calculate the n^2xm sensitivity values. A cumulative sensitivity can be calculated as the averaged effect of each gain element on the overall system dynamic response. This coefficient is defined as follows:

$$\tilde{S}_{ij} = \frac{1}{n} \sum_{k=1}^n S_{C_{ij}}^k \quad (3.192)$$

Using the nxm values of \tilde{S}_{ij} , the elements of the gain matrix can be ranked according to the net effect on the closed-loop system. A group of gains can typically be found which do not affect the closed-loop response. These gains can be eliminated from the system and the eigensystem will be only minimally affected.

The second factor determining the optimality of the response is the mode shapes associated with each eigenvalue. In general, for reasonably separated eigenvalues, if a gain has a small effect on the system time constant, then it will have a correspondingly small effect on the mode. The time response of the system with these gains eliminated will be nearly the same as the full state response. If this is the case, then the increase in the cost function will be small and the system will only be "slightly" suboptimal.

An alternative approach to the problem is to calculate the sensitivity of the optimal cost function exactly. This procedure is somewhat more time consuming. The optimal cost function corresponding to an initial condition is given below:

$$\dot{x} = (F + GC_x)x \quad x(0) = x_0 \quad (3.193)$$

$$J = \text{tr} \left[\int_0^{\infty} \varphi^T(t) (A + C_X^T B C_X) \varphi(t) dt \cdot X_0 \right] \quad (3.194)$$

where

$$X_0 = x_0 x_0^T \quad (3.195)$$

and

$$\varphi(t) = \exp[(F + G C_X)t] \quad (3.196)$$

There are several techniques for simplifying the expression in Eq. (3.194).

The change in the cost due to the elimination of a particular gain element can be directly calculated from the expression. This procedure eliminates the approximation due to the small perturbation assumption required in the linear sensitivity analysis. It also works well when the closed-loop eigenvalues are close together.

3.7.2 Fixed Structure Optimization [56]

Either of the two procedures described in Section 3.7.1 yield a gain matrix with several elements set to zero. This feedback structure yields less than optimal performance with respect to the given performance index. This degraded performance is reflected as an increase in the cost function for a set of initial conditions. However, the fixed structure controller also is not optimal. A secondary optimization procedure can be performed to find the elements of the fixed structure gain matrix which minimize the given cost function (see Appendix A).

3.8 DISCRETE OPTIMAL CONTROL PROBLEM

In the previous discussion, the continuous time solutions to the linear problem have been stressed. This was primarily for economy of notation. The discrete solution to the optimal

control problem is functionally identical to the continuous forms. As the sample interval becomes shorter, it will be shown that the behavior of the optimal discrete feedback system becomes identical to the continuous design [49].

3.8.1 Discrete Time Problem

The continuous time design model is as follows:

$$\dot{x} = Fx + Gu \quad (3.197)$$

$$y = Hx + Du \quad (3.198)$$

The solution to Eqs. (3.197) and (3.198) can be written as follows:

$$x(t) = \varphi(t)x(0) + \int_0^t \varphi(t-\tau) Gu(\tau) d\tau \quad (3.199)$$

$$y = Hx + Gu \quad (3.200)$$

where

$$\varphi(t) = \exp(Ft) \quad (3.201)$$

If the time function, $u(t)$, is sufficiently smooth, the time interval $[0, NT]$ can be broken down to equal intervals as follows:

$$[0, t] = [0, T, 2T, \dots, nT, \dots, NT] \quad (3.202)$$

where the control is approximately constant or

$$u(t) = u(nT) \quad nT \leq t < (n+1)T \quad (3.203)$$

and Eqs. (3.198) and (3.199) can be rewritten in the obvious manner,

$$x(n+1) = x(n) + \Gamma u(n) \quad (3.204)$$

$$y(n) = Hx(n) + Du(n) \quad (3.205)$$

where

$$x(n+1) = x[(n+1)T], \text{ etc.} \quad (3.206)$$

$$\varphi = \exp(FT) \quad (3.207)$$

or

$$\varphi = \sum_{j=0}^{\infty} \frac{1}{j!} F^j T^j \quad (3.208)$$

$$\Gamma = \int_0^T \varphi(\tau) d\tau G \quad (3.209)$$

or, substituting Eq. (3.208) into Eq. (3.209) yields the expansion:

$$\Gamma = \sum_{j=1}^{\infty} \frac{1}{j!} F^{j-1} T^j G \quad (3.210)$$

The variables, $x(n)$, represent the state at the discrete time instants when Eq. (3.203) is satisfied. Also, T can be made small enough that for any n and ϵ ,

$$|x_a(nT) - x_d(n)| < \epsilon$$

where x_a is the actual state vector at $t = nT$ and $x_d(n)$ is the state from Eq. (3.204).

The cost functional which was used to weight states and controls in the continuous problem is given below:

$$J = \frac{1}{2} \int_0^t [x^T(\tau) A x(\tau) + u^T(\tau) B u(\tau)] d\tau \quad (3.211)$$

Substituting Eqs. (3.204) in Eq. (3.209), the following holds:

$$J = \frac{1}{2} \sum_{i=1}^N [x^T(i) A_D x(i) + u^T(i) B_D u(i)] \quad (3.212)$$

where

$$A_D = \int_0^T \varphi^T(\tau) A \varphi(\tau) d\tau \quad (3.213)$$

and

$$B_D = TB + G^T \int_0^T \left[\int_0^t \varphi^T(\xi_1) d\xi_1 \right] A \left[\int_0^t \varphi(\xi_2) d\xi_2 \right] dt G \quad (3.214)$$

The discrete optimal control problem given by Eqs. (3.204) and (3.212) can be solved using dynamic programming [47] and the solution is given below for the steady-state regulator:

$$u(n) = C_D x(n) \quad (3.215)$$

$$C_D = (B + \Gamma^T S_D)^{-1} \Gamma^T S_D \Phi \quad (3.216)$$

where S_D is found as the steady-state solution to the following backward difference equation:

$$\begin{aligned} S(n) &= \Phi^T S(n+1) \Phi - \Phi^T S(n+1) \Gamma [B + \Gamma^T S(n+1) \Gamma]^{-1} \Gamma^T S(n+1) \Phi + A \\ S(\infty) &= 0 \end{aligned} \quad (3.217)$$

The form of the solution, Eq. (3.215), can be interpreted as state feedback where a constant feedback gain matrix is calculated in Eqs. (3.216) and (3.217).

It will be shown that for decreasing sampling interval,

$$C_D \rightarrow C \quad (3.218)$$

where C is the steady-state optimal regulator solution derived in Section 3.2; some guidelines will be given for evaluating this equivalence.

Considering the Taylor series expansion for the state transition matrix φ and defining $||\cdot||$ as any consistent matrix norm, the following relations hold:

$$\varphi(T) = \sum_{j=0}^{\infty} \frac{1}{j!} F^j T^j \quad (3.219)$$

and

$$||\varphi(T) - I - FT|| = ||\sum_{j=2}^{\infty} \frac{1}{j!} F^j T^j|| \quad (3.220)$$

$$\leq \sum_{j=2}^{\infty} \frac{1}{j!} T^j ||F||^j \quad (3.221)$$

$$\leq \exp(||F||T) - 1 - ||F||T \quad (3.222)$$

where Eq. (3.222) represents a bound on the norm of the matrix error taking two terms in the expansion for Φ . There are some matrix norms where

$$||F||T \leq |\lambda_{\max}(F)|T \quad (3.223)$$

and utilizing Eq. (3.223), the norm of the approximation error can be written as follows:

$$|\varphi - (I + FT)| \leq |e^{\alpha} - 1 - \alpha| \quad (3.224)$$

where

$$\alpha = |\lambda_{\max}(F)|T \quad (3.225)$$

In most control applications where a continuous approximation is used, the largest allowable value of α is taken as 0.10 and

$$e^{\alpha} - 1 - \alpha = 0.5\% \quad (3.226)$$

Under these conditions,

$$\varphi(T) \approx I + FT \quad (3.227)$$

Utilizing the same conditions for the expansion, i.e., keeping only terms up to FT , the following approximate formulas are evident:

$$\Gamma = GT \quad (3.228)$$

$$A_D \approx AT \quad (3.229)$$

$$B_D \approx BT \quad (3.230)$$

$$J = \frac{T}{2} \sum_{i=1}^N [x^T A x + u^T B u] \quad (3.231)$$

Substituting the relations in the optimal control solution yields,

$$C_D = B^{-1} G^T S_D \quad (3.232)$$

$$\begin{aligned} \frac{S_D(n) - S_D(n+1)}{T} = & S_D(n+1)F + F^T S_D(n+1) + A \\ & - S_D(n+1)GB^{-1}G^T S_D(n+1) \end{aligned} \quad (3.233)$$

In steady-state, the term on the left hand side of Eq. (3.233) is zero and the solution to the algebraic equation,

$$0 = F^T S_D + S_D F + A - S_D G B^{-1} G^T S_D \quad (3.234)$$

is identical to the steady-state solution of the Riccati equation in the continuous time problem, thus,

$$S_D = S \quad (3.235)$$

$$C_D = C \quad (3.236)$$

where the S and C matrices result from the continuous time solution.

The implication of the above results is important from a design point of view. If the processor capability exists to sample relatively quickly with regard to the time constants of the system as measured by the eigenvalues in Eq. (3.224), and if the closed-loop dynamics in the regulator do not violate Eq. (3.203), then the design can be carried out in the continuous domain and implemented directly in a discrete time form. This fact often allows the designer to work in the familiar frequency domain or S -plane using classical design evaluation techniques and measures (e.g., bandwidth and damping ratio). After a suitable design is developed, the state feedback gains can be directly implemented in the sampled data system.

The certainty equivalence principle used in separating controller and estimator designs is still valid for the discrete case. It is possible to utilize continuous design procedures for the regulator and implement the same feedback gains using a discrete estimator (if the time constant assumptions remain valid). The discrete filter design also formulates the solution as a difference equation directly implementable on the control processors (see Chapter IV).

3.9 SUMMARY

The design techniques for quadratic regulator synthesis have been presented which produce multivariable control laws for linear systems. The basic theoretical background has been summarized for regulator and follower forms which result in proportional state feedback systems. The choice of performance index has been presented for state weighting and for special cases of actuator modeling and output variable augmentation. Various methods for integral control design have been developed which can be implemented in a computationally feasible manner. Plant parameter sensitivity is discussed and procedures to synthesize minimally sensitive controls are reviewed. Finally, the equivalence of the discrete and continuous time formulations are presented and conditions allowing the implementation of continuous gains derived. These linear techniques are utilized in the design of the multivariable controller for the F100 engine. Chapter IV presents the development of a locally linear control synthesis procedure for nonlinear systems within which the techniques of this chapter are applicable.

CHAPTER IV

DESIGN METHODOLOGY FOR A MULTIVARIABLE CONTROLLER

4.1 OVERVIEW

The development of a multivariable control law for nonlinear systems requires many techniques in modeling and design. Locally linear control synthesis is presented below which uses linear quadratic regulator techniques to produce control laws for the complete operating envelope of a nonlinear system.

The synthesis procedure requires linear dynamical equations. Various techniques are presented to develop perturbational design models which contain an appropriate dynamic description of the behavior within a linear region. Extension of the locally linear models to control throughout the envelope requires some form of adaptivity to ambient conditions. Passive adaptivity is discussed in Section 4.4. An operational requirement is to control transitions from one operating point to another. An implementable technique for feedforward synthesis of trajectories is presented. Physical constraints on the system often determine the operating point. These constraints depend on the region of the envelope. A technique of variable structure integral trim is presented to accommodate the set point requirement.

Exact knowledge of the system states has been assumed in Chapter III. Several procedures for compensating sensor signals to more accurately represent the actual state are presented.

Together, these procedures integrate locally linear regulator designs into a control capable of functioning continuously throughout the operating envelope while satisfactorily operating the system to accommodate physical constraints.

4.2 DETERMINISTIC NONLINEAR CONTROL

Optimal control synthesis procedures for nonlinear systems can be formulated theoretically. Practical application of the result is usually not feasible because of physical limitations of the control processor. However, the structure and philosophy can be adapted from the general theory. The procedure for locally linearized control design results from this simplification.

The design process involves the utilization of a mathematical description of the behavior formulated as a series of dynamical equations. For turbine engines, equations from thermodynamics are available to describe the energy and mass flow along the gas path. The model in general can be described as follows:

$$\dot{x} = f[x(t), u(t), \theta(t)] \quad (4.1)$$

where $x(t)$ represents the dynamical variables, $u(t)$ represents the controls, and $\theta(t)$ represents ambient parameters. Relationships of nondynamic variables can be represented as nonlinear, static equations as follows:

$$y(t) = h[x(t), u(t), \theta(t)] \quad (4.2)$$

The nonlinear equations (4.1) and (4.2) produce state and output time histories, $x(t)$, $y(t)$, for given control and ambient inputs, $u(t)$, $\theta(t)$, $t > t_0$, and initial state, $x_0 = x(t_0)$,

which approximate empirically observed results. Simulations solving Eqs. (4.1) and (4.2) for turbine engines typically require orders of magnitude more processor capability than is available from typical minicomputer systems. In addition, even large-scale digital or hybrid simulations produce results which do not exactly match observed behavior.

The general optimization problem minimizes a terminal error and a path integral as follows:

$$J = \varphi[x(t_f), u(t_f)] + \int_{t_0}^{t_f} L[x(t), u(t), \theta(t)] dt \quad (4.3)$$

where the penalties φ and L represent design criteria such as minimum response time or acceptable limit accommodation. The final time, t_f , is somewhat arbitrary. The minimization of Eq. (4.3) can actually be performed utilizing several off-line algorithms [29,57]. A set of open-loop optimal trajectories $u(t)$, $x(t)$ given $\theta(t)$ and $x(t_0)$ is obtained. Storage requirements for a reasonable set of such trajectories is large. An alternative solution approximates trajectories generated from simplified models. The reduction in complexity in this case is striking. This procedure is described in Section 4.5.

Given an approximate set of open-loop trajectories which produce acceptable behavior, a perturbational controller can be designed to keep the system near the nominal trajectory. The perturbational variables are described below:

$$\delta x = x(t) - x_n(t) \quad (4.4)$$

$$\delta y = y(t) - y_n(t) \quad (4.5)$$

$$\delta u = u(t) - u_n(t) \quad (4.6)$$

The structure of the general controller is shown in Figure 4.1.

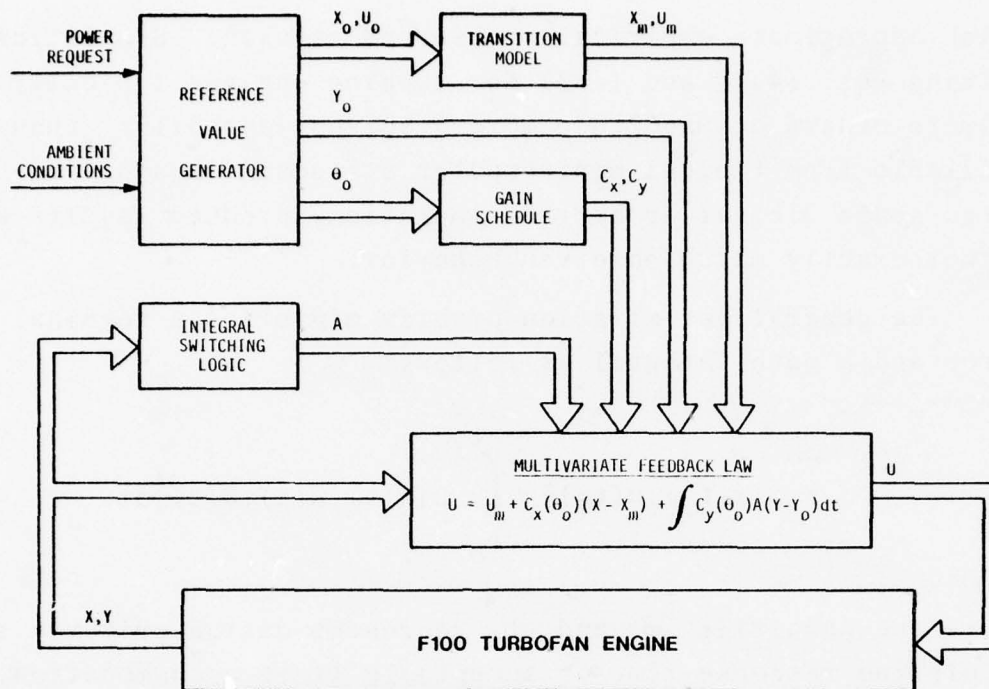


Figure 4.1 F100 Turbofan Multivariable Control Structure

Utilizing perturbational quantities in Eqs. (4.4)-(4.6) and assuming that the actual and nominal trajectories satisfy the same set of equations, e.g., (4.1) and (4.2), then

$$\dot{\delta x} = f[x(t), u(t), \theta(t)] - f[x_0(t), u_0(t), \theta(t)] \quad (4.7)$$

$$\delta y = h[x(t), u(t), \theta(t)] - h[x_0(t), u_0(t), \theta(t)] \quad (4.8)$$

Using a Taylor series expansion of Eqs. (4.7) and (4.8), the following linear equations result:

$$\dot{\delta x} = F(t)\delta x + G(t)\delta u + \mathcal{O}(\delta^2) \quad (4.9)$$

$$\delta y = H(t)\delta x + D(t)\delta u + \mathcal{O}(\delta^2) \quad (4.10)$$

where

$$F(t) = \left. \frac{\partial f[x(t), u_0(t), \theta(t)]}{\partial x} \right|_{x = x_0(t)} \quad (4.11)$$

$$G(t) = \left. \frac{\partial f[x(t), u_0(t), \theta(t)]}{\partial u} \right|_{u = u_0(t)}$$

etc.

and δx is an $n \times 1$ vector of states, δu is an $m \times 1$ vector of controls, δy is a $p \times 1$ output vector with F , G , H , and D representing the compatibly dimensioned constant dynamics matrix, control distribution matrix, and output distribution matrices, respectively. Clearly, ignoring second-order perturbational quantities results in linear equations. However, the linear dynamics are affected by the nominal trajectory chosen. Since this trajectory is fixed by the initial conditions, the dynamics can be considered as simple time-varying functions.

It is also possible to justify the utilization of a quadratic cost functional using Eqs. (4.7) and (4.10). For these equations to be valid, the perturbational quantities to second-order must be kept small during the transient motion [58]. A quadratic cost functional of the type discussed in Chapter III naturally arises. The primary rationale, however, for quadratic performance indices is the static state feedback structure obtained in the optimization.

The controllers which optimize quadratic performance indices using the perturbational dynamics of Eqs. (4.9) and (4.10) are still highly complex and, in general, utilize time-varying gains parameterized by the initial state and dependent on the trajectory.

If it is assumed that the dynamics matrices are constant within a region of the state space, then the equations in (4.9) and (4.10) are constant and independent of initial conditions.

Utilizing this assumption, Eqs. (4.9) and (4.10) reduce to linear, constant coefficient, differential equations and constant state feedback gain procedures presented in Chapter III are applicable. The problem of continuous implementation of the controller in the operating environment remains and will be discussed below. Although this procedure is not strictly optimal in any sense, it is an extremely useful technique in the formulation of suitable control designs for multivariable nonlinear systems.

4.3 ENGINE MODELING FOR CONTROL

As was shown above, a complete mathematical description of turbine engine behavior is exceedingly complex and highly nonlinear. The synthesis procedure is dependent on the selection of a set of tractable design models which may be used to formulate a control law for application throughout the operating envelope. Linear equations are one class of such design models and, as will be shown, can be effectively integrated to provide a nonlinear control function.

The plant can be modeled conceptually as a nonlinear time invariant dynamical system utilizing fundamental aerothermodynamic principles as follows (see Section 4.2):

$$\dot{x} = f(x, u, \theta) \quad (4.12a)$$

$$y = h(x, u, \theta) \quad (4.12b)$$

where states, x , controls, u , outputs, y , and parametric variables, θ , as well as the detailed nonlinear dynamics, $f(\cdot, \cdot, \cdot)$ and $h(\cdot, \cdot, \cdot)$ are chosen by the designer to most expediently achieve his purpose. For engine development, detailed digital simulations including thorough component maps and experimentally correlated gas path equations are utilized

as in the F100 engine transient simulation deck [59,1] shown in Figure 4.2. These programs are too complex for control synthesis, but are useful in evaluating a candidate design.

The central element, therefore, in designing an implementable controller is a systematic method for integrating the completeness of simulation technology with established theoretical and practically validated multivariable design techniques. One multivariable design approach utilizes optimal quadratic regulator theory, but requires a procedure to generate linear models for the design process, and further to incorporate the models into a continuous nonlinear control law. Such a control synthesis procedure subdivides the operating envelope into multiple regions, for example, intervals of power level, altitude, and Mach number. Within each region, the engine dynamical behavior is described by a single set of linear, constant coefficient differential equations. Linear control

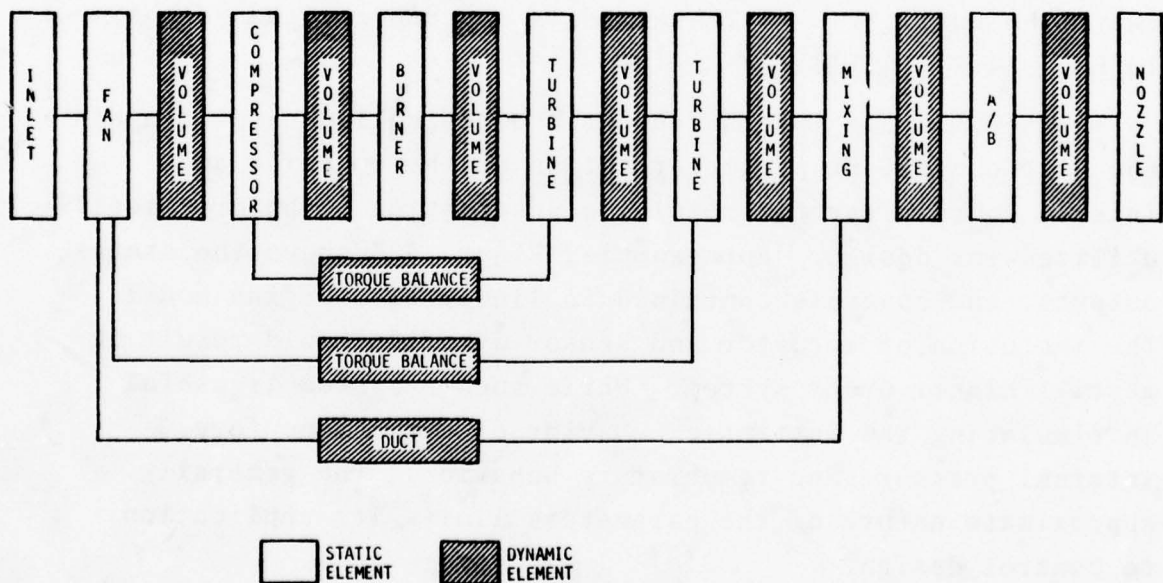


Figure 4.2 Schematic Flow Diagram of F100 Nonlinear Digital Simulation

design techniques are then applied to each region of the envelope. The resulting set of control laws must be suitably linked to form an implementation providing continuous envelope-wide control.

Linear models are generated in many ways, e.g., numerically from nonlinear simulation, or directly from engine data. A common method utilizes a nonlinear hybrid or digital engine simulation. The various dynamic variables and controls are perturbed and state rates calculated. This procedure is computationally efficient; but, often, linearized behavior is dependent on perturbation size [1]. Alternately, the time response to engine inputs can be used with various systems identification procedures [37,60,61,62] to develop models which accurately represent engine behavior over a rather large range. These procedures tend to be computationally demanding and require extensive experience in their application. These linear models are valid in the neighborhood of an equilibrium point (x_o, u_o, θ_o) , and describe perturbation motion, δx , δu , away from equilibrium. These models are represented as shown in Eqs. (4.9)-(4.11).

Often, linear models generated numerically do not contain the most convenient parameterization of the dynamics and, indeed, contain far too complex a description to be practically utilized for design. For example, Figure 4.3 shows the states, outputs, and controls contained in linear F100 engine models. The inclusion of actuator and sensor dynamics would result in a still higher order system. While such a system is useful in simulating the intrinsic behavior of the engine (e.g., internal pressure and temperature behavior), the generally approximate nature of the parameters limits its application to control design.

Some method is required to analyze the dynamic models and establish simpler systems which include only elements important to the desired control function. Without such

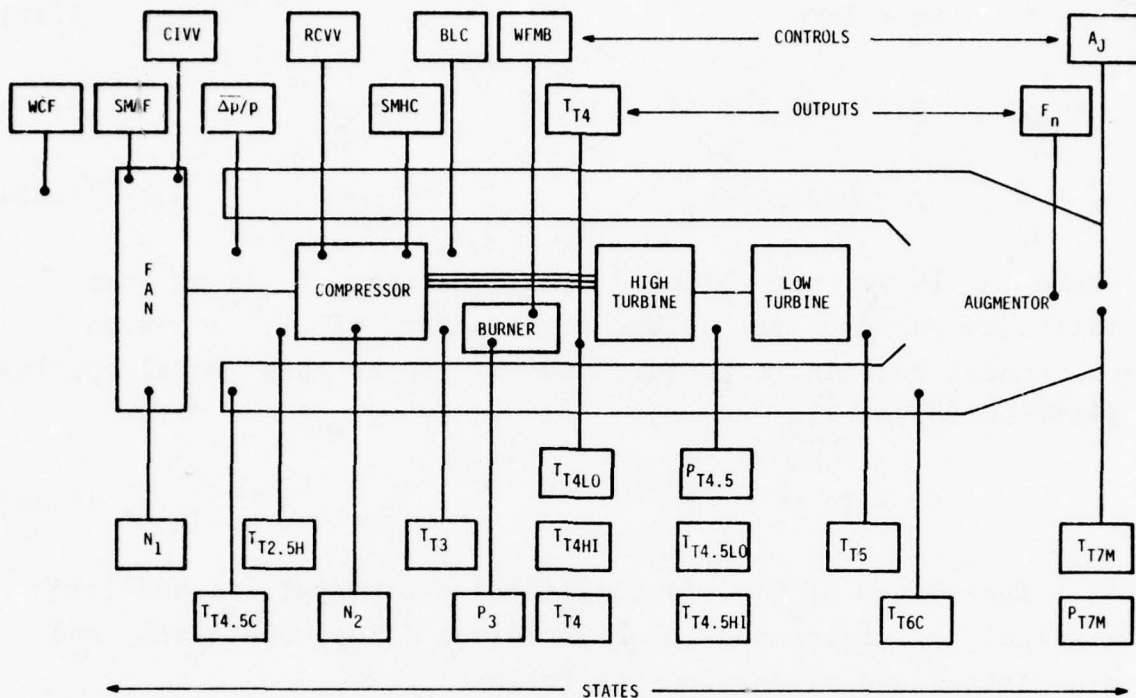


Figure 4.3 States, Outputs, and Controls Modeled in F100 Linear Equations Generated from Nonlinear Digital Simulation Program

simplification, application of design procedures can result in highly complex and parameter sensitive controlled systems. Utilizing the reduced order models, regulator synthesis procedures become physically intuitive and, most significantly, far less sensitive to parameter variation.

A modal decomposition provides the framework for reducing arbitrary linear models to design models containing the appropriate parameterization for the control function. The procedures are well known [63,64,65] and their application to model reduction is described below.

The linear equations (4.9)-(4.11) can be transformed to block diagonal form assuming the $n \times n$ dynamics matrix, F , has no repeated eigenvalues (as is the characteristic of the F100 engine model):

$$\delta x = Tz \quad (4.13)$$

$$\dot{z} = \Lambda z + \Xi \delta u \quad (4.14)$$

$$y = HTz + D\delta u \quad (4.15)$$

where Λ is an $n \times n$ block diagonal matrix, T is an $n \times n$ matrix composed of the column eigenvectors of F , z is an $n \times 1$ modal coordinate vector, and Ξ is the $n \times m$ modal control distribution matrix. Also,

$$FT = T\Lambda \quad (4.16)$$

The system of Eqs. (4.13)-(4.15) can be partitioned into a set of q states and q eigenvalues (time constants) and $n-q$ states and eigenvalues as follows:

$$\begin{bmatrix} \delta x_1 \\ \vdots \\ \delta x_2 \end{bmatrix} = \begin{bmatrix} T_{11} & T_{12} \\ \vdots & \vdots \\ T_{21} & T_{22} \end{bmatrix} \begin{bmatrix} z_1 \\ \vdots \\ z_2 \end{bmatrix} \quad (4.17a)$$

$$\begin{bmatrix} \dot{z}_1 \\ \vdots \\ \dot{z}_2 \end{bmatrix} = \begin{bmatrix} \Lambda_1 & 0 \\ \vdots & \vdots \\ 0 & \Lambda_2 \end{bmatrix} \begin{bmatrix} z_1 \\ \vdots \\ z_2 \end{bmatrix} + \begin{bmatrix} \Xi_1 \\ \vdots \\ \Xi_2 \end{bmatrix} \delta u \quad (4.17b)$$

where δx_1 and z_1 are $q \times 1$ vectors partitioning the states and modes and δx_2 and z_2 are $(n-q) \times 1$ vectors partitioning the remaining states and modes.

Various guidelines for making an appropriate partition will be discussed below. If the following equilibrium relationship is approximately true (within the time frame of control interest),

$$\dot{z}_2 \approx 0 \quad (4.18)$$

then the following reduction can be made:

$$\delta \dot{x}_1 = F_r \delta x_1 + G_r \delta u \quad (4.19)$$

where δx_1 is now the qx_1 state vector, F_r is the qxq dynamics matrix, and G_r is the qxm control distribution matrix. Also,

$$y = [H_1' \ H_2] \begin{bmatrix} \delta x_1 \\ \dots \\ \delta x_2 \end{bmatrix} + Du \quad (4.20)$$

and

$$\begin{bmatrix} \delta x_2 \\ \dots \\ \delta y \end{bmatrix} = \begin{bmatrix} H^* \\ \dots \\ H_r \end{bmatrix} \delta x_1 + \begin{bmatrix} D^* \\ \dots \\ D_r \end{bmatrix} \delta u \quad (4.21)$$

where δx_2 is treated as an additional $(n-q)x_1$ output vector with a $(n-q)xq$ state distribution matrix H^* and a $(n-q)xm$ control distribution matrix D^* . The original output distribution matrices, H and D , are modified to H_r and D_r , respectively. The formulas for these matrices are shown below in terms of the partitioned modal decomposition:

$$F_r = T_{11} \Lambda_1 T_{11}^{-1} \quad (4.22)$$

$$G_r = T_{11} (\Lambda_1 T_{11}^{-1} T_{12} \Lambda_2^{-1} \Xi_2 + \Xi_1) \quad (4.23)$$

$$H^* = T_{21} T_{11}^{-1} \quad (4.24)$$

$$D^* = (T_{21} T_{11}^{-1} T_{12} - T_{22}) \Lambda_2^{-1} \Xi_2 \quad (4.25)$$

$$H_r = H_1 + H_2 H^* \quad (4.26)$$

$$D_r = D + H_2 D^* \quad (4.27)$$

Thus, by assuming $(n-q)$ modes are equilibrated, the n th order system (4.9) is reduced to the q th order system (4.19) with q states and $p+n-q$ outputs. It should be noted also that the q retained states, δx_1 , are chosen by the designer and possess the same physical identification in Eqs. (4.9) and (4.19) if Eq. (4.18) is approximately valid.

The modal decomposition allows the intrinsic structure of the system (4.9) to be exploited in the choice of the q retained modes and states. Initially, nominal values of states and controls are chosen by the designer to scale the dimensional variables of Eq. (4.9) to obtain a nondimensional correspondence. This is a subjective choice but it allows meaningful comparison of dimensional quantities.

The solution to Eq. (4.19) is:

$$\begin{aligned} \delta x_1(t) = & \left\{ \sum_{k=1}^n (u_k v_k^T) \phi_k(t) \right\} \delta x(0) \\ & + \left\{ \sum_{k=1}^n \frac{u_k c_k^T}{\lambda_k} \right\} \mathcal{L}_k(\delta u, t) \end{aligned} \quad (4.28)$$

where the $q \times 1$ column and row eigenvectors, u_k and v_k^T of the reduced system are as follows

$$F_r u_k = \lambda_k u_k \quad (4.29)$$

$$v_k^T F_r = \lambda_k v_k^T \quad (4.30)$$

and the modal impulse responses can be calculated as follows:

$$\Phi_k(t) = \exp(\lambda_k t) \quad (4.31)$$

$$\mathcal{L}_k(\delta u, t) = \lambda_k \int_0^t \phi_k(t-\tau) \delta u(\tau) d\tau \quad (4.32)$$

and the modal control distribution matrix is partitioned by rows,

$$\Xi = \begin{bmatrix} c_1^T \\ \vdots \\ c_n^T \end{bmatrix} \quad (4.33)$$

or, more compactly,

$$\delta x_1(t) = \sum_{k=1}^n \left\{ R_k \phi_k(t) \delta x(0) + S_k \mathcal{L}_k(\delta u, t) \right\} \quad (4.34)$$

where R_k is the $q \times q$ matrix of residues of initial conditions at λ_k and S_k is the $q \times m$ matrix of impulse response residues at λ_k . For clarity of notation, it has been assumed that all eigenvalues are real. The extension to the block diagonal formulation is slight and does not alter the logic [52].

The partitioning of the system is dependent upon the control designer's estimate of the frequency range of the control function. For example, the F100 controller was designed to primarily modulate thrust in transient and steady state operation. The response frequency range extends from 0 rad/sec to around 10 rad/sec, which is the bandwidth of the primary (fuel flow) actuator. The frequency range would be significantly different if, for example, the controller was designed to

transiently modulate compressor stability margin with a high bandwidth variable area turbine actuator. In the F100 engine linear models, the properties of spectral separation can be applied. From Eq. (4.34), if $\delta u(t)$ contains primarily the desired frequency components (for the F100, 0-10 rad/sec), then the following conditions may hold during the majority of the transient for the $(n-q)$ modes chosen in the reduction; either,

$$\left. \begin{array}{l} \varphi_k(t) \approx 0 \\ \mathcal{L}_k(\delta u, t) \approx 1 \end{array} \right\} \text{ if } t \gg 1/\lambda_k \quad (4.35)$$

or

$$\left. \begin{array}{l} \varphi_k(t) \approx 1 \\ \mathcal{L}_k(\delta u, t) \approx 0 \end{array} \right\} \text{ if } t \ll 1/\lambda_k \quad (4.36)$$

with the initial condition modified in the latter case to account for the high frequency control effects.

The implication is that all eigenvalues significantly outside the bandwidth of interest are in equilibrium during the motion. Also, if for a λ_k , c_k is approximately zero, then the mode associated with λ_k is uncontrollable and should be eliminated from the design model regardless of the time constant.

The most powerful property of the modal decomposition is evident in Eq. (4.17). If a group of states can be identified with a null projection into the subspace spanned by a set of modal coordinates (i.e., a partition with $T_{12} \approx 0$), then those modes can be eliminated without affecting the dynamic behavior of the states. This situation occurs when a state is nearly

parallel to a single modal direction. If the outputs of interest are not affected by the particular state, the state and associated dynamics can be removed from the design model without affecting behavior important to the control synthesis. Figure 4.4 shows the normalized eigenvectors associated with two eigenvalues for the F100 engine lying in the bandwidth of control. These modes are associated with temperature lag states at the turbine inlets. Examination of the thrust output equation shows that these states have a relatively small

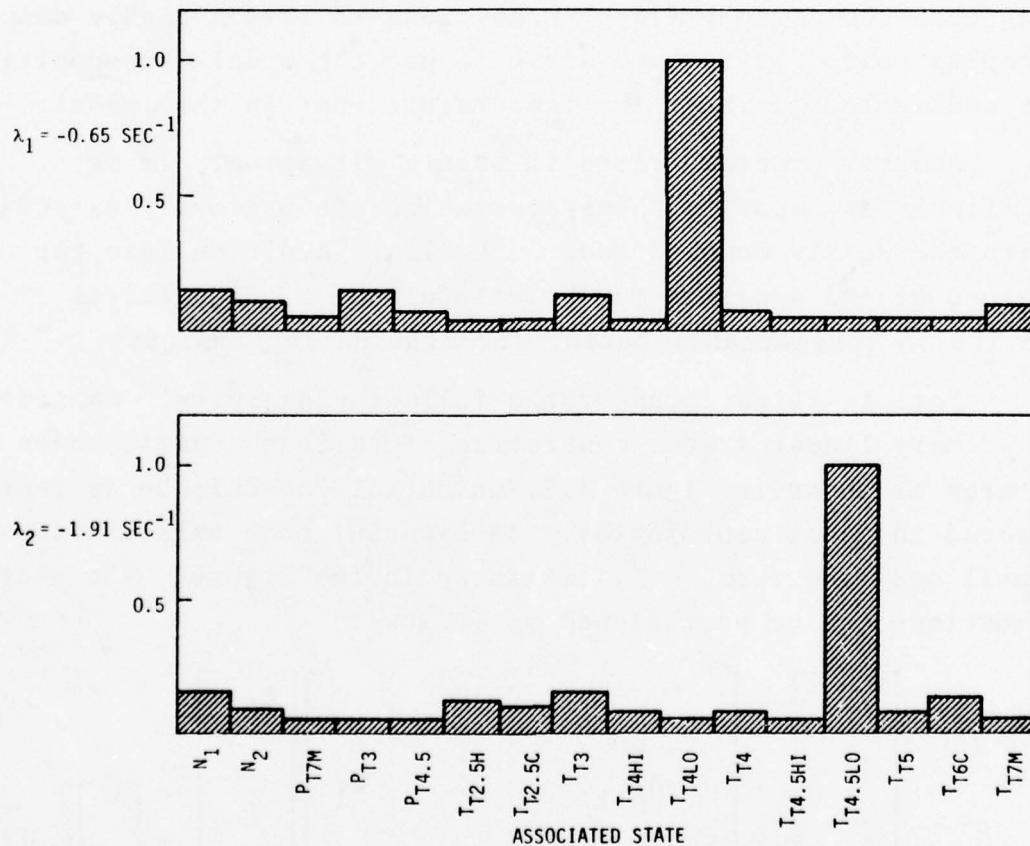


Figure 4.4 Normalized Eigenvector Components for Two Roots Lying in the Bandwidth of Control at Sea Level Static, Intermediate Power Condition for the F100 Turbofan Engine

contribution. Thus, for control design purposes, the two states and the associated modes can be eliminated.

There is one situation which causes the modal decomposition procedure to fail. In this case, a small coupling exists between two modes which have nearly equal time constants. This coupling causes the root locations to merge and become a highly damped complex pair. The modal decomposition procedure cannot eliminate one root of a complex pair. Thus, if the procedure is used, the complex root must be either eliminated or retained. In some situations, this may be troublesome to the designer. For example, in the F100 engine, the mode associated with the high compressor rotor and a turbine inlet temperature lag coalesce at some flight conditions to form a highly damped complex pair. It is impossible to use the modal decomposition procedure to eliminate the temperature root in this model.

Another problem arises in such a situation. It is difficult to identify the states which are primarily associated with the weakly coupled mode. Physical intuition into the nature of the dynamics may be helpful but a mathematical device is considerably better for eliminating ambiguity.

This is illustrated by the following analysis. Consider a primary linear system consisting of various dynamic modes and states as shown in Figure 4.5, which for convenience is represented in modal coordinates. An external mode exists with a small coupling term, ϵ^2 , as shown in the figure. The state equations can be partitioned as follows:

$$\begin{bmatrix} \dot{\xi}_1 \\ \vdots \\ \dot{\xi}_{n-1} \\ \dot{\xi}_n \\ \dot{z} \end{bmatrix} = \begin{bmatrix} & & 0 & & \\ & \Lambda_{n-1} & \vdots & & h_1 \\ & & 0 & & \\ \hline 0 & \dots & 0 & \lambda_n & h_n \\ \hline \epsilon^2 t_i^T & & \epsilon^2 t_n & & -a \end{bmatrix} \begin{bmatrix} \xi_1 \\ \vdots \\ \xi_{n-1} \\ \xi_n \\ z \end{bmatrix} + \begin{bmatrix} G \\ - \\ 0 \end{bmatrix} \delta u \quad (4.37)$$

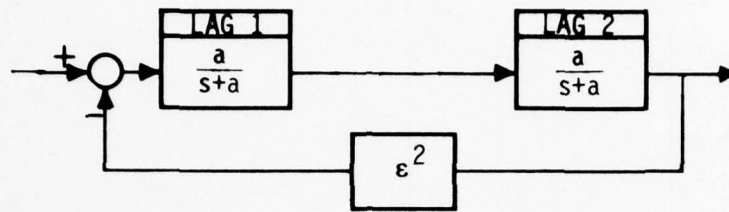


Figure 4.5 Schematic Representation of Lightly Coupled Roots Within the Structure of a High Order Linear System - For Nearly Any Non-Zero ϵ , the System Roots Corresponding to the Two Lags Will be a Complex Pair

All the roots of the primary system have values different from $-a$, except possibly λ_n . As ϵ becomes small, the roots approach the eigenvalues of the primary system with the additional root at $s = -a$. If $\lambda_n = -a$, the roots still approach the uncoupled system for small ϵ . However, for any finite ϵ , there is a root at

$$s = -a(1 \pm j\epsilon\sqrt{h_n t_n}) \quad (4.38)$$

Even for vanishingly small positive coupling, the eigenvalue is complex. It should be stressed that the dynamic response of the system does not markedly change as ϵ reaches zero, even though the mathematical expression relating the response has a different functional form.

Examination of the eigenvector associated with the complex mode shows how to identify the lightly coupled states. In terms of the primary system modal coordinates, the eigenvectors for this root can be written as follows:

$$u = \begin{bmatrix} 0 \\ \vdots \\ 0 \\ 1 \pm 0j \\ 0 \pm \varepsilon a \sqrt{h_n t_n} j \end{bmatrix} \quad (4.39a)$$

and in terms of the original state coordinates as follows:

$$u_x = \begin{bmatrix} u_1 \pm 0j \\ \vdots \\ u_n \pm 0j \\ 0 \pm \varepsilon a \sqrt{h_n t_n} j \end{bmatrix} \quad (4.39b)$$

where u_1, \dots, u_n are real numbers. From Eq. (4.39), it is clear that the state and modal coordinate associated with the lightly coupled behavior will be 90° out of phase relative to the remaining states of the system. An example of this technique is presented in the 16th-order system describing F100 engine behavior in Figure 4.6.

Once the lightly coupled roots are detected in the structure of the dynamics matrix, the dynamic coupling can be eliminated. In this case, the complex pair decomposes into two real roots associated with the primary state variables. This static equilibration is equivalent to the assumption in Eq. (4.37) that

$$\dot{z} = 0 \quad (4.40)$$

Elementary matrix manipulation can be used [66,67] to obtain the reduced form. An example in Table 4.1 shows that the

EIGENVALUE	
$\lambda = -0.67 \pm .22j \text{ (sec}^{-1}\text{)}$	} HIGHLY DAMPED ROOT
$\omega_n = 0.70 \text{ (sec}^{-1}\text{)}$	
$\zeta = 0.95$	

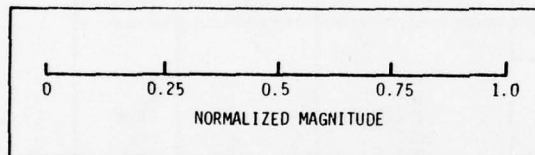
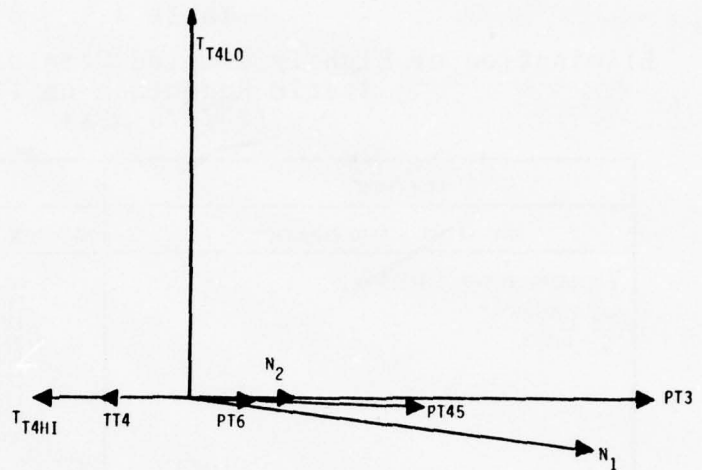


Figure 4.6 Example of Normalized Eigenvector Corresponding to a Lightly Coupled System in the 16th-Order Linear Models of the F100 engine at Sea Level Static, Idle Power Conditions - The Lightly Coupled State, T_{T4L0} , Appears 90° Out-of-Phase of Remaining State Components

reduction does not change the system eigenvalues except to replace the complex pair with a single root.

A number of techniques have been presented for choosing (n-q) modes which can be eliminated along with a group of states. The choice of the retained q states is somewhat arbitrary depending on convenient measurables as well as dependence of the important output quantities. The modal decomposition can be used to assure that the chosen q states strongly span the controlled subspace (T_{11} invertible and

Table 4.1
Elimination of Lightly Coupled Complex Pair by Performing
Static Reduction on TT4LO
(20/0/0 HPX)

EIGENVALUE	EIGENVECTOR		
ROOT BEFORE STATIC REDUCTION	MAGNITUDE (SEC ⁻¹)	ANGLE (DEG)	STATES
$(-6.66340-001)+j(2.17310-001)$ $\omega_n = 0.701$ $\zeta = 0.951$.8696	-14.61	N1
	.2194	.73	N2
	.1353	-11.92	PT7M
	1.0000	.00	PT3
	.4991	-2.16	PT45
	.1278	-6.64	TT25H
	.1331	-5.77	TT25C
	.2725	-1.44	TT3
	.3087	-179.15	TT4HI
	.8226	93.80	TT4LO
	.3548	-179.08	TT4
	.4414	-176.00	TT45HI
	.5674	177.58	TT45LO
	.5378	-176.58	TT5
	.1400	-5.86	TT6C
	.1932	163.61	TT7M
LIGHTLY COUPLED MODE →			
ROOT AFTER STATIC REDUCTION			
$(-7.19412-001)+j(0.00000)$.9131	.0	N1
	.2185	.0	N2
	.1426	.0	PT7M
	1.0000	.0	PT3
	.5062	.0	PT45
	.1354	.0	TT25H
	.1413	.0	TT25C
	.2759	.0	TT3
	-.3063	.0	TT4HI
	-.3522	.0	TT4
	-.4303	.0	TT45HI
	-.5760	.0	TT45LO
	-.5256	.0	TT5
	.1487	.0	TT6C
	-.1999	.0	TT7M

well conditioned. With this partition and associated reduction, the resulting system (4.20) will represent a controllable design model.

The behavior of an F100 design model vis-a-vis the 16th-order linear system and nonlinear simulation is shown in Figure 4.7. In general, the design models match the 16th-order models closer than the 16th-order models match simulated, nonlinear engine response. The discrepancy between linear and nonlinear simulated responses for moderate sized transient behavior is

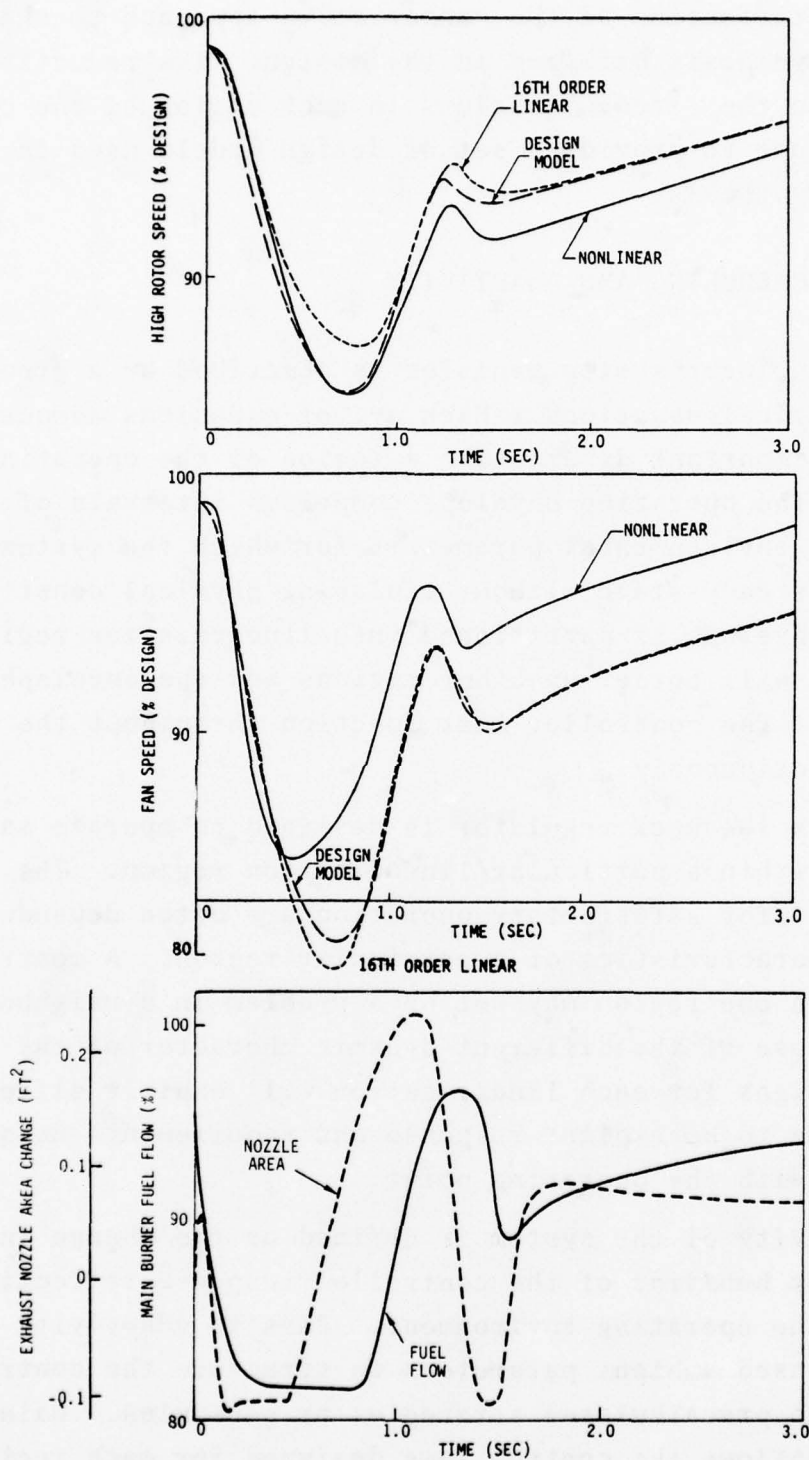


Figure 4.7 Comparison of Small Perturbation Response of the F100 Turbofan Engine at Sea Level Static, Take-off Power Simulated by the Full Nonlinear Digital Deck, the 16th-Order Linearized Model and the Reduced Order Design Linear Model

further justification of the conservative approach to the regulator synthesis utilized in the design. The reduction was performed on the linear equations in each region of the operating envelope to provide a set of design models used in the regulator synthesis.

4.4 GAIN SCHEDULING AND ADAPTIVITY

The nonlinear system behavior is described by a group of linear dynamical equations. Each set of equations adequately models the important dynamics in a region of the operating envelope. The operating envelope comprises intervals of independent environmental parameters for which the system can operate in steady-state without violating physical constraints. Since the envelope is partitioned into linearization regions, each region will border on other regions and the envelope boundaries. The controller must function throughout the envelope continuously.

A state feedback regulator is designed to operate satisfactorily within a particular linearization region. The requirements for satisfactory operation are often dependent upon the characteristics of a particular region. A control "problem" in one region may not be a problem in a neighboring region because of the different dynamic character of the system. Control designs for each linearization will exhibit different behavior due to both plant response and requirements uniquely associated with the operating point.

Adaptivity of the system is defined as the change in structure or behavior of the controlled response reflecting change in the operating environment. Passive adaptivity utilizes sensed ambient parameters to structure the controller according to precalculated strategies or schedules. Gain scheduling allows the control laws designed for each region of the envelope to be linked in a continuous implementation

parameterized by the independent environmental variables. The alternative to passive gain scheduling is an on-line algorithm to optimize a particular performance index or criterion function in real time. Practical utilization of such systems requires significant computational overhead and so far have few successful applications in actual systems.

Methods of designing gain scheduling algorithms range from basic analytical treatments to a posteriori correlation of gain elements. Several of these procedures will be discussed below.

4.4.1 Analytical Approaches

There is no strictly analytical technique to produce optimal variable gains for nonlinear systems from constant, proportional gains designed from linearized behavior. In general, the optimal state feedback gains are time- and trajectory-dependent, even for systems described by a linear differential model. However, successful systems have been synthesized using approximations to optimal values.

One approach is applicable to systems whose dynamics are determined by geometric scaling relationships. If it is assumed that the optimal cost functional can be likewise scaled, then the optimal state feedback "schedule" can be derived from the appropriate scaling factors in the state and control variables.

The procedure can be written as follows. A group of linear dynamical systems, $\{F, G\}_i$, can be calculated for various operating points described by the ambient variable vector,

$$\theta_i = \{\theta_{1_i}, \theta_{2_i}, \dots, \theta_{p_i}\}. \quad (4.41)$$

Because of consistent geometric scaling, the time response of the system may sometimes be written as follows

$$F_i = k(\theta_i) S^{-1}(\theta_i) F^* S(\theta_i) \quad (4.42)$$

$$G_i = k(\theta_i) S^{-1}(\theta_i) F^* R(\theta_i) \quad (4.43)$$

where

$$S = \text{diag}\{s(\theta_i)\} \quad (4.44)$$

$$R = \text{diag}\{r(\theta_i)\} \quad (4.45)$$

and the scaling functions, $k(\theta_i)$, $s(\theta_i)$ and $r(\theta_i)$ have the form of pure geometric factors of the ambient variables, or,

$$f(\theta_i) = c (\theta_1)^{v_1} (\theta_2)^{v_2} (\theta_3)^{v_3} \cdots (\theta_p)^{v_p} \quad (4.46)$$

This transformation is equivalent to the variable scaling defined below

$$x = S^* \quad (4.47)$$

$$u = Ru^* \quad (4.48)$$

$$t = t^*c \quad (4.49)$$

The nondimensional variables, x^* , u^* , t^* describe the system behavior at all operating points. Calculation of the scaling laws, Eqs. (4.42)-(4.46), is cumbersome for high order dynamical systems and adequate fits are not possible for systems whose states cannot be modeled by geometric factors of the ambient environmental quantities. Methods of regression analysis can be utilized to solve such problems.

The cost function,

$$J = \frac{1}{2} \int_{t_0}^{t_f} (x^T A x + u^T B u) dt, \quad (4.50)$$

can be written in terms of the nondimensional quantities, as

$$J^* = \frac{1}{2} \int_{t_0}^{t_f} C(x^{*T} S A S x^* + u^{*T} R B R u^*) dt^* \quad (4.51)$$

If weights A and B can be chosen so that acceptable dimensional response at each flight condition is maintained, then the control law resulting from the optimal regulator design can be written as follows:

$$u^* = C^* x^* \quad (4.52a)$$

or, in dimensional form,

$$u = c(RC^*S^{-1})x \quad (4.52b)$$

The gain schedules are defined from Eqs. (4.52) as follows:

$$C(\theta) = R(\theta) C^* S^{-1}(\theta) \quad (4.53)$$

This procedure produces optimal regulators for each operating point which minimize the scaled cost functional. It is a generalization of the technique used in classical single-loop design to vary gains to maintain a constant time constant or damping. It yields constant, nondimensional weighting of control effort and state deviations as required by the minimization of J^* .

The drawback of the method is that the control criteria may require different weightings at different operating points. In this case, it would not be possible to choose a single group of state and control weightings for the nondimensional system. An alternative which involves fitting gains after the local designs have been made is presented below.

4.4.2 Direct Gain Schedule Development

The result of the linear quadratic regulator design is a group of state feedback matrices. There is one matrix associated with each region of the flight envelope and each matrix reflects the important dynamic couplings and significant control criteria for that region.

A sensitivity analysis of each gain matrix will eliminate those elements which produce an insignificant effect on the closed-loop eigensystem. Reduction of the gain matrix produces control laws that tend not to exhibit numerical problems due to machine precision because values which are "small" have been set to zero.

Since the gain matrices and the flight conditions are given, the problem of gain scheduling reduces to curve fitting. Two procedures are useful: optimal subset regression and splines [60,21]. The problem is stated as follows. For each non-zero element of the gain matrix, C , a value is given corresponding to the optimal regulator design at a point, (x_o, u_o, θ_o) . The gain value should be represented as a function of the operating point as follows:

$$C = f(x_o, u_o, \theta_o) \quad (4.54)$$

If a polynomial in various powers of (x_o, u_o, θ_o) is chosen as the functional form of f , and

$$p_i \in (x_o, u_o, \theta_o) \quad (4.55)$$

then

$$\hat{C} = \sum_{j=1}^Q a_j t_j \quad (4.56)$$

where t_j has the form of a product of the elements p_j to arbitrary power. The task of finding the set of coefficients in Eq. (4.56) to match a given set of gain elements is efficiently accomplished using subset regression techniques.

For a given value of Q , and choice of coefficients, the set of values of a_j which minimize the fit error

$$\epsilon^2 = \sum_{k=1}^N [C(k) - \hat{C}(k)]^2 \quad (4.57)$$

is given as follows

$$a = (H^T H)^{-1} H^T \bar{C} \quad (4.58)$$

where

$$a^T = [a_1, \dots, a_n] \quad (4.59)$$

$$H = \begin{bmatrix} t_1(1) & \dots & t_Q(1) \\ \vdots & & \\ t_1(N) & & t_Q(N) \end{bmatrix} \quad (4.60)$$

$$\bar{C}^T = [C(1), \dots, C(N)] \quad (4.61)$$

However, there are typically a large number of possible elements t_j , and it is desired that the best set of model terms be included. The best set usually contains the smallest number of terms which would produce an adequate fit according to some criteria [60].

Two approaches to the problem of choosing the "best" and smallest subset of coefficients from a given group are stepwise and global regression. In stepwise regression, one term is added to the model and the reduction of the steady-state error calculated. Correlations are used to determine which parameter is chosen. The resulting model may not be the one which yields the minimum error for that number of terms. However, the procedure is computationally efficient. An alternate method calculates every function possible from a group of variables. A procedure for searching the coefficient elements is available which is nearly as efficient as stepwise regression and produces the globally optimal curve fit.

A second technique is more appropriate for a small number of linearization points used to span the operating envelope. Polynomial curves have poor extrapolation properties. Linearization points lie in the center of regions and gains must be extrapolated to the envelope boundary. It is possible that gross errors in estimated gain values will arise as shown in Figure 4.8. This effect can be minimized by assigning fictitious values of gain corresponding to maximum or minimum values at the boundaries of the envelope. This results in a general degradation of the curve fit throughout the envelope.

The feedback gains should ideally be constant within a particular operating region. This can be partially realized by the limiting function for exterior regions as shown in Figure 4.9. At interior points, linear spline interpolation curves can be used to approximate the gain function. These produce easily implemented schedules.

A least squares procedure can be used to calculate linear spline or interpolation schedules from data in an efficient manner. Figure 4.10 illustrates the problem for the univariate function case. The procedure can be formulated as a constrained least squares problem as follows:

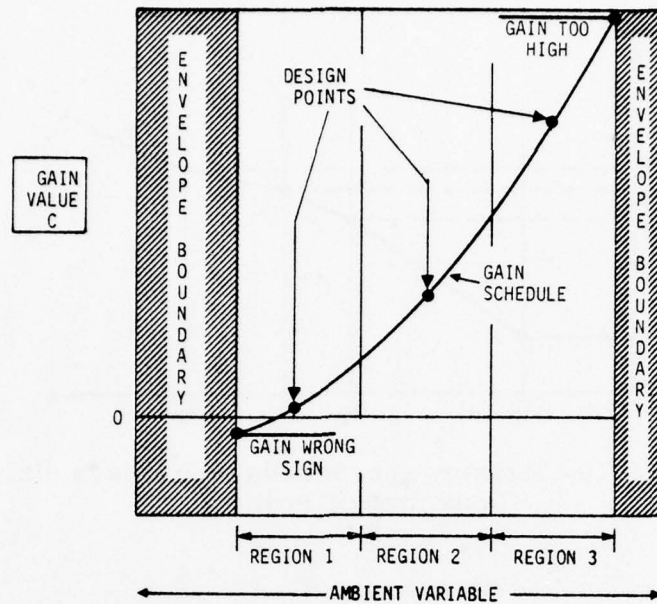


Figure 4.8 Problems Caused by Extrapolation of Polynomial Gain Schedule for a Small Number of Design Points Include Sign Reversal and Overly Large Magnitude

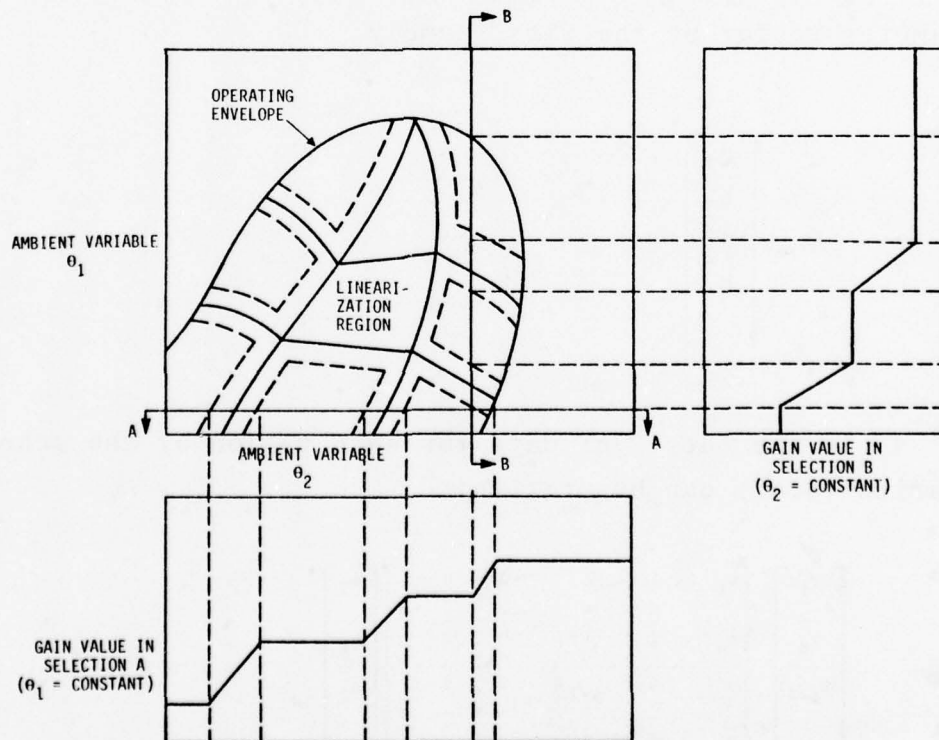


Figure 4.9 Linear Spline Interpolation of a Gain Scheduled Throughout a Bivariate Envelope Linking Design Points Within Each Region and Providing Well Behaved Extrapolation Properties

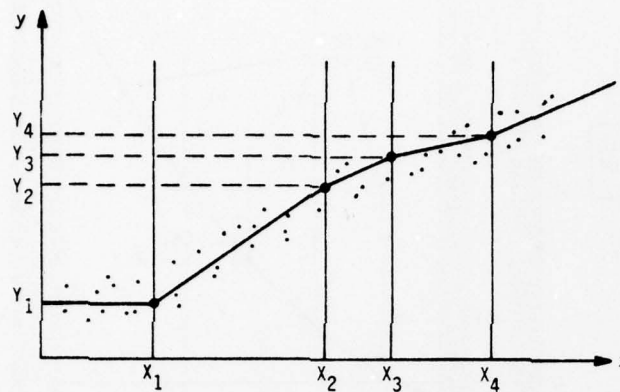


Figure 4.10 Univariate Schedule of Data Using Four Break Points

$$y_j = A\theta \quad (4.62)$$

where y_j is the data to be fit, θ is the interpolation parameter vector of the fits, namely

$$\theta = \begin{bmatrix} a_1 \\ b_1 \\ a_2 \\ b_2 \\ \vdots \end{bmatrix} \quad (4.63)$$

and A is the matrix of data for each region of the schedule. Equation (4.62) can be written:

$$\begin{bmatrix} y_1 \\ \vdots \\ y_p \\ y_{p+1} \\ \vdots \\ y_q \\ y_{q+1} \\ \vdots \end{bmatrix} = \begin{bmatrix} x_1 & 1 & 0 & 0 & 0 \\ \vdots & \vdots & \vdots & \vdots & \vdots \\ x_p & 1 & 0 & 0 & 0 \\ 0 & 0 & x_{p+1} & 1 & 0 \dots \\ \vdots & \vdots & \vdots & \vdots & \vdots \\ 0 & 0 & x_q & 1 & 0 \dots \\ 0 & 0 & 0 & 0 & x_{q+1} \\ \vdots & \vdots & \vdots & \vdots & \vdots \end{bmatrix} \begin{bmatrix} a_1 \\ b_1 \\ a_2 \\ b_2 \\ \vdots \end{bmatrix} \quad (4.64)$$

where

$$X_{j-1} < x_i \leq X_j \quad i=1, \dots, N, \quad j=1, \dots, M \quad (4.65)$$

where X_j is the j th schedule break point and x_i is the i th data point variable.

In the procedure, the error of the fit

$$\tilde{\epsilon} = (y - A\theta)^T (y - A\theta) \quad (4.66)$$

is minimized under the constraint that the schedule line segments be continuous at the break points, namely,

$$Y_i = a_j X_{j+1} + b_i \quad (4.67)$$

$$j = 1, \dots, M$$

$$= a_{j+1} X_{j+1} + b_{j+1} \quad (4.68)$$

where M is the number of break points in the table. The problem can be extended to minimization of the error for a variable set of break points which can be formally written:

$$J^*(M) = \min_{\{X_j\}} [\epsilon] \quad i = 1, \dots, M \quad (4.69)$$

where $\{X_j\}$ contains a given number of break points. If the optimal fit function, $J^*(j)$, for each number of break points is plotted versus the number j , it is possible to choose the minimum number of break points needed to produce a given level of accuracy. This is shown in Figure 4.11.

The extension to multivariate curves is straightforward. For the bivariate case, the equations are given below:

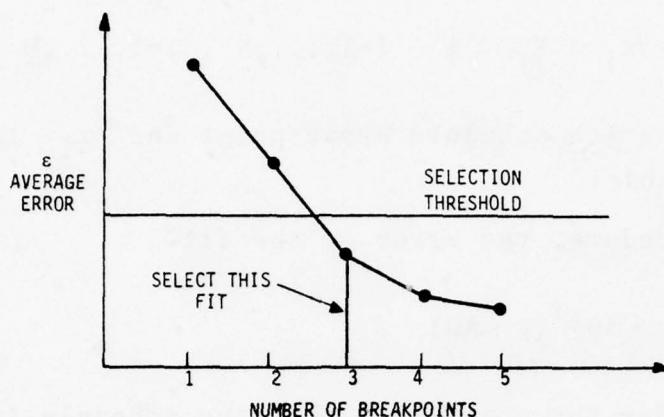


Figure 4.11 Average Error in Filtering Data for Increasing Number of Break Points

Schedule Model

$$y_i = a_{jk}x_i + b_{jk}z_i + c_{jk} \quad \begin{array}{l} i=1, \dots, N \\ j=1, \dots, M \\ k=1, \dots, K \\ x_j < x < x_{j+1} \\ z_k < z < z_{k+1} \end{array} \quad (4.70)$$

Constraints

$$\begin{aligned} y_i &= a_{jk}x_{j+1} + b_{jk}z_{k-1} + c_{ij} \\ &= a_{j+1,k}x_j + b_{j+1,k}z_{k+1} + c_{j+1,k} \\ &= a_{j,k+1}x_{j+1} + b_{j,k+1}z_k + c_{j,k+1} \\ &= a_{j+1,k+1}x_j + b_{j+1,k+1}z_k + c_{j+1,k+1} \end{aligned} \quad (4.71)$$

for M break points along x and K break points along z .

One advantage of this technique is that extrapolation to the envelope boundary is well behaved. Gains which are nearly

constant can be easily implemented as a constant value. There are excellent interpolation algorithms in existence for real time computers which are designed for operation in a typical fixed point arithmetic environment. Appendix J shows an example of this procedure in developing a typical control schedule.

4.5 TRANSITION CONTROL

4.5.1 Requirements

In the development of the optimal nonlinear controller in Section 4.2, it was shown that a feedforward path was required in the perturbation regulator solution. Choice of the trajectory can be based on a priori simulation to optimize a criterion function appropriate to the response. Storage of the required trajectories remains as the most serious drawback of this procedure. The development of the optimal follower solution in Chapter III showed that a trajectory satisfying the linear design model equations used a regulator control law without a time-varying bias term. It is possible to utilize the linear perturbational design models to approximate trajectories which satisfy the linear and nonlinear equations in the neighborhood of an equilibrium. The advantage of this procedure is evident when storage requirements for the feedforward time functions are evaluated.

4.5.2 Generation of Transition Models

The linearized equations about an equilibrium are valid if state and control deviations are relatively small compared to the magnitude of the nonlinearity. Any linear optimal controller which is required to follow a specified state and control trajectory has a simple regulator structure if the trajectory is a solution to the open-loop, linear dynamics.

The solution to the linear perturbation dynamics is an approximate solution to the nonlinear system in the neighborhood of the linearization point.

The linear perturbational equations are as follows:

$$\delta \dot{x} = F\delta x + G\delta u \quad (4.72)$$

$$\delta y = H\delta x + D\delta u \quad (4.73)$$

An asymptotic solution to Eqs. (4.72) can be written such that the states and outputs maintain a constant rate. The required inputs may be calculated from Eq. (4.72) using the following form:

$$\delta u(t) = \delta u(0) + r_u t \quad (4.74)$$

where $\delta u(0)$ is a step component and r_u is a control rate. The problem of existence of solutions of this type can be put in a somewhat general framework. The forced solution to Eqs. (4.72) and (4.73) is as follows:

$$\begin{bmatrix} sI - F & -G \\ H & D \end{bmatrix} \begin{bmatrix} \delta x(s) \\ \delta u(s) \end{bmatrix} = \begin{bmatrix} 0 \\ Y_D(s) \end{bmatrix} \quad (4.75)$$

where $Y_D(s)$ is the Laplace transform of the forcing time function and $\delta x(s)$ and $\delta u(s)$ are the non-homogeneous (or asymptotic) solutions to the linear differential equations given in (4.72) and (4.73).

There are solutions to Eqs. (4.75) when the number of controls equals the number of states and the system in Eqs. (4.72) and (4.73) is both controllable and observable. If there are more outputs than controls, there is no solution in

general. In this situation, a number of outputs can be deleted from Eq. (4.73) [51].

If there are more controls than states, several approaches can be taken. Additional output equations could be specified to build up the system to full rank. An optimization problem minimizing state and control deviations subject to the constraint equations in (4.72) and (4.73) can eliminate ambiguities in the solution.

The solution to Eq. (4.74) can be written as follows:

$$\delta u(s) = [D + H(sI - F)^{-1}G]^{-1}Y_D(s) \quad (4.76)$$

A stable solution to the control time history exists when the roots of Eq. (4.76) lie in the left half complex plane. The transfer function matrix of output to controls must be minimum phase, or, the numerator roots of the following expression must lie in the left half plane [51]:

$$\delta y(s) = [D + H(sI - F)^{-1}G]\delta u(s) \quad (4.77)$$

The asymptotic solutions to Eq. (4.72) have the form:

$$\delta x(t) = \delta x(0) + r_x t \quad (4.78)$$

where $\delta x(0)$ is the intercept of the asymptotic solution at $t = 0$ and r_x is a compatible state rate for the asymptotic solution (see Figure 4.12).

The implementation of Eqs. (4.74) and (4.78) requires only storage of state and control rates. During the transient, the system is controlled to the asymptotic trajectory by the regulator. The calculation of the compatible state and control rates is discussed below.

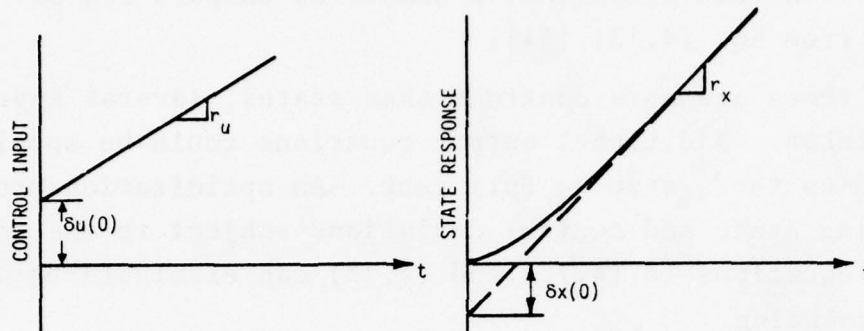


Figure 4.12 Asymptotic Solution to Linear System

The system of Eqs. (4.72) must be partitioned into an mth order and (n-m)th order system as shown below with the following restrictions:

- (1) G_1 invertible
- (2) F_{22} invertible
- (3) $F_{22} - G_2 G_1 F_{12}$ invertible

$$\frac{d}{dt} \begin{bmatrix} \delta x_1 \\ \delta x_2 \end{bmatrix} = \begin{bmatrix} F_{11} & F_{12} \\ F_{21} & F_{22} \end{bmatrix} \begin{bmatrix} \delta x_1 \\ \delta x_2 \end{bmatrix} + \begin{bmatrix} G_1 \\ G_2 \end{bmatrix} \delta u \quad (4.79)$$

$$\delta y = [H_1 \quad H_2] \begin{bmatrix} \delta x_1 \\ \delta x_2 \end{bmatrix} + D \delta u \quad (4.80)$$

The m states should be strongly influenced by the m control deflections. This situation is manifested by strong conditions of the matrices in items (1) and (3) above. Also, an analysis of the modal controllability can be used to select these states. Two types of asymptotic solutions can be derived as shown below:

Type I - Continuous State Asymptotic Solution

$$\delta x_1(0) = 0 \quad (4.81)$$

Type II - Continuous Control Asymptotic Solution

$$\delta u(0) = 0 \quad (4.82)$$

Continuous State Asymptotic Models (Type I)

For continuous state asymptotic solutions, shown in Figure 4.13, the following form is assumed:

$$\begin{bmatrix} \alpha_1 \\ \alpha_2 \end{bmatrix} = \begin{bmatrix} F_{11} & F_{12} \\ F_{21} & F_{22} \end{bmatrix} \begin{bmatrix} \alpha_1 t \\ \alpha_2 t + \delta x_2(0) \end{bmatrix} + \begin{bmatrix} G_1 \\ G_2 \end{bmatrix} [\delta u(0) + r_u t] \quad (4.86)$$

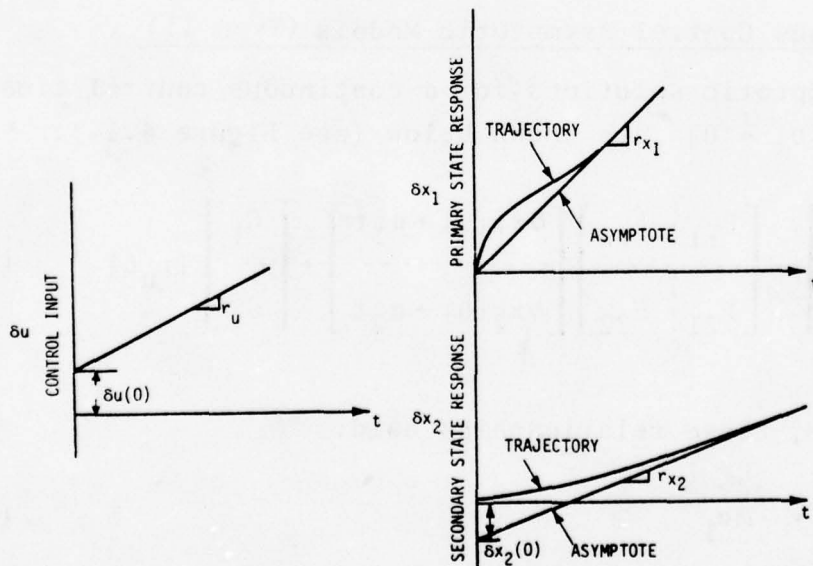


Figure 4.13 Continuous State Asymptotic Solution to Linear System

For this case, these relationships hold:

$$\alpha_2 = -M\alpha_1 \quad (4.87)$$

$$r_u = -G_1^{-1} [F_{11} - F_{12}M]\alpha_1 \quad (4.88)$$

$$\delta x_2(0) = -\bar{F}_2^{-1} [M + G_2 G_1^{-1}] \alpha_1 \quad (4.89)$$

$$\delta u(0) = G_1^{-1} [I + F_{12} \bar{F}_2^{-1} (M + G_2 G_1^{-1})] \alpha_1 \quad (4.90)$$

$$M = \bar{F}_2^{-1} \bar{F}_1 \quad (4.91)$$

$$\bar{F}_2 = F_{22} - G_2 G_1^{-1} F_{12} \quad (4.92)$$

$$\bar{F}_1 = F_{21} - G_2 G_1^{-1} F_{11} \quad (4.93)$$

The free design parameter is α_1 , and guidelines for this choice will be discussed below.

Continuous Control Asymptotic Models (Type II)

The asymptotic solutions for a continuous control time history $[\delta u(0) = 0]$ are shown below (see Figure 4.14):

$$\begin{bmatrix} \alpha_1 \\ \alpha_2 \end{bmatrix} = \begin{bmatrix} F_{11} & F_{12} \\ F_{21} & F_{22} \end{bmatrix} \begin{bmatrix} \delta x_1(0) + \alpha_1 t \\ \delta x_2(0) + \alpha_2 t \end{bmatrix} + \begin{bmatrix} G_1 \\ G_2 \end{bmatrix} [r_u t] \quad (4.94)$$

For this case, these relationships hold:

$$\alpha_2 = -M\alpha_1 \quad (4.95)$$

$$r_u = -G_1^{-1} [F_{11} - F_{12}M]\alpha_1 \quad (4.96)$$

$$\delta x_1(0) = S^{-1} T \alpha_1 \quad (4.97)$$

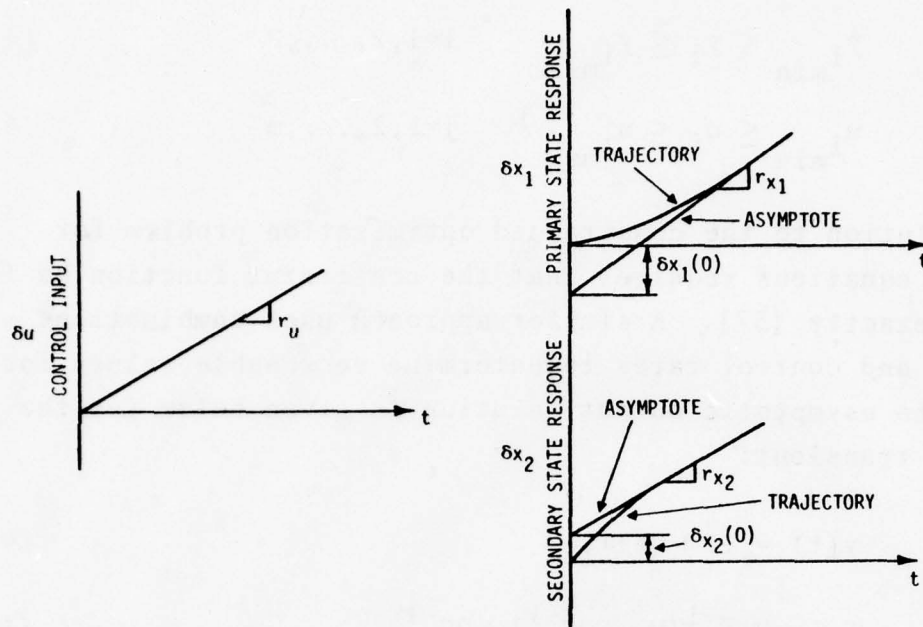


Figure 4.14 Continuous Control Asymptotic Solution to Linear System

$$\delta x_2(0) = -F_{22}^{-1}[F_{21}S^{-1}T + M]\alpha_1 \quad (4.98)$$

$$S = F_{11} - F_{12}F_{22}^{-1}F_{21} \quad (4.99)$$

$$T = I + F_{12}F_{22}^{-1}M \quad (4.100)$$

4.5.3 Rate Design

The transition models developed in the preceding section produce asymptotic solutions to the linear equations assuming that the m free parameters, α_1 , are specified. The choice of design parameter, α_1 , is iterative. The output equations can be used to specify quantities important to the system during transient motion. The asymptotic rates are designed to meet either of the following two types of inequality constraints:

$$y_{i_{\min}} \leq y_i \leq y_{i_{\max}} \quad i=1,2,\dots,P \quad (4.101)$$

$$u_{i_{\min}} \leq u_i \leq u_{i_{\max}} \quad j=1,2,\dots,m \quad (4.102)$$

The solution to the constrained optimization problem for linear equations requires that the constraint function be followed exactly [57]. A simpler approach uses combinations of output and control rates to determine reasonable values for α_1 . The asymptotic output solution is given below for the Type I transient:

$$y(t) = (P + Qt)\alpha_1 \quad (4.103)$$

$$P = -H_2 \bar{F}_2^{-1} [M + G_2 G_1^{-1}] + D G_1^{-1} \quad (4.104)$$

$$Q = H_1 - D G_1^{-1} F_{11} + (H_2 + D G_1^{-1} F_{12})M \quad (4.105)$$

The Type II solution follows directly from the results above.

The equations governing the Type I transient are collected below:

$$\text{Control Rate: } r_u = -G_1^{-1} (F_{11} - F_{12}M)\alpha_1 \quad (4.106)$$

$$\text{Output: } y(0) = P\alpha_1 \quad (4.107)$$

$$\text{Output Rate: } \dot{y} = Q\alpha_1 \quad (4.108)$$

One must choose an initial set of m equations from the $(2p+m)$ equations (4.106)-(4.108) and solve for the α_1 vector. The remaining $2p$ equations can be evaluated to verify that no limits are exceeded by the solution. The procedure is iterative, but it is usually easy to develop

an appropriate set of equations quickly and generate the resulting trajectory.

The result is a group of $n+2m$ quantities for each linear design point. The open-loop trajectories for either a Type I or Type II transient can be directly generated from this small number of quantities. The rates and jumps are scheduled in the normal manner throughout the operating envelope using ambient variables.

4.6 INTEGRAL CONTROL DESIGN PROCEDURES

4.6.1 Integral Control with Variable Structure

Typically, for a system with m control actuators, in a steady-state, m' controls will be saturated and $(m-m')$ (subject to several general controllability requirements) [49] outputs can be held at independent values. The choice of output trim quantities determines the steady-state performance of the system. Modeling errors, measurement bias, and manufacturing tolerances must be considered in developing schedules of the engine set point. Often there are many possibilities and the designer must rely on physical judgment and experience. In the case of the engine, a basic output set point is chosen to obtain rated thrust performance with minimum sensitivity to extractions, deteriorations, and engine-to-engine variations (see Chapter V). However, at many flight conditions, engine limits must be accommodated (i.e., the engine must hold a particular engine state or control above or below a critical value). The limits include minimum/maximum burner pressure, maximum turbine inlet temperature, minimum fuel-to-air ratio, maximum/minimum fuel flow, variable geometry flutter boundaries, and jet area actuator saturation (see Figure 4.15).

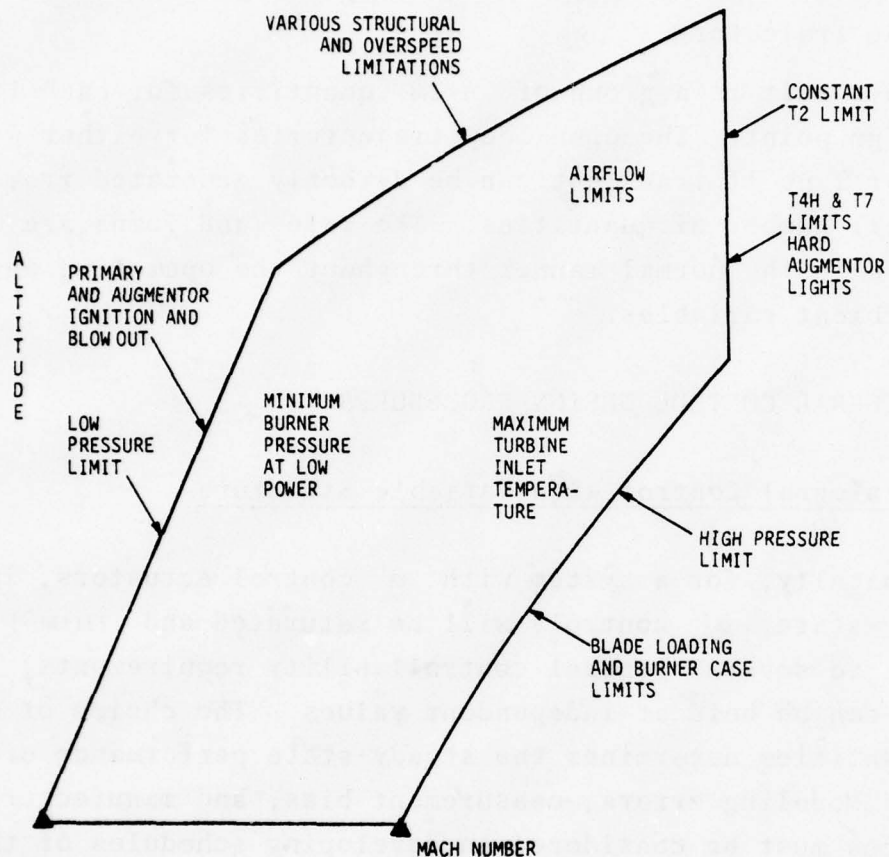


Figure 4.15 Operating Envelope Constraint Limits for the F100 Turbofan Engine

Whenever one or more of these limiting conditions exists, the structure of the trim control must be changed to hold the required limit and switched again to release the limit when the flight or power conditions allow. The switching must be accomplished without exciting unacceptable transient response and switching must occur without adverse interaction with the regulator control.

The engine response requirements are stated in terms of the transient response time or time to obtain, say, 95% of the

output and steady state trim time or the time to bring the engine to full rated performance. The regulator portion of the controller is designed to satisfy the former requirement while the trim control satisfies the latter. This separation, both structurally and spectrally, allows design of a trim control independent of the transient system, allows variable structure switching without unsatisfactory interactions, and allows a control implementation of minimal complexity.

Given the design model and the linear quadratic regulator gains, the closed-loop response to additive inputs may be written as follows:

$$\dot{\delta x} = (F + GC_x)\delta x + G\delta u' \quad (4.109)$$

where

$$\delta u = C_x\delta x + \delta u' \quad (4.110)$$

Assuming that the trim roots are spectrally decoupled from the transient roots, the following is approximately valid:

$$\dot{\delta x} \approx 0 \quad (4.111)$$

This equality implies the following:

$$\delta x = -(F + GC_x)^{-1} G\delta u' \quad (4.112)$$

$$\delta y_s = [-(H + DC_x)(F + GC_x)^{-1}G + D]\delta u' \quad (4.113)$$

or

$$\delta y_s \triangleq \bar{H}\delta u' \quad (4.114)$$

The $m \times 1$ set point vector δy_s is chosen as m measurable quantities which must be held to their reference values in steady-state (controllability is assured then if \bar{H} is invertible).

The trim integrations provide the system dynamics, namely,

$$\dot{b} = \delta y_s \quad . \quad (4.115)$$

The control law is designed,

$$\delta u' = C_{y_s} b \quad (4.116)$$

and the full controller is implemented

$$\delta u = C_x \delta x + \int C_{y_s} A \delta y_s \, dt \quad (4.117)$$

$$A = \text{diag}(\ell_j) \quad j=1, \dots, r \quad \ell_j = 0 \text{ or } 1$$

where the elements of δy_s and C_{y_s} can be switched arbitrarily (with appropriate choice of logic elements, ℓ_j) while maintaining a continuous control time history.

The design of the control law, C_{y_s} , could be performed with a single application of the regulator synthesis procedure in Eq. (4.115) for a particular set point vector. However, because the elements (and dimension) of the δy_s vector change according to engine limit conditions and control saturations, a complete design for all combinations of set point vectors would require an extremely large number of C_{y_s} matrices stored in the processor.

Several alternate procedures exist to accommodate the variable structure requirement and two will be briefly described below (see Chapter V for a complete discussion).

The various couplings in the trim system dynamics, \bar{H} , can be ignored and the integral control can be approximately designed for each output quantity individually, or

$$\delta y_{si} = \bar{h}_i^T \delta u' \quad (4.118)$$

Control weightings are chosen to represent the amount of the j th control, $\delta u_{j_{\max}}$, which should be used to trim the output error, δy_{si} , and the optimal output regulator can be designed to place the single trim root at $s = -\lambda$ as follows:

$$C_{y_{si}} = \frac{-\lambda B^{-1} \bar{h}_i}{\bar{h}_i^T B^{-1} \bar{h}_i}, \quad i=1, \dots, r \quad (4.119)$$

where $B = \text{diag}\{1/\lambda_j\}$, $j=1, \dots, m$ and the $m \times r$ implemented gain matrix, C_y , is constructed as follows:

$$C_y = \begin{bmatrix} C_{y_{s1}} & C_{y_{s2}} & \dots & C_{y_{sr}} \end{bmatrix} \quad (4.120)$$

where $m-s$ columns are chosen in Eq. (4.120) corresponding to the appropriate set point and number of unsaturated controls. All possible output set point quantities, r ($r > m$), are included as columns in the matrix. Equation (4.120) represents a single matrix which can accommodate any subset of output errors as long as a suitable set of actuators is available. The drawback of such a system is that the precise eigenvalue locations of the trim system are only approximately determined because of the neglected cross-couplings in Eq. (4.118) and as a result, the closed-loop system dynamics change with different set point vector components. The problem can be minimized if the weightings are chosen such that each control is primarily used to modulate a single output error. The eigensystem of the closed-loop dynamics must be specifically determined to assure that the exact root locations of the trim and transient system for each set of trim outputs is acceptable. Several iterations are often required.

Alternately, if the closed-loop trim system,

$$\dot{s} = \bar{H} C_{y_s} b \quad (4.121)$$

is chosen such that $\bar{H}C_{y_s}$ is upper triangular, then corresponding rows and columns of C_{y_s} can be deleted without altering the closed-loop dynamics (except eliminating an eigenvalue). Also, it is possible to switch the first element of the output vector independently of the other system elements and not affect the remaining dynamics. The upper triangular structure and eigenvalue placement determines $(m)(m+1)/2$ constraint equations. The remaining $(m)(m-1)/2$ free elements of C_{y_s} can be chosen as zero or a quadratic regulator construction can be used to resolve the ambiguity.

Either method described above produces a single $m \times r$ gain matrix. The implementation of the switching operation is now described. If s controls are saturated, $m-s$ elements of the r output quantities can be chosen for trim. The control law is then implemented as in Eq. (4.117) with the s rows corresponding to the saturated actuators deleted from the C_x and C_y matrices and $(m-s)$ diagonal elements of \underline{A} set to 1. The control is switched when an actuator saturates (delete a row and column), an engine limit must be accommodated (the first column is replaced), or the set point element associated with a saturated control tends to unsaturate the control (add the row and a column). The implementation produces an extremely simple structure for trim and transient control action which can accommodate various engine limits and control saturation, as well as accurately obtain rated engine performance throughout the envelope.

4.7 SENSOR COMPENSATION TECHNIQUES

4.7.1 Optimal Control in the Presence of Noise

In the preceding discussion of control synthesis techniques for linear and nonlinear systems, it has been assumed that the controller has perfect knowledge of the state. In

Section 4.3, a model reduction procedure was introduced which allows the control designer some freedom to choose conveniently measurable quantities as state variables. However, this is not always possible and models containing unmeasured states must sometimes be formulated to accurately describe system response. Measurement errors, model errors and sensor dynamics all tend to make the knowledge of the state only approximate. The dependence of the regulator control law on measurement uncertainties must be analyzed so that the impact on performance can be evaluated.

The regulator gains are assumed independent of the uncertainty in the knowledge of the state. This assumption allows the synthesis procedure to maintain its systematic simplicity and separates the compensation of the transduced signals from the control design. The justification of this assumption is discussed below.

For the general, linear stochastic control problem, the system follows:

$$\dot{\mathbf{x}} = \mathbf{F}\mathbf{x} + \mathbf{G}\mathbf{u} + \mathbf{w} \quad (4.122)$$

$$\mathbf{y} = \mathbf{H}\mathbf{x} + \mathbf{v} \quad (4.123)$$

In this case, \mathbf{w} and \mathbf{v} are zero mean, Gaussian random processes with covariances defined below:

$$\mathbf{E}[\mathbf{w}(\tau)\mathbf{w}^T(t)] = \mathbf{Q}\delta(t-\tau) \quad (4.124)$$

$$\mathbf{E}[\mathbf{v}(\tau)\mathbf{v}^T(t)] = \mathbf{R}\delta(t-\tau) \quad (4.125)$$

Systems acted on by random disturbances and containing random measurement errors can be modeled by Eqs. (4.122) and (4.123).

The performance index for the problem remains unchanged except that the mean value of the cost is minimized:

$$J = \frac{1}{2} E \left\{ \begin{bmatrix} x^T & u^T \end{bmatrix} \begin{bmatrix} A & N \\ N^T & B \end{bmatrix} \begin{bmatrix} x \\ u \end{bmatrix} \right\} \quad (4.126)$$

The solution to the problem follows directly from a change of coordinates. The maximum likelihood estimate of the state given all the measurements to time t is the function $\hat{x}(t)$ that makes the residual process white, i.e., [47]

$$v(t) = y(t) - H\hat{x}(t) \quad (4.127)$$

$$E[v(t) v^T(t)] = M\delta(t - \tau) \quad (4.128)$$

It can be shown that there is an $(n \times p)$ matrix function of time $K(t)$ which will produce the maximum likelihood estimate as follows:

$$\dot{\hat{x}} = F\hat{x} + Gu + K(t)v(t) \quad (4.129)$$

Now, the problem in Eqs. (4.126) and (4.129) can be rewritten with new variables as follows:

$$e = \hat{x} - x \quad (4.130)$$

$$J = \frac{1}{2} E \left\{ \begin{bmatrix} \hat{x}^T & u^T \end{bmatrix} \begin{bmatrix} A & N \\ N^T & B \end{bmatrix} \begin{bmatrix} \hat{x} \\ u \end{bmatrix} \right\} + E[e^T A e] \quad (4.131)$$

The error term, e , follows the linear system relationship,

$$\dot{e} = (F - KH)e + Kv + w \quad (4.132)$$

and is independent of the control. The regulator problem minimizes the first term of Eq. (4.131). The solution is derived in Chapter III as follows:

$$u(t) = C\hat{x}(t) \quad (4.133)$$

where the matrix C is determined under the assumptions of perfect state knowledge.

For nonlinear systems and for systems with non-Gaussian disturbances, this separation principle may not hold. However, it is often approximately true and utilization of separate design procedures for control and estimation yields satisfactory closed-loop systems.

A result of the above discussion is presented below. For the linear system, Eq. (4.122), a filter, not necessarily optimal, can be written as follows:

$$\dot{\hat{x}} = F\hat{x} + Gu + K(y - H\hat{x}) \quad (4.134)$$

where K is any ($n \times p$) constant matrix. The system of Eqs. (4.122), (4.132), and (4.133) can be written in terms of the state vector, x , and the error vector, e , as follows:

$$\begin{bmatrix} \dot{x} \\ \dot{e} \end{bmatrix} = \begin{bmatrix} F + GC & GC \\ 0 & F - KH \end{bmatrix} \begin{bmatrix} x \\ e \end{bmatrix} + \begin{bmatrix} 0 & I \\ K & I \end{bmatrix} \begin{bmatrix} v \\ w \end{bmatrix} \quad (4.135)$$

Here, C is any ($m \times n$) constant feedback. Thus, the closed-loop system dynamics and the filter dynamics can be designed independently by any method. In practice, the system dynamics F , G , and the filter dynamics will not be identical. Therefore, this separation property will be only approximate.

4.7.2 Classical Techniques

The philosophy discussed in Section 4.7.1 has been used for many years in classical design. The goal of sensor compensation is to remove the random error from the signal and produce the best estimate of the measured quantity for control.

There are two criteria used in sensor compensation. If a sensor has a very high bandwidth, spurious, high frequency input may enter the feedback loop and cause unacceptable behavior. The standard remedy is a low pass filter at a bandwidth higher than the closed-loop frequency. The simple lag filter can be represented as follows:

$$\hat{x}(s) = \frac{a}{s+a} y(s) \quad (4.136)$$

or

$$\dot{\hat{x}} = -a\hat{x} + ay(t) \quad (4.137)$$

or

$$\hat{x}(n+1) = e^{-aT}\hat{x}(n) + (1 - e^{-aT}) y(n) \quad (4.138)$$

In most digital control systems, it is standard practice to filter all input signals to eliminate aliasing. Each transduced input will have an ample amount of noise at all frequencies due to line pick-up, power supply fluctuation, EMI, etc. Sampling into this noise can often lead to difficult problems. Higher order filters with steeper attenuation characteristics are sometimes necessary.

Sensor compensation must also improve poor dynamic response relative to the closed-loop dynamics. Many transducers can be modeled by first order lags. If the bandwidth of these sensors is significantly lower than the desired closed-loop bandwidth, poor transient behavior can be anticipated due to the phase lag introduced by the instrument.

Compensation introduces phase angle into the control loop as required. The following form results:

$$\hat{x}(s) = \frac{\tau s + 1}{\alpha \tau s + 1} y(s) \quad 0 < \alpha < 1 \quad (4.139)$$

or

$$\dot{\hat{x}} = -\frac{1}{\alpha \tau} \hat{x} + \frac{1}{\alpha \tau} y + \frac{1}{\alpha} \dot{y} \quad (4.140)$$

or

$$\begin{aligned} \hat{x}(n+1) = e^{-T/\alpha \tau} \hat{x}(n) + (1 - e^{-T/\alpha \tau}) y(n) \\ + \frac{1}{\alpha} [y(n+1) - y(n)] \end{aligned} \quad (4.141)$$

The implicit derivative term in Eq. (4.140) causes amplification of high frequency noise components and this restriction determines the limit on α . Higher order lead networks can be used.

Another classical compensation network is the complementary filter. This uses two measurements of a particular variable. One signal originates from a slow response sensor with high low frequency (i.e., d.c.) accuracy. The other originates from a high response transducer with lower d.c. accuracy. The information content of the signals can be thought of as frequency decoupled. A filter is constructed for the slow response signal consisting of a noise lag shown in Figure 4.16. The complement of this is constructed whose frequency characteristic, when added to the noise roll-off, produces a flat response. This high pass filter is used to eliminate the d.c. bias associated with the fast sensor. Combining the two inputs, the frequency components are most efficiently utilized. The complementary filter is a special case of multivariable filters and Kalman estimators which will be discussed in the next section.

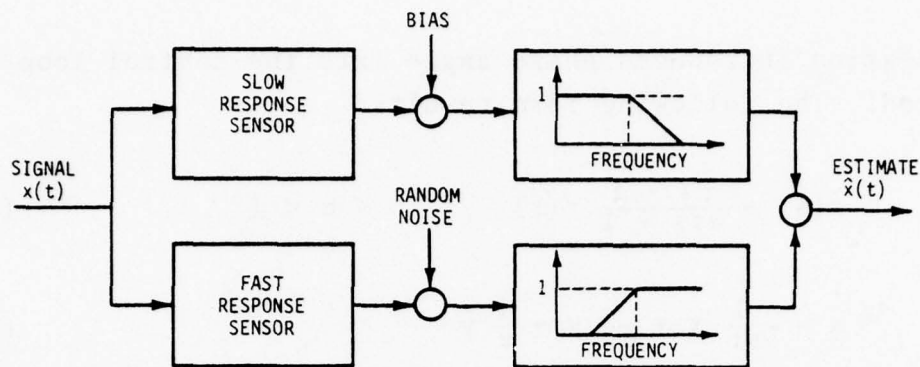


Figure 4.16 Complementary Filter Structure

4.7.3 Multivariable Filter Compensation

Classical compensation philosophy can also be applied [68] to multivariable systems. With many measurements, it is possible to choose the high bandwidth variables to regulate the transient response of the system. Slower, high accuracy sensors can be utilized for trim or bias control. The design proceeds by the appropriate choice of model, quadratic weights and, finally, filter compensation.

It is possible to implement the full order filter in Eq. (4.134) directly. This increases the complexity of the control law from simple proportional feedback to an n th order dynamic compensation. An examination of the optimal filter roots for a group of measurements typically shows that some filter time constants will be well above the closed-loop bandwidth. Single-loop prefiltering can be used to limit noise transmittance in these inputs. The measured variables will naturally decompose into a set of high bandwidth signals with no special filter requirements (i.e., except prefiltering) and a set of low bandwidth signals which are necessary to the

control function but which do not have sufficient response for use directly in the control law.

The system can be formulated as a reduced order filter [68]. Given that measurements of the state vector are made; a group of q measurements will have satisfactory response and noise characteristics and a group of $(n-q)$ measurements will require filtering for excessive high frequency noise components or insufficient bandwidth response. The system can then be partitioned as follows:

$$\begin{bmatrix} \dot{x}_1 \\ \dot{x}_2 \end{bmatrix} = \begin{bmatrix} F_{11} & F_{12} \\ F_{21} & F_{22} \end{bmatrix} \begin{bmatrix} x_1 \\ x_2 \end{bmatrix} + \begin{bmatrix} G_1 \\ G_2 \end{bmatrix} u \quad (4.142)$$

$$y_1 = x_1 \quad (4.143)$$

$$y_2 = x_2 \quad (4.144)$$

For the control law, the following form is used:

$$u = C_1 x_1 + C_2 \hat{x}_2 \quad (4.145)$$

where \hat{x}_2 is the compensated filter output. Since x_1 is known (measured) accurately, the first m equations are available for use in the estimator for x_2 . Thus, treating x_1 as an input to these equations, an estimate of x_1 may be obtained as follows:

$$\dot{\hat{x}}_1 = F_{12} \hat{x}_2 + [G_1 \mid F_{11}] \begin{bmatrix} u \\ \hat{x}_1 \end{bmatrix} \quad (4.146)$$

The filter for x_2 is written in standard form as follows:

$$\dot{\hat{x}}_2 = F_{22}\hat{x}_2 + [G_2 \quad F_{21}] \begin{bmatrix} u \\ y_1 \end{bmatrix} + K_1(y_1 - \hat{x}_1) + K_2(y_2 - \hat{x}_2) \quad (4.147)$$

We can easily combine Eqs. (4.146) and (4.147) if the matrix L is defined as

$$K_1 = LF_{11} \quad (4.148)$$

Substituting Eqs. (4.148) and (4.146) into Eq. (4.147) yields the following:

$$\begin{aligned} \dot{\hat{x}}_2 = & (F_{22} + LF_{12} - K_2)\hat{x}_2 + (F_{21} + LF_{11})y_1 \\ & + (G_2 + LG_1)u + K_2y_2 - L\dot{\hat{x}}_1 \end{aligned} \quad (4.149)$$

The implementation of Eq. (4.149) in filter form is shown below and in Figure 4.17:

$$\hat{x}_2 = \theta - Ly_1 \quad (4.150)$$

$$\begin{aligned} \dot{\theta} = & (F_{22} + LF_{12} - K_2)\theta + (G_2 + LG_1)u + K_2y_2 \\ & + (F_{21} + LF_{11} - F_{22}L - LF_{12}L - K_2L)y_1 \end{aligned} \quad (4.151)$$

The gains L and K_2 are chosen to yield satisfactory response of the estimates of x_2 [68]. An examination of the filter shows that the control inputs, high bandwidth sensor information, and lower bandwidth signals are used in conjunction with the state model to form an estimate of x_2 which has acceptable frequency response and noise characteristics. The filter uses

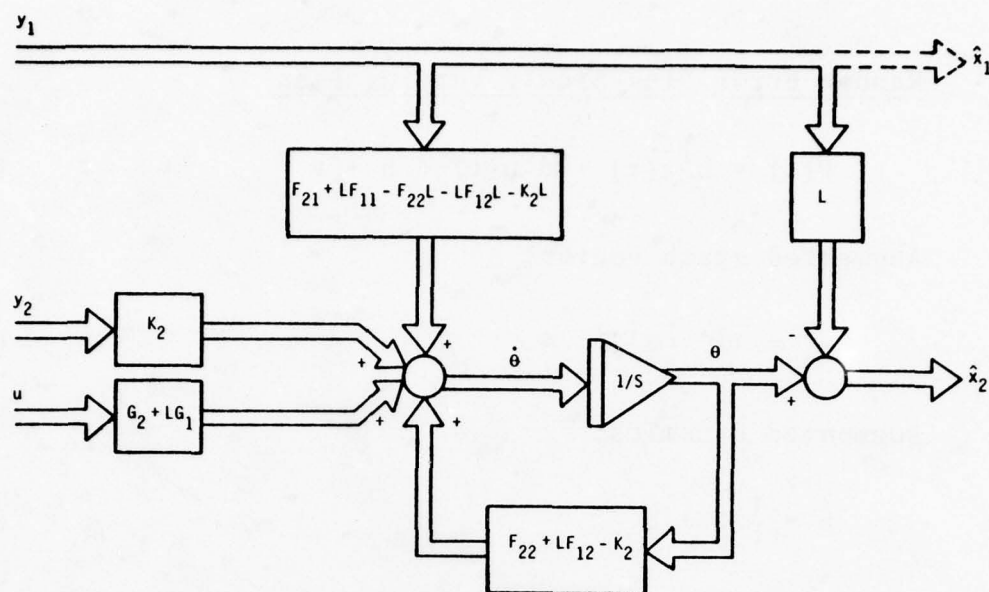


Figure 4.17 Reduced Order Filter Implementation

a blend of inputs in an effective manner to produce an efficient output.

4.7.4 Sensor Error Models

It was stated above that systems driven by random noise and using measurements with random errors could be modeled by Eqs. (4.122) and (4.123), i.e., linear systems with white noise inputs. In order to use this form, the noise process must be white. Examples of the most common models to obtain this form are given below.

Purely Random Error

$$y(t) = h^T x(t) + d^T u(t) + v \quad (4.152)$$

$$E(v) = 0 \quad (4.153)$$

$$E(vv^T) = R\delta(t-\tau) \quad (4.154)$$

Random Error Plus Slowly Varying Bias

$$y(t) = h^T x(t) + d^T u(t) + b + v \quad (4.155)$$

Augmented state vector:

$$x_a^T = [x^T \mid b^T] \quad (4.156)$$

Augmented dynamics:

$$\dot{b} = \frac{1}{\tau} b + \xi \quad (4.157)$$

$$E(\xi) = 0 \quad (4.158)$$

$$E(\xi \xi^T) = 2\bar{b}^2 \tau \quad (4.159)$$

where τ is the estimate of the correlation time of the bias (e.g., the mean time between zero crossings [49]) and \bar{b}^2 is the approximate covariance of the bias.

First Order Sensor Lag

$$y = y_m + \xi \quad (4.160)$$

$$\dot{y}_m = \frac{-1}{\tau} [y_m - h^T x(t) - d^T u(t)] \quad (4.161)$$

or

$$y = h^T x(t) + d^T u(t) + v \quad (4.162)$$

$$\dot{v} = \frac{-1}{\tau} v + \xi \quad (4.163)$$

$$E(\xi) = 0 \quad (4.164)$$

$$E(\xi^T \xi) = \frac{-1}{\tau} \bar{b}^2 \quad (4.165)$$

Higher Order Sensor Dynamics

$$y = y_m + v \quad (4.166)$$

$$\dot{y}_m = F_m y_m + G(h^T x + d^T u) \quad (4.167)$$

$$x_a^T = [x^T \ ; \ y_m^T] \quad (4.168)$$

$$y = [0 \ ; \ I] \begin{bmatrix} x \\ \vdots \\ y_m \end{bmatrix} + v \quad (4.169)$$

4.7.5 Final Value Filter for Nonlinear System

In some physical systems, there is a strict requirement on regulation below some physical limit. The system makes transitions throughout its envelope. At some point, the operation takes it to the boundary, i.e., the state which holds an output at its limiting value. Operation in a manner which exceeds this limit either transiently or in steady-state is forbidden (e.g., material melting points or strength limits). Since the system is typically nonlinear and time-varying, only an approximate model is available and the accuracy of the model in predicting the actual outputs of the system can be too poor to be used. Also, outputs may be measured with slow response transducers relative to the control bandwidth.

Filtering theory can be used to combine information from the control inputs, output measurements, sensor models, and the open-loop trajectory to form an estimate of the output. It is desirable to estimate the value which will be attained in steady-state. If this estimate is available prior to the moment of exceedance, then appropriate limiting action can be initiated to avoid overshoot.

Consider a step change in operating point which produces a state trajectory as discussed in Section 4.1. This is shown schematically in Figure 4.18. For simplicity, let the transition take place in a region of the operating envelope where a constant coefficient, linear model is valid, i.e.,

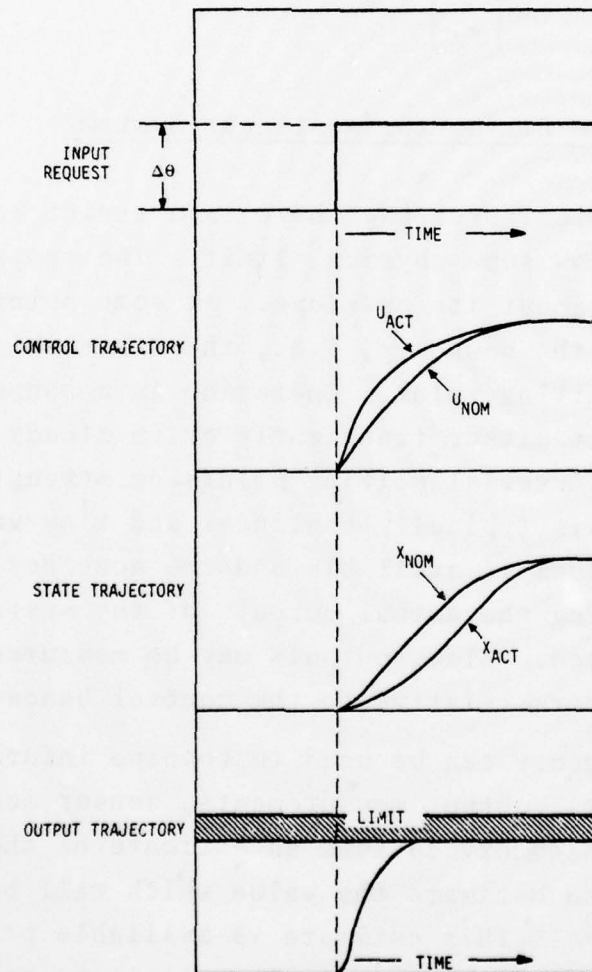


Figure 4.18 Illustration of Step Response of a Nonlinear System During an Output Limited Transient

AD-A052 420

SYSTEMS CONTROL INC PALO ALTO CALIF AERONAUTICAL AND--ETC F/G 21/5
F100 MULTIVARIABLE CONTROL SYNTHESIS PROGRAM. VOLUME 1. DEVELOP--ETC(U)
JUN 77 R L DE HOFF, W E HALL, R J ADAMS F33615-75-C-2053

UNCLASSIFIED

AFAPL-TR-77-35-VOL-1

NL

3 of 4

AD
A052420



$$\dot{\delta x} = F\delta x + G\delta u \quad (4.170)$$

$$\delta u = C\delta x \quad (4.171)$$

$$\delta y = H\delta x + D\delta u \quad (4.172)$$

In steady-state,

$$\delta y_{SS} = H_{CL} \delta u_{SS} \quad (4.173)$$

where H_{CL} is the closed-loop gain of the system,

$$H_{CL} = -(H - DC)(F + GC)^{-1}G + D$$

and

$$\delta u_{SS} = u_{SS} - u_o \quad (4.174)$$

The perturbation, δu_{SS} , is the steady-state control hang-off due to scheduling errors and plant parameter uncertainties (see Appendix B). An estimate of the final value of y is known from the reference schedule as follows:

$$y_o = f(\theta) \quad (4.175)$$

and y_{SS} , the actual output, could be calculated if δy_{SS} was known, i.e.,

$$y_{SS} = y_o + \delta y_{SS} \quad (4.176)$$

The steady-state hang-off in an engine control without integral compensation is due primarily to inaccuracies in the open-loop reference schedules. The mismatch is due to build differences, aging, and approximations in the implementation. The hang-off, however, is equivalent to that caused by a constant disturbance. Thus, compensation can be designed for constant disturbances of unknown origin. This problem is

discussed in Section 3.5. The solution results in a reduced order filter for estimation of the steady-state hang-off [49]. It is extended below to include measurements containing errors.

Consider the system driven by constant disturbances of unknown structure,

$$\delta \dot{x} = F\delta x + G\delta u + \Gamma w \quad (4.177)$$

$$\delta y = H\delta x + D\delta u \quad (4.178)$$

where Γw is an unknown $n \times 1$ vector. In steady-state, the equilibrium of the closed-loop system can be written analogously to Eq. (4.173) assuming no scheduling errors:

$$\delta y_{SS} = H_w \Gamma w \quad (4.179)$$

A filter to estimate the final value of the output due to the unknown disturbance can be formulated in general as follows:

$$\delta \dot{\hat{y}}_{SS} = K(\delta y_{SS} - \delta \hat{y}_{SS}) \quad (4.180)$$

where the "dynamics" of the system are

$$\delta \dot{\hat{y}}_{SS} = 0 \quad (4.181)$$

and K is chosen as a positive definite matrix for stability [49], i.e., the filter converges to the actual steady-state hang-off. From Eq. (4.177),

$$\Gamma w = \dot{x} - F\delta x - G\delta u \quad (4.182)$$

and from Eqs. (4.179) and (4.180), the following holds (dropping the SS subscripts):

$$\dot{\delta \hat{y}} = K [H_w(\delta \dot{x} - F\delta x - G\delta u) - \delta \hat{y}] \quad (4.183)$$

The form of Eq. (4.183) is a reduced order estimator for δy using measurements of δx , δu , and δy . The techniques presented for sensor error modeling are directly applicable. The measurements of δy containing sensor errors (typically slow response characteristics) can be augmented to the system and the filter synthesis carried out.

A specialization of Eq. (4.183) is important in some applications. If the modal components of the output are associated primarily with a portion of the dynamics which is much faster than the dominant control roots, the model reduction procedure will yield an equation of the following form:

$$\delta y \approx D_r \delta u \quad (4.184)$$

where δu has the interpretation of the control deviation away from the trajectory which produces the correct final value, namely $\delta y_{SS} = 0$. In this case, δy can be interpreted as a measure of the final deviation in the output calculated during the transition. Since this deviation is not known because of trajectory inaccuracies, Eq. (4.184) can be treated as a biased measurement of the final output and can be used as an auxiliary measurement equation. An augmented, reduced order estimator under these assumptions is given below:

$$\dot{\delta \hat{y}} = K_1 (D_r \delta u - \delta \hat{y} - \hat{b}) + K_2 (\delta \hat{y}_m - \delta \hat{y}) \quad (4.185)$$

$$\dot{\hat{b}} = K_3 (D_r \delta u - \delta \hat{y} - \hat{b}) \quad (4.186)$$

$$\dot{\delta \hat{y}}_m = \alpha (\delta \hat{y} - \delta \hat{y}_m) + K_4 (\delta y_m - \delta \hat{y}_m) \quad (4.187)$$

where a transducer input, δy_m , with time constant $\tau = 1/\alpha$ is used.

The algorithm tends to act as a complementary filter using the control deviations as high frequency information. A specific application is discussed in detail in Chapter V for estimating turbine inlet hang-offs above physical limits.

4.8 SUMMARY

The principal techniques of locally linear control design and implementation for nonlinear systems is presented. The theoretical foundations are reviewed and the assumptions necessary for application of the procedure stated. Modeling of the nonlinear system using locally linear perturbations is described. Techniques for manipulating the model into a form containing convenient parameterization and important dynamics is discussed.

For full envelope operation, a method for integrating locally linear model controls together is needed. A passive adaptive technique is discussed which is inherently suited for minicomputer implementation.

A successful control implementation must handle large transitions as well as account for system degradation and variation. A transition control structure is described with integral trims to produce the desired properties. Set point variation and control saturations are also accommodated by the approach.

Sensed variables of the system are often corrupted by error sources due to the transducer. Various techniques for sensor compensation are discussed and their impact on control performance is evaluated.

CHAPTER V

DESIGN OF A MULTIVARIABLE CONTROLLER FOR THE F100 ENGINE

5.1 INTRODUCTION AND OVERVIEW

In Chapter II, the important issues in the design of turbine engine controls are discussed along with the approach of previous work in utilizing classical and optimal design tools. In Chapter III, important linear techniques are presented for multivariate feedback control laws. In Chapter IV, techniques from linear theory to derive nonlinear controllers which function throughout the operating envelope of the system, accommodate large and small inputs, and produce robust regulation in the presence of disturbances are illustrated. In this chapter, an application of these principles is described for the F100 turbofan engine. The numerical outputs are accumulated in Appendices C through H.

The perturbational control structure chosen for the F100 engine is described. Input and output characteristics are presented. Each component subsystem is then derived in more detail. The reference point schedule algorithm produces feed-forward state and control information. The linear engine model is developed for which design models for linear quadratic regulator synthesis are calculated. Modification of the resulting state feedback matrices to accommodate full envelope operation is controlled by the gain scheduling algorithm. Integral control modes, sensor compensation, and switching are next presented to illustrate accommodation of practical constraints. Finally, the design for large transients is made using linear models as first-order approximations to

the nonlinear trajectory. The resulting logic is an implementable control for full envelope operation well within the requirements of the control criteria.

5.2 F100 ENGINE SYSTEM

5.2.1 F100 Turbofan Engine

The Pratt & Whitney F100 turbofan engine is an example of a production, high technology, propulsion system (see Figure 5.1). The F100 is a low bypass ratio, twin spool, axial flow aircraft turbine with the following characteristics:

- (1) three-stage fan driven by a two-stage turbine;
- (2) ten-stage compressor driven by an air-cooled, two-stage turbine;
- (3) annular fan duct discharging into a mixed flow augmentor;
- (4) variable area nozzle;
- (5) variable geometry fan inlet guide vanes;
- (6) variable geometry stators in the compressor; and
- (7) variable compressor discharge bleeds.

The production fuel control of the F100 engine is basically a hydromechanical implementation with an engine-mounted electronic supervisory control. Because of test availability of an engine under the NASA Full Scale Engine Research Program and the multivariable nature of the F100, it was chosen as a test bed for the demonstration of the LQR synthesis described in this report. A more complete description of the F100 engine is presented in Ref. 1.

5.2.2 Sensor and Actuator Characteristics

The dynamic characteristics of the control actuators and sensors modeled on the nonlinear digital simulation and the NASA LeRC hybrid simulation are completely described in Refs. 1 and 2. A brief description is presented below.

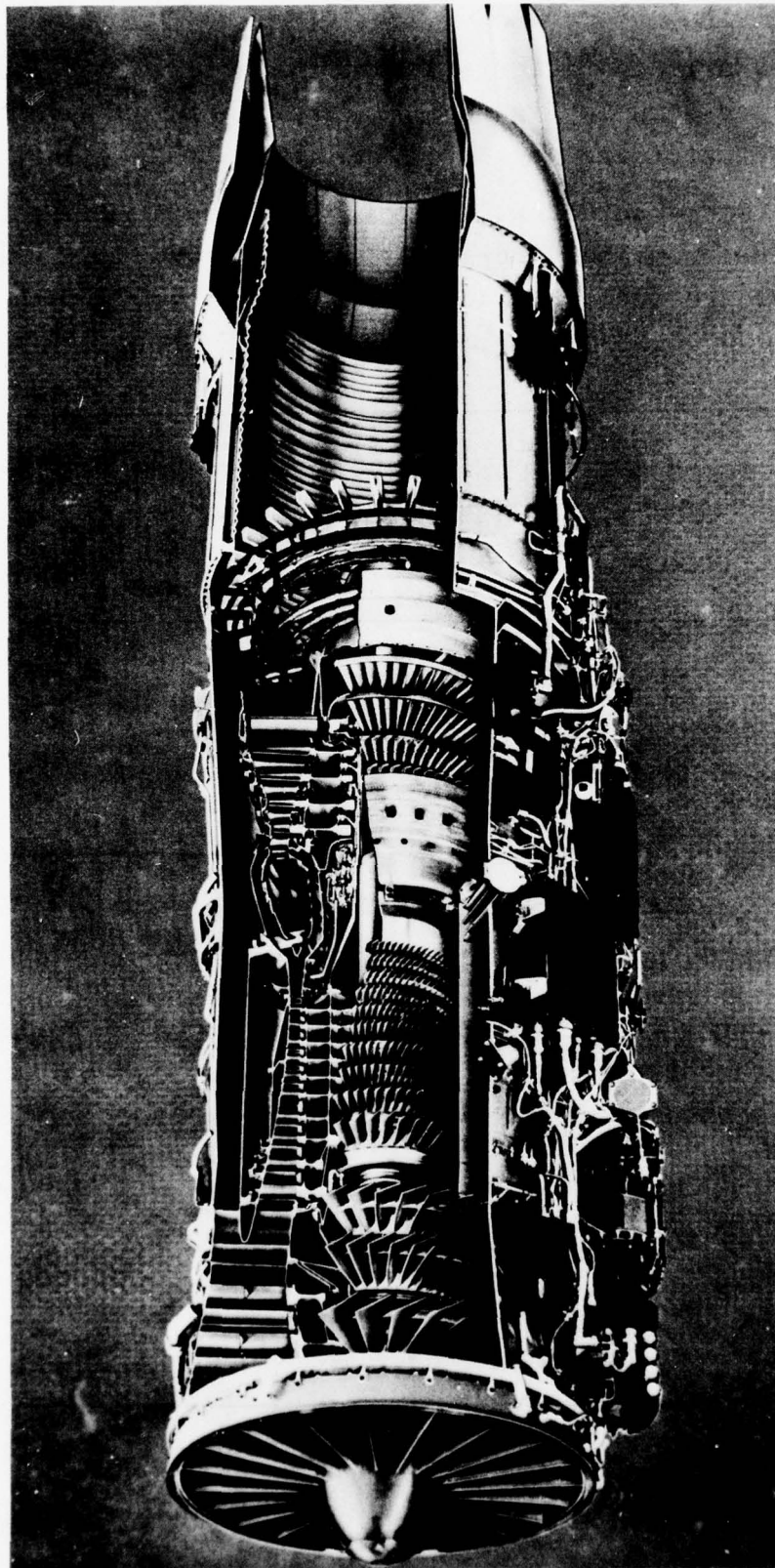


Figure 5.1 F100 Turbofan Engine

Actuators

The dynamic characteristics of the actuators are presented in linearized form in Figure 5.2. The characteristic values for each actuator are presented in Table 5.1.

The primary actuated variable is the main burner fuel supply. Fuel commands are supplied to a hydromechanical control for the fuel pump and regulating valve. There are

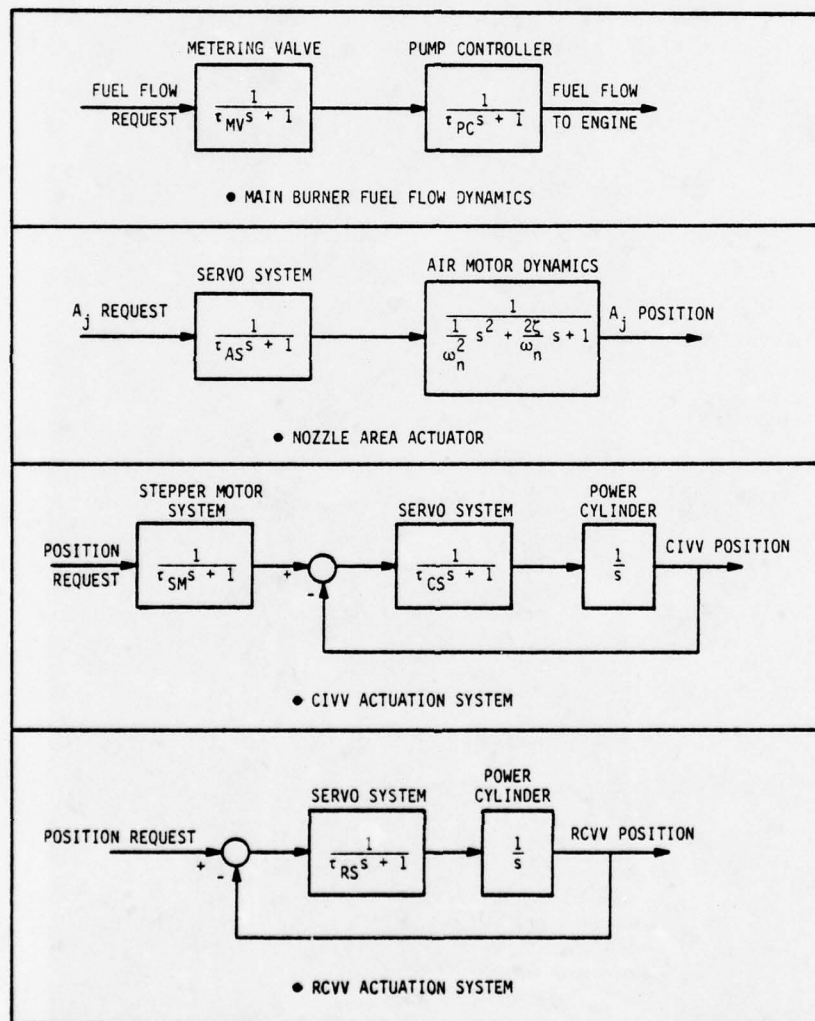


Figure 5.2 Linearized Actuator Dynamical Models

Table 5.1
Characteristic Actuator Time Constants
(see Fig. 5.2)

ACTUATOR	TIME CONSTANT
Main Fuel Pump (WFMB)	$\tau_{MV} = 0.02 \text{ sec}$ $\tau_{PC} = 0.1 \text{ sec}$
Area Actuator (A_J)	$\tau_{AS} = 0.01 \text{ sec}$ $\omega_n = 3-6 \text{ Hz}^*$ $\zeta = 0.27 - 0.57^*$
Compressor Inlet Variable Vanes (CIVV)	$\tau_{SM} = 0.02 \text{ sec}$ $\tau_{CS} = 0.01 \text{ sec}$
Rear Compressor Variable Vanes (RCVV)	$\tau_{RS} = 0.01 \text{ sec}$

* Depending on altitude and Mach number

first-order dynamics associated with the metering valve response and the pump servo regulator. Of these two, the servo pump response predominates. There is hysteresis in the system resulting from backlash in linkages and other hydro-mechanical elements. For the research control actuator, the hysteresis is negligible.

The rear servo compressor variable stator vane (RCVV) system is a complex servo system with nonlinear rate limits and hysteresis characteristics. The response rates of the system are extremely fast relative to the fuel pump dynamics. The system is linearized by removing the hysteresis and rate limit effects as shown in Figure 5.2.

The compressor inlet vane (CIVV) system is a stepper motor actuated servo loop. Electronics is provided for loop compensation of the servo system and the resulting linear behavior is shown in Figure 5.2. Hysteresis and step quantization effects are negligible.

The jet area actuator is an air-driven system whose response characteristics are dependent on the engine operating conditions. The important aspects of the response to small perturbations are the 18-36 rad/sec bandwidth and fairly low ($\zeta = 0.27 - 0.56$) damping ratio.

The linearized dynamics shown in Figure 5.2 are the basis for the analysis of actuator models used in the regulator control. The most efficient representation is included in the synthesis procedure. The effect of nonlinearities such as hysteresis, rate limits, variable time constants, etc., are then evaluated on the full nonlinear simulation of the engine/actuation system.

Sensors for the NASA Controls Research Engine

The transducers sensing the important aerothermodynamic quantities in the engine gas path are listed in Table 5.2. For multivariable control, typical state-of-the-art transducers are used with response times shown in the table. The time constants of the rotor speeds and pressure transducers are generally faster than 20 rad/sec. The engine face temperature probe time constant of 1.5 sec is typical of a shielded thermocouple.

The fan turbine inlet temperature (FTIT) dynamics are shown in Figure 5.3. The probe dynamics have this form because a harness configuration is used to withstand the adverse environment. This model was developed by Pratt & Whitney Aircraft Group to represent the behavior of the sensor throughout the flight envelope. The time constants are somewhat slower than the typical response time constants of the engine and represent a critical controlling quantity. A steady-state filter for the fan turbine inlet temperature was developed to provide the increased response needed for control without degrading the accurate steady-state characteristic. This system will be discussed in Section 5.9.

Table 5.2
Engine Sensor List

SENSOR LOCATION	SYMBOL	TYPE	TIME CONSTANT
Engine Face Temperature	TT2	Thermocouple	1.5 sec
Engine Face Pressure	PT2	Strain Gauge	0.02 sec
Fan Discharge Temperature	TT25C	Thermocouple	1.5 sec
Fan Exit $\Delta p/p$	DP25	Strain Gauge	0.02 sec
Fan Speed	N_1	Tachometer	0.03 sec
Compressor Speed	N_2	Tachometer	0.05 sec
Burner Pressure	P_B	Strain Gauge	0.02 sec
Fan Turbine Inlet Temperature	TT45	See Fig. 5.3	See Fig. 5.3
Augmentor Entrance Pressure	PT6	Strain Gauge	0.02 sec
Main Burner Fuel Flow	WFMB	Flowmeter	0.05 sec
Jet Area Servo Stroke	A_J	Position Transducer	See Table 5.1
Inlet Guide Vane Deflection	CIVV	Servo Feedback	See Table 5.1
Compressor Vane Deflection	RCVV	Servo Feedback	See Table 5.1

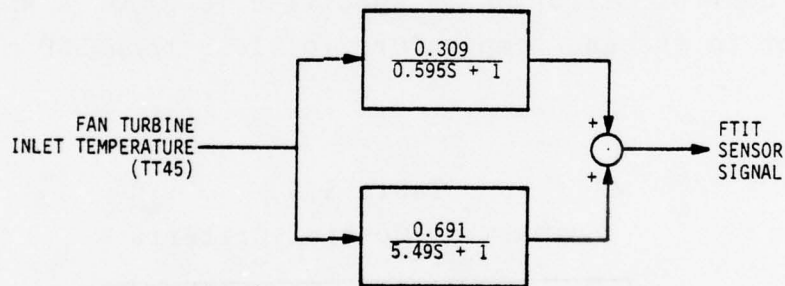


Figure 5.3 Fan Turbine Inlet Temperature (FTIT)
Sensor Model

5.2.3 Engine Envelope and Control Criteria

High performance turbine engines inevitably operate at or near design limits of speed, pressure, temperature and airflow. Accurate control of these quantities is necessary to achieve performance levels without producing unacceptable deterioration

of the components. The operating envelope of the engine is often determined by these limiting aspects. A detailed discussion of the control criteria for the F100 engine is given in Refs. 1 and 2. The impact of the criteria on control design is summarized below and in Table 5.3.

Temperature Limits

Temperature limits are encountered in operation of the engine at various stations throughout the core stream gas path. Since transducing accuracy and response times are poor within the burner section of the engine, the control requirement for all core stream temperature limiting is expressed as a limit on the gas temperature at the low pressure turbine entrance. At this point, the cooler environment allows placement of accurate and durable probes which correlate well with other unmeasurable sense points in the burner section.

In order to meet transient response specifications, the current control criterion is specified to allow a small (2%) overshoot in the gas temperature for less than 500 msec. This

Table 5.3
Summary of Control Criteria

- | |
|--------------------------------------------|
| 1. Engine Protection |
| • Temperature Limits |
| • Speed Limits |
| • Pressure Limits |
| • Engine Fluctuations |
| • Fan and Compressor Stall Margins |
| • Augmentor Spikes |
| • Structural Stability |
| 2. Compatibility with Inlet/Aircraft |
| • Airflow Corridor |
| • Minimum Burner Pressure |
| 3. Steady-State Performance |
| • Thrust and Fuel Consumption Requirements |
| • Control Sensitivity |
| Deterioration |
| Installation |
| Inlet Conditions |
| • Repeatability |
| 4. Transient Requirements |

criterion is evaluated in the simulation only because the engine probes are too slow to accurately produce measurements of this overshoot.

The steady-state temperature limit is used to set engine operating point performance at intermediate power throughout most of the operating envelope. The controller is required to modulate the engine to attain exactly this temperature in steady-state.

Speed Limits

Because of physical limitations of rotors operating at high temperatures, overspeed limits were placed on the compressor and fan spools. These limits were roughly 2% and 4% of the intermediate operating values, respectively. These limits represented transient requirements, since the engine never operates exactly at the overspeed limit.

Pressure Limit

Maximum burner pressure is restricted to assure structural integrity. At several flight conditions, engine intermediate power performance is set by operation at the maximum burner pressure limit. Minimum burner pressure is specified at 48 psia to provide an air source for auxiliary usage. Idle power is set by operation on the minimum burner pressure limit at most subsonic, altitude points within the envelope.

A conflict in the minimum burner pressure and maximum turbine inlet temperature occasionally occurs. Operation at the maximum temperature produces too low a burner pressure while operation at minimum burner pressure produces an over-temperature condition. In these cases, the control is required to hold the maximum turbine temperature even though this results in substantially lower burner pressures than otherwise allowed.

Structural Stability

The variable geometries (CIVV and RCVV) have a limited motion due to physical stops and aerodynamic flutter boundaries. Also, to keep geometry motion within the regions of accurate modeling, the geometry excursions are limited to $\pm 6^\circ$ and $\pm 8^\circ$ from the nominal hardware schedules, respectively. At some operating conditions, the vanes must be exactly at a physical stop to produce the specified performance.

Airflow Corridor

Engine airflow is set by inlet requirements. At supersonic flight points, the airflow corridor is restrictive and the engine can operate on the limit in several regions. No direct measurement of airflow is made by the control. The airflow requirement is translated into restrictions in power level such that at supersonic conditions, engine idle is set by a minimum throttle position and at many supersonic conditions the engine cannot operate below intermediate power. This restriction makes the controller's task at supersonic conditions one of only disturbance regulation.

Transient Control Criteria

To develop regulators, it is necessary to formulate a performance index representing a group of design parameters. It is critical to provide transient control criteria including both quantitative and qualitative specification of the desired small perturbation response. The specific transient control criteria developed for the F100 are discussed below and more completely in Ref. 1.

The regulator must provide smooth tracking of the reference trajectory. Rapid and smooth response to small perturbations is important. It is difficult to assign the desired response time constants because the engine has a wide range

of natural response characteristics. For example, a fast controller at 0K/1.2 would probably be too stiff at 45K/0.9 where the engine natural response is much slower. The criterion of fast response is not as important as other aspects of the closed-loop behavior.

The most important transient consideration is regulation near critical structural limits without exceeding them. Near intermediate power, small accelerations must be controlled so that the maximum operating temperature and/or pressure is not exceeded. Rotor overspeeds are only slightly greater than the normal speeds at intermediate power. Transients to intermediate power should be well damped. Minimum burner pressure and minimum fuel-to-air ratio must be accommodated during deceleration near idle power at most subsonic points. Variable geometry limits are imposed on RCVV and CIVV motion to avoid excursions into flutter and stall regions. Surge margin limits on the fan and compressor cause an implied limit on fuel flow and jet area modulations at low power.

The protection limits are natural extensions of steady-state operating requirements. A group unique to transient operation is also specified. When the augmentor is ignited, pressure tends to quickly increase in the duct and cause the fan to run at a reduced stability margin. Typically, the nozzle is opened to reduce the increased pressure and relieve the loading on the fan. Due to slight mismatches in coordination between nozzle area and augmentor ignition, small pressure pulses are experienced at the fan discharge station. Positive pulses are caused by too slow or too small a nozzle area and negative pulses from the reverse situation. These pulses can cause significant performance degradation from fan surge and augmentor blowout at subsonic altitude points where operating pressures are low. The control should modulate the geometry to reduce the effects of this pulse. This function is complex and suited to the multivariable aspect of the

regulator. Control action to accommodate a positive pressure pulse sensed by the augmentor pressure probe would be to close the inlet guide vanes and open the nozzle area. As the fan speed drops, added fuel flow and trim of the geometry should proceed in a coordinated fashion.

A second transient criterion is the limiting of temperature overshoots. Small overtemperatures are allowed to permit rapid thrust response. Reducing the overshoot without significant degradation in response is a desired goal.

An objective of the regulator is small signal stability in the presence of actuator hysteresis, dead zones, and significant time constants in thermal response and sensor outputs. The control criteria limit variations in thrust at any frequency to be less than 1% of the intermediate level. This thrust requirement translates to about 0.25% of intermediate airflow regulation and about ± 20 RPM rotor speed. This accuracy requirement can be compared to the ± 20 RPM accuracy of the rotor speed sensors themselves.

Qualitative transient criteria provide goodness factors to compare designs which otherwise satisfy the quantitative specifications. The requirements include reduced sensitivity to instrument errors. Single-loop control designs utilize a single measurement input. If a failure or degradation of this sensor occurs, the system response degrades. In a multivariable control, there is redundant information available from sensors and if the control is properly designed, single sensor sensitivity can be reduced. Conflicting with this is the desirability of fast and accurate response, manifested by smooth thrust recovery, engine limit protection and disturbance attenuation.

The transient control criteria form the qualitative and quantitative framework for the development of the control cost function as well as the choice of dynamic model of the engine.

Miscellaneous Steady-State Requirements

The controller was required to operate satisfactorily in the presence of specified deterioration, power extractions and bleed flow in comparison to the F100 production control.

5.3 OVERVIEW OF THE CONTROL STRUCTURE

The control structure is shown in Figure 5.4. The design of each block will be described in the following section. References to the theoretical foundations described in Chapters III and IV are made extensively to simplify the treatment.

The controller is basically a perturbational regulator. State feedback is used to modulate control variables to track a synthesized trajectory. Integral control is provided to obtain defined steady-state performance. The integral control has a variable structure to accommodate varying set points and

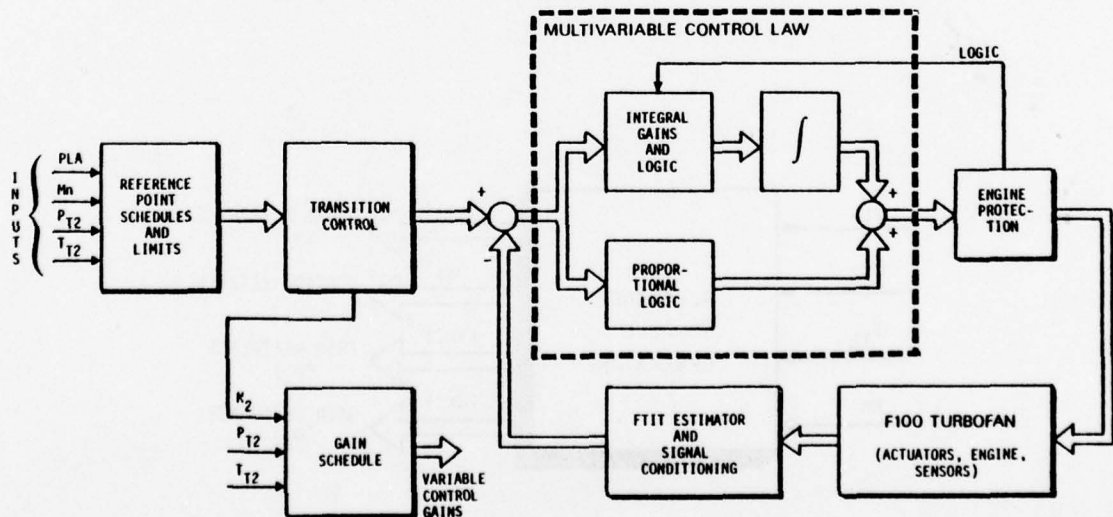


Figure 5.4 F100 Turbofan Multivariable Control Structure

actuator limits. The reference trajectory is approximated from reference point schedules and a trajectory synthesis algorithm. Gains are scheduled as a function of power and flight point.

The following sections, 5.4-5.9, detail the five principal control logic elements.

5.4 REFERENCE POINT SCHEDULES

5.4.1 Purpose

The control must produce inputs which cause the system to operate with outputs appropriate to the power level and flight condition. In the F100 control, the transformation from ambient conditions and power lever angle to rotor speeds, pressures and temperatures is performed by the reference point scheduling algorithm (see Figure 5.5).

The F100 engine has five actuators to modulate steady-state engine conditions. Assuming that the bleeds are closed and the variable geometry has attained the prescribed hardware schedules for maximum efficiency, there are two remaining

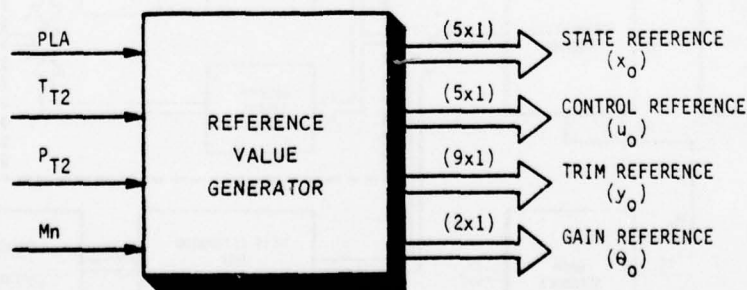


Figure 5.5 Reference Schedule Algorithm

degrees of freedom of the operating point represented by the main burner fuel flow and the exhaust nozzle area.

Typically, the problem of the engine operating point is addressed during the engine design and various rating points are developed at which the engine must produce given levels of performance. The control system is then designed to operate at the rated performance points and to modulate the engine between rating points smoothly and efficiently. In the F100 production control, the engine is operated to meet rated performance in this manner using a supervisory trim and a hydro-mechanical governor.

In this research control program, the reference points were specified at the conditions (e.g., fuel flow and jet area) held by the production control. While this procedure does not exploit the full versatility of the digital computer in running extremely detailed and optimal set point maps, it did provide a demonstration of the flexibility of the control in matching a given set of performance data as represented by the production control.

5.4.2 Implementation Procedure

The reference schedule generation uses steady-state data representative of the set points held by the production control. A number of points were generated at subsonic and supersonic conditions from the nonlinear digital simulation. The data spans the engine operating line from sea level to high altitude and from intermediate to idle power. It represents rotor speeds, fuel flow, pressures, temperatures, and areas attained at the power lever angles, ambient pressures, temperatures, and Mach numbers.

The technique for linear break point interpolation is used to approximate nondimensional steady-state data. This approximation produced small errors in state and control matches.

The set of speeds, pressures, and temperatures calculated by the schedules is not precisely an equilibrium point. This does not degrade the performance because the integral control logic applies the required trim. State and control feedforward scheduling produces an improved transient response characteristic. This concept is discussed in Section 4.5 and Appendix B.

Figure 5.6 shows a simplified diagram of the reference point schedules. The algorithm schedules the fan stream and core stream variables separately. Fan airflow is the independent variable for the fan stream and compressor speed schedules the core variables. A nondimensional parameterization is used.

5.4.3 Approximation Techniques

In the computer implementation, the reference point schedule data is stored in tabular format. The tables are derived from data points generated at various steady-state conditions. There is a trade-off in accuracy and storage/execution time of the algorithm. A least squares procedure for accurate break point interpolation table construction is discussed in Section 4.4.

5.4.4 Description of Implementation

The reference schedules are shown in Appendix C. A description of each block is given below.

Fan Stream Schedules

The principle scheduling variable for the fan stream parameters is airflow (see Figure 5.7). The power lever angle is translated into a requested airflow to set the performance of

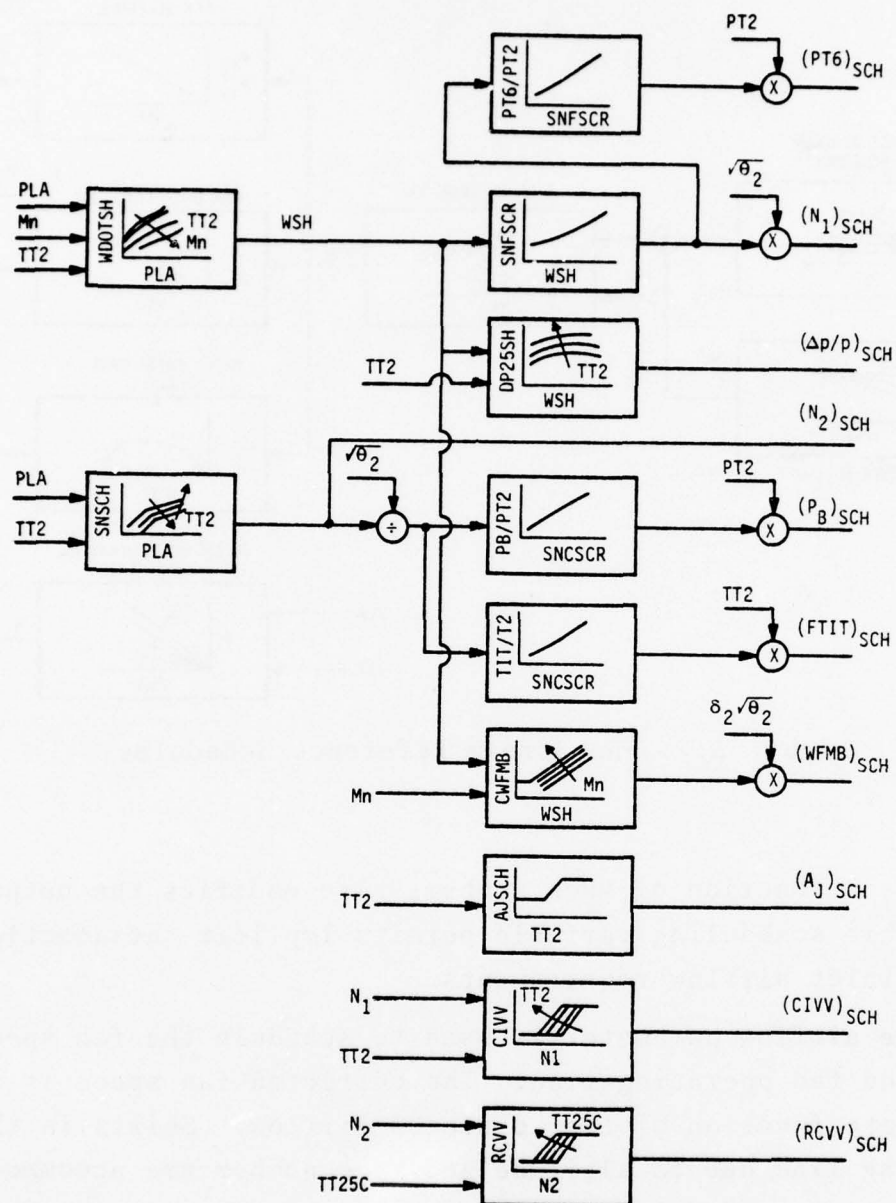


Figure 5.6 Reference Point Scheduling Algorithm - Overview

the engine. This relationship is a function of the ambient temperature. The airflow is modified at lower power and low Mach number to mimic the production control in generating the rated sea level static, idle thrust. The airflow corridor,

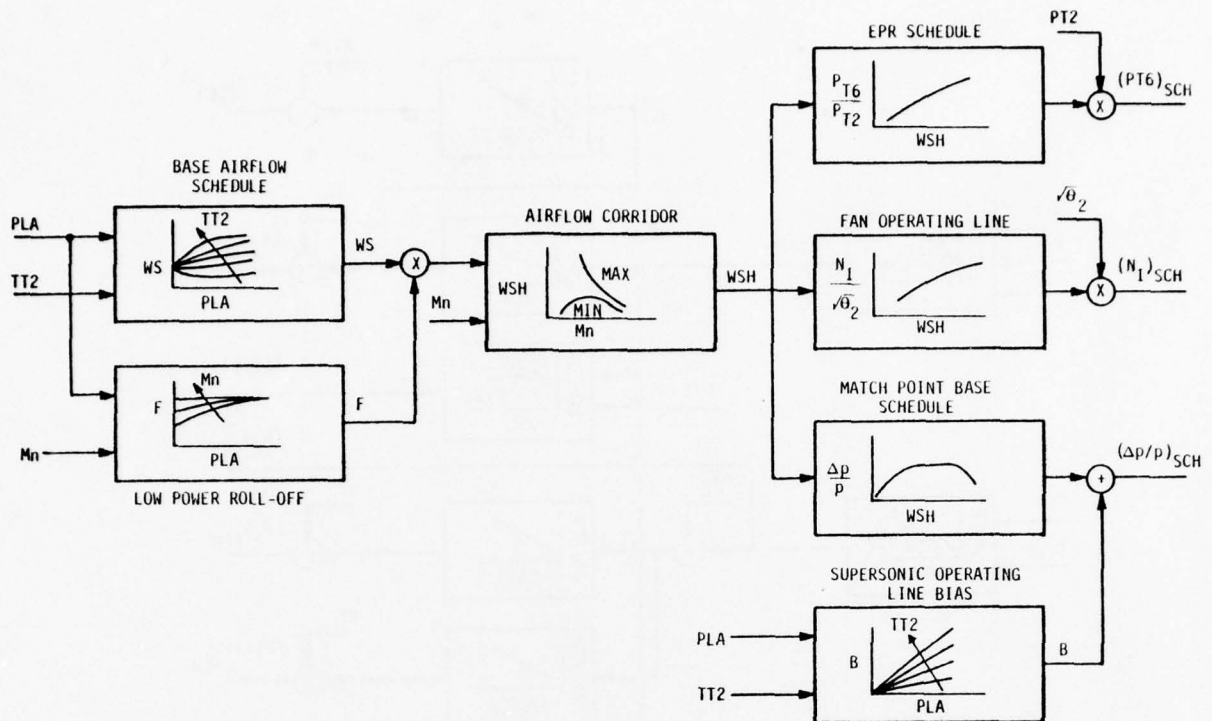


Figure 5.7 Fan Stream Reference Schedules

which is a function of Mach number, also modifies the output. Using this scheduling variable permits implicit satisfaction of the inlet airflow requirements.

The airflow parameter is used to schedule the fan speed along the fan operating line. The corrected fan speed is a univariate function of the corrected airflow. Shifts in the operating line due to altitude and Mach number are accommodated in the $\Delta p/p$ schedule.

The averaged fan exit Mach number parameter, $\Delta p/p$, is defined (but not necessarily synthesized) as follows:

$$\Delta p/p = \frac{1}{2} \left\{ \frac{(P_{2.5C})_T - (P_{2.5C})_S}{(P_{2.5C})_T} + \frac{(P_{2.5H})_T - (P_{2.5H})_S}{(P_{2.5H})_T} \right\}$$

This parameter represents a direct fan operating point measurement [29]. The averaging reduces bypass ratio effects which can produce poor performance if interior or exterior fan exit measurements are used alone. The parameter's relationship to other fan variables is schematically shown in Figure 5.8. $\Delta p/p$ is used for trim because it determines the fan match point shift as a function of altitude and Mach number. It is scheduled as a function of corrected airflow and temperature to represent these effects. The augmentor entrance pressure is scheduled by fan airflow.

Core Stream Schedules

The independent variable for the gas generator is compressor speed (see Figure 5.9). The compressor speed is scheduled as a function of the engine face temperature and the power lever angle.

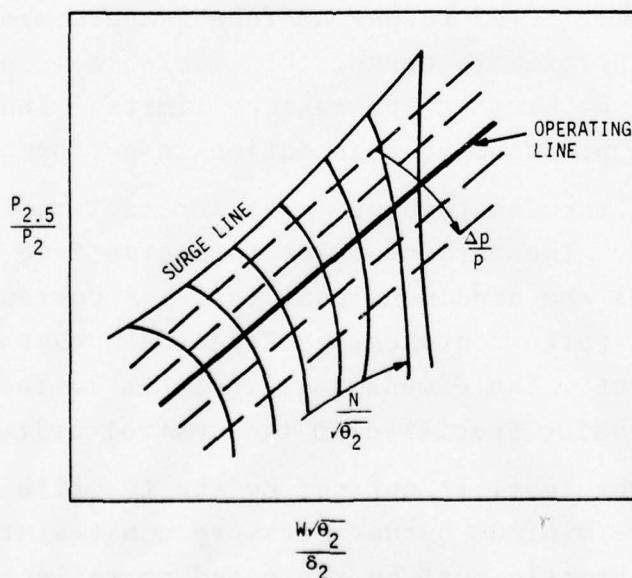


Figure 5.8 Relationship of Fan Component Parameters to $\Delta p/p$

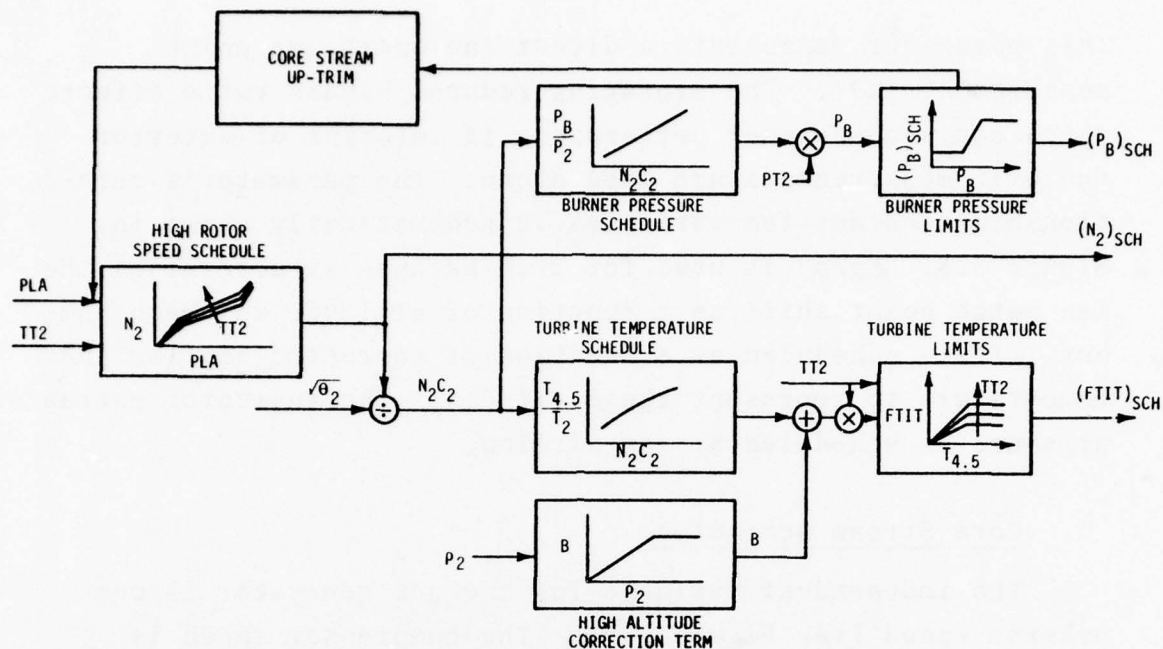


Figure 5.9 Core Stream Reference Point Algorithm

The burner pressure schedule is a univariate function of the core speed corrected to engine face temperature. While it is only an approximate curve, this variable is not used for trim except at minimum and maximum limits. Thus, the slight mismatch produces no degradation in performance.

Similarly, the fan turbine inlet temperature is scheduled with core speed. The turbine inlet-to-engine face temperature ratio is used as the nondimensional form. A correction is applied to this ratio representing Reynolds number effects at high altitudes. The dimensional variable is then limited by the maximum value specified in the control criteria.

Engine power level is not set by the throttle at flight conditions where minimum burner pressure constraints apply. The requested throttle must be increased to reflect the higher power required to maintain sufficient combustion stability.

The reference point scheduling logic is used to increase the requested PLA at low pressure conditions as shown in Figure 5.10.

The initial power lever angle is used to calculate compressor speed and then burner pressure. If the burner pressure scheduled is below the minimum (48 psia), then the scheduled burner pressure is set to the minimum. This value is used in an inverse pressure versus rotor speed curve to calculate the higher value of rotor speed necessary to hold this pressure. Finally, the rotor speed and engine face temperature are used to enter the PLA versus rotor speed schedule to calculate the up-trimmed throttle position. The higher PLA is an estimate of the throttle position for minimum burner pressure. This new PLA is used to calculate the appropriate reference state and control vectors for the equilibrium point in the normal manner.

Control Schedules

The engine fuel flow is scheduled against engine corrected airflow and Mach number. It was found that this relationship

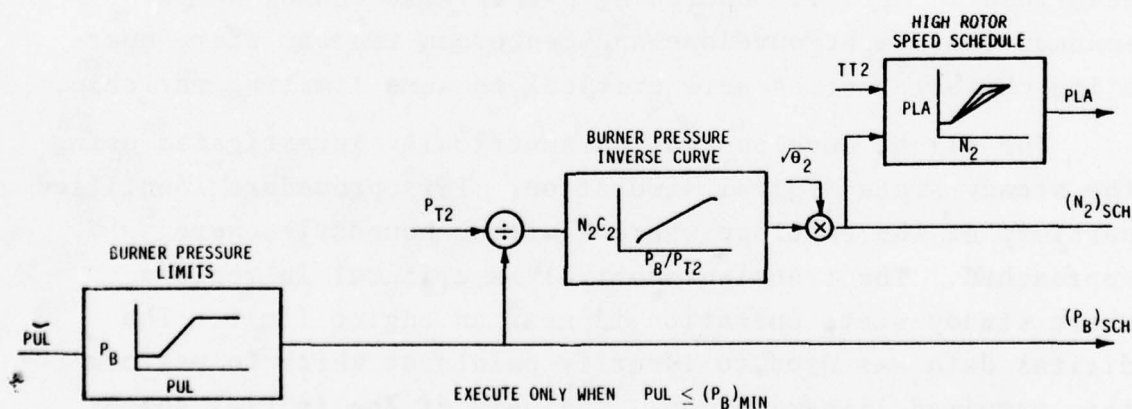


Figure 5.10 Core Stream Uptrim Logic

gave the closest correlation to the operating conditions specified by the production control. Since this variable is not used to trim the engine performance, the inaccuracies associated with the scheduling produce only minor effects.

The variable geometry curves are taken from the hardware schedules supplied by the engine manufacturer. The base bleed schedule is closed.

The nozzle jet area is scheduled as a function of engine inlet temperature to match the production control schedules so that direct compatibility with the augmentor control logic is maintained (see Figure 6.20).

Utilizing the reference point algorithm, the ambient conditions, namely PT2, TT2, Mn and the throttle input (PLA) are translated into an approximate reference point vector (see Figure 5.6). This vector includes the engines states, outputs and controls.

5.5 ENGINE LINEAR MODEL DESCRIPTION

Linear models were generated by Pratt & Whitney Aircraft Group using the F100 nonlinear simulation. This procedure is described in Ref. 1. Operating points were chosen which spanned the flight envelope and center on regions where operating characteristics were critical to some limiting variable.

The flight envelope was parametrically investigated using the steady-state digital simulation. This procedure identified portions of the envelope where limiting boundaries were approached. The transient control is critical in regions where steady-state operation is near an engine limit. The digital data was used to identify points at which to perform this required linearization. Analysis of the initial set of linear models yielded information concerning the engine

dynamic behavior which was combined with steady-state data to identify additional linearization points.

As part of the investigation of the operating envelope, a group of steady-state operating points for the production control were run on the nonlinear digital simulation. Data were acquired on: (a) component stability limits, and (b) engine protection limits including physical rotor speeds, turbine inlet temperature and burner pressure limits. Data were calculated for standard day conditions as a function of altitude and Mach number within the limits of a nominal envelope of operation for a typical aircraft application. The results of this analysis will identify those envelope regions where particular physical limits are important relative to the control criteria specifications. This analysis will, therefore, lead to: (a) further linear model generation points, (b) control design operating points, and (c) a good physical understanding of important terms to be weighted heavily in the LQR performance index.

Figure 5.11 shows component stability results. The control criteria [1] specifies a minimum component stability margin for the fan and compressor of 15% and 5%, respectively. It is observed from the data that fan stability is well above this level except at high power, high altitude and low Mach number conditions, or at low altitude, power and Mach number where the steady state operating stability margin is actually below the minimum. For the compressor, the stability limits are always maintained in steady state by the production control. Areas where the limits are approached occur at low power, altitude and Mach number or high power, altitude and Mach number. These results indicate that stability margins are important transient constraints at conditions like sea level static, idle power. High altitude points of low component stability lie outside the transient

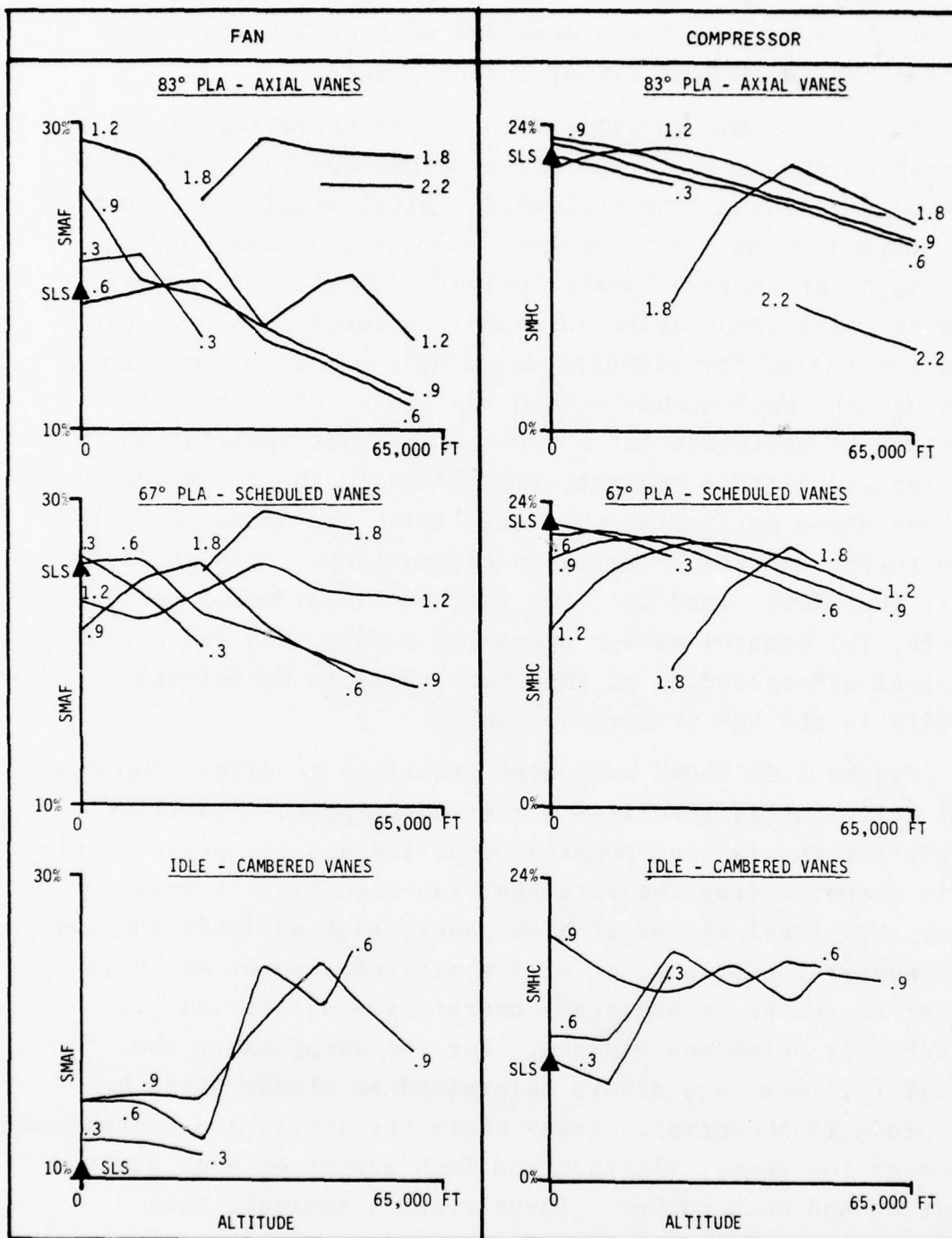


Figure 5.11 Fan and Compressor Stability at Various Power Conditions, Altitudes, and Mach Numbers

operating corridor so these conditions (e.g., 83°/65K/0.9 or 83°/65K/2.5) are important for steady state scheduling considerations.

A similar analysis was performed on engine limits. Insight into important transient criteria for engine protection was sought since those points which operate near a limit at a particular condition should have regulator gains designed for stiff control of that variable. Figure 5.12 shows the data from the production control simulation deck. The results indicate that FTIT limits set engine intermediate performance about $Mn \approx 0.9$. Fan rotor speed limits are approached at high altitudes and Mach numbers. Compressor speed limits are approached at low altitudes and transonic Mach numbers. Maximum burner pressure is a design point for sea level, maximum Mach number operation. The minimum burner curves indicate that idle is defined by this limit at most operating points. The engine limit and component stability results were utilized with the preliminary linear models to specify a group of linearization points for full envelope operation.

Figure 5.13 shows the operating envelope spanned by the chosen set of linearization points. Table 5.4 lists the linear models. The transient operating corridor shown in Figure 5.14 represents the region where modulation of engine power is not constrained by either burner pressure, airflow, or temperature limitations. Elsewhere, engine power conditions are limited to intermediate throttle at constant airflow.

A description of the linear model analysis is given below. A complete list of the linearized dynamics is given in Ref. 1. Appendix D gives a detailed analysis of the characteristics of the linear models.

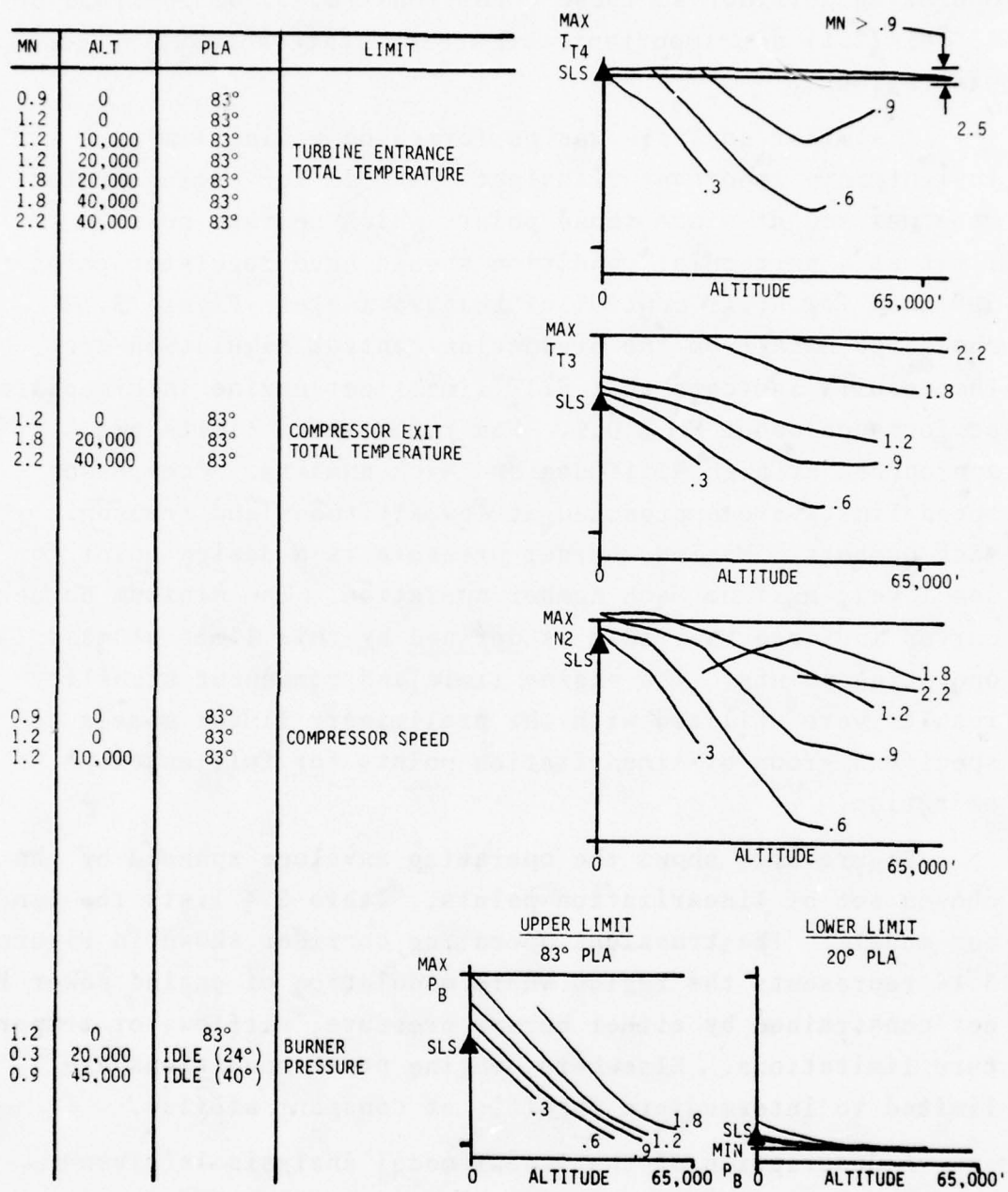


Figure 5.12 Engine Protection Limits for Various Altitudes and Mach Numbers

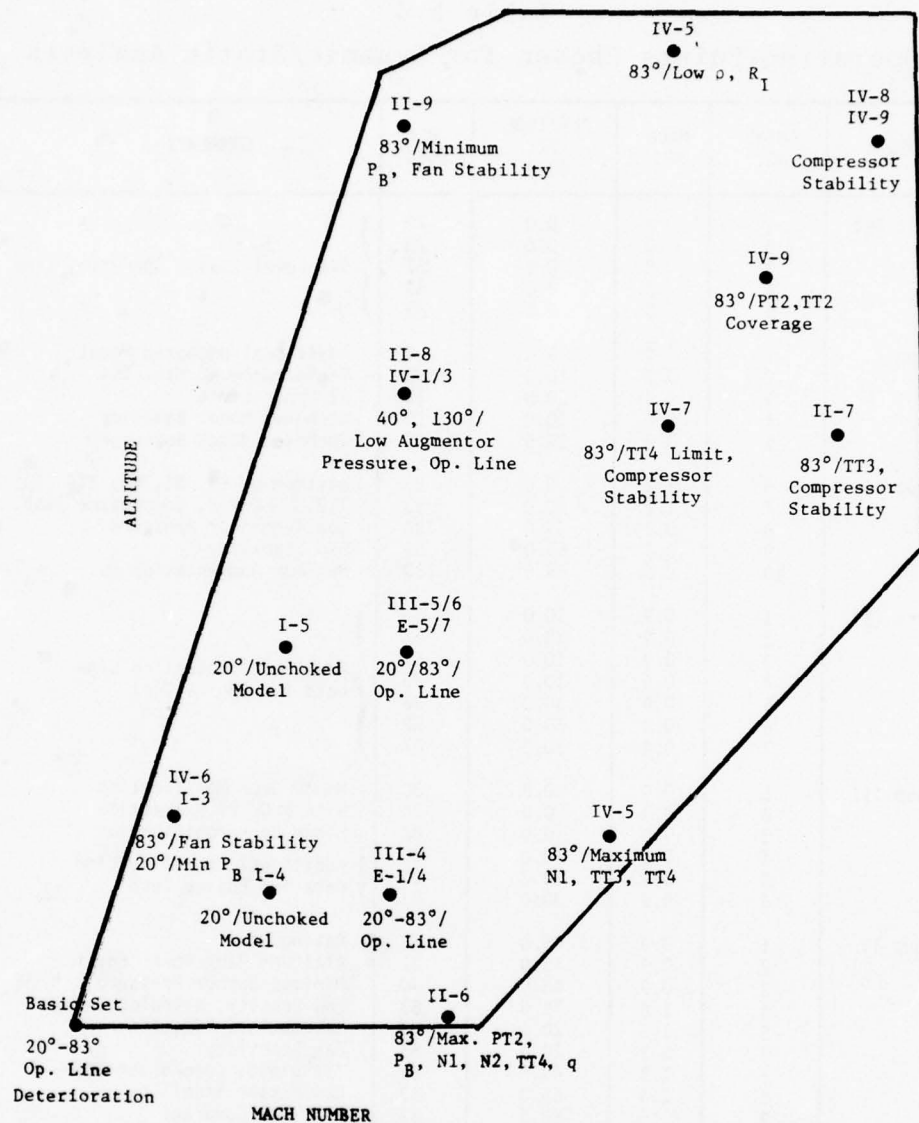


Figure 5.13 Relative Operating Point Location and Significance
Linear Model Generation Schedule

5.5.1 Linear Model Analysis

Linear models were analyzed to determine the important physical interactions occurring in the engine and to develop insight into the various effects of power condition, altitude,

Table 5.4
Operating Points Chosen for Dynamic/Static Analysis

CODE	POINT NO.	MACH NO.	ALTITUDE FT. (000)	PLA (DEG)	COMMENTS
Basic Set	1	0	0.0	20	} Sea Level Static Operating Line
	2	0	0.0	36	
	3	0	0.0	52	
	4	0	0.0	67	
	5	0	0.0	83	
Group I	1	0	0.0	24	Additional Unchoked Model
	2	0.9	10.0	83	Performance at Max. TT4
	3	0.3	20.0	24	PB Lower Limit
	4	0.6	10.0	20	Unchoked Model Behavior
	5	0.6	30.0	24	Unchoked Model Behavior
Group II	6	1.2	0.0	83	Maximum q, PR, N1, N2, TT4
	7	2.2	40.0	83	TT3, TT4 Limit, Compressor Stab.
	8	0.9	45.0	130	Low Augmentor Pressure
	9	0.9	65.0	83	Fan Stability
	10	2.5	65.0	130	Maximum Augmentation
Extra (E)	1	0.9	10.0	36	} Additional Operating Line Data for Engine Test
	2	0.9	10.0	52	
	3	0.9	10.0	67	
	4	0.9	10.0	83	
	5	0.9	30.0	36	
	6	0.9	30.0	52	
	7	0.9	30.0	67	
Group III	1	0.0	0.0	20	Minor Deck Modification
	2	0.0	0.0	20	With BLD/HPX Extraction
	3	0.0	0.0	83	Minor Deck Modification
	4	0.9	10.0	20	} Additional Operating Line Data for Engine Test
	5	0.9	30.0	20	
	6	0.9	30.0	83	
Group IV	1	0.9	45.0	83	Rating Point
	2	0.9	45.0	52	Altitude Part Power Point
	3	0.9	45.0	40	Minimum Burner Pressure
	4	1.8	75.0	83	Low Density, Reynolds Index
	5	1.8	20.0	83	Maximum N1, TT3, TT4
	6	0.3	20.0	83	Fan Stability
	7	1.8	40.0	83	TT4 Limit, Compressor Stab.
	8	2.5	65.0	83	Compressor Stability
	9	2.15	58.5	83	PT2, TT2 Coverage

and Mach number on the character of the transient response. Initially, the linear models for the sea level static operating line were used to investigate the effects of power condition at a single flight point. Subsonic operating line model response was related to the behavior at sea level static.

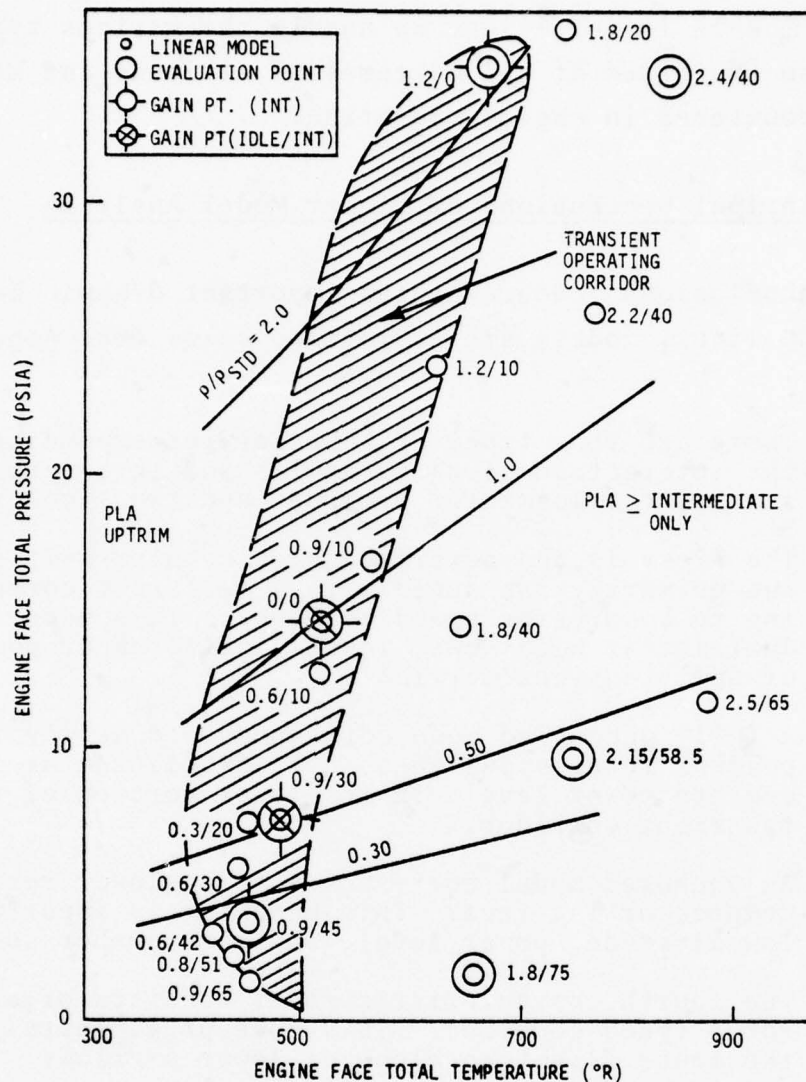


Figure 5.14 Linear Model Generation Points

Various supersonic points were used to compute the time constants of the engine operating at these conditions. The details of the evolution of the linear reduced order models are described in Appendix D. The net result was a group of design models for control synthesis. The models contain all the dynamic information concerning the interaction between states and inputs to design practical control algorithms. The

number of models is sufficient to handle the various types of response exhibited at all extremes of altitude and Mach number encountered in engine operation.

5.5.2 Principal Conclusions of Linear Model Analysis

The conclusions concerning the important dynamic behavior of the F100 linear models are summarized below (see Appendix D):

- (1) There are four types of behavior corresponding to the interaction of the dynamics and three principal states, the augmentor pressure and two spool speeds.
- (2) The first is characterized by a complex pair involving primarily fan speed with a real root corresponding to compressor speed response. This mode is dominant at high power levels in the upper portion of the transient corridor.
- (3) A fully uncoupled mode corresponds to nearly independent rotor speed lags. It is dominant at intermediate power levels in the lower portion of the transient corridor.
- (4) An unchoked model corresponds to a slower response compressor lag root. This behavior is important at low altitude, power level, and Mach number conditions.
- (5) The fourth characteristic model consists of a complex rotor speed coupling. This mode predominates in the lower flight envelope at lower airflows.
- (6) Supersonic flight point response does not consistently correspond to pressure, temperature or density correlation with subsonic conditions. In general, coupling terms in the dynamics are different functions of ambient conditions.

*

A more detailed discussion of model dynamics, parameterization as well as questions of identification of system parameters from real data is presented in Ref. 36.

5.6 LINEAR QUADRATIC REGULATOR DESIGNS

5.6.1 Introduction

The linear quadratic regulator uses processed sensor data to form the actuator commands (see Figure 5.15). It uses simplified state feedback gain matrices calculated from optimal theory. The regulator function alters the natural system dynamics to satisfy transient criteria and control acceptability guidelines. Steady-state trim or integral control is provided by decoupled logic which is described in Section 5.8. Constant coefficient linear models are used to represent the behavior within regions of the envelope. The resulting control laws are parameterized by ambient conditions to form a continuous implementation.

5.6.2 Selection of Design and Evaluation Models

The results of the linear model analysis have been presented in Section 5.5. Along with the transient control criteria, these are used in the development of design models to

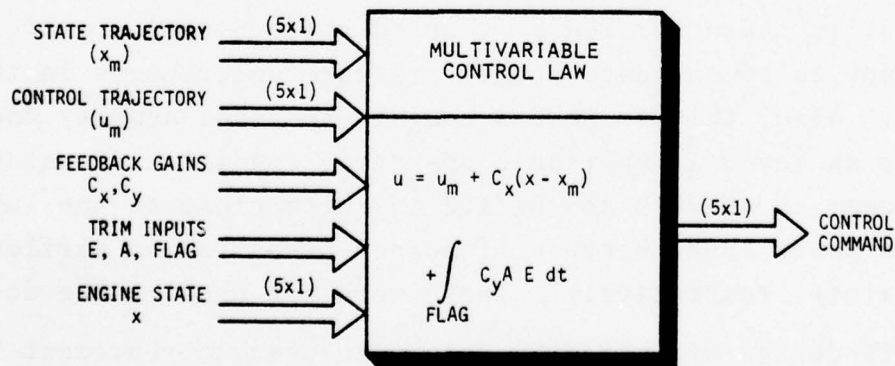


Figure 5.15 Multivariable Feedback Control Law

calculate the optimal state feedback gain matrices. Design models are generated from the high order linear systems using modal reduction described in Section 4.3. This method allows important dynamic modes to be retained and important, measurable quantities included as state variables in the system. Evaluation points are also chosen in the design process to verify off-design behavior.

Design models were obtained from the high order models selected on the basis of the response characteristics discussed in Section 5.5. There were four models chosen near intermediate power. The conditions chosen were 45K/0.9, 30K/0.9, 0K/0, and 0K/1.2. The 45K/0.9 point represented uncoupled response in the lower end of the envelope. This model is similar to the 65K/0.9 and 75K/1.8 points. The operating point is also in a region of hard augmentor lights and fan stability sensitivity to augmentor ignition. The 30K/0.9 model represents uncoupled behavior at intermediate power. This is a typical cruise point in an aircraft envelope. The 0K/0 condition at intermediate power is in the central portion of the transient corridor. Finally, the 0K/1.2 point lies at the top of the transient corridor and has the fastest response. Idle power models are chosen at 0K/0 and 30K/0.9. The 0K/0 condition represents low airflow, unchoked turbine behavior. Sensitive surge margin response is typical. At 30K/0.9, the behavior is characterized by coupled rotor dynamics. It is important to accommodate burner pressure undershoots in this region. Also, this point has roughly the same density and airflow as several supersonic operating conditions considered. Idle power at 45K/0.9 and 0K/1.2 is quite close to the intermediate power level because of burner pressure and airflow constraints, respectively. These were not used in the design.

Off-design evaluation models were used to represent the off-design, closed-loop response of the regulator. Three evaluation models were chosen in the supersonic envelope. Low,

middle, and high pressure conditions were selected at 75K/1.8, 58.5K/2.15 and 40K/2.2, respectively. The 0K/1.2 feedback gains were used at the 40K/2.2 supersonic point. The 30K/0.9 and 45K/0.9 gains were used at 58.5K/2.15 and 75K/1.8, respectively. Satisfactory regulation of pressure disturbances at supersonic conditions can be attained using the feedback matrices at the six subsonic design points. This simplifies the implementation and scheduling requirements substantially.

5.6.3 Design Model Structure and Performance Indices

The design points were discussed in the preceding section. Using the transient controls criteria and the linear model analysis, one can choose the important dynamics and states for control in a state feedback law. The dynamic response represented in the linear equations has been analyzed. The fundamental thrust response is determined primarily by the three principle states. The remaining 13 eigenvalues in the 16th-order linear models were eliminated. A fourth important dynamical element is the time lag of the servo pump regulating main burner fuel flow. The 0.1 second time constant in this actuator produces significant effects on closed-loop response at higher frequencies.

The analysis indicated that the two rotor speeds and augmentor pressure represented important engine dynamics at each flight condition. All three variables are measurable. These three quantities are sensed by high response/high accuracy probes on the NASA research control engine. The main burner fuel flow is chosen as a state modeling the servo pump lag. It would have been possible to use another variable, e.g., TT3 or PT4, as a state describing this behavior. However, a measurement of the fuel flow is provided in the instrumentation and is conveniently included in the state equations.

The four states provide a complete description of the response suitable for design purposes. An examination of the instrumentation set shows that all high accuracy/high response gas path transducers are used in the control except the burner pressure probe. The transient requirements specify explicit limits to burner pressure overshoots and undershoots. However, the burner pressure flow dynamics have a time constant always less than 0.01 sec. Therefore, this mode is equilibrated during typical transients and can be represented as a linear combination of the chosen state variables or, alternatively, as an output.

One method of explicitly including the probe signal into the control is to formulate an estimate for the four state variables using five inputs, namely, N_1 , N_2 , PT6, WFMB, and P_B . This implementation utilizes the burner pressure measurement to improve the accuracy of the estimated states. The control is designed to produce adequate burner pressure response by weighting appropriate linear combinations of N_1 , N_2 , PT6 and WFMB in the performance index. This method is discussed in Chapter IV. However, the state variable measurements are accurate enough to be used without extensive filtering and an alternative is attractive to remove further explicit dependence of the control on the linear models through a filter algorithm.

The burner pressure probe signal can be included in the control law and the performance index explicitly if the high frequency dynamics are included in the design. In this way, the design model has five states and only four dominant response time constants. The state weightings explicitly include burner pressure with an adjustable design parameter. As shown in Chapter III, when a spectrally decoupled model is used in optimal quadratic synthesis, the following occurs: (1) weighting the "slow" response states does not affect the high response root, (2) weighting the high response state

acts like an output weighting on the slow response roots, and (3) the effect of high response state weighting on the high response root increases its closed-loop frequency and maintains spectral decoupling from the lower frequencies. Based on these results, burner pressure is included along with its large eigenvalue in the design model.

Once the design models are calculated and the important operating points specified, selection of the performance index is quite straightforward. The state weighting performance index is shown below:

$$J = \frac{1}{2} \int_0^{\infty} \left[A_{11} \delta N_1^2 + A_{22} \delta N_2^2 + A_{33} (\delta PT6)^2 + A_{44} (\delta W_f)^2 \right. \\ \left. + A_{55} (\delta PB)^2 + B_{11} (\delta W_{fc})^2 + B_{22} (\delta A_j)^2 + B_{33} (\delta CIVV)^2 \right. \\ \left. + B_{44} (\delta RCVV)^2 + B_{55} (\delta BLC)^2 \right] dt \quad (5.1)$$

When the state equations are normalized by typical small perturbation response magnitudes, the state weighting parameters become nondimensional fractions and can easily be manipulated during the design procedure. The initial guess for state weighting becomes the following:

$$A_{ii} = B_{jj} = 1 \quad i, j = 1, \dots, 5$$

The linear perturbation response and eigensystem of the closed-loop behavior is calculated for each design model. The parameters are adjusted reflecting the results of each iteration and the cycle repeats until an acceptable response is obtained. The results of the regulator designs and state weighting are summarized in Appendix E.

Adjustments to the weights follow from linear simulation, sensitivity calculations of closed-loop dynamics, and an intuitive understanding of the model response (see Chapter III).

5.6.4 Results of the Regulator Design

The design model structure, performance index, and transient control criteria were discussed above. Weighting elements were chosen for each design model to produce acceptable response to small perturbations vis-a-vis the control criteria. The resulting closed-loop systems are shown in Figure 5.16 and discussed below for each design point. The relative closed-loop weights are shown in Figure 5.17.

At 45K/0.9, the two important transient criteria are augmentor and burner pressure control. The feedback has approximately doubled the compressor speed response (see Figure 5.16 and Appendix E) and increased fan response by about 50%. The augmentor pressure root is coupled lightly with fuel flow. The feedback terms on PT6M and P_B cause the actuators to respond satisfactorily to augmentor disturbances and burner pressure transients.

At 30K/0.9 there are design models at intermediate and idle power. At intermediate, the engine is not pressure or temperature limited. At idle power, the engine operates at minimum burner pressure. The intermediate system shows about a 50% increase in response time. The idle power design point exhibited open-loop rotor coupled response at a natural frequency and damping ratio of 1.3 rad/sec and 0.95, respectively. The closed-loop roots have roughly twice the frequency response at the same damping.

There are also two design models at sea level static conditions. At intermediate power, temperature limiting is important and at idle, surge protection is a factor. Adequate verification of the idle design requires nonlinear simulation.

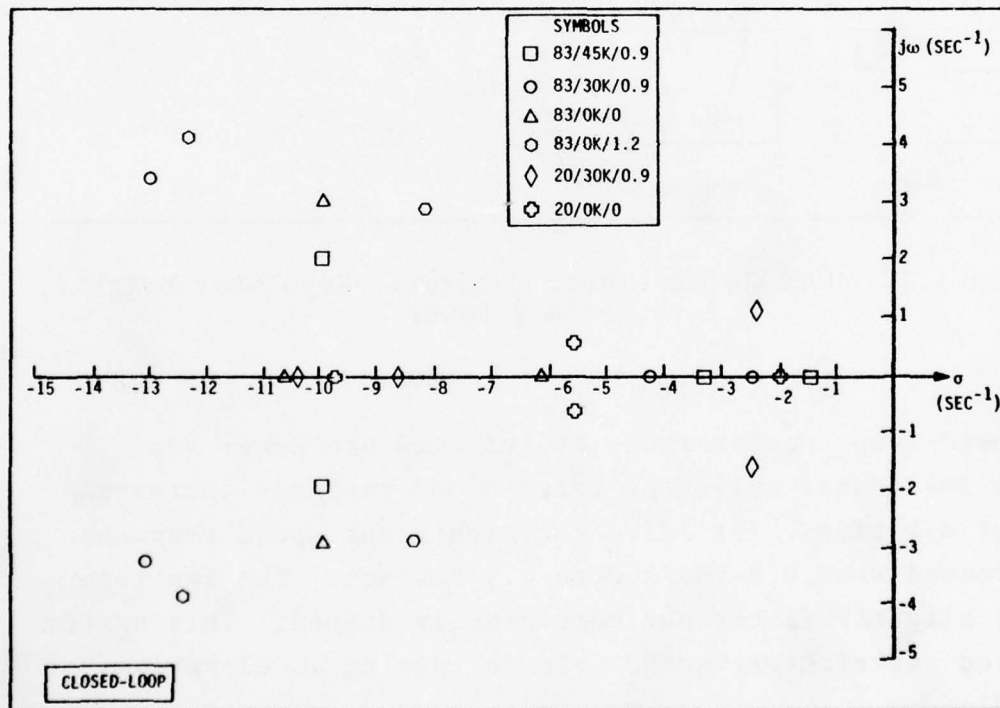
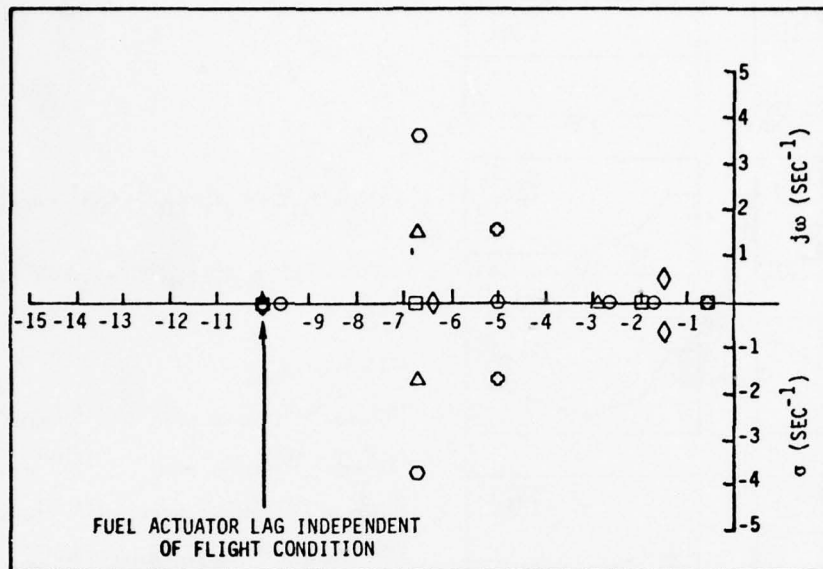


Figure 5.16 Open- and Closed-Loop Root Locations for Six Design Points from LQR Synthesis

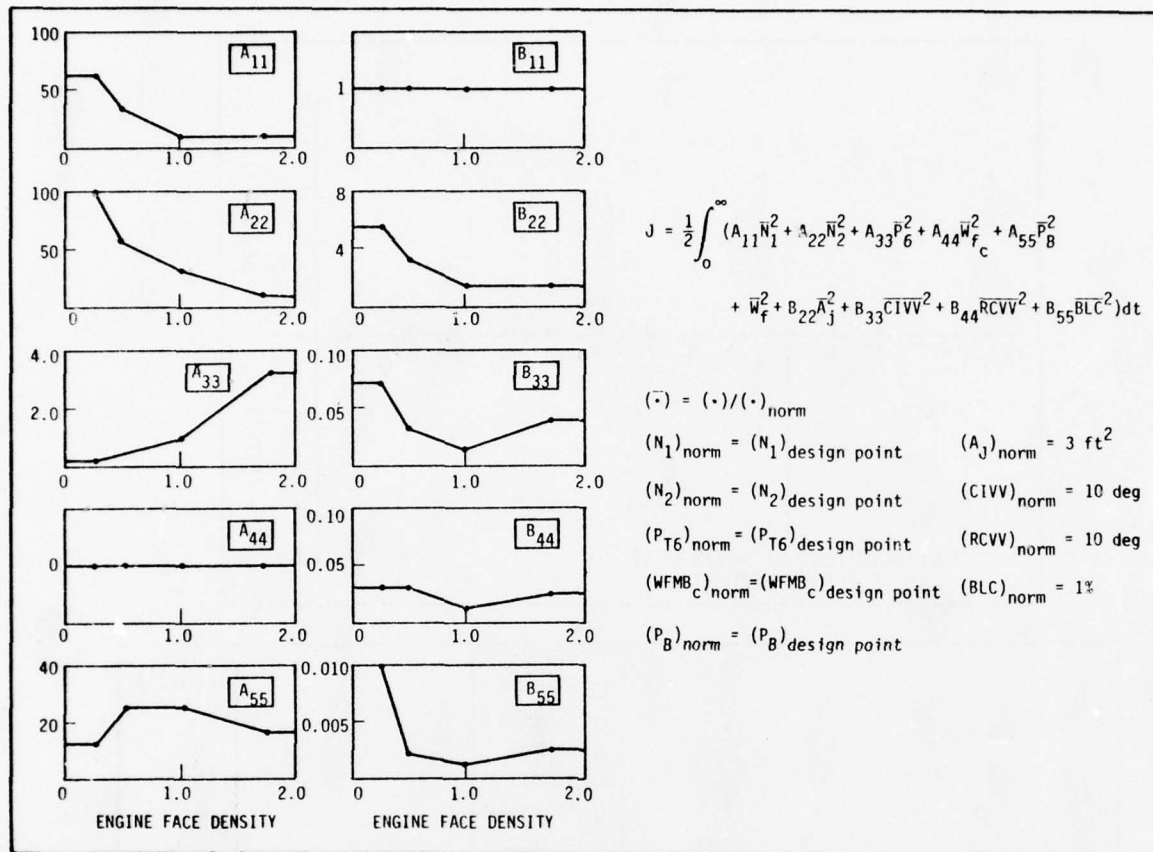


Figure 5.17 Normalized Linear Quadratic Regulator Weights, Intermediate Power

The closed-loop complex roots at intermediate power are roughly 50% faster while the rotor speed response increases by about 2.5 times. At idle, the high rotor speed response is increased from 0.8 rad/sec to 1.9 rad/sec. The fan rotor root is slightly faster but more heavily damped. This system exhibited satisfactory surge behavior during accelerations from idle.

The regulators are selected to satisfy control criteria on the small perturbation transient response. The gain matrices are also used to calculate the closed-loop response

at evaluation points to partially assess the off-design performance. The verification cycle is shown in Table 5.5.

There is a single design point at 0K/1.2 representing intermediate power. The system operates near maximum burner pressure and turbine inlet temperature. The open-loop complex root has a damping ratio near 0.85. The compressor root is at 5 rad/sec. The closed-loop system has two complex roots. The faster complex pair comes from the original complex root at a higher damping and about 50% faster response. The root at 9 rad/sec and a damping ratio of 0.93 is associated with

Table 5.5

Typical Multivariable Design Cycle

(This table shows the effect of model reductions and state variable feedback design on the eigenvalues of a perturbed and unperturbed linear model at sea level static, idle power condition)

20/0/0 16TH ORDER	20/0/0 15TH ORDER	20/0/0 5TH ORDER	5TH ORDER CLOSED-LOOP	16TH ORDER CLOSED-LOOP	20/0/0 (WITH BLEED EXTRACTIONS) OPEN-LOOP	20/0/0 (WITH BLEED EXTRACTIONS) CLOSED-LOOP
-827	-830	-830 ^{d/}	-830	-830	-827	-846
-146	-144			-144	-161	-164
-51±9j	-50±10j			-50±10j	-50	-50
-52	-87			-85	-84	-85
-44	-24			-28	-50	-50
-25±4j	-25±8j			-26±8j	-20j±0.1j	-26±8j
-20	-20			-20	-26	-20±0.9j
-20	-20			-20	-24±0.8j	-22
-21	-21			-21	-21	-18
-2	-2			-2	-1	-2
-4.7±2j	-5.1±2.2j	-5.1±2.2j ^{c/}	-8.3±1.2j	-8±1j	-4.8±2.1j	-4.7±2j
-0.67±0.22j	-0.75	-0.75 ^{b/}	-3.4±0.9j	-3.2±0.7j	-0.72	-8.2
↑ UNCOUPLED COMPRESSOR/TURBINE INLET TEMPERATURE DYNAMICS		-10.0 ^{a/}			-10.0 ^{a/}	
ORIGINAL SYSTEM	QUASI- STATIC REDUCTION	MODAL REDUCTION	MULTI- VARIABLE DESIGN RESULT	EFFECT OF FEEDBACK ON FULL STATE MODEL	PERTURBED MODEL	ROOTS WITH FEEDBACK DESIGNED WITHOUT EXTRACTION

NOTES: a/ - Fuel flow valve dynamics; b/ - Compressor speed; c/ - Fan speed/augmentor pressure;
d/ - Main burner pressure

a coupling between the compressor lag and the servo pump lag. The response time shows a 50% improvement.

The regulator designs consistently showed improved response to the limits of actuator capability. Transient control criteria were met without unacceptable sensitivity to either sensor inputs or model parameters. The reduction of the state feedback matrices, verification on the full order linear system, and implementation as continuous gain schedules throughout the envelope are discussed in the next section.

5.7 DEVELOPMENT OF REGULATOR GAIN SCHEDULES

5.7.1 Introduction

The development of linear quadratic regulators for a group of design models has been described. The gain matrices designed at intermediate power conditions were used to determine closed-loop response at the supersonic evaluation points. These show acceptable dynamic behavior and the results are included in Appendix E. The next step in the synthesis is to utilize the linear analysis results to schedule the gain elements at each design point on ambient and power conditions (see Figure 5.18). The scheduled gains are then evaluated on the full order models to investigate the effect of gain matrix simplification and scheduling. Additional data is contained

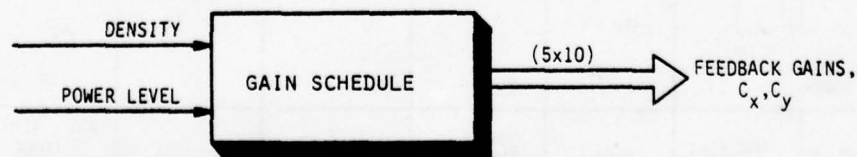


Figure 5.18 Gain Schedule

in Appendix F. A discussion of the theoretical foundation of the procedures can be found in Section 4.4.

5.7.2 Simplification of Feedback Matrices

The feedback gains calculated during the regulator synthesis are all non-zero. For each design model, a gain matrix contains 25 elements. Because of the model and type of closed-loop response specified, a group of these gain elements can be eliminated without adversely affecting the response. These elements are determined by the sensitivity of closed-loop pole locations to feedback gains. Examples of such calculation are included in Appendix F.

The sensitivity calculations for each of the six design points can be used in two ways. First, those elements which do not affect the response at any of the six points can be eliminated from the control completely. This reduces control processor storage and cycle time requirements. Table 5.6 shows the gain matrix after elimination of these elements.

The sensitivity calculations show 9 of the 25 gain elements can be removed without significant impact on the closed-loop response. An additional eight elements showed low sensitivity at one or more design points. These elements were averaged over the ambient conditions. The gain element becomes a constant value or a value dependent only on one scheduling parameter. The remaining eight gains required scheduling as a function of both the ambient conditions and power level.

5.7.3 Scheduling Parameter Development

The sensitivity analysis indicated the relative importance of each gain. The linear model analysis gives the designer an understanding of the dependence of the response on various ambient and power variables. These two aspects can

Table 5.6
Regulator Feedback Gain Matrix Structure
After Reduction

ROW	COLUMN				
	N1	N2	PT6M	WFCOM	PT4
WFMB	X	X	X	□	□
AJ	X	□	X	0	0
CIVV	□	0	X	0	0
RCVV	□	□	X	0	0
BLC	□	□	0	0	X

0 → Set to Zero for All Matrices

□ → Smoothed

X → Sensitive Element

be used to select interpolation parameters used in gain scheduling at off-design conditions. Formal procedures are discussed in Section 4.4. In the F100 engine, the characteristic modes of the linear models were used to deduce scheduling variables for the gain elements.

Transition from one power level to another which resulted in a change of the model characteristics occurred at the 30K/0.9 and 0K/0 design points. At sea level static, the change was correlated with the occurrence of a choked flow condition of the low pressure turbine and exhaust nozzle in the 20°-28° PLA region. At 30K/0.9, the transition from uncoupled to coupled spool behavior occurred in the region of 42°-67° PLA. These observations were used to select a scheduling parameter for power excursions. The parameter had the characteristics shown in Figure 5.19. It indicates the current

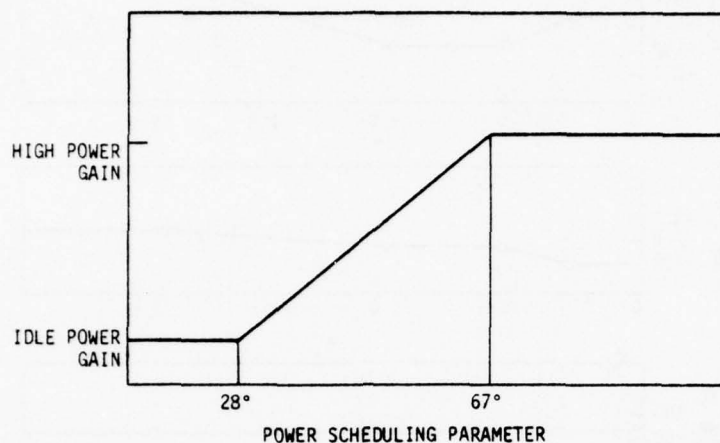


Figure 5.19 Gain Schedule Function for Power Level

power state of the engine. For small transitions at high or low power, the feedback gains are constant. During middle power transition, the gains are scheduled between the high power and low power values using a linear interpolation procedure as follows:

$$C_{ij} = [C_{ij}]_{HP} (1 - \alpha) + [C_{ij}]_{LP} \alpha \quad 0 < \alpha < 1 \quad (5.2)$$

$$28^\circ < PLA < 67^\circ$$

The interpolation requires scheduling between two idle and four intermediate power gain points. Engine face density was chosen as the ambient scheduling parameter. Points at a lower density than the 45K/0.9 (e.g., 65K/0.9 and 75K/1.8) had satisfactory closed-loop response using the 45K/0.9 gains. The supersonic evaluation points indicated that the density parameter interpolation would yield acceptable behavior at all flight conditions. Scheduling of several regulator gain elements is shown in Figure 5.20. A detailed gain schedule listing is included in Appendix F.

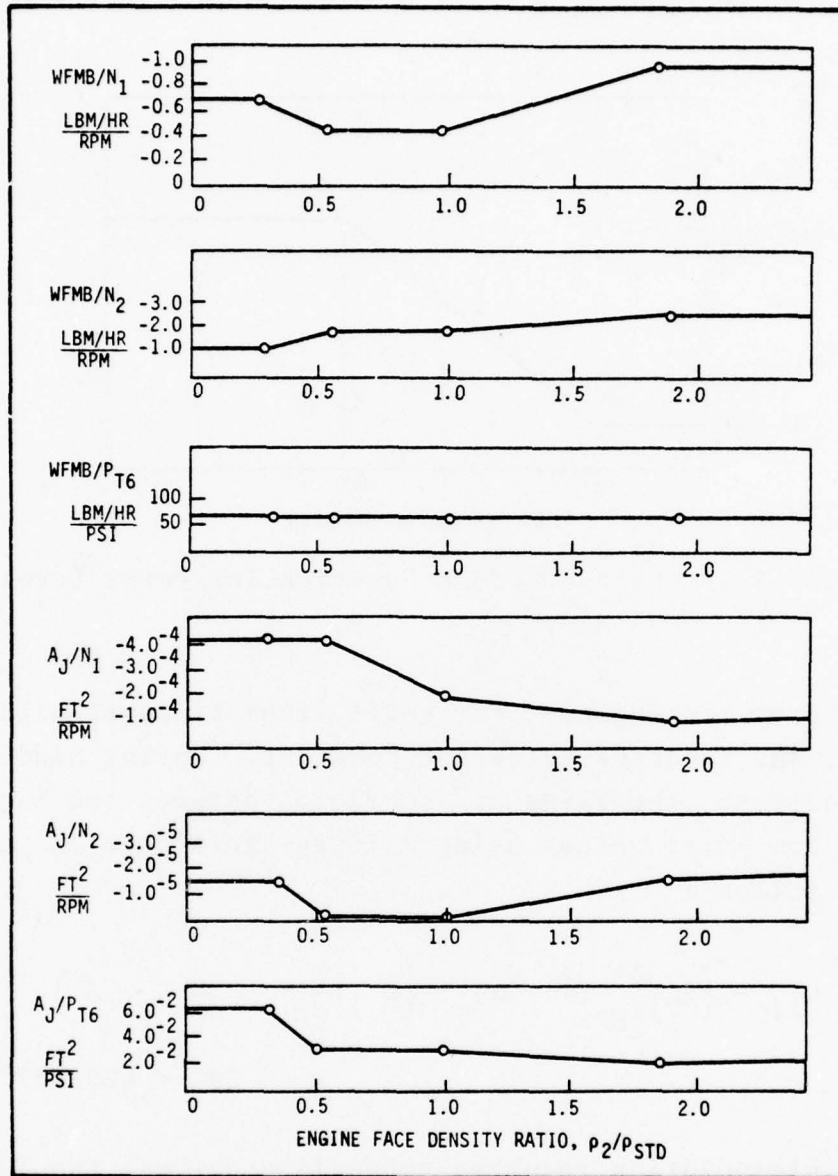


Figure 5.20 Selected Elements of Regulator Gain Schedule Intermediate Power

5.7.4 Verification of Scheduled Response

The gain schedules are developed for off-design point operation. Closed-loop response with the scheduled feedback gains can be evaluated using the 16th-order linear models.

The resulting closed-loop eigensystem should represent behavior which is acceptable according to the transient requirements at the operating point. A typical design evaluation for supersonic, off-design conditions is shown in Figure 5.21. Several examples of off-design linear model data are included in Appendix E. Linear simulation techniques are used in addition to this verification procedure. It was found, however, that the system response was best evaluated on a detailed nonlinear digital or hybrid simulation (see Figure 5.22). In this way, a complete representation of the engine, sensors and actuators was included. The design cycle is flexible enough to accommodate changes dictated by unsatisfactory performance found in the simulation phase. The hybrid and digital evaluation points are shown in Table 5.7. The results of these evaluations are discussed in Chapter VI.

5.8 INTEGRAL CONTROL DESIGN

5.8.1 Introduction

The theoretical foundations of decoupled integral control are presented in Chapter III. The application to the F100 engine is presented in Section 4.4. In this section, the details of the design and incorporation into the control system are presented (see Figure 5.23).

In the preceding sections, the development of a reference point scheduling algorithm was presented. The practical considerations in designing a locally linear regulator for full envelope operation was described. The steady-state performance of the engine is controlled by two independent quantities at each ambient/power condition. Three controls are scheduled in steady-state. The reference point schedules produce five control and five state values to generate the regulator error. Because of the approximations in the scheduling algorithm and

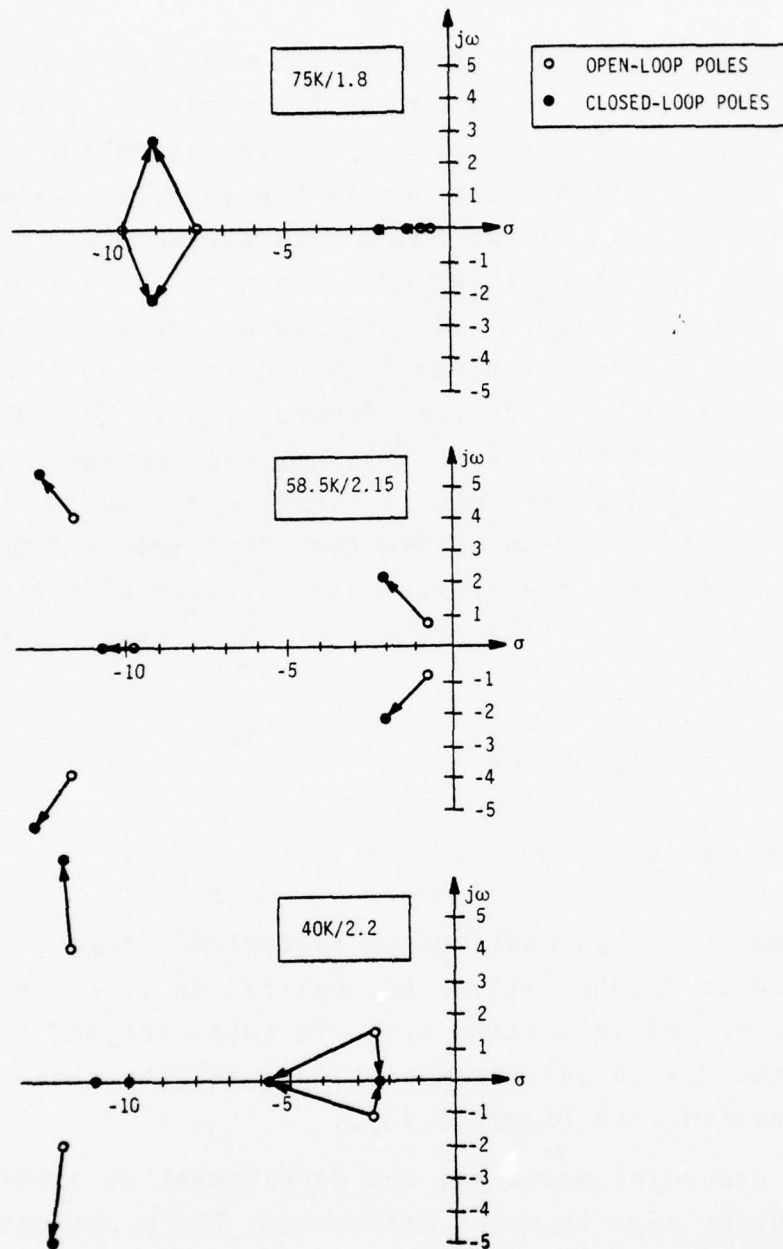


Figure 5.21 Dominant Open- and Closed-Loop Regulator Poles at Three Supersonic Evaluation Points Using Gains Scheduled from Subsonic Design Models and Calculated on 16th-Order Linear Systems at the Three Conditions

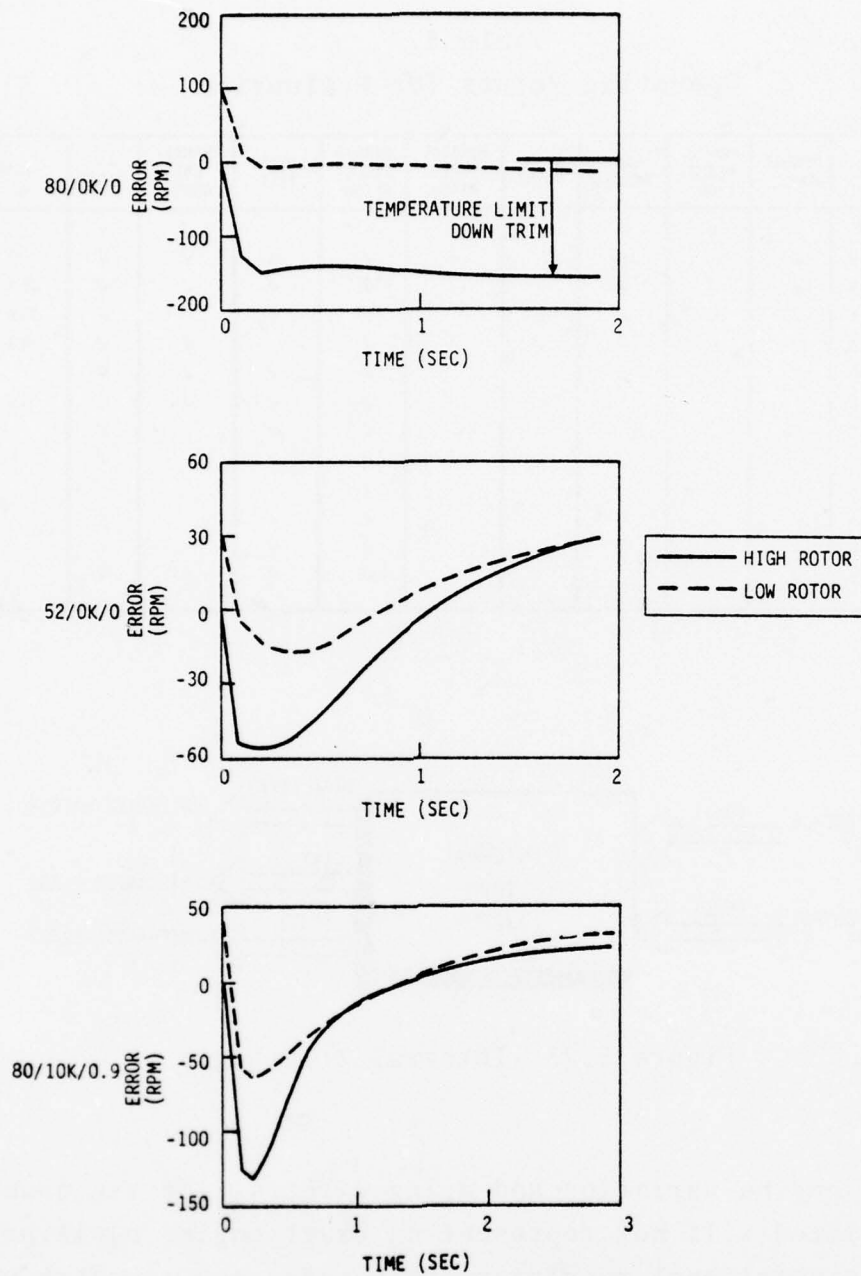


Figure 5.22 Rotor Speed Error Signal Response to Small Perturbation ($\Delta PLA = +3^\circ$) Step Input at Three Flight Conditions from Nonlinear Digital Evaluation

Table 5.7
Operating Points for Evaluation

ALTITUDE	Mn	LINEAR MODEL	MODEL REDUC- TION	LQR DESIGN	GAIN POINT	DIGITAL EVALU- ATION	HYBRID EVALU- ATION	ENGINE TEST	TRANSI- ENT RUNS	Δp TESTS	COMMENTS
0	0	✓	✓	✓	✓	✓	✓		✓	✓	
10K	0.9	✓	✓			✓	✓	✓	✓	✓	
30K	0.9	✓	✓	✓	✓	✓	✓	✓	✓	✓	PLA $\geq 24^\circ$
45K	0.9	✓	✓	✓	✓		✓	✓	✓	✓	PLA $\geq 40^\circ$
0	1.2	✓	✓	✓	✓	✓	✓		✓	✓	PLA $\geq 57^\circ$
10K	0.6	✓					✓	✓	✓	✓	
10K	1.2						✓	✓	✓		PLA $\geq 57^\circ$
20K	1.8	✓					✓	✓		✓	
40K	2.2	✓	✓	✓			✓	✓		✓	
65K	2.5	✓					✓			✓	
58.5K	2.15	✓	✓	✓			✓	✓		✓	
75K	1.8	✓	✓	✓			✓	✓		✓	
65K	0.9	✓					✓	✓		✓	

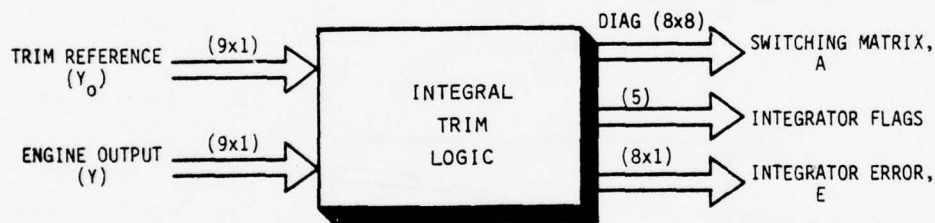


Figure 5.23 Integral Trim Logic

engine-to-engine variation and aging effects, the ten quantities specified will not represent an exact engine equilibrium. With the proportional regulator, this reference mismatch will cause the resulting steady-state to "hang-off" at a point determined by the feedback gains. Such "hang-off" could be small but none is allowed by the control criteria. Thrust sensitivity to airflow and rotor speed errors tends to be large, e.g., 1% thrust change will be caused by only a 20 RPM shift in fan speed at many operating conditions. In order to

obtain acceptable performance, trim integrations are required on a subset of the reference vector.

5.8.2 Set Point Vector Specification

The theory of the variable set point, decoupled design procedure is discussed in Chapters III and IV. The set point vector for the F100 is shown in Table 5.8. The criterion for steady-state performance is stated as follows. The bleed valve should be closed. The vanes should be on hardware schedules (functions of rotor speeds and temperatures) and the remaining two degrees of freedom used to match performance specified by the production control.

The three scheduled actuators are provided with decoupled integral loops. The time constant for the integral poles is set at 1 rad/sec. Switching logic for these error signals is activated when the actuator is driven to a limit. For example, if the error signal or scheduled reference for the CIVV drives

Table 5.8
Integral Set Point Vector Specification

ELEMENT	OUTPUT ERROR	ASSOCIATED CONTROL
y_1	$\begin{cases} N_1 - (N_1)_{SCH} \\ T_{T4.5} - (T_{T4.5})_{MAX} \\ P_B - (P_B)_{MAX} \\ P_B - (P_B)_{MIN} \end{cases}$	WFMB
y_2	$(\Delta p/p) - (\Delta p/p)_{SCH}$	A_J
y_3	$CIVV - (CIVV)_{SCH}$	CIVV
y_4	$RCVV - (RCVV)_{SCH}$	RCVV
y_5	$BLD - (BLD)_{SCH}$	BLD

it to a stop, authority limit ($\pm 6^\circ$), or flutter boundary, it is limited and the integration is held. A test on the integrator error signal is made during each cycle. If the error signal has the appropriate sign to unlimit the command, the integration is resumed. In this way, switching during actuator saturation is accomplished without integrator windup or unacceptable transients. Figures 5.24 and 5.25 show the implementation of this logic. A dead-zone on the integrator input is required of the actuator hysteresis width to prevent wander or "hunting." An example of an actuator switch in saturation is shown in Figure 5.26. The small dead zone in the RCVV system causes a variation in intermediate thrust which violates the accuracy, repeatability and stability requirements of the control criteria. To eliminate this, the geometry schedules are extended above the physical stops to drive the vanes and stators to their scheduled values (typically full axial) in the presence of the hysteresis and dead-zone at intermediate power.

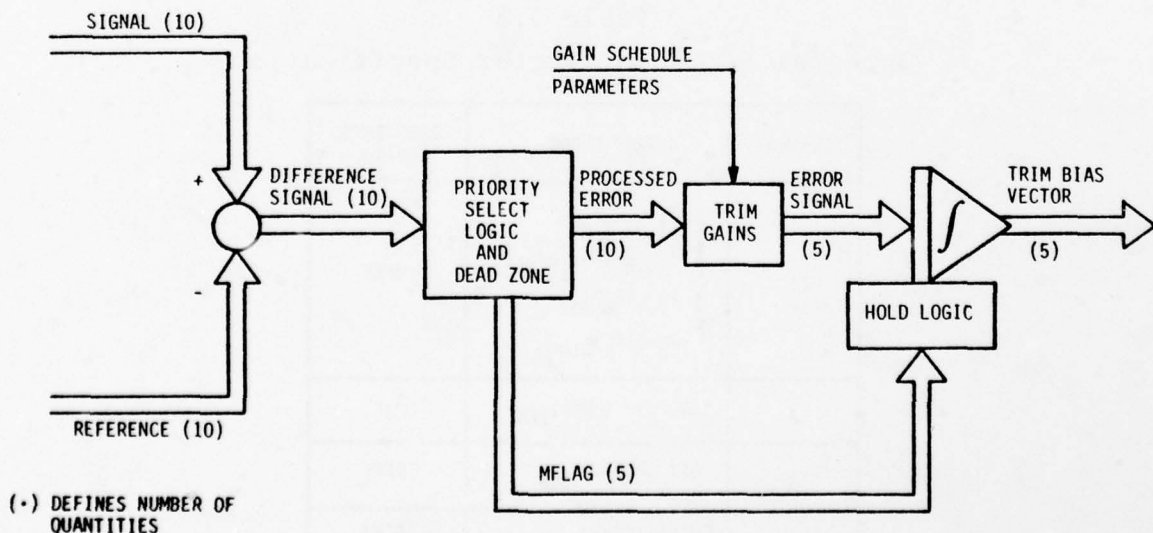
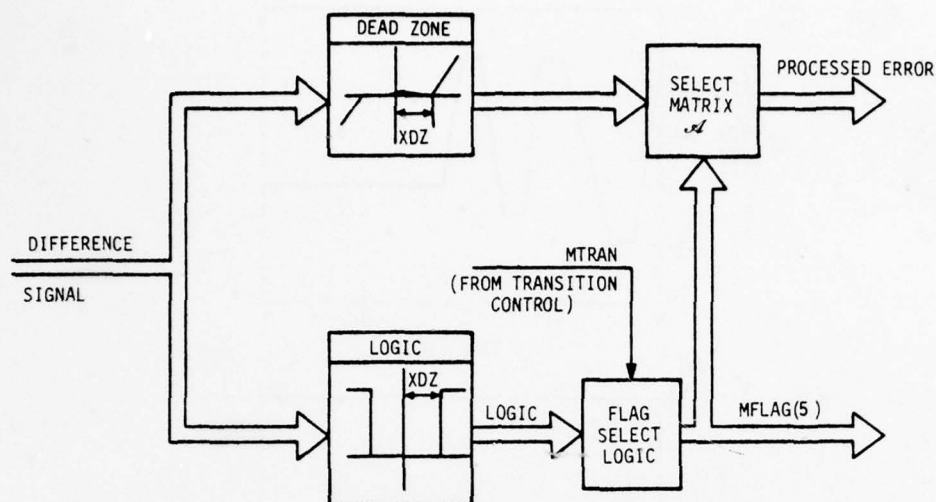


Figure 5.24 Implementation of Integral Trim - Overview



SIGNAL	REFERENCE	XDZ	LOGIC	MFLAG	LOGICAL OPERATION
$\Delta p/p$	$(\Delta p/p)_{NOM}$	0.005	LFDP	MAJFLG	$LFAJ \cup MTRAN$
N_1	$(N_1)_{NOM}$	25 RPM	LFN1	MCVFLG	$LFCIVV \cup MTRAN$
FTIT	$(FTIT)_{MAX}$	4.0°F	LFT45	MRCFLG	$LFRCVV \cup MTRAN$
P_B	$(P_B)_{MAX}$	4 PSI	LFPBHI	MBLFLG	$LFBLD \cup MTRAN$
P_B	$(P_B)_{MIN}$	4 PSI	LFPBLO	MWFFLG	$LFWF \cup MTRAN \cap$ $(LFT45 \cup LFPBMX \cup LFPBMN)$
CIVV	$(CIVV)_{LIMIT}$	1°	LFCIVV	MN1FLG	$MFTFLG \cup MPBHI \cup MPBLO$
RCVV	$(RCVV)_{LIMIT}$	1°	LFRCVV	MFTFLG	LFT45
BLD	$(BLD)_{LIMIT}$	0.1%	LFBLD	MPBHI	$LFPBHI \cup MFTFLG$
WFMB	$(WFMB)_{LIMIT}$	150 LBM/HR	LFWF	MPBLO	$LFPBLO \cup MFTFLG$
ANMIX	$(ANMIX)_{LIMIT}$	0.02 FT ²	LFAJ		

TO CONTROL

$$\mathcal{A} = \text{diag}(\text{MAJFLG}, \text{MCVFLG}, \text{MRCFLG}, \text{MBLFLG}, \text{MN1FLG}, \text{MFTFLG}, \text{MPBHI}, \text{MPBLO})^*$$

* The \mathcal{A} matrix contains 1's or 0's depending on the logic states of the MFLAG variables.

Figure 5.25 Priority Select Logic and Dead Zone in Integral Control Algorithm

Since the geometry and bleed trims have uncoupled loops, the remaining two degrees of trim freedom determine the choice of fuel flow and jet area. The input to the trim system is dependent upon the flight and power condition. The trim quantities are chosen to provide accurate performance in the

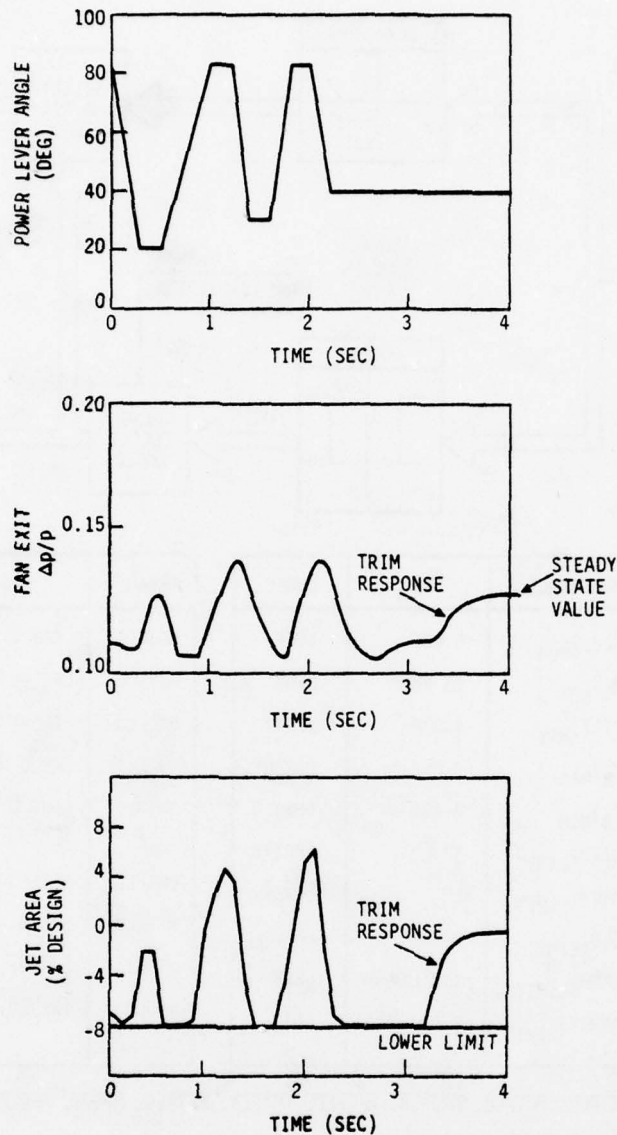


Figure 5.26 Cyclic PLA Response Shows Nozzle Moving In and Out of Saturation (At the end of input sequence, jet area unsaturates to trim engine match point, sea level static conditions from nonlinear digital simulation)

presence of modeling uncertainties, sensor errors, engine-to-engine variation and deterioration. They are also chosen for engine limit protection. Finally, trim quantities are chosen to provide acceptable saturated actuator behavior. This concept will be discussed below.

An additional logical element is used in the trim control. During large power level transients, the engine is not near a trim condition. A logical flag, MTRAN, generated in the transition control (see Figure 5.25) indicates when the engine is undergoing a large motion. This flag inhibits integral trim action until the engine is in the neighborhood of a trim point as indicated by MTRAN acquiring the false condition. An exception to this logic occurs if there is a measured or anticipated limit overshoot. In this case, the fuel flow integrater is allowed to trim back from the limit as an additional component of the control law.

At off-intermediate power, the engine usually operates away from temperature and pressure limits. Fuel flow and jet area must be adjusted to give the desired thrust at acceptable fuel consumption and airflow values. This defines a locus of operating points on the fan and compressor map. For a given thrust, there is a unique operating point for optimum performance. Locating match points on the compressor and fan maps represent four degrees of freedom. It is only possible to specify two of these with fuel flow and jet area. Thus, there are several possibilities for setting performance in these regimes.

One set of trim variables contains the two spool speeds. This choice is attractive for instrumentation considerations because the rotor speed measurements are the most accurate transduced signals in the engine. It would be possible to set the performance of the engine by specifying the rotor speeds independently and using jet area and fuel flow to match these two quantities. Fixing the rotor speeds still allows match point movement along constant speed lines on the fan and compressor map. The match point on the fan is deduced from rotor speeds and an inferred equilibrium model of the thermodynamic cycle. Effects such as deterioration, power extractions, and bleed flow will degrade the model and cause the

match to change with corresponding shifts in performance. A practical variation of this concept will be discussed below.

Alternately, quantities determining the fan match point can be specified. Two independent quantities which determine the fan performance are chosen. Fixing the fan match point causes the compressor match to float, i.e., the compressor speed and core airflow are determined by thermodynamic equilibrium. No inferred model is necessary in this procedure because measured quantities set the fan trim point exactly. This approach is also attractive because the compressor operates in a much lower speed range and variations of the compressor operating point tend to be small. With small variations, the compressor is less likely to operate far from its high efficiency design point.

Choice of direct match point measurements is determined by sensitivity, accuracy, and equipment reliability. One variable will be the fan speed itself. The second trim variable has been the subject of much discussion within the industry. This measurement reflects the fan loading at a particular speed and thus is a pressure or flow quantity. Pressure measurements tend to reflect distortion due to inlet air nonhomogeneity, wakes and other effects caused by mechanical projections in the flow path. Three variables are presently considered. These are fan pressure ratio, fan exit pressure ratio and engine pressure ratio. Fan pressure ratio tends to suffer from non-uniform radial and circumferential distortion at the engine face. Also, lines of constant pressure ratio tend to lie at an angle to the desired operating line. This causes a lack of precision in specifying the match point [29].

Fan average delta pressure ratio is defined as follows:

$$\frac{\Delta p}{P}_{AVG} = \frac{1}{2} \left\{ \left(\frac{P_T - P_S}{P_T} \right)_H + \left(\frac{P_T - P_S}{P_T} \right)_C \right\}$$

where circumferentially averaged core stream and tip stream measurements are radially summed. This parameter is insensitive to bypass ratio effects but it requires multiple probe locations and signal processing to derive the measurement. Lines of constant $\Delta p/p$ lie nearly parallel to the desired fan operating line. Operating line shifts due to altitude and Mach number effects can be easily scheduled. Also, distortion effects are theoretically averaged due to the fan, resulting in less sensitivity than obtained with measurements at the engine face. Engine pressure ratio is much like fan pressure ratio. High accuracy is needed to specify the schedule. It has the advantage of using the augmentor pressure signal which is less sensitive to flow effects than fan discharge pressure. The problem of accurate installed engine face pressure measurement remains, however.

For the F100 control, the averaged fan $\Delta p/p$ parameter was chosen along with low rotor speed to trim the engine. Deterioration and installation effects were evaluated using the digital simulation. Measurement errors in the $\Delta p/p$ probes were evaluated using worst case thrust shifts. The results of this evaluation are presented in Chapter VI.

In unlimited engine operation, the fuel flow and nozzle area are used to trim the fan speed and scheduled $\Delta p/p$ to obtain adequate performance. When an engine quantity reaches a structural limit or when an actuator reaches a saturation limit, the set point must be modified. The results of the set point switching algorithm are discussed below. Figure 5.27 illustrates set point switching caused by unsaturating the CIVV's and RCVV's.

When the jet area reaches its lower limit, the fan match point can no longer be maintained. In this case, the jet area integrator is held and the $\Delta p/p$ error term is eliminated from the control law as illustrated in Figure 5.26.

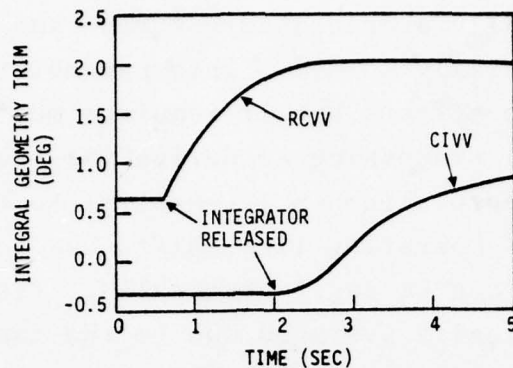


Figure 5.27 An Example of Integral Trim Accommodation of Control Saturation During a Step Power Lever Response. Geometry Integrators Release When Controls Unsaturate and Trim to New Steady-State Condition (Acceleration at sea level static conditions from nonlinear digital simulation)

When jet area is saturated at the closed stop, the fan match tends to move down a constant speed line and away from surge. When the $\Delta p/p$ error term changes sign so that the actuator will move out of saturation, the integration is continued. A set point switch also occurs when the required fuel flow exceeds the pump limits. In this case, integrators are held during large transients to eliminate tracking of large error terms. An example of fuel flow integrator switching is shown in Figure 5.28.

The engine operates at the fan turbine inlet temperature (FTIT) limit at many of the intermediate power points throughout the envelope. When FTIT is at its maximum, the trim point is controlled by $\Delta p/p$ and FTIT error terms. Movement on the fan map in such a situation is along lines of constant $\Delta p/p$. The operating line is nearly along a constant $\Delta p/p$ and no logic modification or switch is necessary between limited and unlimited operation. Using pressure ratio or compressor speed trims, movement would not be in this direction. As a result,

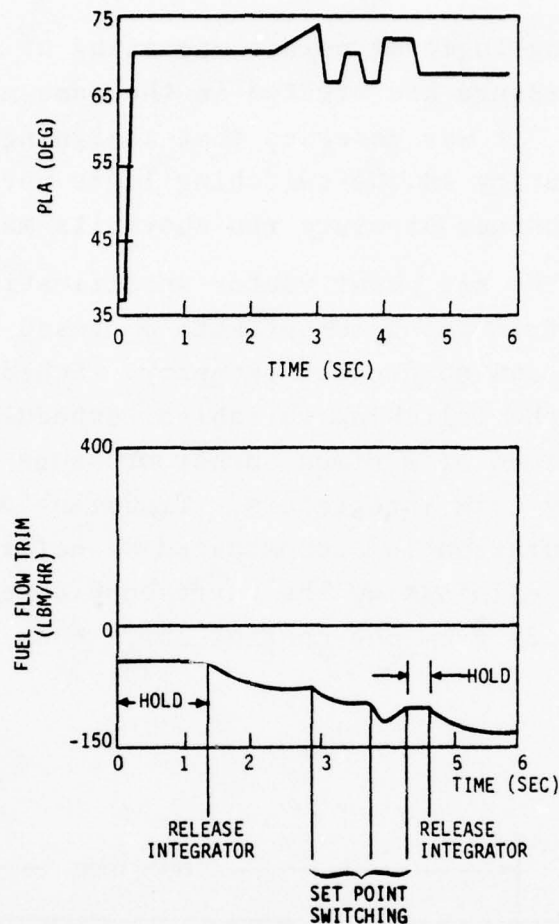


Figure 5.28 Example of Fuel Flow Integrator Switching During Cyclic PLA Input at Sea Level Static

these trim schemes require a separate schedule to handle match point migration under limited conditions. The rotor speed match uses a schedule representing the nominal fan operating line parameterized by fan speed as a function of high rotor speed. This procedure requires further complexity to accommodate altitude effects and the degradation in spool match due to installation and deterioration. Similar results are obtained for pressure ratio trim. A comparison of the effect of deterioration and installation on performance is presented in Chapter VI.

Trim switching logic at points operating at maximum or minimum burner pressure are treated in the same manner as overtemperatures. It was observed that assigning the FTIT limit highest priority in the switching logic never produced situations where burner pressure ran above its maximum limit.

In summary, the set point vector specification is described as follows. The trim point is set with a closed bleed valve and scheduled fan and compressor geometry. Scheduled fan exit $\Delta p/p$ and one of the following variables--scheduled fan speed, maximum FTIT, maximum or minimum burner pressure--are held at their schedules by trim integrators. Transient or steady-state control saturation is accommodated by holding the integrator output and eliminating the corresponding error term shown in Figure 5.29 from the control law. When the error

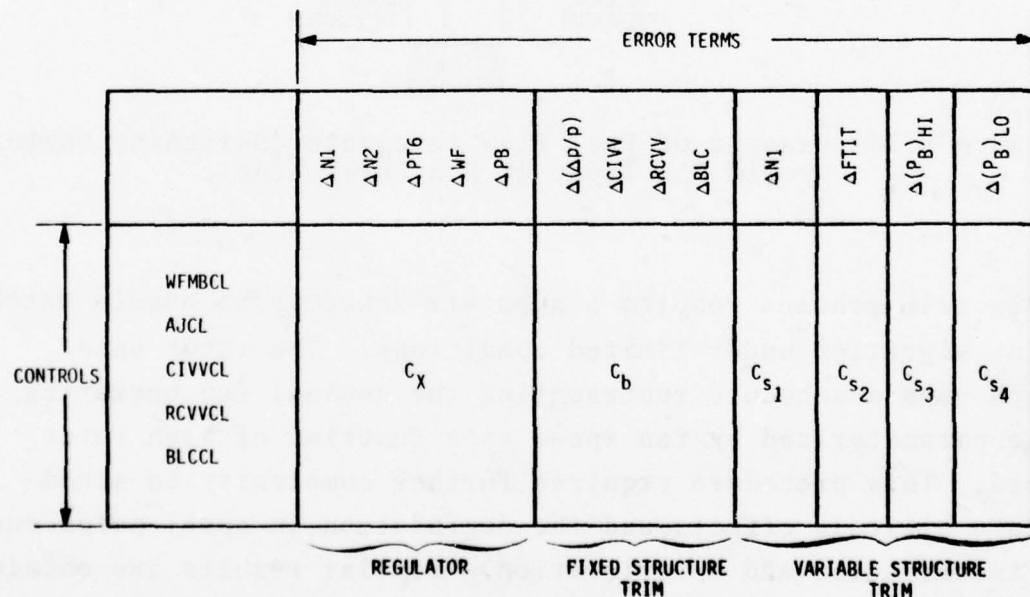


Figure 5.29 Multivariable Controller Feedback Gain Matrix Structure Containing Regulator and Variable Set Point Integral Trim Terms

term takes the correct sign to unsaturate the actuator, the integration is resumed.

5.8.3 Integral Control Design Method

The procedure for deriving integral trim gains from the locally linear control designs is described in Chapter IV. Specific design results are presented in Appendix G. The design method and application to the F100 is described below.

The design procedure was used to synthesize coupled trim controls for fuel flow and exhaust nozzle area. The three uncoupled integral loops on the CIVV, RCVV, and bleed schedules were designed separately; however, the dynamics of the complete system had to be included in the evaluation because of inherent interactions of all integrations.

Design points for the integral trim system were the same as the regulator. This provided a convenient implementation advantage because the feedback gain matrix could be scheduled along with the LQR state feedbacks. The structure of the feedback gain matrix is shown in Figure 5.29. The columns feeding back the integrated $\Delta p/p$, N_1 , FTIT, $(P_B)_{\max}$, $(P_B)_{\min}$ error signals to the fuel flow and nozzle area were designed using the procedure described in Chapter IV.

The variable structure allows one column (or error signal) to be switched into the trim system. In this case, the $\Delta p/p$ feedback term always remains in the design and one of the four remaining terms is included in the feedback law. The structure of the system for design purposes is shown below:

$$\frac{d}{dt} b_1 = \Delta p/p - (\Delta p/p)_{sch} = \delta \Delta p/p$$

$$\frac{d}{dt} \dot{b}_2 = \left\{ \begin{array}{l} N_1 - (N_1)_{sch} = \delta N_1 \\ FTIT - (FTIT)_{sch} = \delta FTIT \\ P_B - (P_B)_{max} = \delta P_{Bmax} \\ P_B - (P_B)_{min} = \delta P_{Bmin} \end{array} \right\} \quad \begin{array}{l} \text{Switched} \\ \text{by limiting} \\ \text{logic} \end{array}$$

For each choice of \dot{b}_2 , the trim dynamics can be written as follows:

$$\begin{bmatrix} \dot{b}_1 \\ \dot{b}_2 \end{bmatrix} = \begin{bmatrix} g_{11} & g_{12} \\ g_{21} & g_{22} \end{bmatrix} \begin{bmatrix} C_{11} & C_{12} \\ C_{21} & C_{22} \end{bmatrix} \begin{bmatrix} b_1 \\ b_2 \end{bmatrix}$$

where C_{ij} is a feedback gain element and g_{ij} represents an element of the closed-loop gain from the error term to the control with the LQR regulator active, or, for example,

$$\begin{bmatrix} \delta \Delta p/p \\ \delta N_1 \end{bmatrix} = \begin{bmatrix} g_{11} & g_{12} \\ g_{21} & g_{22} \end{bmatrix} \begin{bmatrix} \delta W_f \\ \delta A_j \end{bmatrix}$$

where δW_f and δA_j represent perturbations away from the scheduled equilibrium.

The trim system dynamics matrix is defined as follows:

$$\bar{F} = \begin{bmatrix} g_{11}C_{11} + g_{12}C_{21} & g_{11}C_{12} + g_{12}C_{22} \\ g_{21}C_{11} + g_{22}C_{21} & g_{21}C_{12} + g_{22}C_{22} \end{bmatrix}$$

The following observations can be made. If the dynamics matrix is forced to be lower triangular, i.e.,

$$g_{11}C_{12} + g_{12}C_{22} = 0$$

then the eigenvalues of the trim system can be written as follows:

$$\lambda_1 = g_{11}c_{11} + g_{12}c_{21}$$

$$\lambda_2 = g_{21}c_{12} + g_{22}c_{22}$$

The first eigenvalue is independent of the elements of the second column of the gain matrix and first row of the g matrix. It follows for any feedback in the second position and the associated gain matrix satisfying the triangularity condition that the gains for the first position are independent of the second. The assignment of b_2 to a particular error term requires satisfaction of the triangularity condition for each column of C and row of g . These columns can be switched into the system while maintaining the same system response dynamics.

The design procedure is sequential. First, the $\Delta p/p$ trim system is calculated. This fixes λ_1 , c_{11} , c_{21} , g_{11} , and g_{12} . Then, for each possible trim error term, the appropriate steady-state gains are calculated for the second row of g and the feedback gains for the second column of C are derived. The formulas for this procedure are shown below.

For the $\Delta p/p$ system, the trim dynamics are not sufficient to fix the gains uniquely. An optimal system with respect to the cost function shown below can be calculated (as presented in Chapter III):

$$\text{COST:} \quad J = \frac{1}{2} \int_0^{\infty} [b_1^2 + B_1(\delta W_{FMB})^2 + B_2(\delta A_J)]^2 dt$$

$$\text{SYSTEM:} \quad \dot{b}_1 = g_{11}\delta W_{FMB} + g_{12}\delta A_J$$

$$\text{FEEDBACK*}: \quad \delta W_{FMB} = c_{11} b_1$$

$$\delta A_J = c_{21} b_1$$

$$\text{CONSTRAINT}: \quad g_{11} c_{11} + g_{12} c_{21} = \lambda_1 = \text{given}$$

$$\text{SOLUTION}: \quad \begin{bmatrix} c_{11} \\ c_{21} \end{bmatrix} = S \begin{bmatrix} 1/B_1 & 0 \\ 0 & 1/B_2 \end{bmatrix} \begin{bmatrix} g_{11} \\ g_{12} \end{bmatrix}$$

$$S = \frac{-\lambda_1}{\frac{g_{11}^2}{B_1} + \frac{g_{12}^2}{B_2}}$$

In general,

$$C = S B^{-1} g^T$$

$$S = \frac{-\lambda}{g^T B^{-1} g}$$

The trim root, λ_1 , is chosen to represent suitably fast trim (e.g., as specified in the control criteria). B_1 and B_2 weight the relative effort used by the fuel flow and jet area in trimming $\Delta p/p$ errors.

Once c_{11} and c_{21} are calculated, each possible set point quantity is used in the calculation of a column of the feedback matrix as follows:

* Note that another actuator input, e.g., δC_{IVV} , can be included at this point without affecting the variable set point structure in the following.

$$\begin{bmatrix} c_{12} \\ c_{22} \end{bmatrix} = \begin{bmatrix} g_{21} & g_{22} \\ g_{11} & g_{12} \end{bmatrix}^{-1} \begin{bmatrix} \lambda_2 \\ 0 \end{bmatrix}$$

In this case, the gains are completely determined. The time constant, λ_2 , is chosen for suitably fast trim while keeping the decoupled character of the overall system. The procedure is a special case of a general result. For higher order systems, a variation on the optimal design is required as presented in Chapter III.

The decoupled assumptions must be checked to assure stable behavior of the full system. This validation is provided initially by calculation of the full (16th) order closed-loop linear system response with five integral gains and the LQR regulator feedback. Unacceptable results are corrected by iteration in the design cycle. Such an evaluation is shown in Appendix G.

5.8.4 Summary

Integral trims are provided to satisfy steady-state control criteria and accommodate engine operating limits in the presence of aging, build differences and disturbances. The trim requirements vary over the flight/power envelope and a variable structure trim system is used to accommodate this phenomena. Trim gains are chosen to provide a decoupled behavior which reduces the complexity of the implementation and allows switching without poor response. Evaluation has shown that this procedure accommodates the operating point throughout the practical environment of the engine.

5.9 TRANSITION CONTROL DESIGN

5.9.1 Introduction

The design of the reference point generator, regulator and trim system has been discussed above. These blocks are sufficient to provide rapid and accurate response to small perturbation changes around a steady-state operating point. The regulator is robust to small changes and therefore contains reasonably large gain elements in the proportional feedback law. A large step input, however, from idle to intermediate power, causes a large change in the reference signal. This change results in proportionally large actuator commands which add to the scheduled actuator signal. The effect is to saturate the actuators and the response would be uncertain. Since the engine is not globally linear and the actuators have a limited range, the perturbationally optimal regulator is not appropriate for large transitions.

Three alternatives are available for large transition logic. The regulator outputs can be limited, the regulator inputs can be limited and the gains can be reduced during large transients.

Limiting regulator outputs requires scheduling engine protection and actuator dynamic ranges as a function of actuator inputs. For example, fuel flow can be transiently scheduled during accelerations to provide surge protection, temperature limiting, and rotor speed overshoot protection. On decelerations, it can be limited by fuel-to-air ratio and minimum burner pressure constraints. The drawback of this solution is that the calculation of such limits for multivariable control systems under some optimality criterion is difficult [57]. The character of large transition becomes a schedule "riding" proposition with the regulator response

being overridden for all but the smallest perturbation by the acceleration or deceleration limits.

Gains in the regulator can be varied as a function of the "size" of the transition as measured in the difference of the present and scheduled value of an engine variable [67]. Such a procedure requires significant iteration. Each magnitude of transition should be evaluated to choose appropriate proportionality factors. The resulting control law does not use the constant gains assumed in the regulator design.

The third solution limits the inputs. A simple example of this is the rate limited power lever input which is used on production engines. This constrains the transient nominal path to lie along the corresponding steady-state operating line. This procedure does not allow any direct control of the transient trajectory. A procedure is described below and more theoretically in Chapter IV which provides this capability.

5.9.2 Transition Control Design Principles

The transition logic is designed to produce a trajectory reference for the regulator which takes the system from one power condition to another (see Figure 5.30). If this trajectory were a consistent path, the regulator action would be a perturbation response only. Since the regulator is designed for this, the resulting behavior along the trajectory would presumably be satisfactory. This method produces transients which are controlled by the trajectory generator in a gross sense and are controlled by the regulator in a perturbational sense (see Figure 5.31).

Unfortunately, it is extremely difficult and impractical to calculate precise open-loop trajectories for all transitions throughout the envelope. Some procedures are available to approximate this trajectory [26,57] and a procedure to produce an easily calculated trajectory is described below.

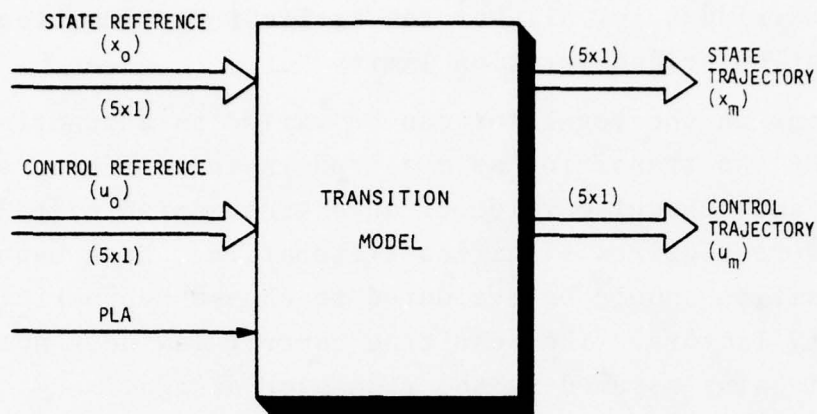


Figure 5.30 Transition Model

The approximate nature of the trajectory does not invalidate the separation of control effort. Since the approximate trajectory will not be a free trajectory, the regulator must control a time-varying perturbational input (equivalent to a disturbing force) during the motion. Linear quadratic regulators have shown excellent characteristics in such situations as long as the inputs are small enough to excite no significant actuator or plant nonlinearities. Using this property of the regulator, an easily implemented trajectory generation scheme provides direct and flexible control of large transient motion.

5.9.3 Description of the Designs

The first order approximation to free transitions (i.e., equilibrium motion) developed in Chapter IV was used to produce the transition logic in the F100 multivariable control. The various operating constraints allow power level transitions in a corridor of the envelope as shown in Figure 5.14. The design points for transition rate calculation using the linear models were high, middle, and low power conditions at 0K/1.2, 0K/0, and 30K/0.9.

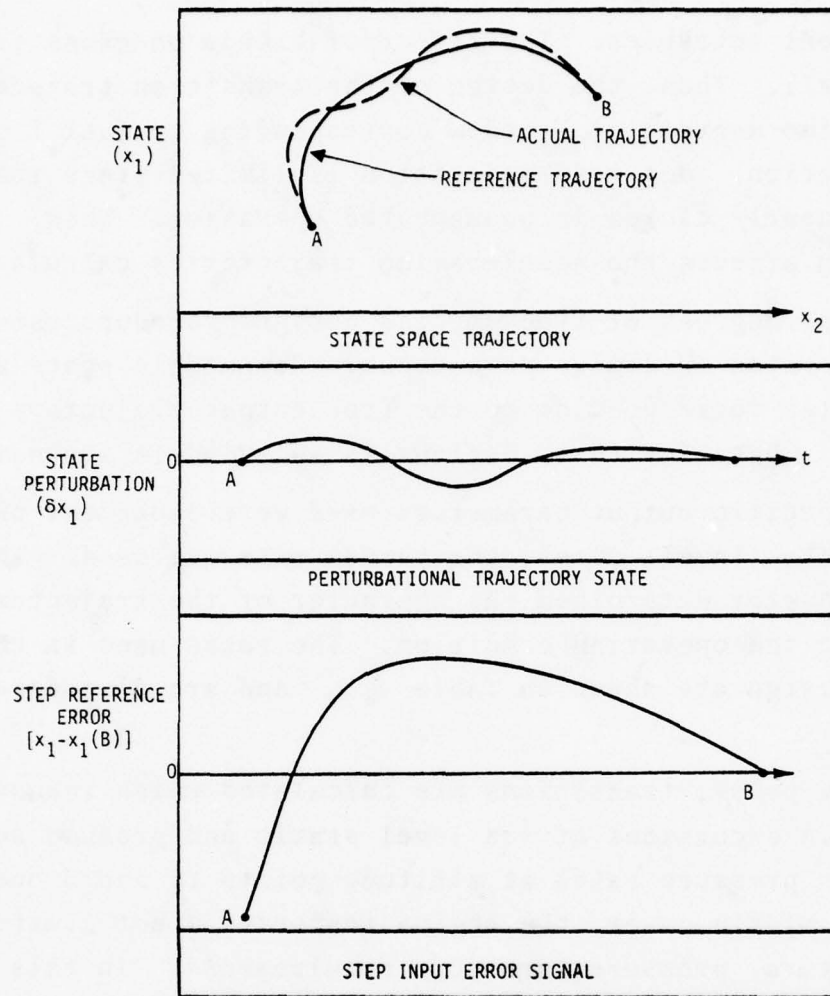


Figure 5.31 Illustration of the Differences Between Perturbation Error Signal and Reference Error in a Large Transient from Point A to Point B Shown as State Space Trajectory, Perturbation Trajectory, and Step Input Error Signal

There were five control variables considered in the regulator design. The fuel flow is the primary power modulation variable during large transients. Jet area also provides a small capability of fast thrust response. The variable geometry is, however, restricted to small deflections away from

the component schedules. The effect of bleeds on gross transients is small. Thus, the design of the transition trajectory used only two degrees of freedom corresponding to fuel flow and jet area motion. Jet area modulation is limited since the nozzle is nearly closed in unaugmented operation. This restriction affects the acceleration trajectories calculated.

For two degrees of freedom, the design procedure uses two output rates as design parameters. Compatible state and control rates corresponding to the free output trajectory are calculated. Data for these designs is included in Appendix H.

The specific output parameters used were dependent on the design point. In all cases, the thrust rate was used. The second parameter determined the character of the trajectory peculiar to the operating condition. The rates used in the original design are shown in Table 5.9, and are discussed below.

At low power, transitions are calculated which reduce surge margin excursions at sea level static and produce acceptable burner pressure rates at altitude points to avoid undershoot. At middle power, the engine response is not limited by temperature, pressure, or surge requirements. In this case, the turbine inlet temperature rates were specified to produce smooth and rapid thrust responses. At intermediate power, lower turbine inlet temperature rates were specified to modulate this variable near its upper limit.

The algorithm produces rates for the state and control reference vector which are asymptotic solutions. The procedure can also produce jumps as discussed in Chapter IV. It is not necessary to include the jumps in the logic. Practical implementation of reference point discontinuities requires a significant amount of logic to assure smooth response for all types of PLA inputs. The step logic was not used in the controller except in the one case discussed below.

Table 5.9
Scheduled Rate Values and Derived Output Values
Calculated as a Function of Ambient Conditions
at Four Design Points

STATE/ CONTROL RATES	AMBIENT FACTOR				DESIGN POINTS												UNITS
					HIGH				MID				LOW				
	A	B	C	D	A	B	C	D	A	B	C	D	A	B	C	D	
$\alpha_1 = \dot{N}_1$	1.2	1.0	.93	.83	960	800	742	662	3230	2690	2500	2230	1450	1190	1110	988	rpm/sec
$\alpha_2 = \dot{N}_2$	1.2	1.0	.93	.83	900	750	695	623	1820	1520	1410	1260	1080	600	558	498	rpm/sec
WFMB	1.8	1.0	.45	.18	5510	3060	1380	551	6710	3730	1680	671	1300	980	325	130	lbm/hr/sec
\dot{A}_J	1.8	1.0	.45	.18	.35	.29	.13	.05	0	0	0	0	-.045	-.025	-.011	-.005	ft ² /sec
\dot{P}_{T6}	1.8	1.0	.45	.18	15.1	8.4	3.8	1.5	15.5	8.6	3.9	1.6	7.7	4.3	1.9	.78	psi/sec
\dot{P}_B	1.8	1.0	.45	.18	135	75	34	14	218	121	54.5	22	77	43	19	7.8	psi/sec
OUTPUT RATES																	
Net Thrust					5800	3260	1200	500	---	5441	1320	767	---	1360	670	---	lbf/sec
Turbine Temp.					572	290	272	230	---	464	650	490	---	120	260	---	°R/sec
Comp Surge Margin					12	-0.4	-0.3	-0.2	---	17	-10	5	---	10	-5		%/sec

DESIGN POINT INDEX			
	HIGH	MID	LOW
A	83/OK/1.2	---	---
B	83/OK/0	52/OK/0	20/OK/0
C	83/30K/0.9	52/30K/0.9	23/30K/0.9
D	83/45K/0.9	52/30K/0.9	---

There is one condition where reference value steps can be used to produce significantly improved response. The thrust and temperature rates chosen at the high power design point are used to implicitly limit temperature overshoots caused by open-loop modulation of the controls. This yields state and control rates which are smaller than the middle power values. However, during a deceleration from intermediate power, the trajectory will follow the acceleration path in reverse. This produces slower decelerations than would be normally possible.

By implementing a fuel flow and jet area step for decelerations in this portion of the power range, fast decelerations and temperature limited accelerations are produced. The implementation of the transient logic is described below.

5.9.4 Implementation of Logic

The output of the transition control design is a set of state and control rates for each power and flight condition, as follows:

$$\dot{x} = r_x$$

$$\dot{u} = r_u$$

The implementation of this system is shown in Figures 5.32 and 5.33. The rates at each power condition are scheduled by a multiplicative function of engine face density to approximate the rate parameters at the design conditions. There were two scheduling functions for the six state and control rates used as illustrated in Figure 5.32 and Table 5.10. The rates were interpolated as a function of the engine power condition to produce a smooth nominal trajectory. These rate schedules are included in Appendix H. Using this method, an appropriate state and control rate vector can be calculated for each operating condition.

Implementation of a smooth trajectory for any type of PLA input is accomplished by using a rate limited servo form driven by the reference vector as shown in Figure 5.32. Figure 5.33 shows the structure which produces a smooth transition from one operating point to another without unsatisfactory switching. The servo loop gain is chosen to produce transitions from the rate limited behavior to the proportional behavior at a small off-set from the steady-state. The linear

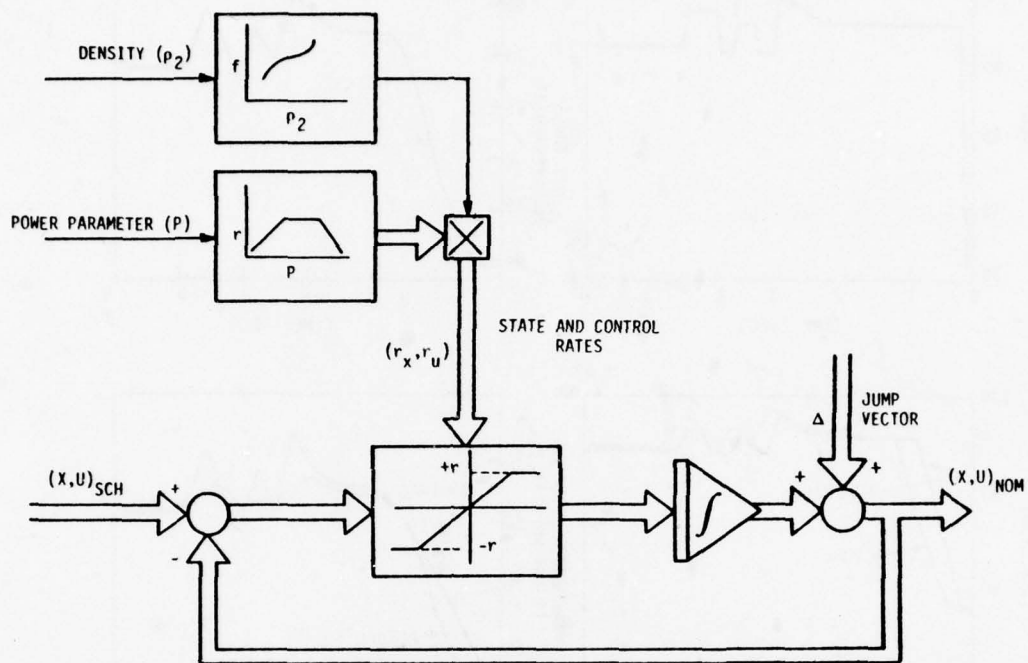


Figure 5.32 Transition Trajectory Generation Algorithm is Formed from a Rate Limited Servomechanism Structure With Variable Rate Saturation Forming the Gross Trajectory and the Proportional Response Providing Continuity with the Steady-State Reference

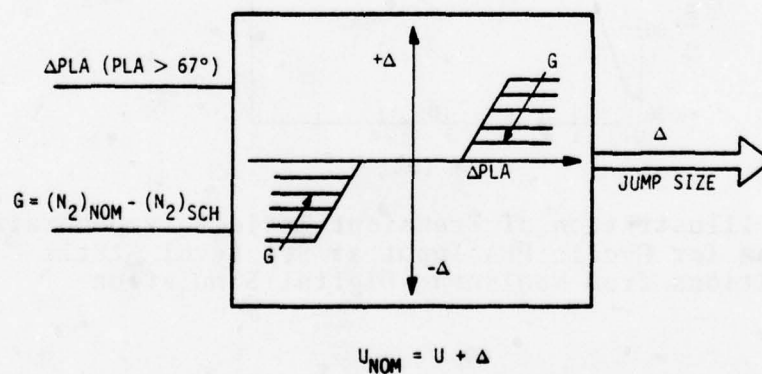


Figure 5.33 Generation of Control Step Inputs as a Function of Power Lever Angle Change and Current Trajectory State

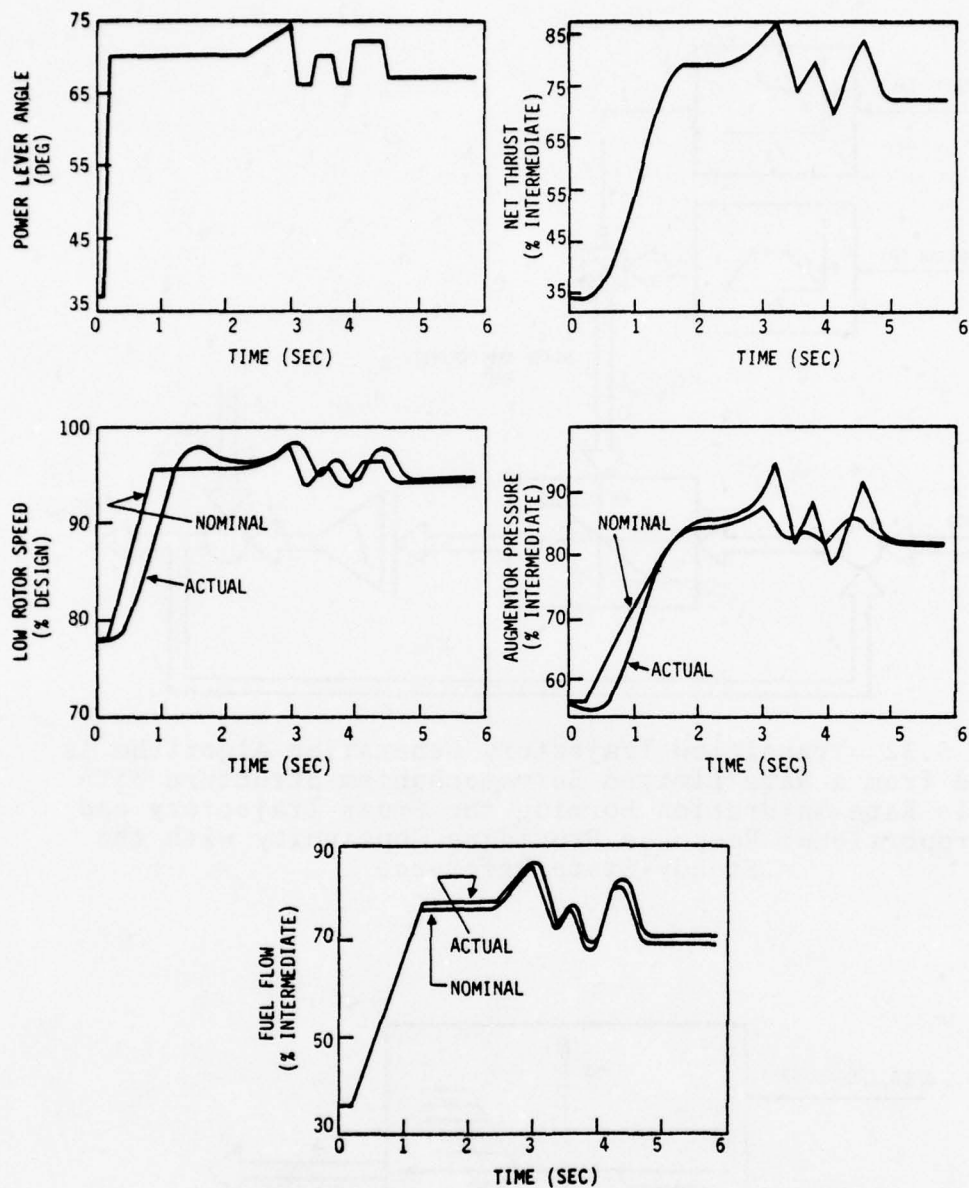


Figure 5.34 Illustration of Transient Trajectory Generation Algorithm for Cyclic PLA Input at Sea Level Static Conditions from Nonlinear Digital Simulation

region of the "servo" loop is chosen to have a time constant compatible with the trajectory rates to ensure a smooth transition. This time constant was chosen as $\tau = 0.2$ sec for all flight conditions for simplicity. The logic results in an exponential response near steady-state and the trajectory is continuous with continuous time derivatives.

Implementation of the algorithm as shown above requires very little control logic and storage. The performance is excellent and the processing overhead minimal.

Discontinuities in the output of the trajectory generator must be included to accommodate inputs of arbitrary form, magnitude and frequency without "ratcheting" or other unacceptable behavior. The MVC implementation uses the sample difference of PLA to schedule the step magnitude. The time at the particular power level reduces this magnitude. Short steps to one level and back will not cause a change in power. This procedure is illustrated in Figure 5.33. Performance of the system is shown in Figure 5.34 for a cyclic PLA input.

For the implementation of the multivariable controller on the SEL 810B to control a real engine in an altitude cell, an additional functional block was included in the controller as protection against erratic or unpredicted operation of the control. This logic was tested initially on the hybrid to verify operation of the engine protection logic in conjunction with the multivariable control.

The logic was developed to incorporate specific actuator deflection limits and override schedules provided by the engine manufacturer. The limits specified were maximum and minimum fuel flow as a function of compressor speed, inlet temperature and burner pressure, RCVV stall boundaries as a function of compressor speed and fan discharge temperature, and CIVV flutter boundaries as a function of fan speed, engine face temperature and pressure. These schedules were implemented as variable actuator limits and directly integrated

with the integral trim logic as shown in Figure 3.25. Additional maximum deflection limits of $\pm 8^\circ$ and $\pm 6^\circ$ were placed on CIVV and RCVV motion, respectively, because simulation modeling of larger, off-schedule deflection was considered uncertain by the engine manufacturer.

5.9.5 Summary

The purpose of the transition control is to generate a state and control reference trajectory taking the system from one reference point to another. The regulator produces robust small signal regulation to move the system along the open-loop trajectory. A design procedure is presented for calculating the approximate trajectories as a function of design parameters from the linear models. An implementation is presented which schedules the rates and implements them to form a trajectory in a smooth and reliable manner. A procedure for adding discontinuous inputs is presented which produces acceptable responses.

5.10 FAN TURBINE INLET TEMPERATURE SENSOR COMPENSATION

Temperature limiting during transient and steady-state operation is a critical function of the multivariable control. The maximum temperatures specified for compressor discharge and turbine inlet stations in the gas path are implicitly limited by the maximum fan turbine inlet temperature criterion discussed in Section 5.2. Accurate measurement of this variable is crucial to successful engine control. Unfortunately, the characteristics of desirable temperature probes in this environment are severely restrictive to the control operation because of low bandwidth response relative to the temperature overshoot criterion. Compensation of this sensor signal is required for adequate temperature limiting during transient maneuvers. The compensation must not degrade the high d.c.

accuracy of the signal because this measurement sets intermediate thrust at a majority of flight points.

The techniques for sensor compensation discussed in Section 4.6 were applied to the FTIT sensor. A steady-state, reduced order filter was used for simplicity. In this case, choice of filter parameters can be directly related to classical, frequency domain considerations.

The FTIT sensor consists of a thermocouple harness with multiple circumferential probes at the low pressure turbine entrance. The dynamic model of the transient response is shown in Figure 5.35. The model is simplified to include only the dynamics associated with the slow response component of the measurement. A comparison with the linearized model presented in Section 5.2 is shown in the figure for a step input. After an initial mismatch, the two outputs are nearly identical. This behavior is used in the filter implementation discussed below. The implementation logic, which is discussed below, deactivates the filter during the initial portion of large transients. The filter is forced to track the sensor in the initial portion of the transient so the effects of the initial mismatch are substantially reduced. For small transients, this forced tracking does not occur, but in this case, the initial error is small relative to the overall accuracy of the actuators and the error is insignificant.

The equations used for the sensor filter are derived in detail in Appendix K and are repeated here as follows:

$$\begin{bmatrix} \dot{\hat{\theta}} \\ \dot{\hat{b}} \\ \dot{\hat{\epsilon}} \end{bmatrix} = \begin{bmatrix} 0 & 0 & 0 \\ 0 & 0 & 0 \\ 0 & 0 & -a \end{bmatrix} \begin{bmatrix} \hat{\theta} \\ \hat{b} \\ \hat{\epsilon} \end{bmatrix} + \begin{bmatrix} k_{11} & k_{12} \\ k_{21} & k_{22} \\ k_{31} & k_{32} \end{bmatrix} \begin{bmatrix} g(p)\delta W_{FMB} - \delta \hat{T} - \hat{b} \\ \delta T_m - \delta \hat{T} - \hat{\epsilon} \end{bmatrix}$$

$$\delta \hat{T} = \theta + \alpha g(p)\delta W_{FMB}$$

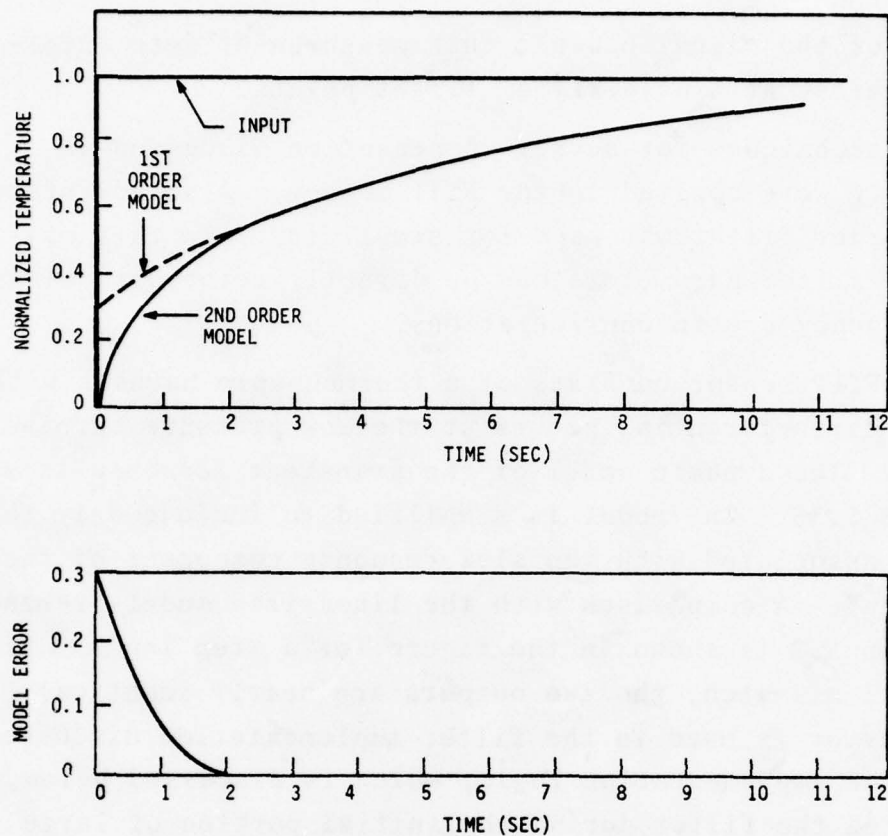


Figure 5.35 Step Response of FTIT Sensor Models Indicating That Error in Using First Order Approximation is Small Compared to Overall Sensor Output Response

The compensation is third-order. The sensor output relative to the scheduled final value, δT_m , contains correlated noise, ϵ , due to the sensor response. The deviation of the fuel flow from its nominal trajectory is treated as a biased measurement of the final temperature. The bias state is b . The scale factor $g(\rho)$ is a scheduled, steady-state gain of fuel flow to FTIT derived from the six design models. Values of the gain matrix are chosen to produce the desired frequency response of the estimate to the inputs. The transfer functions of each input to the temperature estimate are shown below:

$$\frac{\theta}{\delta W_{FMB}} = g(\rho) \frac{k_{11}(1-\alpha)s(s+a+k_{32})-\alpha k_{12}(s+a)(s+k_{21})}{s(s+k_{21}+k_{11})(s+k_{32}+a)+k_{12}(s+a)(s+k_{21})}$$

$$\frac{\theta}{\delta T_m} = \frac{k_{12}(s+k_{21})(s+a)}{s(s+k_{21}+k_{11})(s+k_{32}+a)+k_{12}(s+a)(s+k_{21})}$$

$$\delta \hat{T}(s) = \theta(s) + \alpha g(\rho) \delta W_{FMB}(s)$$

The relations are plotted in Figure 5.36. The fuel flow input affects the temperature estimate during transients only.

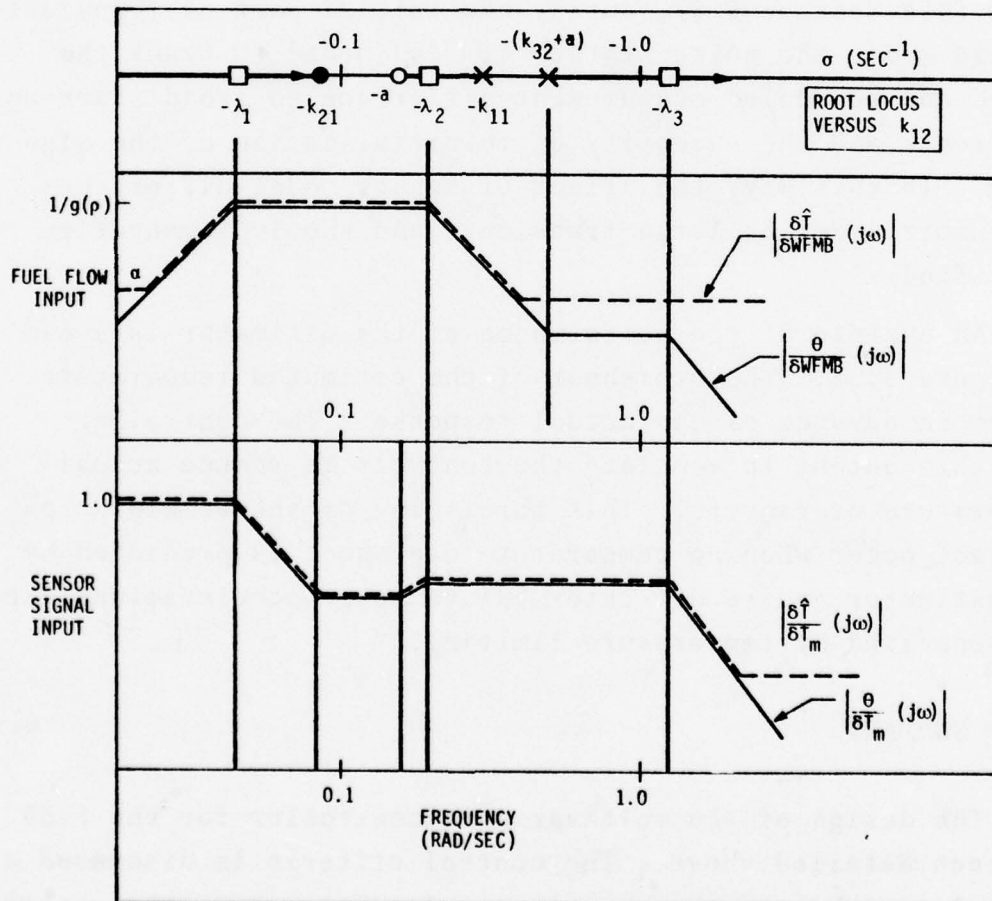


Figure 5.36 Asymptotes of Frequency Response of FTIT Sensor Compensation Showing Pole-Zero Locations as a Function of Estimator Gains and Feedforward Parameter

The filter bias state, b , nulls the effect of this measurement in steady-state. Scheduling errors in fuel flow will not cause hang-offs with this procedure. The sensor output is attenuated at frequencies greater than its slowest response time constant. The gain of the estimator to the sensor input in steady-state is unity preserving the high d.c. accuracy of the measurement. The filter functions like a complementary filter in blending inputs of two types to form a system with acceptable dynamic response and accuracy.

The implementation of the filter is shown in Figure 5.37. The input from the sensor is deactivated by the logic flag, MTRAN (see Section 5.8), during the initial part of transients. In this mode, the noise state, ϵ , is forced to track the sensed and scheduled measurement difference to avoid start-up transients and the necessity of reinitialization of the algorithm. In this way, the effect of sensor model differences is minimized during large transients and the implementation simplified.

An example of the performance of the estimator is shown in Figure 5.38. The overshoot of the estimated temperature occurs in advance of the actual response. The controller uses this output to modulate the controls to reduce actual temperature overshoots. This throttling of the acceleration does not occur when no temperature overshoot is predicted by the estimator and so off-intermediate power accelerations are not penalized by temperature limiting.

5.11 SUMMARY

The design of the multivariable controller for the F100 has been detailed above. The control criteria is discussed and its relationship to the structure and substance of the control law presented. The engine actuators and sensors have been

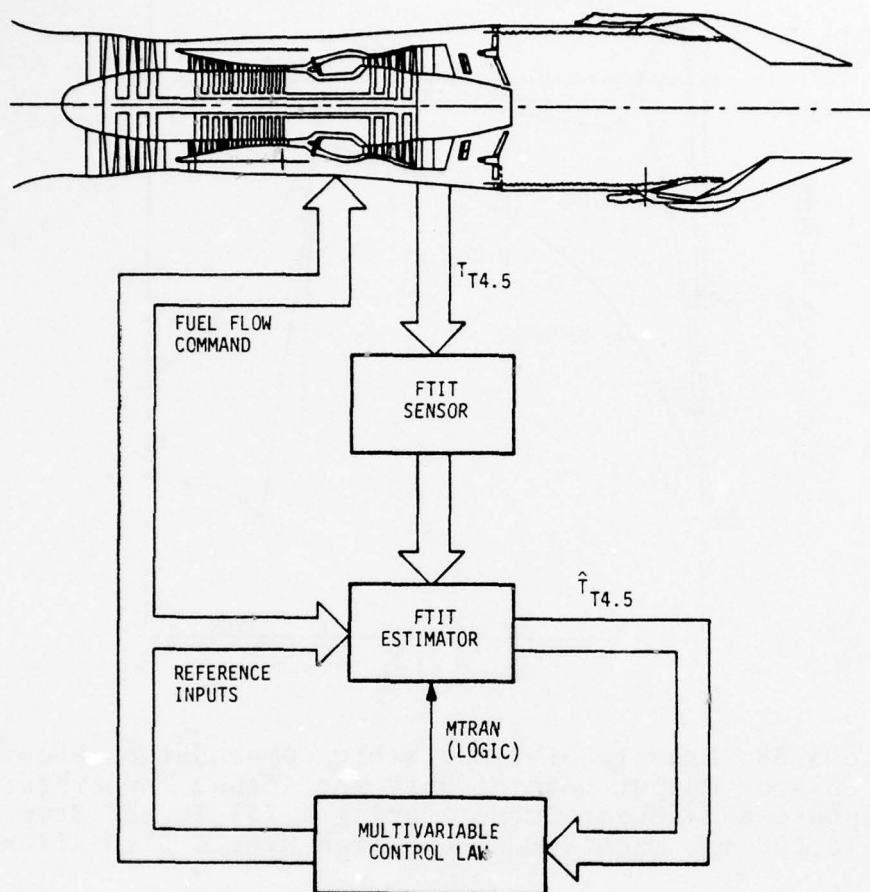


Figure 5.37 Implementation of Fan Turbine Inlet Temperature Estimator in Multivariable Control System

analyzed. The operating envelope has been explored using steady and linearized model analyses. These considerations have been combined to produce linear quadratic regulator designs at a series of design points spanning the envelope. A gain scheduling algorithm has been developed to link these designs into a continuous implementation. Integral trim logic has been designed to control the engine accurately, safely and efficiently throughout the envelope in the presence of sensor inaccuracies, plant variation and deterioration effects. A

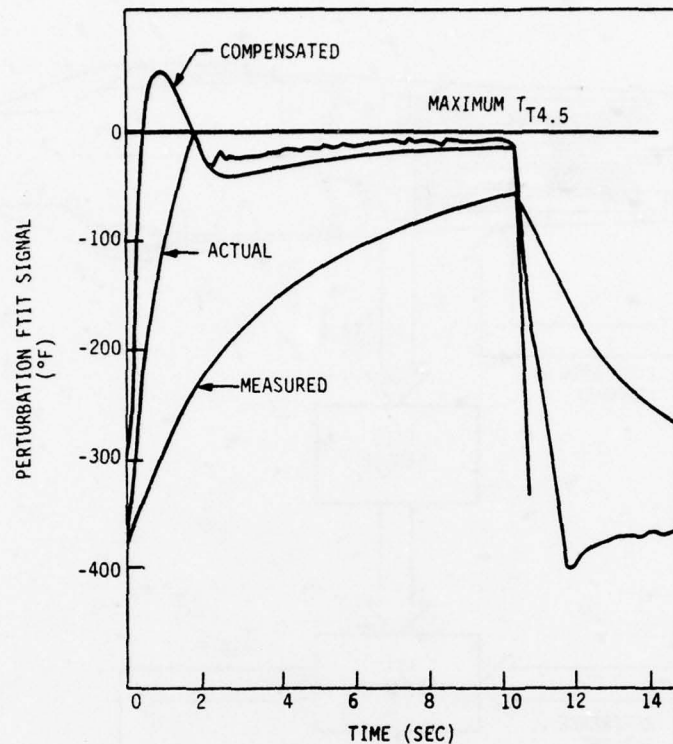


Figure 5.38 Example of Temperature Compensation Showing Compensator Output Leading Both the Actual Temperature Response and Sensor Output During a 75% Thrust Step at 10,000 ft, Mach Number 0.9 from Hybrid Simulation

transient control algorithm has been derived to produce nominal, open-loop trajectories to modulate gross thrust commands smoothly and stably at all flight conditions. The blocks have been integrated in a single full authority, digital, electronic control system for the engine. This system has been implemented on an SEL 810B computer and evaluated at NASA LeRC. The results of this evaluation and preliminary digital tests are summarized in Chapter VI.

CHAPTER VI

EVALUATION OF THE F100 MULTIVARIABLE CONTROLLER

6.1 INTRODUCTION

The multivariable control for the F100 engine described in Chapter V was developed and tested using a nonlinear, digital engine simulation from Pratt and Whitney Aircraft, the CCD 1103-1.0 deck. The algorithm was coded in FORTRAN and initially evaluated to verify satisfaction of the control criteria. Design iteration, both in the synthesis of linear quadratic regulator gains and the adjustment of other parameters in the control system, was facilitated by the complete model of the dynamic characteristics included in the simulation program.

A digital evaluation of the preliminary design was undertaken to verify steady-state and transient characteristics. Revisions were made as a result and the controller was implemented on the hybrid simulation at NASA LeRC. For a description of the digital tests see Ref. 1. The results of the hybrid simulation and implementation at NASA LeRC is described in Ref. 2.

In this chapter, a summary of the digital and hybrid evaluation is presented to illustrate the synthesis procedure. In Section 6.2, steady-state performance including deterioration and installation effects is presented. In Section 6.3, selected digital and hybrid transient runs are described with reference to the action of the controller in generating the response.

6.2 STEADY-STATE EVALUATION

6.2.1 Introduction

The steady-state evaluation consisted of three parts, each performed on the nonlinear digital simulation. The reference schedules were tested to determine the accuracy of the match point at a few conditions and to verify safe steady-state operation throughout the envelope. The controller trim logic was used to determine the effect of typical deterioration, power extraction, and bleed flow on baseline engine performance. Finally, the effect of instrument errors on steady-state performance was assessed. The evaluation test points are listed in Table 6.1.

6.2.2 Reference Schedules

Multivariable controller performance was required to match production control performance at ten power/flight points for study purposes during the preliminary digital evaluation.

Table 6.1
Operating Points for Evaluation

ALTITUDE	Mn	LINEAR MODEL	MODEL REDUC- TION	LQR DESIGN	GAIN POINT	DIGITAL EVALU- ATION	HYBRID EVALU- ATION	ENGINE TEST	TRANSI- ENT RUNS	Δp TESTS	COMMENTS
0	0	✓	✓	✓	✓	✓	✓		✓	✓	
10K	0.9	✓	✓			✓	✓	✓	✓	✓	
30K	0.9	✓	✓	✓	✓	✓	✓	✓	✓	✓	PLA $\geq 24^\circ$
45K	0.9	✓	✓	✓	✓		✓	✓	✓	✓	PLA $\geq 40^\circ$
0	1.2	✓	✓	✓	✓	✓	✓		✓	✓	PLA $\geq 57^\circ$
10K	0.6	✓					✓	✓	✓	✓	
10K	1.2						✓	✓	✓		PLA $\geq 57^\circ$
20K	1.8	✓					✓	✓		✓	
40K	2.2	✓	✓	✓			✓	✓		✓	
65K	2.5	✓					✓			✓	
58.5K	2.15	✓	✓	✓			✓	✓		✓	
75K	1.8	✓	✓	✓			✓	✓		✓	
65K	0.9	✓					✓	✓		✓	

These study points were intermediate power ($PLA = 83^\circ$) at 0K/0, 30K/0.9, 10K/0.9, 0K/1.2; idle power at 0K/0, 30K/0.9, 10K/0.9, and at 0K/0; PLA's of 67° , 52° , and 36° . The requirement for comparable performance was to facilitate the control evaluation. The tolerance for matching governor performance was specified as 1% of point thrust, 2% of point thrust specific fuel consumption (TSFC) with vanes and bleeds on schedule. Idle power is defined as the highest thrust level of the following: $PLA = 20^\circ$, $P_B = 48$ psia, or operation on the minimum airflow boundary at supersonic conditions. Operation of the controller in the remaining portions of the envelope was constrained to be within the specified control criteria limits discussed in Chapter V. The performance of the reference point schedules at the ten study points is shown in Table 6.2 for comparative purposes.

Table 6.2
Digital Evaluation of Reference Point Schedules Comparing
the Steady Operating Point of the Production and
Multivariable Controller at Ten Study Flight Conditions

MAGNITUDE OF DIFFERENCE AS PER CENT OF POINT VALUE	STUDY FLIGHT CONDITIONS									
	83/0K/0	67/0K/0	52/0K/0	36/0K/0	20/0K/0	83/10K/0.9	20/10K/0.9	83/30K/0.9	20/30K/0.9	83/0K/1.2
Net Thrust	0.2	0.1	0.5	0.1	0.0	0.4	25*	0.7	----**	(2.1) [†]
Thrust Specific Fuel Consumption	0.0	0.0	0.1	0.1	0.1	0.0	33*	0.1	----**	(4.7) [†]
Fan Speed	0.0	0.1	0.0	0.2	0.0	0.1	0.2	0.0	---	2.1
Compressor Speed	0.0	0.0	0.1	0.0	0.0	0.0	0.1	0.1	---	0.3
Augmentor Pressure	0.2	0.4	0.5	0.3	0.0	0.8	1.5	0.9	---	5.4
Burner Pressure	0.2	0.0	0.3	0.1	0.1	0.4	0.6	0.8	0.0	0.9
Fan Turbine Inlet Temperature	0.0	0.0	0.2	0.1	0.1	0.0	0.6	0.0	---	0.2
Fuel Flow	0.2	0.1	0.4	0.1	0.1	0.4	1.8	0.7	---	0.3
Jet Area	0.2	0.4	0.3	0.7	1.7	1.0	1.7	0.5	---	8.0

* Low Net Thrust Point - Actual $\Delta F_n < 50$ lbf

** Production Control Does Not Run to Idle Power (i.e., $P_B = 48$ psia)

[†] Slightly Different Thrust Calculations in Simulation Between Production Control and Multivariable Control Runs

Matching the sea level, static operating line and fixing the end points at a few altitude conditions produces a correspondence with the overall performance of the governor control. This is illustrated in Figures 6.1 and 6.2 (see Ref. 2 for a detailed discussion). Using thrust and TSFC as the comparison variables produces an extremely accurate match of all other engine quantities. The curved thrust to PLA relation, characteristic of the hydromechanical governor (see Figure 6.1), is quite satisfactory for engine operation. For the reference point schedules to follow this curve increases the resulting implementation complexity. If the controller had been designed to meet various performance rating points at intermediate power and idle only, the operating line schedule (e.g., $\Delta p/p$ vs. airflow) could have been simplified. However, matching the governor curves shows the flexibility of the method in providing full control of engine operating points.

6.2.3 Installation and Deterioration Effects

The reference point schedules determine the operating conditions throughout the flight envelope. In the first part of the steady-state evaluation, the reference schedules were developed to match ten production control points and to schedule the engine safely throughout the remaining envelope. The second part of the digital evaluation assessed the effect of installation and deterioration. Loss of component efficiency and extractions cause a variation in thrust, TSFC, or both. In general, there are no quantitative requirements on variations of either of these quantities. Qualitatively, the changes should be kept small. The engine must be operated in a safe and stable manner in the presence of these effects. The fan match point trim mode was evaluated against the production control operation. For this test, a set of flight points was chosen as shown in Table 6.1. Typical installation

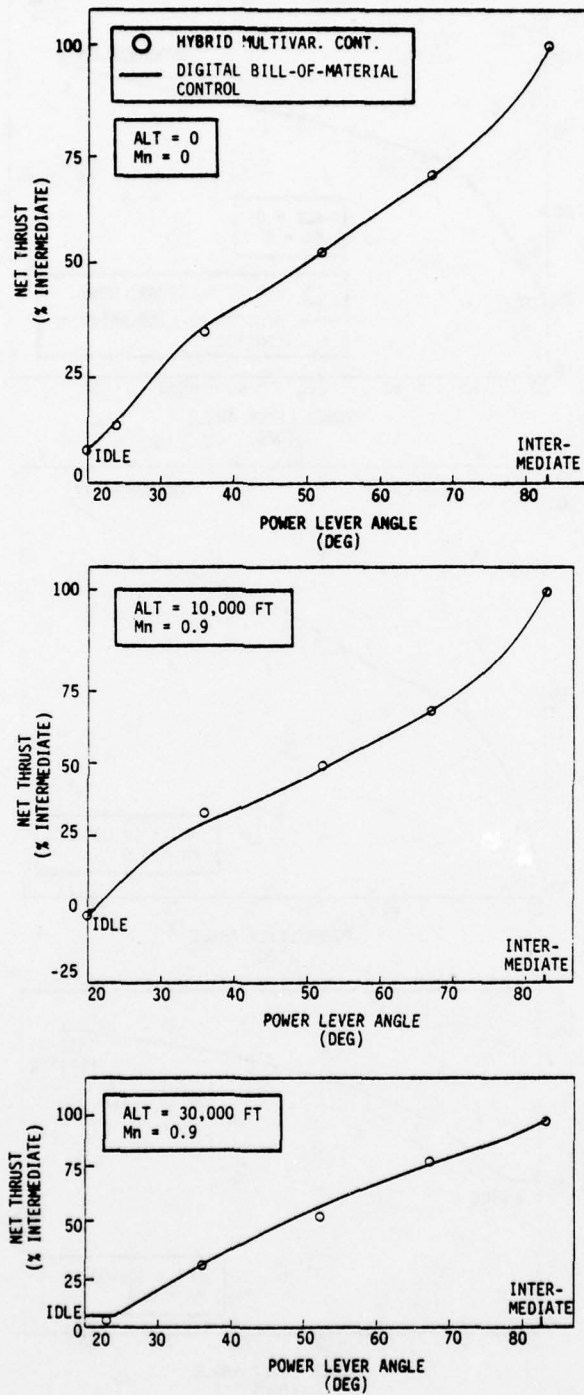


Figure 6.1 Comparison of Multivariable Controller Steady-State Operating Points with the Production Controller at Three Flight Conditions - Net Thrust

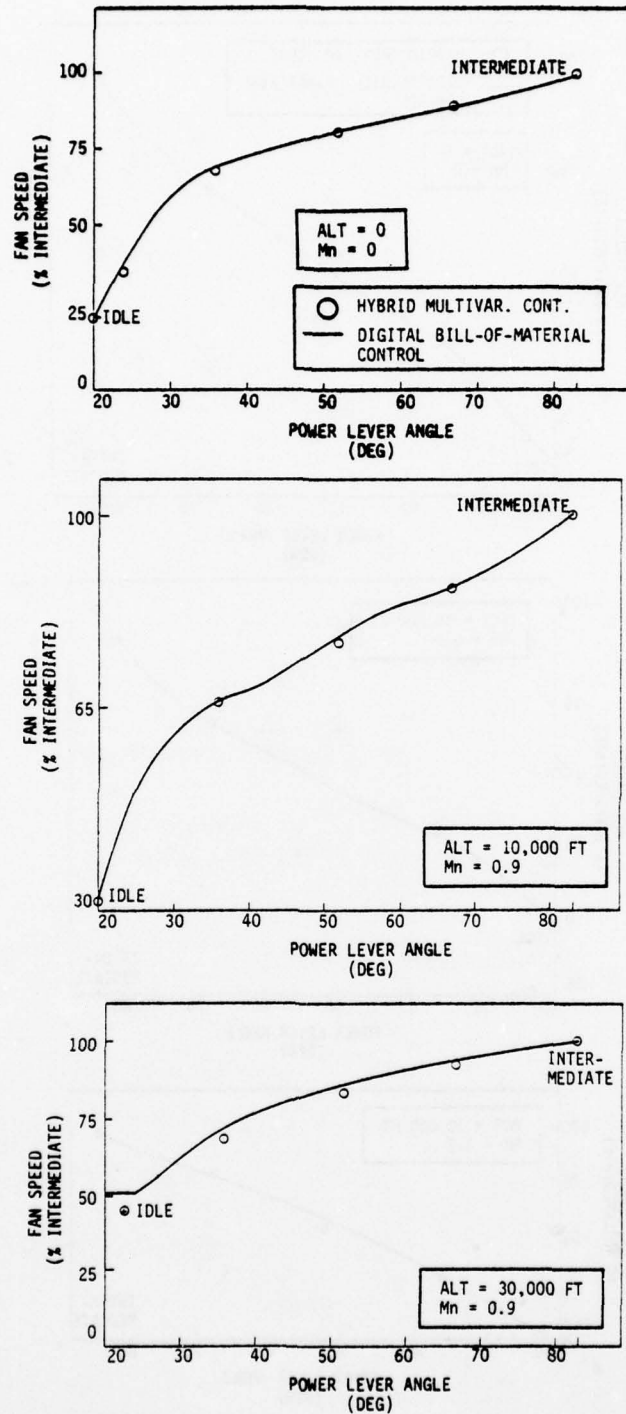


Figure 6.2 Comparison of Multivariable Controller Steady-State Operating Points with the Production Controller at Three Flight Conditions - Fan Speed

effects including deterioration of components, horsepower extraction, and customer bleed flow were specified by the engine manufacturer to be representative of the F15 aircraft application of the F100 engine. The values of these quantities are shown in Table 6.3.

The multivariable controller was run in the steady-state mode to investigate performance changes. The results were tabulated for half-nominal and nominal changes for each effect and all effects together. The details of these results are shown in Appendix I. A summary of these is presented in Figures 6.3 through 6.6. The conclusions are summarized in Table 6.4 and discussed briefly below.

Figures 6.3 and 6.4 show full deterioration and installation effects along the sea level static operating line. Near intermediate power, the engine efficiency losses cause the operating point to be turbine temperature limited. In this

Table 6.3
Typical Component Deterioration and Installation
Effects for the F15

ALTITUDE (FT)	Mn (-)	PLA (DEG)	NOMINAL HP EXTRACTION (HP)	NOMINAL BLEED (PPS)	NOMINAL DETERIORATION
0	0	20	54.0	1.71	(Fan (%)) = -1.0 (Comp (%)) = -2.0 (High Turbine (%)) = -2.5
0	0	52	59.6	1.93	Same as above
0	0	83	65.0	2.14	"
10K	0.9	20	58.4	1.40	"
10K	0.9	52	62.4	1.40	"
10K	0.9	83	66.2	1.40	"
30K	0.9	20	58.4	1.34	"
30K	0.9	52	62.4	1.34	"
40K	0.9	83	66.2	1.34	"
45K	0.9	30	59.6	1.06	"
45K	0.9	62	62.4	1.06	"
45K	0.9	83	66.2	1.06	"
65K	0.9	83	66.2	1.06	"
20K	1.8	83	67.2	1.66	"
58.5K	2.15	83	67.6	1.33	"

case, the fan match point cannot be maintained. The multivariable controller holds a constant $\Delta p/p$ and the production controller schedules N_1 as a function of N_2 . Both controllers cause thrust to decrease at a small increase in fuel consumption.

At middle power conditions, thrust is held nearly constant and fuel flow adds the required energy. The multivariable controller's direct match point trim limits thrust variations slightly more than the production control. The differences, however, are small. Near idle power, the multivariable control continues to add fuel and decrease the nozzle area

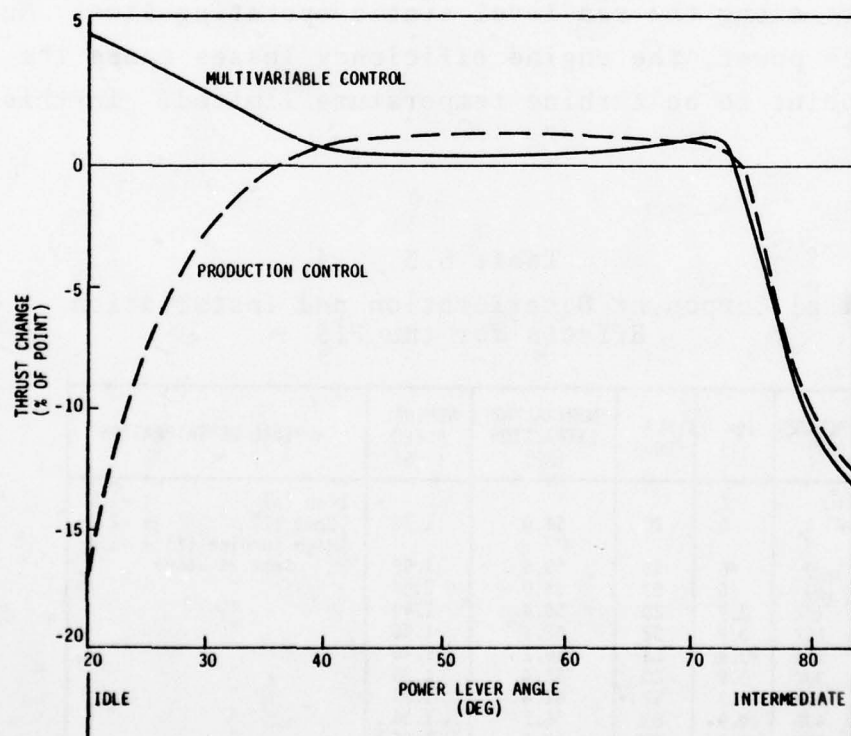


Figure 6.3 Effect of Deterioration and Installation on Net Thrust - Seal Level Static Conditions

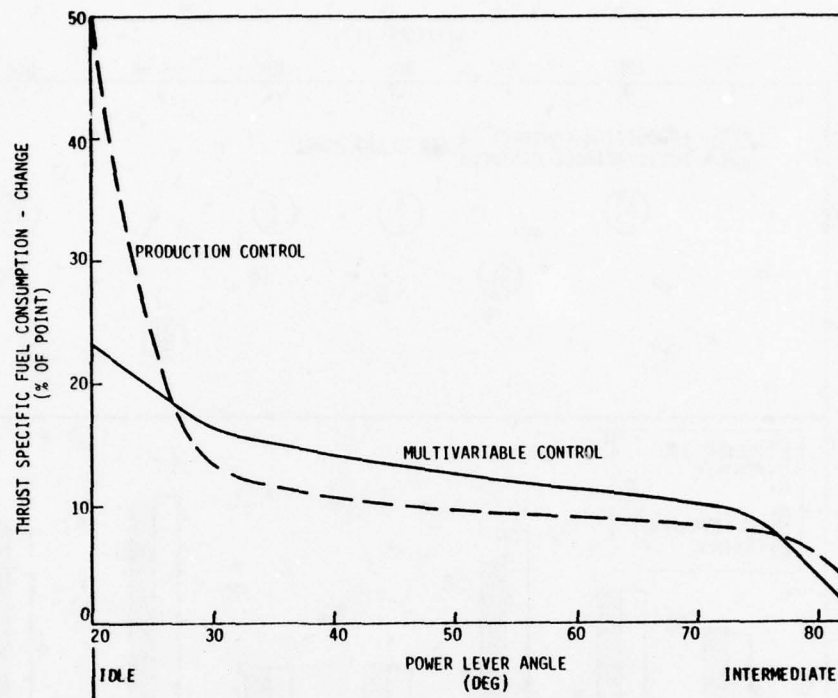


Figure 6.4 Effect of Deterioration and Installation on Thrust Specific Fuel Consumption - Sea Level Static Conditions

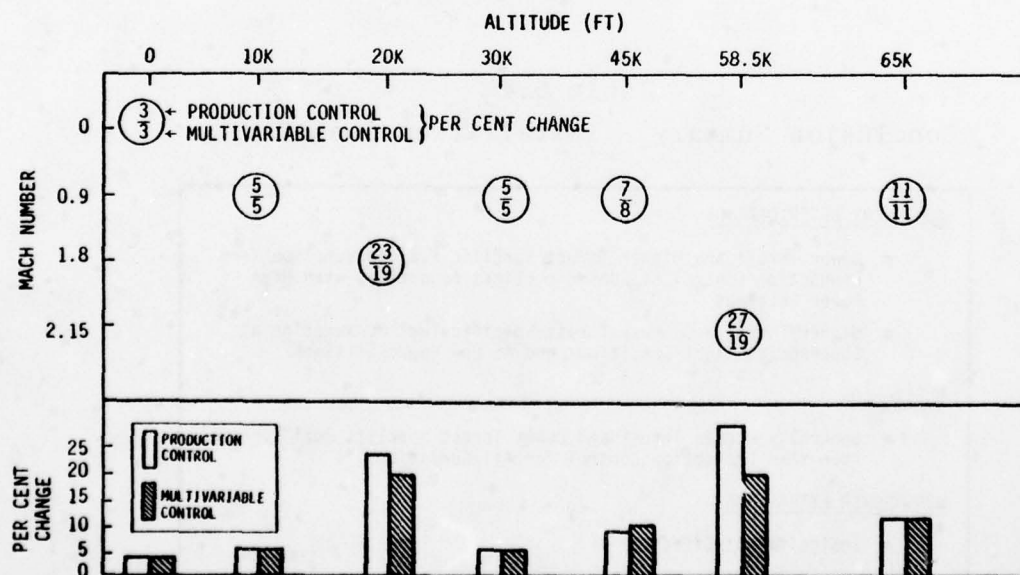


Figure 6.5 Effect of Deterioration and Installation on Net Thrust (% of Point) at Altitude Points, Intermediate Power Level Shown as the Magnitude of the Variation

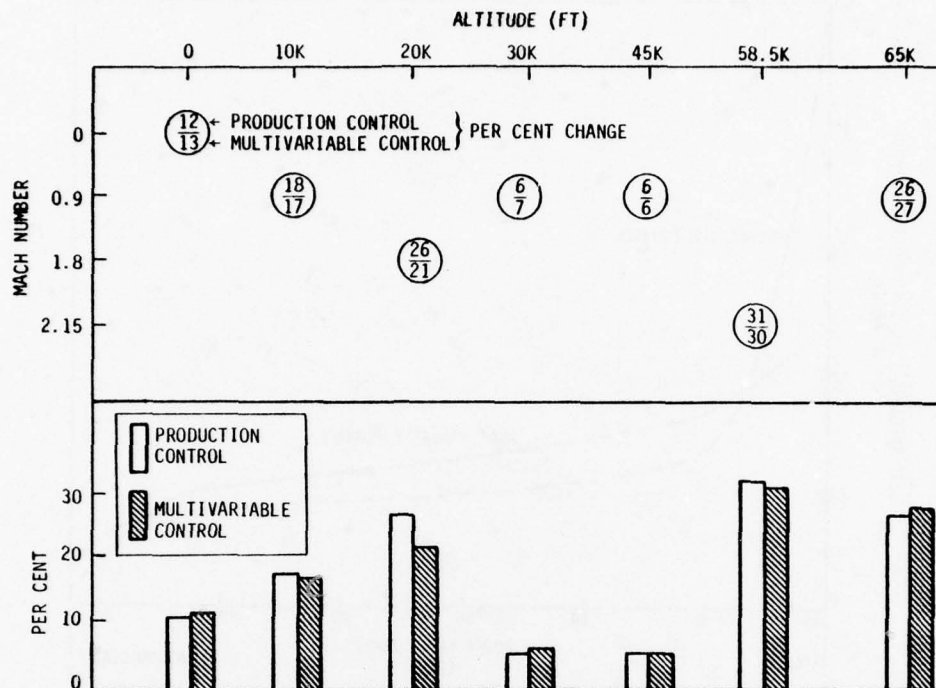


Figure 6.6 Effect of Deterioration and Installation on Thrust Specific Fuel Consumption (% of Point) at Altitude Points, Intermediate Power Level Shown as the Magnitude of the Variation

Table 6.4
Conclusion Summary - Installation Sensitivity

<u>COMPONENT DETERIORATION</u>	
•	Lower Thrust and Higher Thrust Specific Fuel Consumption Than Production Control at Subsonic Flight Conditions with High Power Settings
•	Higher Thrust and Lower Thrust Specific Fuel Consumption at Supersonic Flight Conditions and At Low Power Settings
<u>BLEED FLOW</u>	
•	Generally Higher Thrust and Lower Thrust Specific Fuel Consumption than Production Control for All Conditions
<u>HORSEPOWER EXTRACTION</u>	
•	Insignificant Effect
<u>COMBINED EFFECTS</u>	
•	Generally Higher Thrust and Lower Thrust Specific Fuel Consumption than Production Control at Supersonic Flight Conditions and at Low Power Settings

to produce constant thrust. In this region, the production control maintains fixed nozzle area and runs to a lower rotor speed which produces the lower thrust and higher SFC at these points.

The important conclusions are that the controller reference schedules produce stable and safe operation of the engine. The effects of extractions are comparable to the production control except that the controlled fan match point has a smaller sensitivity at low power settings and supersonic conditions than the production control.

6.2.4 Fan Exit Pressure Measurement

The effect of transducer errors in the measurement of $\Delta p/p$ was assessed. Flow distortion characteristics at the fan exit are more difficult to evaluate using the simulation. The type of measurement error should be investigated during the engine test.

The sensor complement specified for the $\Delta p/p$ measurement is shown in Figure 6.7. The algorithm for calculating the $\Delta p/p$ parameter is also shown in the figure. This parameter maintains the desirable characteristics of the average $\Delta p/p$ which has been previously defined. In addition, because both numerator and denominator terms are averaged separately, the calculation is more accurate when random measurement errors are present. The pressure transducers represent strain gauge instruments with adequate range to accommodate full envelope operation. The error terms are calculated by including the maximum specified accuracy deviation in the calculation. This worst case figure is then inserted as a sensor bias in the controller input. The controller trims the engine to the incorrect value of $\Delta p/p$ and the effect on engine performance is determined. This type of test is considered worst case since sensor errors will normally be

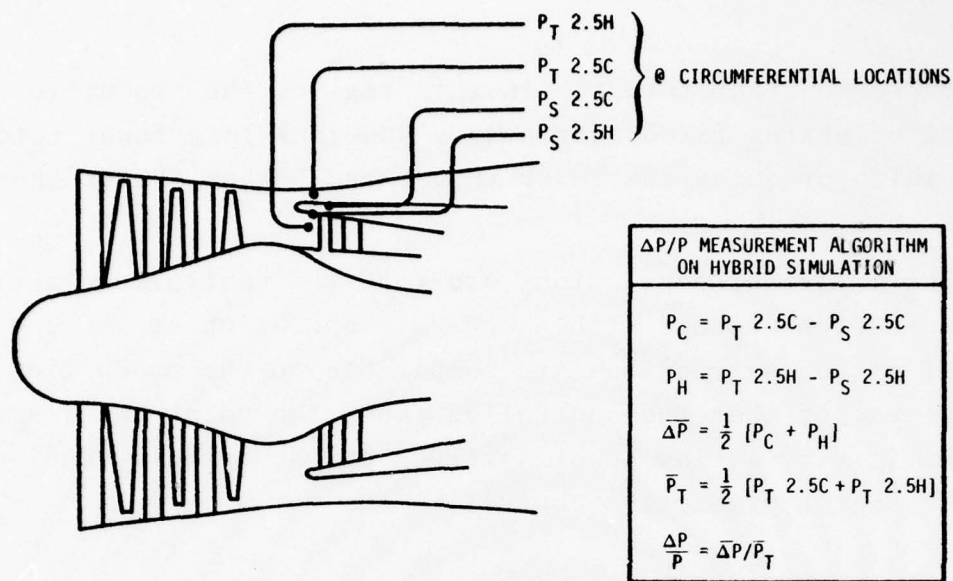


Figure 6.7 Schematic of Instrumentation for Fan Exit Pressure Measurement

averaged by the number of pick-off points used. Also, specified instrument nonrepeatability consists of random (i.e., white noise) components as well as bias shift and scale factor errors. In the operation of the control, a change in performance will be caused only by a shift in the overall bias level of the transducers. The magnitude of this type of error is probably less than the worst performance calculated.

Figure 6.8 illustrates the performance shift at the evaluation points throughout the envelope. In general, the thrust variation is greatest at middle power. At low power, trim authority limits the perturbation. The performance of the system with these sensor errors does not cause unsafe or unstable operation of the engine at any flight point.

AD-A052 420

SYSTEMS CONTROL INC PALO ALTO CALIF AERONAUTICAL AND--ETC F/G 21/5
F100 MULTIVARIABLE CONTROL SYNTHESIS PROGRAM. VOLUME 1. DEVELOP--ETC(U)
JUN 77 R L DE HOFF, W E HALL, R J ADAMS F33615-75-C-2053

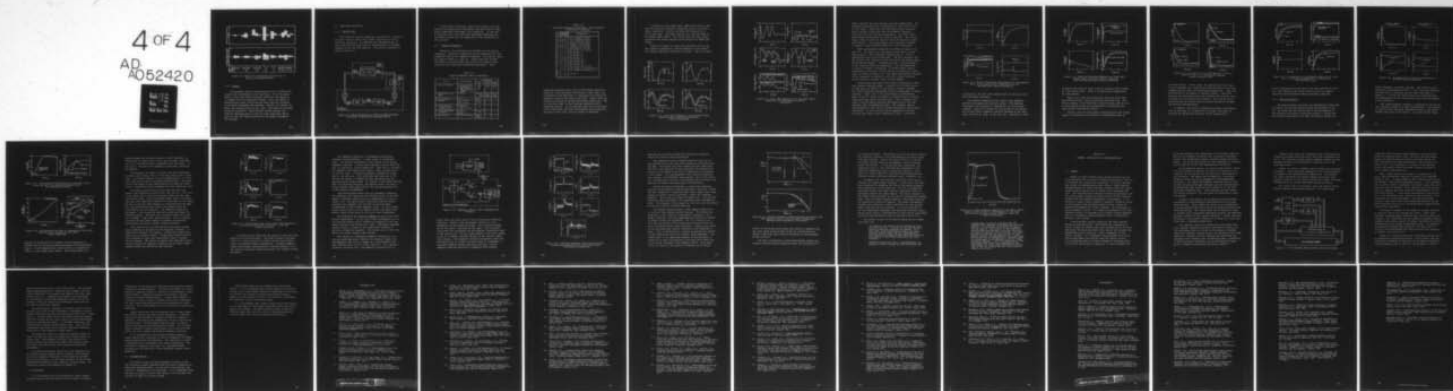
UNCLASSIFIED

AFAPL-TR-77-35-VOL-1

NL

4 OF 4

AD
A052420



END

DATE
FILMED

5-78

DDC

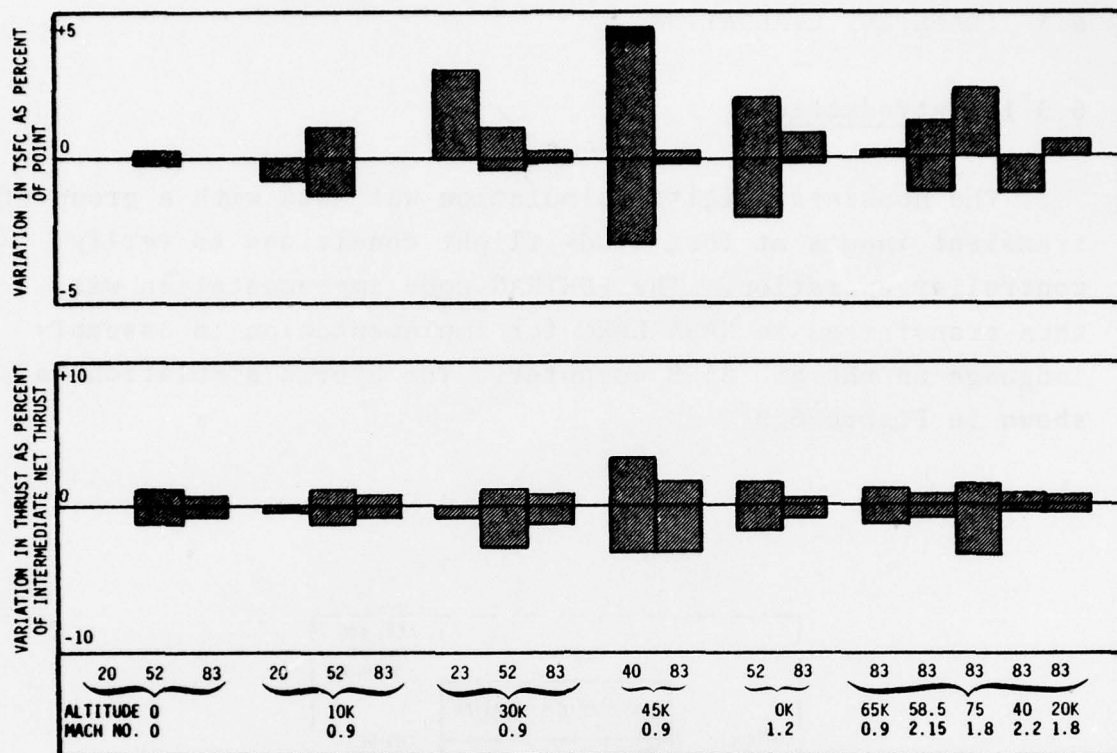


Figure 6.8 Worst Case Performance Sensitivity to $(\Delta p/p)_{2.5}$ Sensing Accuracy

6.2.5 Summary

The nonlinear digital simulation was used to validate the steady-state performance of the controller. First the match point at ten study flight and power conditions was adjusted to compare with the production control. Next, the effect of deterioration, power extraction and bleed flow was evaluated at 40 points throughout the envelope. Finally, the effects of worst case sensing errors on the $\Delta p/p$ trim mode were assessed using the simulation. Multivariable control matches the required operating point at the ten study conditions and results in safe and stable operation of the engine throughout the envelope.

6.3 TRANSIENT EVALUATION

6.3.1 Introduction

The nonlinear digital simulation was used with a group of transient inputs at four study flight conditions to verify controller operation. The FORTRAN code implementation was then transferred to NASA LeRC for implementation in assembly language on the SEL 810B computer. The hybrid simulation is shown in Figure 6.9.

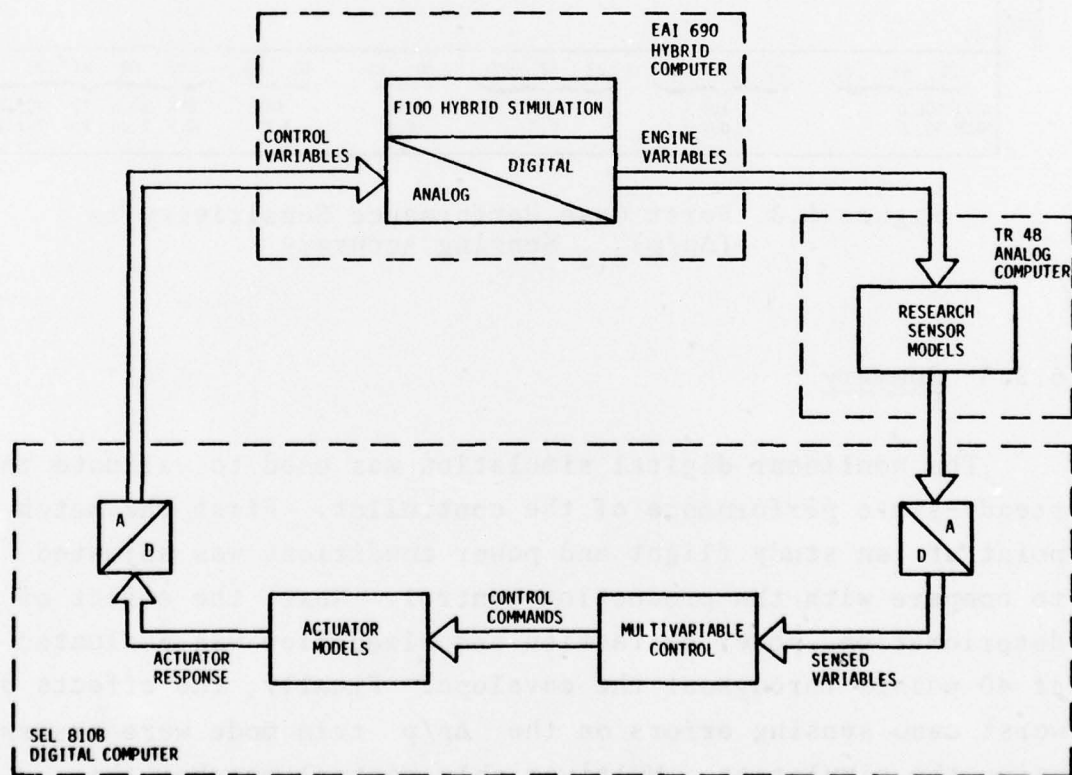


Figure 6.9 Hybrid Simulation of F100 and Multivariable Controller at NASA Lewis Research Center

In the hybrid evaluation, inputs were chosen to be compatible with engine test requirements and specified at flight points compatible with engine test capability. In this way, a controller and a test plan were developed simultaneously. The hybrid results will be summarized in the second half of this section.

6.3.2 Digital Evaluation

Initially, the controller was validated on the digital simulation. Transient responses were also generated with the production control for comparison purposes. The control inputs are shown in Tables 6.5 and 6.6. Large transients between intermediate and idle power were used to test engine limit protection and transition controller performance. Small

Table 6.5
Digital Computer Control Evaluation

TEST ITEM	INPUT SPECIFICATION	FLIGHT CONDITION		
		OK/0	10K/0.9	30K/0.9
1. Large Transient Response	a. Idle to intermediate b. Intermediate to Idle c. Bodie Transient d. Δ PLA = 3,000 lbs Below Intermediate to Intermediate	(1ai) (1bi) (1c) (1d)	(1aii) (1bii) ----- -----	(1aiii) (1biii) ----- -----
2. Small Amplitude Transient Response	+3 Deg PLA	PLA=30 (2c) 52 (2b) 80 (2a)	80° (2d) (Intermediate)	80° (2e) (Intermediate)
3. No Holds Barred PLA	4 runs	8a-8d		
4. Disturbances	ΔP_{T7} = 4 per cent ΔP_{T2} = 2 per cent	83° (4a) 83° (4b)	----- -----	----- -----
5. Transient Limit Check ● P_B Limited (FTIT Limit is Addressed in Item 1)	● Set PLA at 60°. Δ PLA = 23° At Mn = 1.2, Alt = 0	----- (5)	-----	-----
6. Transient Saturation Check - A_j = Constant	● Lock A_j ● Δ PLA = 10°	At PLA of 73° (6)	-----	-----
7. Idle Die Out Check	Max HPX + BLD Specified	Idle (7) Δ PLA = 20°-35°	-----	-----

Table 6.6
Transient Simulation Data Index - Multivariable
Controller Evaluation

ITEM	FLIGHT POINT		INPUT SPECIFICATION
	ALT	Mn	
1ai	0	0	Idle to intermediate PLA transient
1aii	10K	0.9	Idle to intermediate PLA transient
1aiii	30K	0.9	Idle to intermediate PLA transient
1bi	0	0	Intermediate to idle PLA transient
1bii	10K	0.9	Intermediate to idle PLA transient
1biii	30K	0.9	Intermediate to idle PLA transient
1c	0	0	Bodie transient (83° - 20° - 83°)
1d	0	0	PLA = 72°, Δ PLA = + 11° (+3,000 lbs)
2a	0	0	PLA = 80°, Δ PLA = + 3°
2b	0	0	PLA = 52°, Δ PLA = + 3°
2c	0	0	PLA = 20°, Δ PLA = + 3°
2d	10K	0.9	PLA = 80°, Δ PLA = + 3°
2c	30K	0.9	PLA = 80°, Δ PLA = + 3°
4a	0	0	Δ PT7 = +4% (Δ AJ = -0.20 ft ²)
4b	0	0	Δ PT2 = +1% (0.147 psi)
5	0	1.2	PLA = 50°, Δ PLA = + 23°
6	0	0	PLA = 73°, Δ PLA = +10°, AJ \equiv 3.0 ft ²
7	0	0	PLA = 20°, Δ PLA = + 15°, HPX = 54, BLCD = 1.8%
8a	0	0	Idle \rightarrow Intermediate PLA, Lowered W_f/P_B limit
8b			
8c	0	0	Cyclic PLA
8d			

amplitude transients were used to investigate regulation stability in the presence of hysteresis, dead zones, etc. Disturbances were generated to investigate the effects of augmentor ignition and inlet distortion. Engine limit protection was tested at maximum and minimum conditions. The jet area was fixed to test transient operation with a saturated control. An acceleration from idle at sea level static conditions with full deterioration and extractions was used to test this critical regime of operation.

A series of cyclic power lever inputs were used to validate the transition and gain scheduling logic at sea level static conditions. Figure 6.10 shows the response to a cyclic PLA input. The input consists of steps and ramps in the middle power region. The figure shows the rotor speed trajectory and thrust response of the engine are smooth and stable.

Figure 6.11 shows the cyclic PLA maneuver used to test the transient temperature limiting behavior of the control. The turbine temperature was well controlled. The FTIT sensor

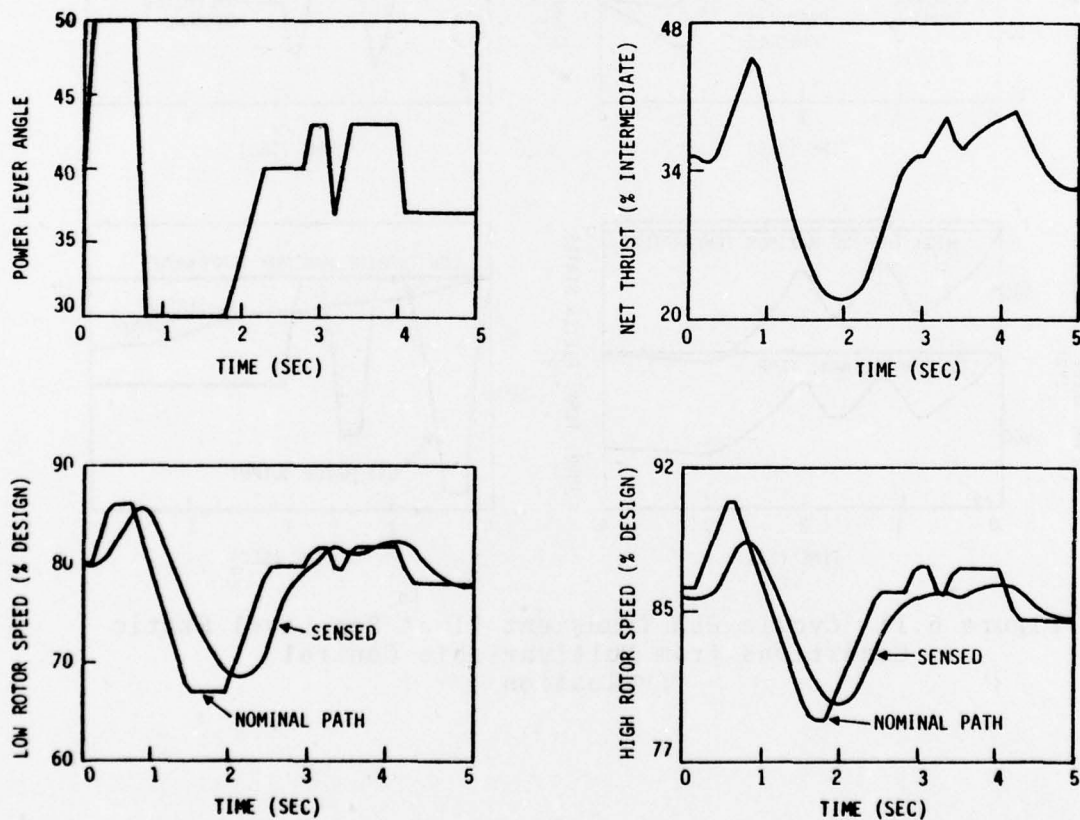


Figure 6.10 Cyclic PLA Transient I at Sea Level Static Condition from Digital Multivariable Control Evaluation

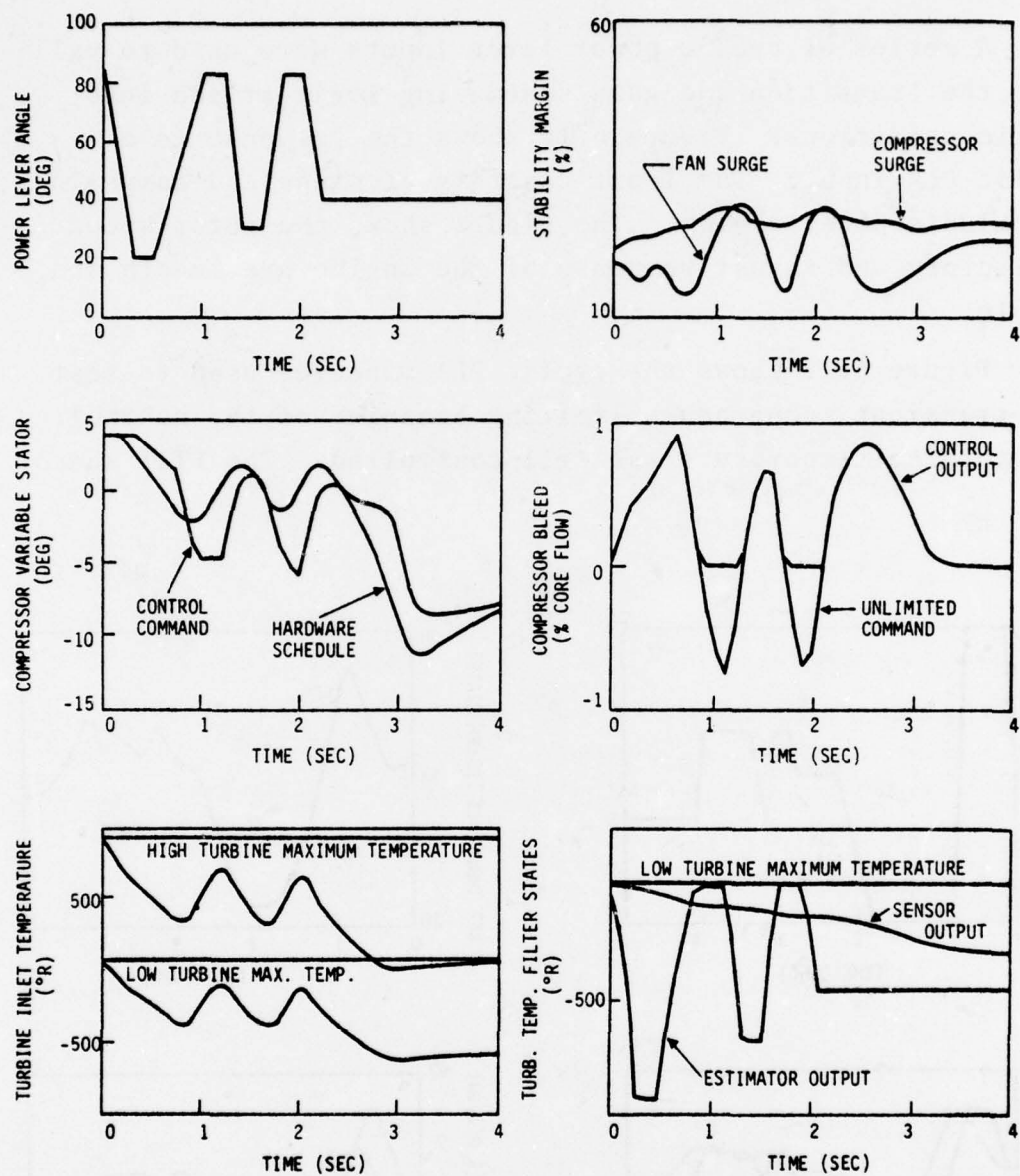


Figure 6.11 Cyclic PLA Transient II at Sea Level Static Conditions from Multivariable Control Evaluation

output reflects the slow response from the thermocouple. The estimated temperature uses scheduled fuel flow error as the driving input. Compressor vane deflection shows regulator inputs causing a deviation from the hardware schedules, typically more axial during deceleration. The bleed valve opens during deceleration as would be expected. The control output tends to close the valve as would be expected during accelerations. The surge margins show acceptable response. In general, large transient behavior is well controlled.

Small perturbation transients are shown in Figures 6.12 and 6.13. In Figure 6.12, the engine accelerates to intermediate power. The system must switch from N_1 trim to temperature trim in this transition. The FTIT estimator output reflects the response of fuel flow while the actual sensor output barely changes. Acceleration time is slowed because of the limiting action on temperature. No overtemperature or thrust overshoot is observed. In middle power regions, temperature is not near a limit and the acceleration is more rapid as shown in Figure 6.13. The small perturbation response of the regulator is visible in the error signal transient. Thrust control is smooth, rapid and well damped.

Several runs were made in the digital evaluation to validate engine protection modes. Figure 6.14 is a deceleration to idle power at 30K/0.9 to test burner pressure response. The results show fast deceleration with no undershoot in burner pressure. Figure 6.15 is an acceleration to intermediate power at 0K/1.2, where the engine is operating near a turbine temperature and burner pressure limit. This evaluation was used to isolate burner pressure overshoots and to test the integral limit accommodation logic. The response shows a down-trimming of fuel flow to prevent temperature and pressure overshoots. It also verifies the accommodation of burner pressure and turbine inlet temperature limits. During the

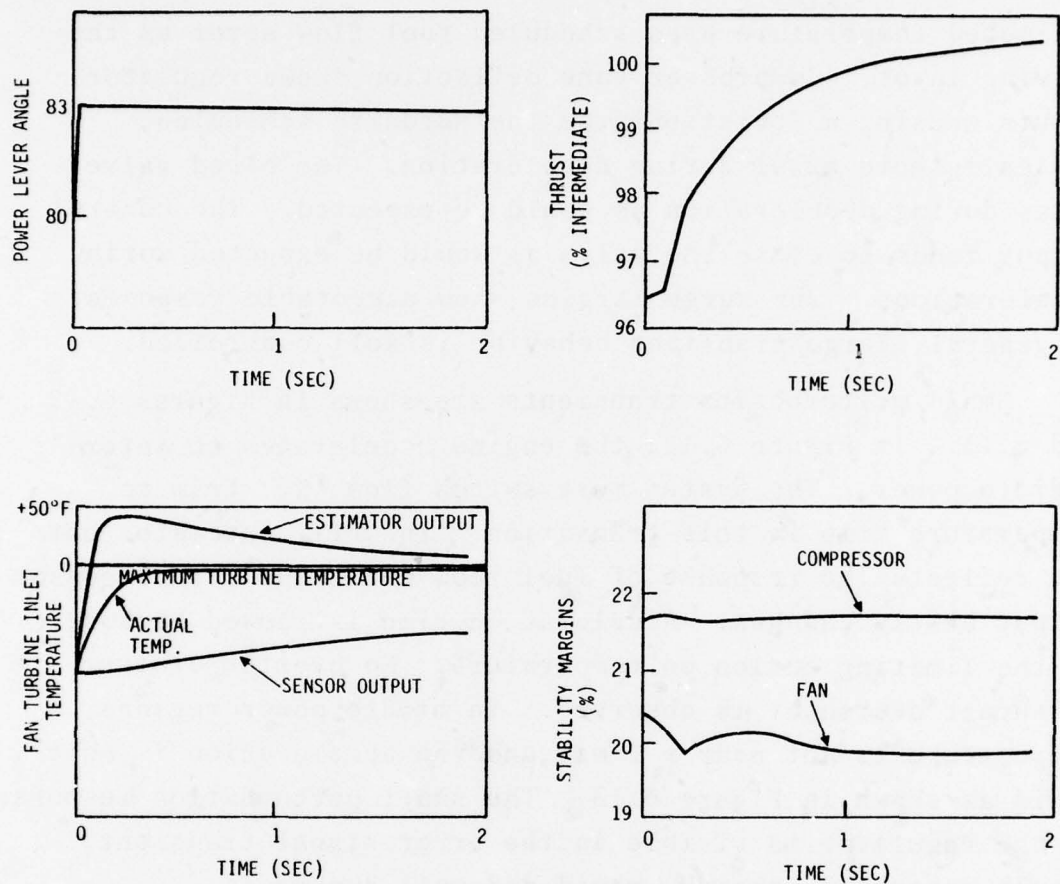


Figure 6.12 Small Perturbation Step Response to Intermediate Power at Sea Level Static Conditions from the Multivariable Control Evaluation

acceleration, the fuel flow response does not show any integral switching transients.

Disturbance compensation was tested using augmentor pressure and engine face pressure inputs. The augmentor disturbance was produced by stepping the jet area closed slightly. Figure 6.16 shows the trim action of the control due to both direct augmentor pressure feedback in the regulator and trim on $\Delta p/p$ at the fan exit. Similarly, a step

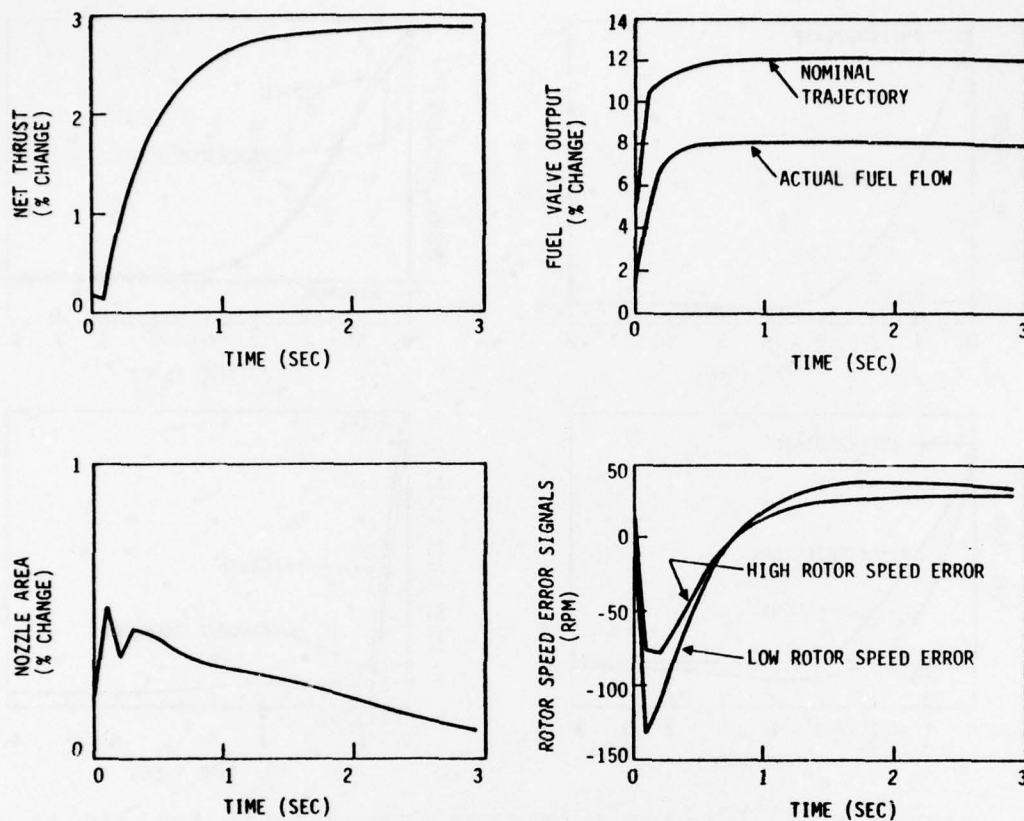


Figure 6.13 Small Perturbation Response to a Step Input - Middle Power, Sea Level Static Conditions from the Multivariable Control Evaluation

in engine face pressure shows a thrust change quickly trimmed to a new steady-state. There is no appreciable degradation in surge margins.

Figure 6.17 shows an acceleration from idle power with full deteriorations, power extractions and bleed flow. The thrust response is not affected by deteriorations and the loss of surge margin during the acceleration is negligibly more than without installation effects.

Finally, the fail safe engine protection logic was tested. Figure 6.18 shows an acceleration to intermediate power at

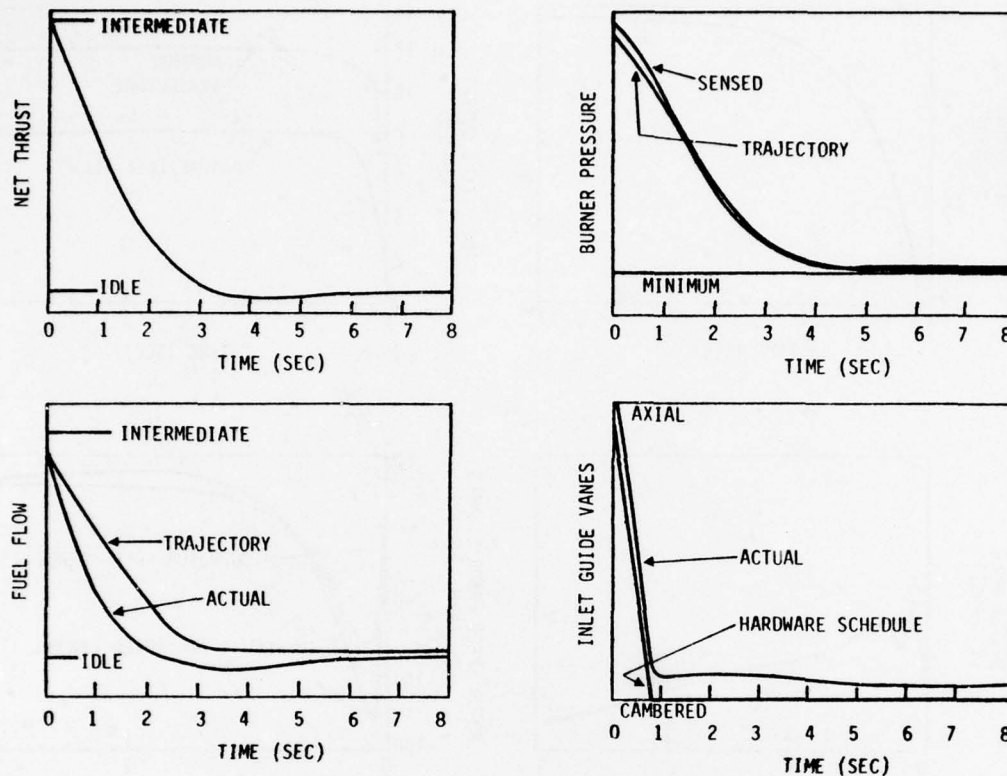


Figure 6.14 Deceleration from Intermediate to Idle at 30,000 Ft, $M_n = 0.9$, Holding the Minimum Burner Pressure Limit

sea level static. In this case, the maximum fuel flow limit is set (scheduled as a function of burner pressure) to be only slightly greater than the equilibrium running line. Thus, the acceleration of the engine is limited severely. This test verifies the protection logic and validates the actuator limiting logic in the integral trim control. This type of run is useful during the initial phase of engine testing to validate the hardware implementation.

In summary, the digital evaluation provided a preliminary test of the logic at a limited set of flight conditions to validate the design and structure of the control and to

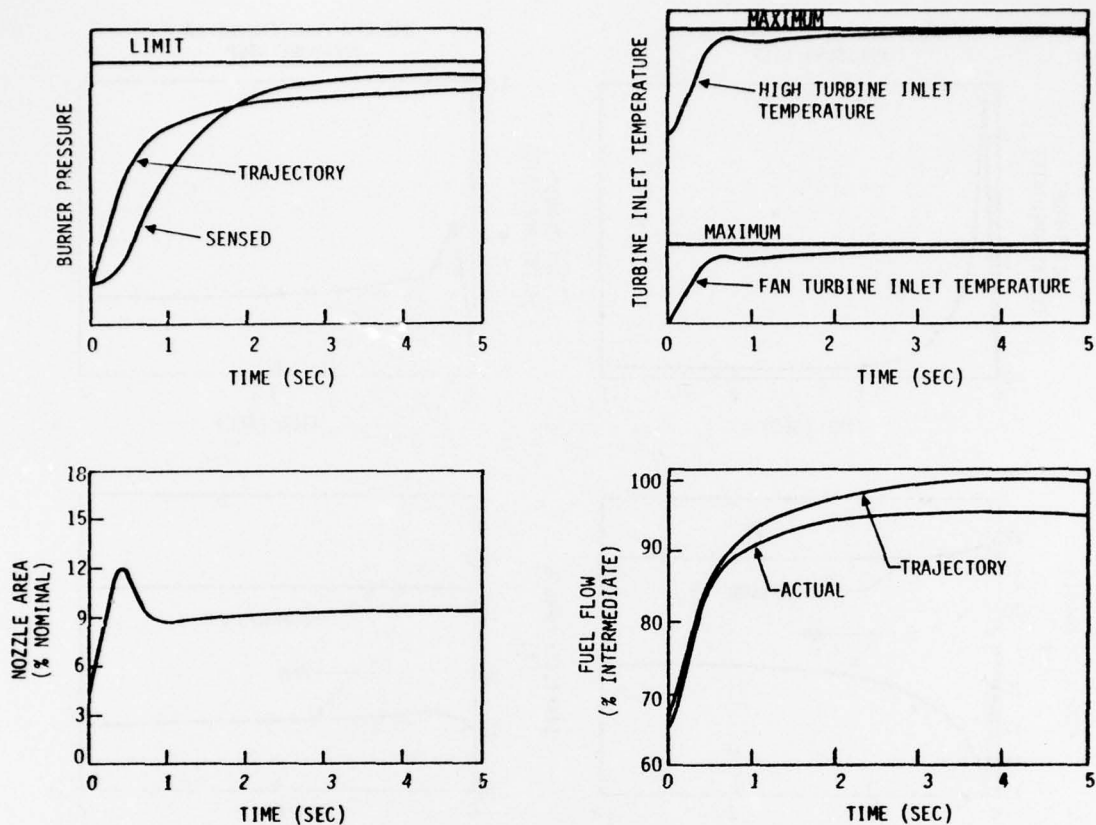


Figure 6.15 Acceleration to Intermediate Power at Sea Level, $M_n = 1.2$ Showing Accommodation of Temperature and Pressure Limits

justify implementation and test on the NASA LeRC hybrid facility. The transient and Steady-State criteria for engine protection and performance were successfully achieved.

6.3.3 Hybrid Evaluation

The multivariable controller was implemented at NASA LeRC to operate the detailed hybrid simulation described in Ref. 90. An evaluation and verification of the performance of the controller was made in sufficient detail to assure safe and reliable operation of the logic and digital hardware at

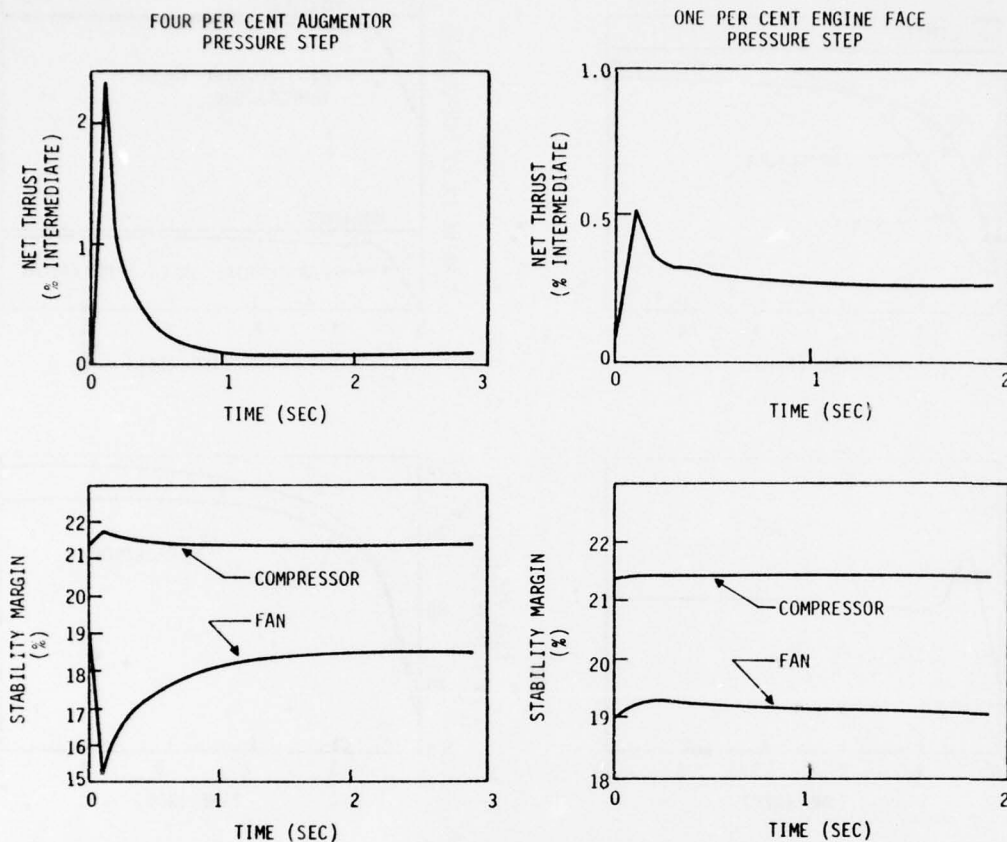


Figure 6.16 Accommodation of Pressure Disturbances at Sea Level Static Conditions

points throughout the flight envelope. The results of this evaluation are presented in Ref. 2. Data from this evaluation has been used to illustrate various topics described in Chapter V. A few of the hybrid results are presented below for completeness and for illustration of the total performance of the controller.

The linear quadratic regulator is designed for smooth and well controlled response to small perturbations. This behavior is used for small and large transients because of the perturbational form used in the control. Also, the locally linear

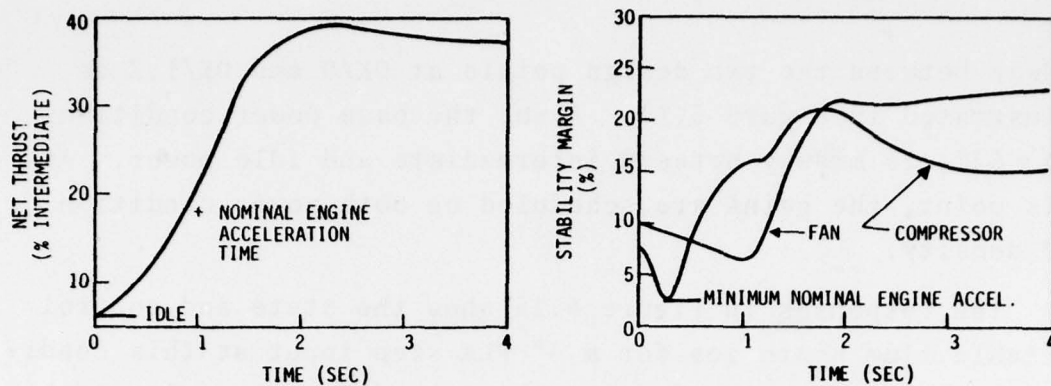


Figure 6.17 Acceleration from Idle Power at Sea Level Static Conditions with Full Specified Deterioration and Installation Effects.

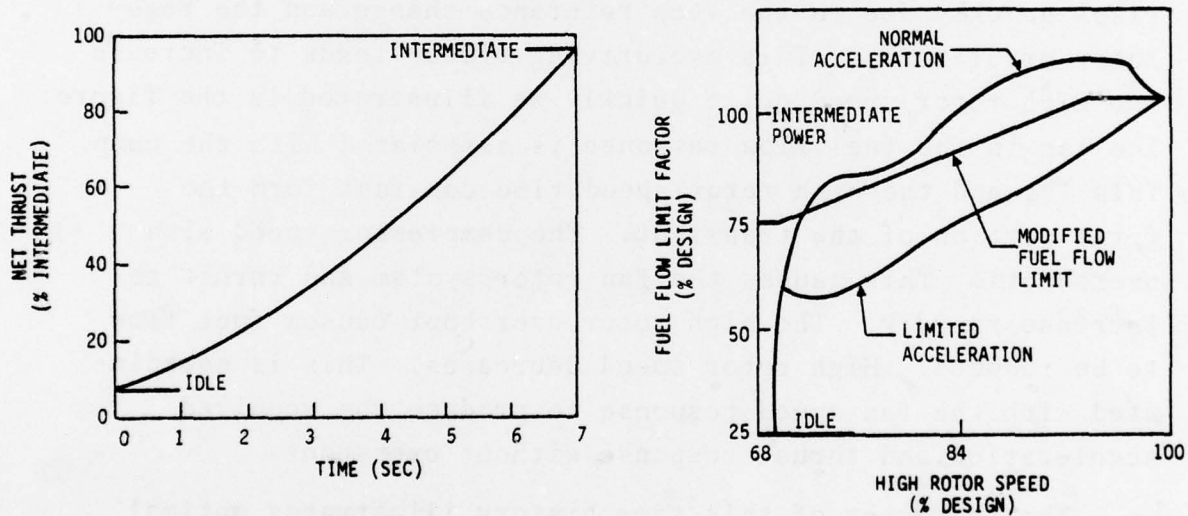


Figure 6.18 Acceleration from Idle to Intermediate Power with Fuel Flow Limit Lowered at Sea Level Static Conditions

analysis is predicted on the ability of the controller to perform well at off-design conditions between two linearization points. In the example below, the controller is operated at 10K/1.2 in the middle power region. This flight point lies

midway between the two design points at 0K/0 and 0K/1.2 as illustrated in Figure 5.14. Also, the base power condition, $PLA = 52^\circ$, is midway between intermediate and idle power. At this point, the gains are scheduled on both power condition and density.

The responses in Figure 6.19 show the state and control variable time histories for a 3° PLA step input at this condition. The thrust response is also included because it is the most sensitive to poorly controlled accelerations. The operation of the engine is not constrained by any physical limits. Trim is accomplished using scheduled low rotor speed and $\Delta p/p$.

The engine acceleration proceeds when the PLA input changes the references on both states and controls. Fuel flow rises quickly due to the step reference change and the regulator error terms. This overdriving effect tends to increase the high rotor speed quite quickly as illustrated in the figure. The lag in the fuel flow response is associated with the pump. This lag and the high rotor speed time constant form the first portion of the transient. The compressor speed also overshoots. This causes the fan rotor system and thrust to increase rapidly. The high rotor overshoot causes fuel flow to be reduced. High rotor speed decreases. This is coordinated with the fan speed response to produce the required acceleration and thrust response without overshoot.

The character of this time history illustrates optimal thrust behavior as specified in the regulator synthesis. It would not be optimal, for example, if high rotor speed excursions were of primary concern. A controller characterized by less overshoot in high rotor speed would result in slower thrust response. The ability to specify the important control criteria during the regulator synthesis process makes linear optimal design very attractive and flexible.

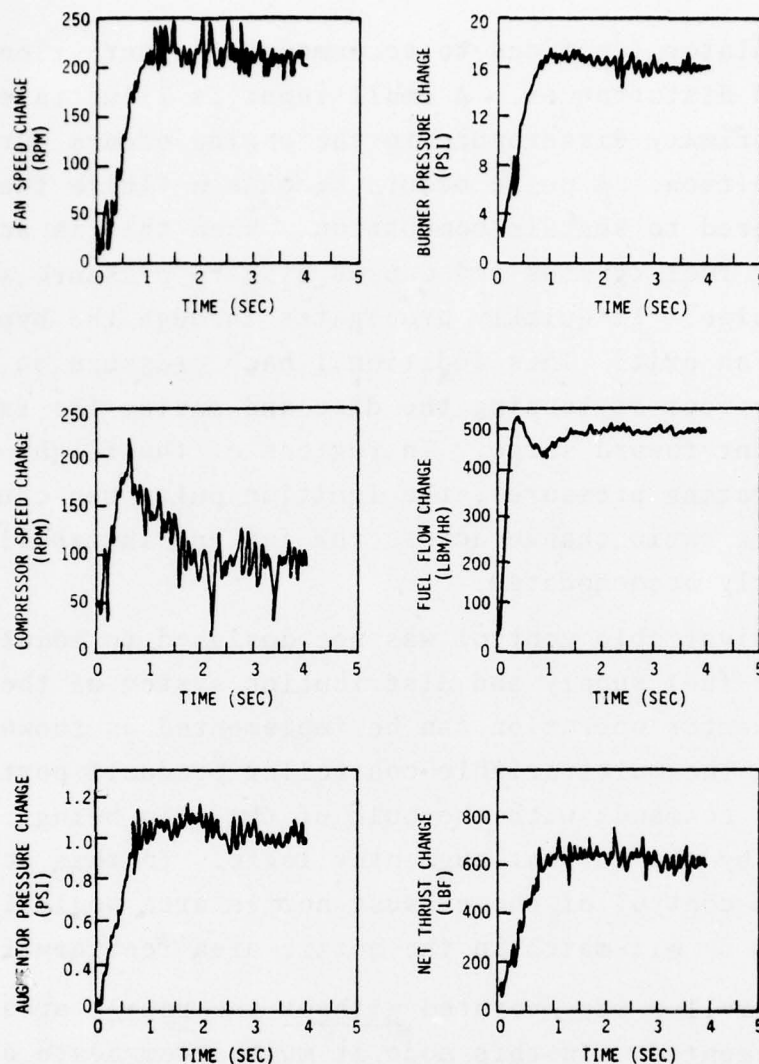


Figure 6.19 Three Degree Power Lever Angle Step Response at an Off-Design Condition, 52/10K/1.2, from the Hybrid Simulation

It should be noted that only the aspects of the fuel flow behavior are discussed above. The other actuators are modulated in a similar fashion to produce control forces which cause a coordinated engine acceleration. Problems common in single-loop designs associated with "crossed controls" (i.e., two controls producing cancelling effects) are avoided in this procedure.

The regulator functions to accommodate perturbation responses and disturbances. A small input is illustrated above. The primary disturbance to the engine occurs during augmentor ignition. A pulse occurs because a finite fuel flow rate is required to sustain combustion. When this is achieved, the augmentor fuel ignites and causes a sharp pressure spike in the tail pipe. It quickly propagates through the bypass duct to the fan exit. This additional back pressure on the fan has the effect of loading the disc and moving the fan operating point toward surge. In regions of the flight envelope with low operating pressures, the ignition pulse can cause a large pressure ratio change across the fan and instabilities if not properly accommodated.

The multivariable control was not designed to modulate the augmentor fuel supply and distribution system of the F100. However, augmentor operation can be implemented as shown in Figure 6.20. The multivariable controller produces perturbational area commands with the bulk of the trim being accommodated by the current augmentor logic. In this scheme, multivariable control of the exhaust nozzle area would limit pulses caused by mis-match in the nozzle area feedforward.

The controller was operated without the nozzle area feedforward implemented. In this mode it must accommodate all of the ignition pressure pulse through the feedbacks on the augmentor pressure, and the fan exit $\Delta p/p$. The higher bandwidth control action is caused by the proportional feedback of pressure through the regulator. The nozzle area is then trimmed at the slower integral time constant.

The results of a simulated augmentor ignition at a low pressure operating point, 65K/0.9, are shown in Figure 6.21. The augmentor fuel flow is stepped to a representative segment ignition value at this flight condition. This ignition produces a pressure step. The augmentor pressure pulse is

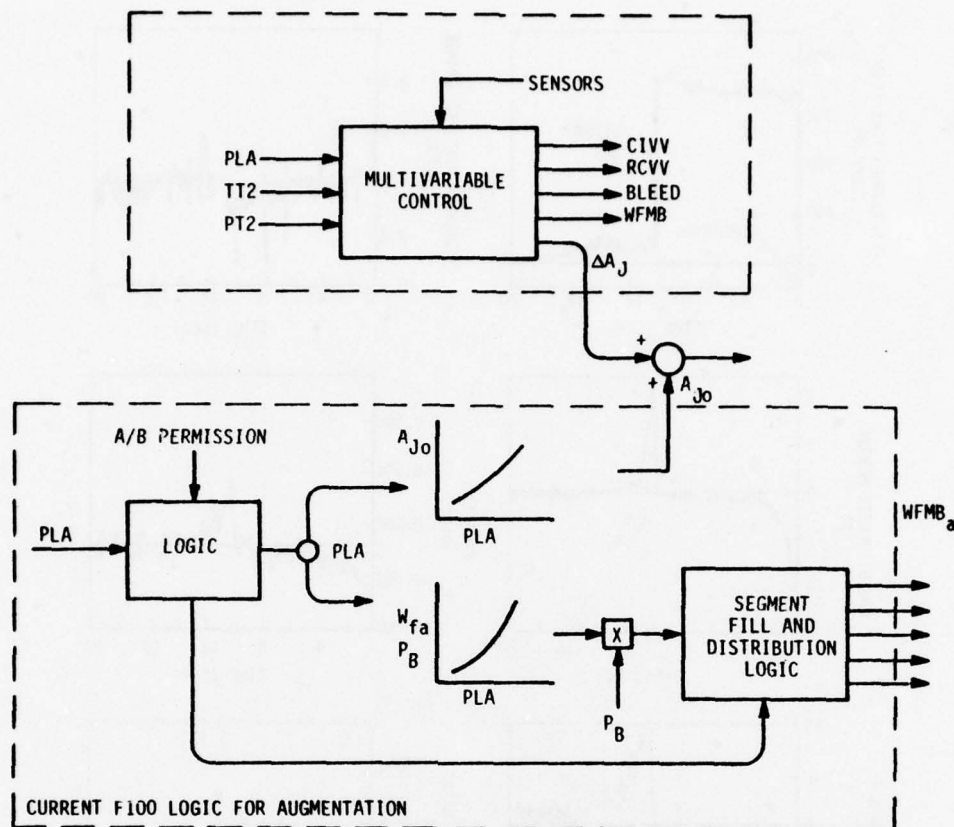


Figure 6.20 Augmentor Control Logic Implementation Schematic

barely above the noise level at this low pressure operating condition. However, this disturbance results in a 30% degradation in fan stability margin. The increased loading on the fan causes a decrease in fan speed. This transient illustrates the requirement for anticipatory feedforward logic on the nozzle area. The fan speed response is not fast enough to act as a feedback variable because of the inherent speed time constant. The augmentor pressure measurement senses the disturbance but it contains too much noise to accommodate a high gain feedback without excessive filtering. Direct augmentor ignition detection or augmentor fuel manifold

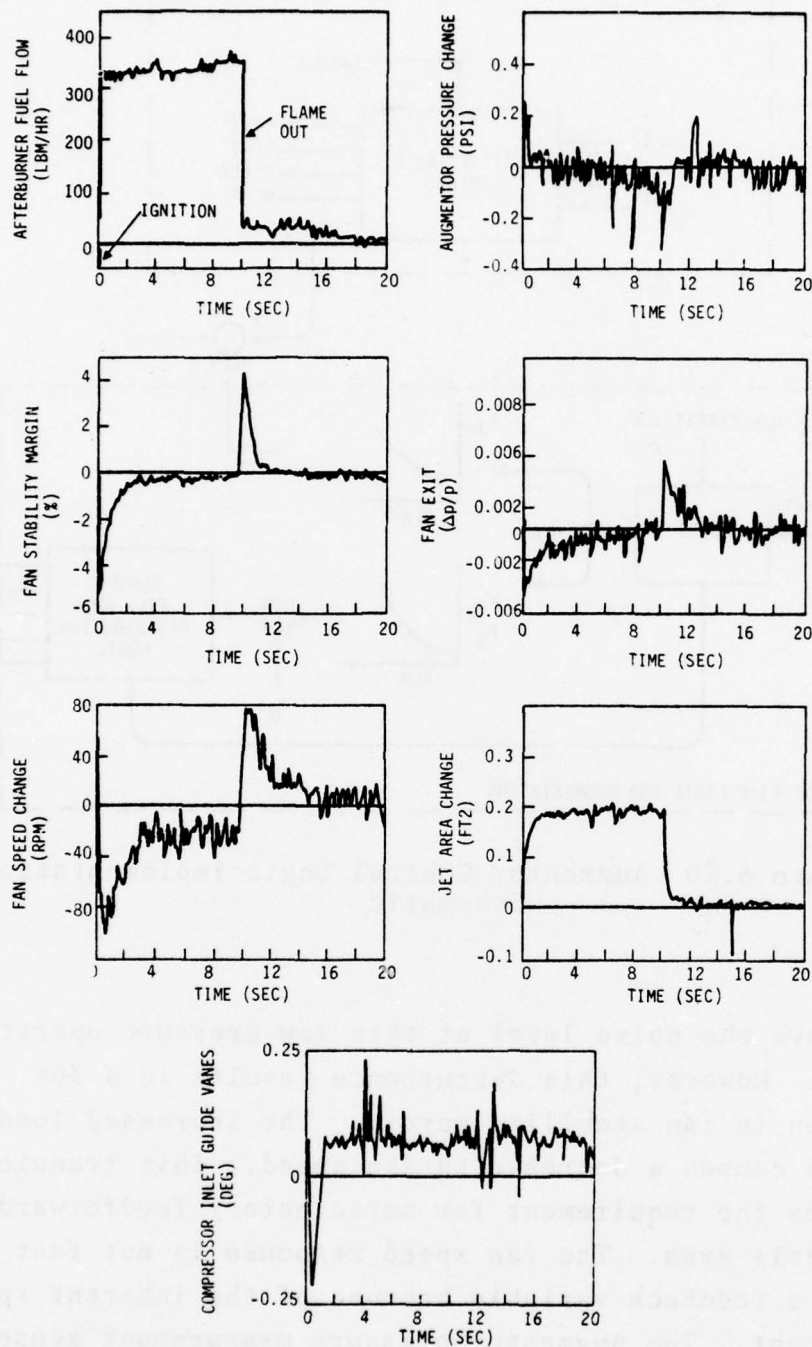


Figure 6.21 Simulated Augmentor Ignition Disturbance Accommodation Without Nozzle Area Feedforward (from Hybrid Simulation)

modeling the controller could also provide the necessary signal for pressure spike attenuation.

The augmentor pressure feedback provides about 30% of the required nozzle area and CIVV response on the pulse leading edge. The nozzle area then follows the fan speed error. The CIVV's are deflected to help alleviate the overpressure. Finally, the integral trim action is dominant as illustrated in the figure. The high bandwidth rotor speed perturbation and, finally, low bandwidth, high accuracy $\Delta p/p$ trim action are simultaneously utilized to accommodate the disturbance and maintain the engine operating point satisfactorily.

During the hybrid evaluation, a closed-loop frequency response was performed on the multivariable controller running the F100 simulation. Sinusoidal power lever inputs were large enough to produce readily detectable outputs for frequency analysis. The results are shown in Figure 6.22. The altitude condition chosen was 45K/0.9 at conditions below intermediate power. The response of the engine for this test was represented by the PLA to thrust transfer function.

The transfer function shows a well damped complex pair or two real roots dominating the response. The closed-loop bandwidth of the system is significantly improved at this flight condition. The lower magnitude PLA input has a slightly higher closed-loop bandwidth. This is a result of the rate limiting nature of the transition controller which protects the engine during large transients. However, the effect of the perturbational control structure on the bandwidth is small. This is indicative of a robust perturbational controller and transition rates of a suitably large magnitude. The slight droop in the amplitude response at mid-frequency is caused by the near cancellation of the high rotor speed root in the thrust response by the feedback system. This cancellation is forced by the quadratic weighting of the thrust

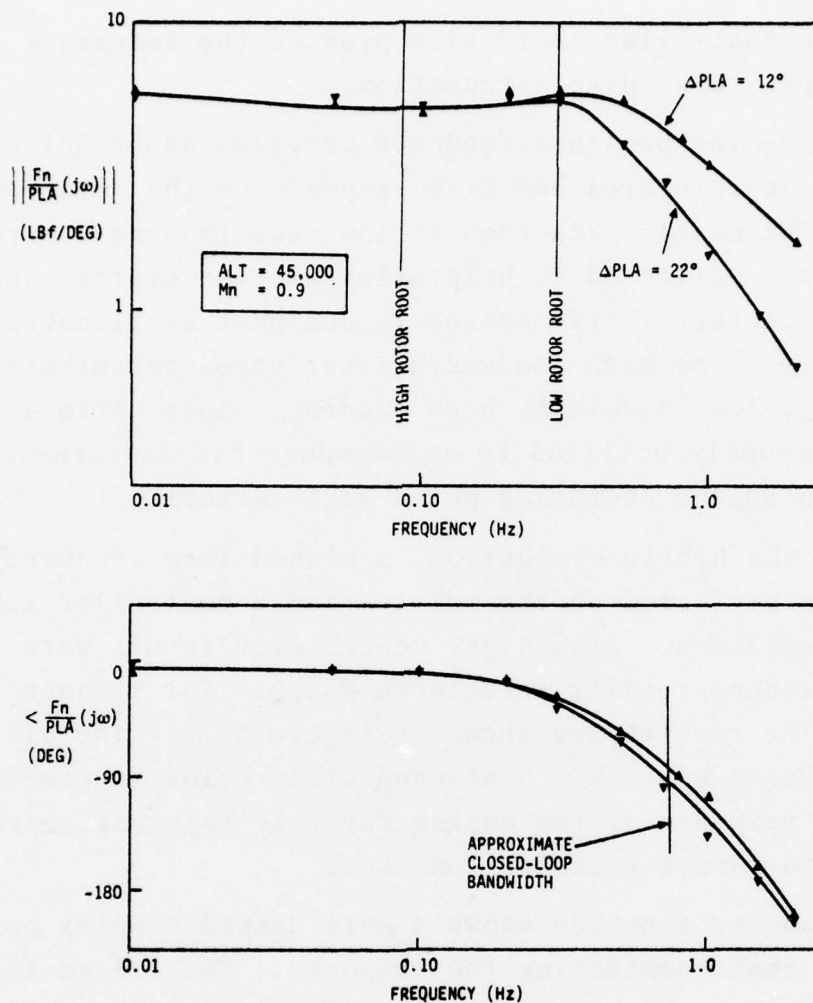


Figure 6.22 Frequency Response of Multivariable Controller and F100 Engine at 45K/0.9 from the hybrid Evaluation Showing Thrust Response to PLA Inputs

states in the design which causes the control to modulate the low rotor speed system quickly while not controlling overshoots in the high rotor speed as discussed at the beginning of this section.

The final illustration of the multivariable control performance from the hybrid evaluation shows the flexibility of

the design procedure. One problem in classical engine control for transient response is the development of accurate engine limiting schedules. Output and Input Limiting is required to produce systems which can accommodate large transients safely and quickly. In the multivariable controller, the transition logic is self-contained and independent of the reference scheduling, trim, or regulator function. Thus, there is a direct control of the acceleration/deceleration response without affecting regulator gains, schedules, etc.

In Figure 6.23, the baseline transition rates were re-designed for faster thrust response. In this case, the rates were calculated by doubling the thrust rate design parameter and assuming zero nozzle area rate. The set of compatible state and control rates were directly substituted into the controller without any other change. The thrust responses in the figure show a decrease in the idle to intermediate response time. This increased response produces a decreased surge margin initially as would be expected. The small perturbation response and responses to other transients at other flight/power conditions are not affected. It is also possible to use this functional modularity for optimized transient trajectories which reflect a minimization of some type of constrained objective function such as time to 90% thrust level [57].

The overall results of the hybrid evaluation are summarized below [2]:

"In general, the results of the evaluation indicate that the engine testing of the multivariable control should be conducted as planned. It is felt that, with minor modifications, the multivariable control logic and its implementation will provide acceptable steady-state and transient performance at all flight conditions and power settings.

Considering the fact that, in approximately ten months, a control design for the F100 engine was

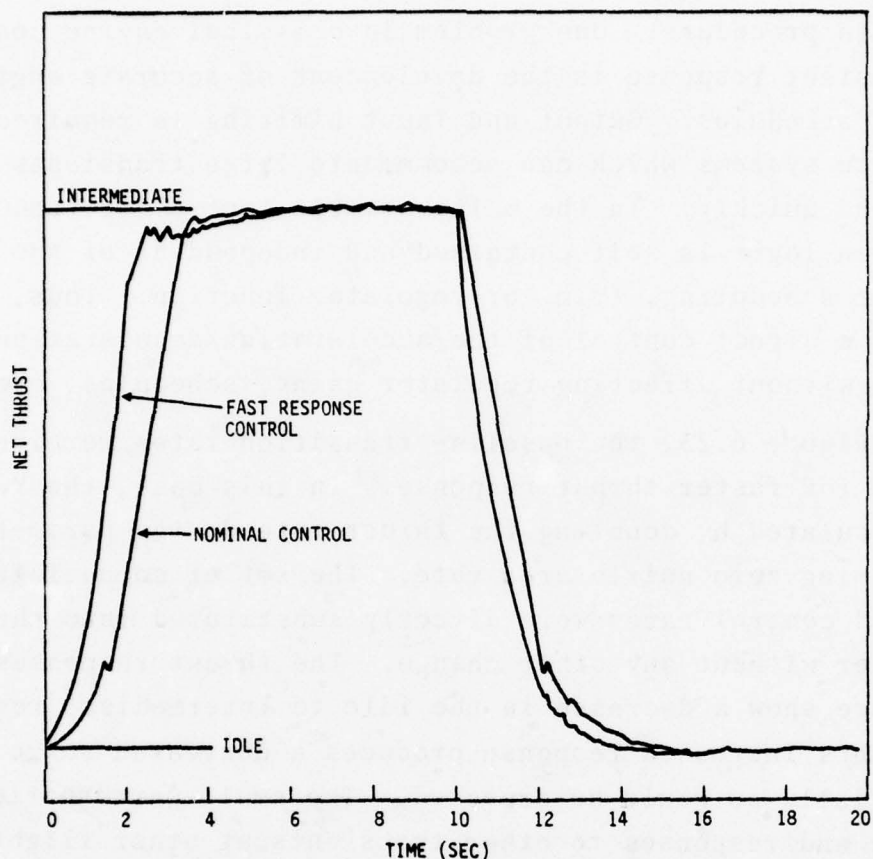


Figure 6.23 Engine Response Comparison at Sea Level, Static Conditions for an Idle to Intermediate to Idle Input with the Fast Response Control Parameters (from the Hybrid Simulation)

accomplished, it must be concluded that the computer-aided approach to designing multivariable controls is a practical solution to the engine control problem. The results of the evaluation indicate that the approach to solving the nonlinear control problem is also practical. The implementation of the control logic on the SEL 810B digital computer has demonstrated that a practical LQR control can be implemented on a digital computer having many of the characteristics of flight-qualified computers. The core requirements (7.1K) and update time (10 ms) are comparable to the requirements of flight-qualified digital controls such as the IPCS control and the F100 Electronic Supervisory Control."

CHAPTER VII

SUMMARY, CONCLUSIONS AND RECOMMENDATIONS

7.1 SUMMARY

Modern aircraft turbine engine designs provide the controls engineer with a variety of sensors and actuators for use in transient and steady-state operations. Classical designs have relied on hydromechanical fuel control--speed governor implementations for gross transient response with more sophisticated control action used in steady-state regulation and trim. The incorporation of digital processing capability into the system allows integrated control action to meet advanced steady-state and transient performance requirements. It is possible to apply linear, quadratic regulator synthesis theory to the design of multivariable engine control systems for operation throughout the flight envelope. The advantages of such procedures include: (1) enhanced performance from cross-coupled controls, (2) maximum use of engine variable geometry, and (3) a systematic design procedure which is efficiently applied to new systems.

A multivariable control system for the F100 turbofan engine has been described. The theoretical foundations of locally linearized control have been reviewed and it has been shown that the resulting form of the control law dictates the implemented control structure. Basic components of the control include: (1) a reference value generator for deriving an approximate equilibrium state and control vector, (2) a transition model to produce compatible reference point trajectories during gross transients, (3) gain schedules for

producing feedback terms appropriate to the flight condition, and (4) the integral switching logic to produce acceptable steady-state performance without exceeding engine operating limits. The design philosophy for each component is described and the details of the F100 implementation presented.

The fundamental aspects of locally linear control synthesis are discussed in Chapters III and IV as applied to the synthesis of the control and the functional requirements of the structure. The engine may be modeled as a nonlinear dynamical system utilizing fundamental aerothermodynamic principles. For engine development, detailed digital simulations including thorough component maps and experimentally correlated gas path equations are utilized as in the F100 transient simulation deck. These programs are too complex for control synthesis, but are useful in evaluating a candidate design.

Locally linear models can be generated from nonlinear simulations or experimentally from engine data via system identification. These models are valid in the neighborhood of an equilibrium point and describe perturbation motion away from equilibrium. The linear model can be reduced in order to include only conveniently measurable elements and important dynamics relative to the control objective. A modal reduction procedure is described in Chapter IV to bring the linear equations into a tractable design form.

The regulator matrix is synthesized using linear quadratic optimal regulator procedures described in Chapter III. The performance index is chosen by the designer to weight important transient response factors for the particular flight condition. Examples of such transient specifications are adequate thrust response near intermediate power, elimination of burner pressure undershoots at low power/high altitude points, adequate surge margin and thrust stability.

Integral trim gains are calculated using a multivariable synthesis procedure which specifies spectrally decoupled trim roots. The piecewise linear control commands produced by this procedure do not excite unfavorable transients due to the switching action.

Figure 7.1 shows a schematic representation of the digital controller. Each functional component of the system produces an element of the multivariable feedback law. The feedback law itself represents an optimal regulator structure with integral trims for steady-state accuracy and a model following implementation to prevent saturation during transients.

The control law is written for state and control perturbations about an equilibrium condition. The equilibrium

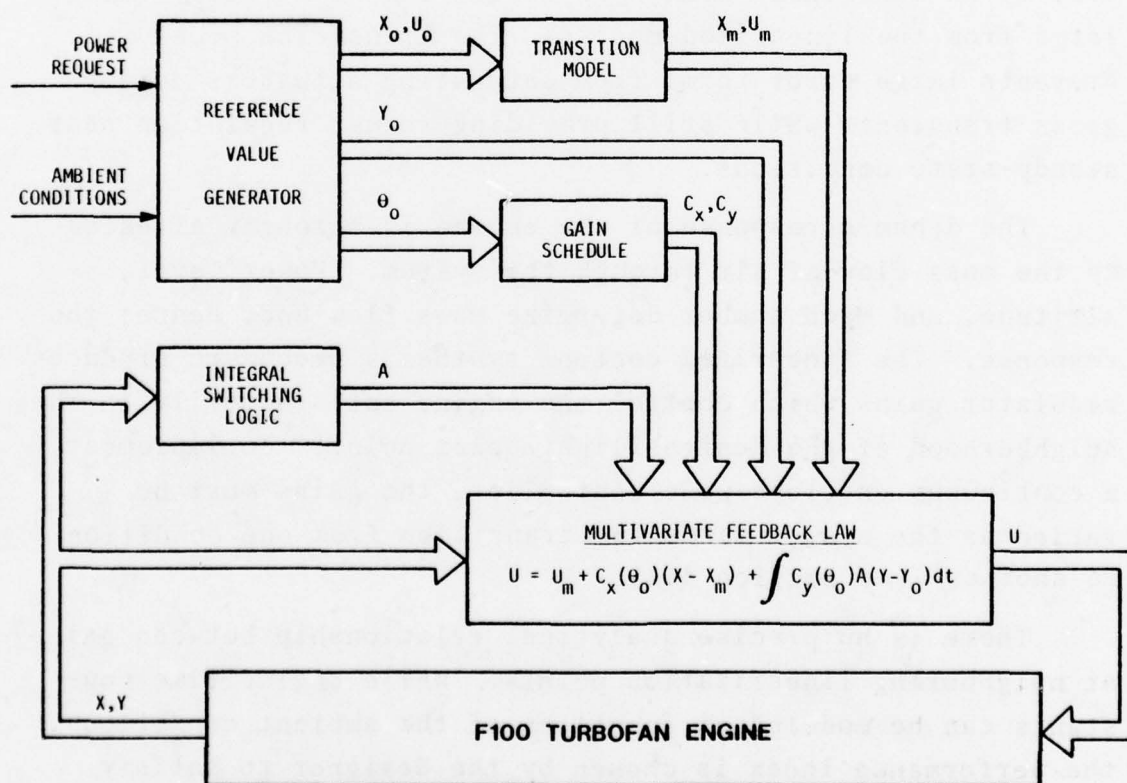


Figure 7.1 F100 Turbofan Multivariable Control Structure

conditions must be derived approximately by the controller given the requested power level, altitude, and Mach number. Because of manufacturing tolerances and engine aging, an exact expression for these quantities is not possible (see Section 5.4). The regulator is tolerant of the schedule errors and produces smooth transient responses without an overly complex implementation.

When a large transition in power is requested by the pilot, the perturbation character assumed in the regulator design is lost. A large change in the reference state vector will produce significantly nonlinear behavior. The regulator can be used to track a compatible trajectory taking the system from one state to another. Exact calculation of such trajectories is complex and their practical implementation has not been investigated. A first-order approximation (see Section 4.5) to an achievable state trajectory can be directly calculated from the linearized models. The transition model prevents large error terms from saturating actuators during gross transients while still providing robust regulation near steady-state conditions.

The dynamic response of the engine is strongly affected by the mass flow of air through the system. Power level, altitude, and Mach number determine mass flow and, hence, the response. The linearized control synthesis procedure produces regulator gains which control the engine satisfactorily in the neighborhood of the design flight/power point. To implement a continuous envelope-wide controller, the gains must be varied as the system makes the transition from one condition to another (see Section 4.4).

There is no precise analytical relationship between gains at neighboring linearization points. While engine time constants can be modeled as functions of the ambient conditions, the performance index is chosen by the designer to satisfy

specifications particular to the flight point. The procedure adopted approximately fits important gain elements with univariate functions of the engine face density and rotor speed (see Section 5.7). Dominant gain elements are determined by assessing the closed-loop eigenvalue sensitivity of the system to each gain element and eliminating those which do not affect closed-loop response.

The characteristic behavior of aircraft turbine engines dictates that steady-state performance is obtained at various flight conditions only when a particular physical limit is held exactly. At lower power levels, the engine operation should cause the airflow and low rotor speed to attain predetermined values for optimum efficiency. At altitude conditions, the minimum burner pressure defines engine idle. Inlet airflow requirements and burner burst pressure determine operating conditions at some supersonic flight points.

The engine set point is a group of reference values of states and controls which the engine must attain exactly in steady-state. The integral trim logic (see Section 5.8) provides smooth and controlled engine transitions in power and flight conditions which yield optimum envelope-wide performance.

The F100 multivariable control has been implemented on an SEL 810B general-purpose digital computer and evaluated on a hybrid computer simulation of the engine at the NASA Lewis Research Center. It has been evaluated on the digital simulation developed by Pratt & Whitney Aircraft Group. The evaluation results are presented in Chapter VI.

7.2 CONCLUSIONS

It is concluded that the multivariable control design procedure used on the F100 engine offers a highly systematic

methodology for designing and integrating multivariable control systems for advanced engines. The basic requirement for linear quadratic regulator design is a method for determining a linear control model. Simulation methods provide models accurate enough for control design purposes. Linear model analysis is required to resolve issues of minimum sensitivity, compatibility with large transient operation and implementation considerations. These requirements can be satisfied with specialized algorithms.

Linear controllers can be integrated into a large transient control design utilizing several procedures. A detailed analysis of the envelope is required to identify regimes of operation. Reference point feedforward is used to specify the operating point. Multivariable transient logic is used to specify trajectories and avoid physical limits. For the F100 engine, decoupled integral trim control can be used to accommodate set point changes and minimize boundary violations.

It is concluded that the design procedure produces a highly modularized controller to easily accommodate refinement, engine modifications and additions. The controller is robust to modeling error, disturbances and sensor degradation. The controller, designed on the basis of a continuous model, performs well for specified, finite bandwidth computer implementation.

7.3 RECOMMENDATIONS

The control logic has been evaluated in detail on the full nonlinear digital simulation and the hybrid simulation at NASA Lewis Research Center. At the latter installation, the control is implemented on the SEL 810B. It is recommended that the logic be used to run the F100 engine in the altitude test facility in Phase II of this program.

Linear model analysis has produced many interesting results. It is recommended that further analysis and verification of the linear model behavior be undertaken to correlate the results and evaluate the model generation procedure. Engine test data should be used in this analysis to validate the nonlinear, digital simulation models.

It is recommended that further integration of the controller be undertaken to investigate couplings between the inlet, engine and airframe. The multivariable control structure is directly compatible with this type of integration and such a system would offer unusual propulsion versatility.

REFERENCE LIST

1. Miller, R.J. and Hackney, R.D., "F100 Multivariable Control System Engine Models/Design Criteria," Pratt & Whitney Aircraft Group, Government Products Division, report to AFAPL, Contract F33615-75-C-2048, Final Report for period 1 June 1975 - 31 August 1976, AFAPL-TR-76-74, Nov. 1976.
2. Szuch, J.S., Soeder, J.F., Seldner, K., Cwynar, D.S., "F100 Multivariable Control Synthesis Program-Evaluation of a Multivariable Control Using a Real Time Engine Simulation", NASA Technical Paper 1056, October 1977.
3. Bentz, C.E., "The Role of Computers in Future Propulsion Controls", AGARD Conference Proceedings No. 151 on Power Plant Controls for Aero-Gas Turbine Engines, AGARD-CP-151, Advisory Group for Aerospace Research and Development, France, 1975.
4. Bentz, C.E., and Zeller, J.R., "Integrated Propulsion Control System Program", presented at the SAE Air Transportation Meeting, Miami, Florida, 24-26 April 1973, No. 730359.
5. Billig, Leon, "Integrated Propulsion Control System," Final Report, AFAPL-TR-76-61, Air Force Aero-Propulsion Laboratory, August, 1976.
6. Billig, L., Kniat, J. and Schmidt, R.D., "IPCS Implications for Future Supersonic Transport Aircraft", presented at NASA ACT Conference, 11 July 1974.
7. Lampard, G.W.N., Batka, J.J., "Development of an Integrated Propulsion Control System", AIAA/SAE 11th Propulsion Conference, AIAA Paper No. 75-1178, Sept. 1975.
8. Seldner, K., Mihalow, J.R. and Blaha, R.J., "Generalized Simulation Technique for Turbojet Engine System Analysis", NASA TN D-6610, Feb. 1972.
9. Sellers, James, Teren, Fred, "Generalized Dynamic Engine Simulation Techniques for the Digital Computer", AGARD-CP-151, Advisory Group for Aerospace Research and Development, France, 1975.

10. Szuch, J.R. and Bruton, W.M., "Real Time Simulation of the TF30-P-3 Turbofan Engine Using a Hybrid Computer", NASA TM-X-3106, Oct. 1974.
11. Szuch, John R., Seldner, Kurt, "Real-Time Simulation of F100-PW-100 Turbofan Engine Using the Hybrid Computer", NASA TM X-3261, August 1975.
12. Zeller, J.R., Arpasi, D.J. and Lehtinen, B., "A Digital Computer Propulsion Control Facility - Description of Capabilities and Summary of Experimental Program Results", presented at NASA ACT Conference, 11 July 1974.
13. Brown, S.C., "Analysis of a Bypass Air Control System for a Supersonic Mixed-Compression Inlet", NASA TN D-4032, June 1967.
14. Willoh, R.G., "A Mathematical Analysis of Supersonic Inlet Dynamics", NASA TN D-4969, December 1968.
15. Cole, G.L., Neiner, G.H. and Wallhagen, R.E., "Coupled Supersonic Inlet-Engine Control Using Overboard Bypass Doors and Engine Speed to Control Normal Shock Position", NASA TN D-6019, December 1970.
16. Paulovich, F.G., Neiner, G.H. and Hagedorn, R.E., "A Supersonic Inlet-Engine Control Using Engine Speed as a Primary Variable for Controlling Normal Shock Position", NASA TN D-6021, March 1971.
17. Lehtinen, B., Zeller, J.R. and Geyser, L.C., "Optimal Control of Supersonic Inlets to Minimize Unstarts", NASA TN D-6408, July 1971.
18. Arpasi, D., Zeller, J.R. and Batterton, P.G., "A General Purpose Digital System for On-Line Control of Air Breathing Propulsion Systems", NASA TM-X-2168, Feb. 1971.
19. Cwynar, D.S., Batterton, P.G., "Digital Implementation of the TP30-P-3 Turbofan Engine Control", NASA TM X-3105, February 1975.
20. Seitz, W.R., "Integrated Flight/Propulsion Control by State Regulation", The Bendix Corporation, presented at AIAA Guidance and Control Conference, August 1975.

21. Hatt, F. George, Hancock, Dain M., "Recent Flight Experience with the F100 Engine in the YF-16", General Dynamics Corp., Journal of Aircraft, Vol. 12, No. 12.
22. Elliott, J.G., Seitz, W.R., "Application of Modern Control Theory to the Design of Integrated Airframe/Engine Control Systems", The Bendix Corp., Technical Report BRL/TR-75-7669.
23. Gilyard, G.B., Berry, D.T., Belte, D., "Analysis of a Lateral-Directional Airframe/Propulsion System Interaction of a Mach 3 Cruise Aircraft", AIAA 2nd Atmospheric Flight Mechanics Conference, Sept. 1972.
24. Kleinman, D.L., Killingsworth, W.R., Smith, R.G., "Automatic Depth Keeping for the Trident Submarine", SCI report to NSRDC, July 1973 (Classified).
25. Kleinman, D.L. and Killingsworth, W.R., "A Predictive Pilot Model for STOL Aircraft Landing", SCI report to NASA Langley Research Center on Contract NAS1-11727, October 1973.
26. Gupta, N.K., Bryson, A.E., "Guidance for a Tilt-Rotor VTOL Aircraft During Takeoff and Landing", Stanford University, SUDAAR No. 448, December 1972.
27. Anon., Mil Spec MIL-E-5007D, 15 October 1973, "General Specification for Turbojet and Turbofan Engines", Supersedes MIL-E-5007C (30 December 1965).
28. Tervo, W.K., Tringali, J.M., "Control Design Considerations for Variable Geometry Engines", AGARD-CP-151, Advisory Group for Aerospace Research and Development, France, 1975.
29. Beattie, E.C., "Control Mode Studies for Advanced Variable-Geometry Turbine Engines", Pratt & Whitney Aircraft, Commercial Products Division, United Aircraft Corp., Technical Report AFAPL-TR-75-7, November 1974.
30. Scott, J.E., "Performance Characteristics of Aero Gas Turbine Engines", AGARD Conference Proceedings No. 151 on Power Plant Controls for Aero-Gas Turbine Engines, AGARD-CP-151, Advisory Group for Aerospace Research and Development, France, 1975.

31. Bates, Arthur L., "Dynamic Analysis Techniques for Turbine Engine Controls", Hamilton Standard Div., United Aircraft Corp., Technical Report AFAPL-TR-67-117, October 1967.
32. Beattie, E.C., Carlisle, L.B., Katzer, T.J., Spock, W.R., "Attitude Control/Engine Control Systems", Final Report, NAPTC Contract N00019-72-C-0612, December 1975.
33. Beattie, E., Spock, W., "Application of Multivariable Optimal Control Techniques to a Variable Area Turbine Engine", 1976 JACC Paper, Purdue University, Lafayette, Indiana, July 1976.
34. MacFarlane, A.G.J., McMorran, P.D., Dixon, B.A. and Hodge, S.S., "Applications of Multivariable Control Techniques to Aircraft Gas Turbines", Conf. on Multivariable Control Systems Design and Application, Sept. 1-3, 1971.
35. McMorran, P.D., "Design of Gas Turbine Controller Using Inverse Nyquist Method", Proceedings of IEEE, Vol. 117, No. 10, October 1970, pp. 2050-2056.
36. DeHoff, R.L. and Hall, W.E., "System Identification Principles Applied to Multivariable Control Synthesis of the F100 Turbofan Engine", presented at the 1977 JACC, San Francisco, California, June 1977.
37. Hall, W.E., Gupta, N.K., and Tyler, J.S., "Model Structure Determination and Identification in Nonlinear Flight Regimes", Presented to the AGARD Symposium on State and Parameter Estimation, NASA Langley Research Center, Hampton, Virginia, November 1974.
38. Stone, C.R., Miller, N.E., Ward, M.D., Schmidt, R.D., "Turbine Engine Control Synthesis", Technical Report AFAPL-TR-75, March 1975.
39. Michael, G.J., Farrar, F.A., "An Analytical Method for the Synthesis of Nonlinear Multivariable Feedback Control", United Aircraft Research Labs, ONR Contract N00014-72-C-0414, NR 041-435, AD 762797, June 1973.
40. Michael, G.J. and Farrar, F.A., "Development of Optimal Control Modes for Advanced Technology Propulsion Systems", Interim Report prepared for Office of Naval Research under Contract N00014-73-C-0281, February 1974.

41. Michael, Gerald J., Farrar, Florence A., "Development of Optimal Control Modes for Advanced Technology Propulsion Systems", Annual Technical Report, United Aircraft Research Laboratories, ONR Contract N00014-73-C0281, NR215-219, Report N911620-2, March 1974.
42. Gupta, N.K., Bryson, A.E., "Automatic Control of a Helicopter with a Hanging Load", Stanford University, SUDAAR No. 459, June 1973.
43. Slater, G.L., "A Unified Approach to Digital Flight Control Algorithms", AIAA Paper No. 74-884, August 1974.
44. Sancedo, R. and Schiring, E.E., Introduction to Continuous and Digital Control Systems, The MacMillian Co., New York, 1968.
45. Katz, P. and Powell, J.D., "Selection of Sampling Rate for Digital Control of Aircraft", Dept. of Aeronautics and Astronautics, Stanford University, Stanford, California, SUDAAR No. 486, September 1974.
46. Stubbs, G.S., et al., "Digital Autopilots for Thrust Vector Control of the Apollo CSM/LM Vehicles", AIAA Paper No. 68-847, August 1969.
47. Bryson, A.E. and Ho, Y.C., Applied Optimal Control, Ginn Blaisdell, Waltham, Mass., 1969.
48. Bryson, A.E., Hall, W.E., "Optimal Control and Filter Synthesis by Eigenvector Decomposition", Stanford University, SUDAAR No. 436, November 1971.
49. Holley, W.E., Bryson, A.E., "Multi-Input, Multi-Output Regulator Design for Constant Disturbances and Non-Zero Set Points with Application to Automatic Landing in a Crosswind", Stanford University, SUDAAR No. 465, August 1973.
50. Trankle, T.L., Bryson, A.E., "Autopilot Logic for the Flare Maneuver of STOL Aircraft", Stanford University, SUDAAR No. 494, May 1975.
51. Hadass, Z., "Design of State-Feedback Controllers Including Sensitivity Reduction, with Applications to Precision Pointing", Stanford University, SUDAAR No. 482, August 1974.

52. Porter B. and Crossley, R., Modal Control - Theory and Applications, Barnes and Noble, London, England, 1972.
53. Tashker, M.G., "Integral Control of a Spinning Drag-Free Satellite", Stanford University, SUDAAR No. 472, April 1974.
54. Harvey, C.A. and Pope, R.E., "Synthesis Techniques for Insensitive Aircraft Control Systems", presented at 1976 IEEE Conference on Decision and Control, Clearwater Beach, Florida, December 1976.
55. Salmon, D.M., "Minimax Controller Design", IEEE Transactions on Automatic Control, Vol. AC-13, August 1968.
56. Hadass, Z. and Powell, J.D., "A Design Method for Minimizing Sensitivity to Plant Parameter Variations", AIAA Paper No. 74-927, August 1974.
57. Teren, F., "Minimum Time Acceleration of Aircraft Turbine Engines", NASA TM X-73624, June, 1977.
58. Cockshutt, E.P., "Equilibrium Performance Analysis of Gas Turbine Engines Using Influence Coefficient Techniques", AGARD-CP-151, Advisory Group for Aerospace Research and Development, France, 1975.
59. Pratt & Whitney Aircraft, "F100-PW-100 (3) Transient Engine Simulation Deck User's Manual for Deck CCD1103-0.0", FR-6867, March 1975.
60. Hall, W.E., Gupta, N.K. and Smith, R.G., "Identification of Aircraft Stability and Control Coefficients for the High Angle-of-Attack Regime", SCI final report to Office of Naval Research on Contract N00014-72-C-0327, March 1974.
61. Gupta, N.K. and Mehra, R., "Computational Aspects of Maximum Likelihood Estimation and Reduction in Sensitivity Functions Computation", IEEE Transactions on Automatic Control, Vol. AC-19, pp. 774-783, December 1974.
62. Michael, G.J. and Farrar, F.A., "Identification of Multivariable Gas Turbine Dynamics from Stochastic Input-Output Data", Annual Tech. Report prepared for Office of Naval Research under Contract N00014-73-C-0281, March 1975.

63. Teren, F., "Solution of Transient Optimization Problems by Using an Algorithm Based on Nonlinear Programming," NASA TM X-73618, June 1977.
64. DeHoff, R.L. and Hall, W.E., "Jet Engine Systems Modeling-State Space Techniques and Modeling for Control", Advances in Control and Dynamic Systems, Vol. XIV, C.T. Leondes, Editor, Academic Press, New York, N.Y., 1977.
65. DeHoff, R.L., Hall, W.E., "Design of a Multivariable Controller for an Advanced Turbofan Engine", presented at the 1976 IEEE Conference on Decision and Control, Clearwater Beach, Florida, December 1976.
66. Weinberg, M.S., "Direct Reduction of High Order Systems by State Variable Techniques", ENJE-TM-75-6, Wright Patterson Air Force Base, February 1975.
67. Weinberg, Marc S., "A Multivariable Control for the F100 Engine Operating at Sea Level Static", ASD-TR-75-28, November 1975.
68. Powell, J.D., Lange, B.O., "Control of a Spinning Drag-Free Satellite with an Application of Estimation Theory", Stanford University, SUDAAR No. 402, May 1970.
69. Otto, Edward W., Taylor, Burt L. III, "Dynamics of a Turbojet Engine Considered as a Quasi-Static System", NACA TN-2091, May 1950.
70. McGregor, W.K., Russell, D.W., Messick, R.W., Burns, L.F., "Analysis of Gas Flow Systems for Dynamic Control Purposes", AEDC-TR-55-11, April 1956.

BIBLIOGRAPHY

Adams, R.J., DeHoff, R.L., and Hall, W.E., "Modeling and Instrumentation Requirements for Multivariable Control of the F100 Turbofan Engine", presented at the AIAA/SAE 13th Propulsion Conference, Orlando, Florida, July, 1977.

Aoki, M., "Control of Large Scale Dynamic Systems by Aggregation", Proceedings 1967 JACC, June, 1967.

Arnett, Samuel E., "Turbine Engine Control Synthesis", Energy Controls Division, The Bendix Corp., Technical Report AFAPL-TR-74-113, December 1974.

Bartlett, C.R. and Turner, E.E., "Performance Evaluation Methods for the High-Bypass-Ratio Turbofan", AIAA Paper No. 75-1206.

Bauerfeind, K., "PRAC-A, New Aero Gas Turbine Engine Control Concept", AGARD-CP-151, Advisory Group for Aerospace Research and Development, France, 1975.

Beattie, E.C., "Control Considerations for Lift-Cruise Engines in a V/STOL Fighter Aircraft," AIAA Paper No. 75-1177.

Bowles, R.J., "Sub-Optimal Control of a Gas Turbine Engine", AD-777852, Master of Science Thesis, AF Institute of Technology, Wright Patterson AFB, Ohio, December 1973.

Brown, S.C., "Computer Simulation of Aircraft Motions and Propulsion System Dynamics for the YF-12 Aircraft at Supersonic Cruise Conditions", NASA Technical Memo, NASA TM X-62.245, August 1973.

Bullock, T.E., "Computation of Optimal Controls by a Method Based on Second Variations", Stanford University, SUDAAR No. 297, December 1966.

Coalson, M.S. and Csavina, F.L., "An Investigation of the Interaction Between Advanced Turbofan Controls and Assumed Performance Correction Models", AIAA Paper No. 75-1175.

PRECEDING PAGE BLANK-NOT FILMED

Cottingham, R.V., "Total Powerplant Simulation", AGARD-CP-151, Advisory Group for Aerospace Research and Development, France, 1975.

DeHoff, R.L. and Hall, W.E., "A Turbofan Engine Controller Utilizing Multivariable Feedback", presented at the 1976 IFAC Multivariable Technology Symposium, Fredrickton, New Brunswick, Canada, July 1977.

DeHoff, R.L., Hall, W.E., "Multivariable Control Design Principles with Application to the F100 Turbofan Engine", presented at the 1976 JACC Meeting, Purdue University, July 1976.

Fawke, A.J., Saravanamuttoo, H.I.H., "Experimental Investigation of Methods for Improving the Dynamic Response of a Twin-Spool Turbojet Engine", Transactions of the ASME, October 1971.

Francis, J.G.F., "The QR Transformation Parts I and II", Computer Journal, Vol. 4., No. 3, 1965.

Goodwine, J.K., "Powerplants for Wide-Bodied Aircraft--What We Bought and What We Got", AIAA Paper No. 75-1204.

Griffiths, D.M., Powell, R.D., "The Use of Digital Control for Complex Power Plant Management", AGARD Conference Proceedings No. 151 on Power Plant Controls for Aero-Gas Turbine Engines, AGARD-CP-151, Advisory Group for Aerospace Research and Development, France, 1975.

Hall, W.E., "Computational Methods for the Synthesis of Rotary Wing VTOL Aircraft Control Systems", Ph.D. Dissertation, Stanford University, Stanford, California, August 1971.

Kamper, P.W., "An Airframe Manufacturer's Requirements for Future Propulsion Controls", AGARD Conference Proceedings No. 151 on Power Plant Controls for Aero-Gas Turbine Engines, AGARD-CP-151, Advisory Group for Aerospace Research and Development, France, 1975.

Ketchum, J.R., Craig, R.T., "Simulation of Linearized Dynamics of Gas-Turbine Engines", National Advisory Committee for Aeronautics, TN 2826, November 1952.

MacIsaac, B.D., and Saravanamuttoo, H.I.H., "Aerothermodynamic Factors Governing and Response Rate of Gas Turbines", AGARD-CP-151, Advisory Group for Aerospace Research and Development, France, 1975.

Markunas, A.L., "Modeling, Simulation, and Control of Gas Turbines", Masters Thesis, MIT, June 1972.

Marscher, W.F., "Linear Analysis of Aircraft Gas Turbine Control Systems Dynamics", Masters Thesis, MIT, March 1960.

Matthews, C.W., "Numerical Study of Control of Dynamic Properties of a Supersonic Inlet Using Bypass Bleed", NASA TN D-6144, Jan. 1971.

McGregor, W.K., Russel, D.W., Messick, R.W., Burns, L.F., "Analysis of Gas Flow Systems for Dynamic Control Purposes", AEDC-TR-55-11, April 1956.

Michael, G.J., Farrar, F.A., "Stochastic Regulation of Nonlinear Multivariable Dynamic Systems", Final Report for period 1 Feb. 1973 through 31 January 1976, Report ONR-CR-215-219-4F.

Novik, David, "Some Linear Dynamics of Two-Spool Turbojet Engines", National Advisory Committee for Aeronautics TN 3274, June 1956.

Nugent, R.F., "Assessment of Engine Problem Areas in Gas Turbine-Powered Commercial Aircraft", AIAA Paper No. 75-1203.

Nye, S., and Vickers, R.J., "Use of Simulation in the Design, Development, and Testing of Power Plant Control Systems", AGARD-CP-151, Advisory Group for Aerospace Research and Development, France, 1975.

Reukauf, Paul J., Burcham, Frank W., Jr., Holzman, Jon K., "Status of a Digital Integrated Propulsion/Flight Control System for the YF-12 Airplane", AIAA/SAE 11th Propulsion Conference, Sept. 1975. AIAA Paper No. 75-1180.

Robinson, K., "Afterburning Regulation Concepts", AGARD-CP-151, Advisory Group for Aerospace Research and Development, France, 1975.

Saravanamuttoo, H.I.H. and Fawke, A.J., "Simulation of Gas Turbine Dynamic Performance", ASME Journal, May 1970.

Thompson, B., "Basic Transient Effects of Aero Gas Turbines", AGARD-CP-151, Advisory Group for Aerospace Research and Development, France, 1975.

Urban, L.A., "Gas Turbine Engine Parameter Interrelationships", United Aircraft Corp., 1967.

Vaughan, D.R., "A Non-Recursive Solution of the Discrete Matrix Riccati Equation", IEEE Transaction on Automatic Control, October 1970.

Weinberg, Marc S., "Low Order Linearized Models of Turbine Engines", ASD-TR-75-24, Wright Patterson Air Force Base, July 1975.